

University of Warwick institutional repository: <http://go.warwick.ac.uk/wrap>

A Thesis Submitted for the Degree of PhD at the University of Warwick

<http://go.warwick.ac.uk/wrap/62024>

This thesis is made available online and is protected by original copyright.

Please scroll down to view the document itself.

Please refer to the repository record for this item for information to help you to cite it. Our policy information is available from the repository home page.

Incorporation of amino acids into polymeric
structures for use in chiral resolution, catalysis and
fluorescence studies

Submitted for the degree of Doctor of Philosophy

February 2014

Beth Moore

Department of Chemistry

THE UNIVERSITY OF
WARWICK

Contents

Declaration of authorship	XXII
Acknowledgements	XXIII
List of Publications	XXIV
Abbreviations	XXV
Thesis Summary	XXIX
Polymerization Techniques	2
1.1.1 Reversible-Deactivation Radical Polymerization	2
1.1.2 Heterogeneous and emulsion polymerization	10
1.2 Amino Acids in Polymers and Structures	13
1.1.2 Amino acid monomers	13
1.2.2 Polymeric structures incorporating amino acids	15
1.3 Enantiomer Resolution	19
1.4 Catalysis	23
1.4.1 Immobilized Catalysts	23
1.4.2 MacMillan Catalysis	32
1.5 Fluorescence	39
1.5.1 Forster resonance energy transfer	41
1.6 Summary	44
1.7 References	45
2.1 Abstract	58

2.2 Introduction	59
2.3 Results and Discussion.....	66
2.3.1 Synthesis of Monomers	66
2.3.2 Polymerization Investigation	68
2.3.3 Synthesis of poly(M 2.1) <i>via</i> a pentafluorophenylacrylate scaffold	76
2.3.4 Interaction between chiral monomers and BINOL.....	84
2.3.5 Interactions between chiral polymers and BINOL	95
2.3.6 Physical Separation	99
2.4 Conclusions	106
2.5 Experimental	107
2.5.1 Instrumentation.....	107
2.5.2 Methods and Techniques	108
2.6 References	116
3. 1 Abstract	121
3.2 Introduction	123
3.3 Results and discussion	129
3.3.1 Monomer Synthesis	129
3.3.2 Polymer Synthesis	133
3.3.3 Polymer properties.....	140
3.3.4 Diels-Alder Catalysis.....	147
3.3.5 Polymer recycling.....	158

3.4 Conclusions	163
3.5 Experimental	164
3.5.1 Instrumentation	164
3.5.2 Methods and Techniques	165
3.6 References	172
4.1 Abstract	176
4.2 Introduction	177
4.2 Introduction	177
4.3 Results and Discussion.....	182
4.3.1 Nanogel Synthesis	182
4.3.2 Diels-Alder catalysis.....	192
4.3.3 Selectivity	203
4.3.4 Hydrophobic effect/concentrator effect.....	209
4.4 Conclusions	222
4.5 Experimental	223
4.5.1 Instrumentation	223
4.5.2 Methods and Techniques	224
4.6 References	226
5.2 Introduction	232
5.3 Results and Discussion.....	241
5.3.1 Monomer Synthesis	241

5.3.2 Nanogel synthesis	248
5.3.4 FRET experiments	262
5.5.1 Instrumentation	279
5.5.2 Methods and Techniques	280
Conclusions	290
Table of Figures, Schemes and Tables	VI

Table of Figures, Schemes and Tables

Figure 1.1. The structure of TEMPO, a common NMP initiator.	5
Figure 1.2. The structures of the different common types of CTA.....	5
Figure 1.3. The structures of MAMs and LAMs.	6
Figure 1.4. The resonance structures that can be formed by xanthates and dithiocarbamates which help to stabilize the radical.....	7
Figure 1.5. The generally accepted mechanism for RAFT polymerization.....	8
Figure 1.6. A representation of the synthetic process for emulsion polymerization..	11
Figure 1.7. A reproduction of a the different synthetic routes available for the synthesis of poly(amino acids).....	14
Figure 1.8. A representation of two enantiomers based on a tetrahedral carbon atom.	15
Figure 1.9. A reproduction of an overview of the differing stabilities afforded from mixtures of chiral leucine polymers.....	17
Figure 1.10. The structure of the pH-responsive tryptophan polymer.....	17
Figure 1.11. A reproduction of the fluorescence microscopy images that were used in alongside other data to demonstrate the negligible cytotoxicity effect of poly(tryptophan).....	18
Figure 1.12. A reproduction of a representation of the chemical and 3D structure of cyclodextrins.	20
Figure 1.13. A reproduction of a representation of how templating is used to form MIPs.....	21
Figure 1.14. A reproduction of an overview of the work carried out by Kristensen <i>et al.</i>	24

Figure 1.15. A representation of an LCST phase diagram showing the relationship between LCST cloud point and composition. The LCST is the minimum temperature.....	26
Figure 1.16. A representation of how a catalyst (green circles) could be immobilized into a cross-linked surfactant stabilized nanogel.	28
Figure 1.17. A reproduction of the conversion of the reaction between vinyl epoxide and phenyl boronic acid catalyzed by either palladium supported within a micelle or in a small molecule.....	29
Figure 1.18. A reproduction of an overview of the compartmentalized catalysts used in a cascade reaction.....	30
Figure 1.19. A reproduction of an overview of how the proline moieties (depicted in red) are in different environments dependent on the structure of the polymer. ¹³⁶	31
Figure 1.20. The structure of the MacMillan catalyst.....	32
Figure 1.21. A schematic representation of the reactions that the MacMillan catalyst has successfully catalyzed.....	33
Figure 1.22. A 3D representation of the transition state reproduced from MacMillan's paper. In this depiction the benzyl group is shielding the top side of the dieneophile from attack.....	34
Figure 1.23. A schematic illustrating the advantages of the 2 nd generation MacMillan catalyst reproduced from MacMillan's paper. Here the catalyst is being used for indole alkylations which uses the same catalytic control as the DA reaction. The nitrogen lone pair is more exposed, the top face (<i>si</i> -face) is more covered and the <i>re</i> -face is more accessible. Models 1 and 2 show the differing lone pair accessibility of both catalysts: model 1 shows the interaction between the CH ₃ group and the lone pair which has been removed in model 2 of the 2 nd generation MacMillan catalyst,	

which makes the lone pair more exposed. Models 3 and 4 illustrate the difference in <i>re</i> -face coverage with model 3 having some steric hindrance on the <i>re</i> -face which is not the case for the 2 nd generation catalyst in model 4.	36
Figure 1.24. A reproduction of an overview of the immobilized MacMillan catalyst being used in a flow set-up for the catalysis of the DA reaction.	37
Figure 1.25. Jablonski diagram illustrating the process of fluorescence.	39
Figure 1.26. Jablonski diagram illustrating the process of fluorescence.	41
Figure 1.27. A reproduction of the fluorescence emission spectrum of tryptophan and the ribonucleoside FRET pair. The left hand spectra shows the emission (solid line) and absorption spectra (dashed line) of the tryptophan (blue) and the ribonucleoside FRET pair (red). The right hand spectra show that the tryptophan emission is decreasing and ribonucleoside emission increasing with increased concentrations of the ribonucleoside. The inset shows the emission spectrum at saturation.	43
Figure 2.1. A reproduction of the table of contents figure for the work published by De <i>et al.</i>	58
Figure 2.2. A reproduction of the table of contents figure for the work published by Mori <i>et al.</i>	59
Figure 2.3. The structures of (<i>S</i>)- and (<i>R</i>)- BINOL with the phenolic protons highlighted which give rise to the trackable signal.	61
Figure 2.4. A reproduction of an image of the separation of (<i>rac</i>)-BINOL enantiomers in ¹ H NMR spectroscopy caused by a leucine monomer.	62
Figure 2.5. A reproduction of the ¹ H NMR spectrum from the work conducted by Redando <i>et al.</i> The bottom spectrum shows a ¹ H NMR spectrum of omeprazole on its own and the top spectrum a ¹ H NMR spectrum of omeprazole in the presence of	

(S)-BINOL. The top spectrum shows how the proton, highlighted on the structure, has shifted and split into the two enantiomers.	63
Figure 2.6. ¹ H NMR (300 MHz) spectrum for L- M 2.1 in CDCl ₃	65
Figure 2.7. ¹³ C NMR (75 MHz) spectrum for L- M 2.1 in CDCl ₃	65
Figure 2.8. The CTAs used and a selection of SEC traces for entries 1, 3, 14, 15, 23 and 25 from Table 2.1.	68
Figure 2.9. The structure of M 2.1 and an acrylamide based monomer of tryptophan (L-A-Trp-OH) with a free carboxylic acid which is easily polymerized <i>via</i> RAFT synthesized by Kumar ¹⁵ and Mori ¹⁴ and a tryptophan monomer functionalized through the carboxylic acid synthesized by De (Boc-L-Trp-HEMA).	69
Figure 2.10. ¹ H NMR (300 MHz) of M 2.2 in CDCl ₃	72
Figure 2.11. ¹ H NMR (300 MHz) spectrum in CDCl ₃ of the original M 2.2 and the end product of the four reactions outlined in Table 2.2 focussing on the proton signal for the proton adjacent to the bromine.	73
Figure 2.12. ¹ H NMR (300 MHz) spectrum (top) and ¹⁹ F NMR (282 MHz) spectrum (bottom) of M 2.3 in CDCl ₃	76
Figure 2.13. ¹⁹ F NMR (375 MHz) spectrum of M 2.3 (top) and poly(M 2.3) (bottom) in CDCl ₃	77
Figure 2.14. ¹⁹ F NMR (375 MHz) spectra of poly(M 2.3) before (top) and after substitution (bottom) in CDCl ₃	78
Figure 2.15. ¹ H NMR (300 MHz) spectrum of poly(M 2.1) in CDCl ₃	78
Figure 2.16. SEC traces of a) poly(M 2.3) in CHCl ₃ and b) poly(M 2.1) in DMF. .	79
Figure 2.17. MALDI-TOF spectra of poly(M 2.1). MALDI-ToF was collected on poly(M 2.1) of DP 18 calculated from the ¹ H NMR spectrum, using dithranol as a matrix and NaTFA as the cationizing agent.	80

Figure 2.18. IR of M 2.1 , poly(M 2.3), and poly(M 2.1).	81
Figure 2.19. ¹ H NMR (300 MHz) spectrum of L- M 2.4 in CDCl ₃	83
Figure 2.20. The monomers, polymers and their combinations with (<i>rac</i>)-BINOL..	84
Figure 2.21. The chemical structure of the two enantiomers of (<i>rac</i>)-BINOL. The protons highlighted in the box are those used to examine the interactions.....	84
Figure 2.22. ¹ H NMR (300 MHz) spectrum showing the interaction of the four monomers with (<i>rac</i>)-BINOL. a) (<i>rac</i>)-BINOL with no monomers; b) (<i>rac</i>)-BINOL + L- M 2.4 ; c) (<i>rac</i>)-BINOL + D M 2.4 ; d) (<i>rac</i>)-BINOL + L- M 2.1 and e) (<i>rac</i>)-BINOL + D- M 2.1 . At 1.0:1.0 molar ratio of (<i>rac</i>)-BINOL:monomer.in CDCl ₃	86
Figure 2.23. ¹ H NMR (300 MHz) spectrum showing the effect of altering the molar ratios of (<i>rac</i>)-BINOL and L- M 2.4 . a) (<i>rac</i>)-BINOL with no added monomer; b) (<i>rac</i>)-BINOL: L- M 2.4 1.0:0.6; c) 1.0:1.0; d) 1.0:1.2; e) 1.0:1.5; f) 1.0:1.9 and g) 1.0:2.4 in CDCl ₃	87
Figure 2.24. ¹ H NMR (300 MHz) spectrum of (<i>R</i>)-BINOL before and post exposure to D ₂ O in CDCl ₃ . The phenolic peaks have been highlighted with the relative integration falling from 0.97 in the (<i>R</i>)-BINOL ¹ H NMR spectrum to 0.79 in the deuterated (<i>R</i>)-BINOL ¹ H NMR spectrum.	88
Figure 2.25. ¹ H NMR (300 MHz) spectrum showing the interaction of (<i>rac</i>)-BINOL with part deuterated (<i>R</i>)-BINOL with (A) L- M 2.4 ; (B) D- M 2.4 ; (C) L- M 2.1 and (D) D- M 2.4 in CDCl ₃ . The furthest shifted enantiomer has been labelled as either (<i>R</i>)- of (<i>S</i>)- BINOL and the spectra have been labelled to indicate if the monomer is either L- or D-.	89
Figure 2.26. ¹ H NMR (300 MHz) spectrum of a racemic mixture of M 2.4 with a) no added BINOL b) (<i>R</i>)-BINOL added and c) (<i>S</i>)-BINOL added at a molar ratio of 2:1 aligned to CDCl ₃	90

Figure 2.27. ¹ H NMR (300 MHz) spectra of (S)- BINOL with b) racemic M 2.4 c) D- M 2.4 (blue line) d) L- M 2.4 (red line) all with CH ₂ Cl ₂ as an internal standard and a) racemic M 2.4 as a standard in CDCl ₃	91
Figure 2.28. ¹ H NMR (300 MHz) spectra of a) (<i>rac</i>)-BINOL at a 1.0:1.0 ratio of (<i>rac</i>)-BINOL to residues with polymers with b) poly(L- M 2.4)(DP 38) and c) poly(L- M 2.1) (DP 150) and d) poly(L- M 2.1) (DP 66) in CDCl ₃	93
Figure 2.29. ¹ H NMR (300 MHz) spectra of a) (<i>rac</i>)-BINOL and poly(L-(M 2.1) (DP 150) polymer at varying ratios of residue: (<i>rac</i>)-BINOL of b) 1.0:0.8, c) 1.0:0.9 d) 1.0:1.0 and e) 1.0:1.1 in CDCl ₃	94
Figure 2.30. ¹ H NMR (300 MHz) spectrum of a) (<i>rac</i>)-BINOL and the spectra showing the interactions of (<i>rac</i>)-BINOL with poly(L- M 2.4) varies with temperature b) 198 K c) 303 K d) 308 K e) 313 K f) 318 K in CDCl ₃	95
Figure 2.31. CD spectrum of poly(M 2.1) at 1 mg mL ⁻¹ in dioxane measured in an 0.1 mm cell.....	96
Figure 2.32. CD spectra of 1 mg mL ⁻¹ M 2.1 in 0.1 mm cell in dioxane (blue line) and the same sample with 0.01 mL of 1 mg mL ⁻¹ (<i>rac</i>)-BINOL in dioxane (red line).	96
Figure 2.33. A reproduction of the TOC of Deng <i>et al.</i> work along with the release data for the proline enantiomers from their chiral-APCN and the structure of the L-alanine monomer used in this work.	97
Figure 2.34. ¹ H NMR spectrum (300 MHz) of M 2.4-OH in DMSO.....	99
Figure 2.35 ¹ H NMR (300 MHz) spectrum for the synthesized monomer M-PDMS in CDCl ₃	100
Figure 2.36. IR of the chiral-APCN with peaks from the two monomers highlighted.	101

Figure 3.1. The chemical structures of the MacMillan catalyst and the newly synthesized MacMillan monomer, where HX is an acid salt.....	121
Figure 3.2. A representative of the energy overlap of the p orbital of the DA reaction highlighting the symmetry and energy overlap of the HOMO of the diene and LUMO of the dienophile.....	125
Figure 3.3. A 3D representation of the transition state reproduced from MacMillans paper. ¹ In this depiction the benzyl group is shielding the top side of the dienophile from attack.	126
Figure 3.4. The structure of the methacrylic MacMillan monomer used by Kristensen <i>et al.</i> and the resulting cross-linked polymer beads.	127
Figure 3.5. ¹ H NMR (300 MHz) spectrum of M 3.1 in CD ₃ OD.	131
Figure 3.6. ¹³ C NMR (75 MHz) spectrum of M 3.1 in CD ₃ OD.....	131
Figure 3.7. IR spectrum of M 3.1 indicating the presence of a secondary amine, carbonyl groups and carbon-carbon double bond. Other significant absorbencies around 1130 cm ⁻¹ are attributed to C-O bonds and 1030 cm ⁻¹ to C-N bonds.	132
Figure 3.8. A representative ¹ H NMR spectrum (300 MHz) in CD ₃ OD of the synthesized functional copolymers; polymer presented is P 3.2 . The relative incorporation of the two monomers was determined from the signals of g and l, here integrated to 1.00 and 2.86. (1.00/3.86*100% = 26%)	134
Figure 3.9. HPLC chromatogram of a sample containing both (<i>S</i>)- and (<i>R</i>)-MacMillan catalyst (black line) and recovered <i>S</i> -MacMillan catalyst after exposure to polymerization conditions (red line). Only the (<i>S</i>)-catalyst is detected after exposure to the polymerization conditions.....	136
Figure 3.10. A schematic illustration of the different reactions that can take place during co-polymerization of two different monomers.	137

Figure 3.11. A representation of the different polymer structures that can be synthesized depending on the reactivity ratios of the co-monomers.	138
Figure 3.12. Plot of monomer fraction in the initial feed and in resulting co-polymer of M 3.1 and DEGMA, used to determine reactivity ratios.....	139
Figure 3.13. A photo of the polymer P 3.1 – P 3.7 , as the catalyst incorporation increases the polymers' physical appearance changes from a yellow sticky solid to a white fluffy solid.....	141
Figure 3.14. A reproduction of graphs highlighting the dependence of temperature on composition for both LCST and UCST systems.....	143
Figure 3.15. Cloud point data for poly(DEGMA), P 3.1 and P 3.2 across a range of concentrations in water. The data was recorded at 500 nm with a heating/cooling rate of 1 °C min ⁻¹ . The cloud point was taken at the temperature when the absorbance equalled 0.5 after the data had been normalized between 0 and 1 absorbance units.	144
Figure 3.16. LCST cloud point measurements traces taken at 0.5 mg mL ⁻¹ and measured at 500 nm with the temperature taken at 0.5 absorbance units after the data had been normalized between 0 and 1 for a) poly(DEGMA) (blue line) b) P 3.1 (red line) and c) P 3.2 (green line).....	146
Figure 3.17. A representative ¹ H NMR (300 MHz) spectrum in CDCl ₃ of the DA products.....	148
Figure 3.18. A representative GC chromatogram of the DA products.	148
Figure 3.19 The structures of M 3.1 and the MacMillan catalyst.....	149
Figure 3.20. The conversions and selectivities of the data highlighting the similarity between the two solvent systems.	152

Figure 3.21. Kinetic plots for the DA reaction between cyclopentadiene and <i>trans</i> -hexen-1-al catalyzed by P 3.6 and P 3.2 fitted to a logarithmic trendline.	153
Figure 3.22. The conversions and selectivities for the DA reaction between cyclopentadiene and <i>trans</i> -hexen-1-al after 4 h for M 3.1 , P 3.2 and P 3.7 at different temperatures (4, 20, 40 and 60 °C) at 5 mol%.	156
Figure 3.23. THF SEC UV 309 nm trace of P 3.6 before (black line) and after end group removal (red line), along with the structures of the two polymers.	157
Figure 4.1. The structures of the dendrimers used in the experiments which demonstrated the concentrator effect by Fréchet and co-workers ⁹ (left) and the structure of the catalyst DMAP (right) that was investigated.	178
Figure 4.2. Conversions of the monomers in the nanogel with EMA (blue line) (relative conversion) and M 3.1 (red line). The integration of monomer: polymer for M 3.1 was used to determine conversion. As EMA monomer will have been removed on removal of THF, the final ¹ H NMR spectrum was taken to be 100% conversion for EMA and the relative integration of EMA polymer to M 3.1 polymer was used to determine the conversion of EMA.	184
Figure 4.3. Number (blue line), Volume (red line) and Intensity (green line) DLS traces for the nanogels N 4.1 – N 4.9	187
Figure 4.4. The correlation coefficient for the DLS measurement of N 4.4	188
Figure 4.5. TEM image and frequency count of the nanogels incorporating the MacMillan catalyst. TEM samples were prepared by drop deposition of a 0.1 mg mL ⁻¹ polymer solution in water onto copper/carbon grids that had been pre-treated with oxygen plasma and analyzed by using a JEOL TEM-2100 microscope operating at 200 kV.	190

Figure 4.6. The structures of the co-monomers used in nanogel synthesis of methyl methacrylate (MMA), ethyl methacrylate (EMA) and <i>n</i> BuMA (butyl methacrylate).	191
Figure 4.7. A schematic representation of reactions carried out varying the nanogel concentration and catalyst concentration (as affected by the difference in catalyst DoF), represented with arbitrary DoF of 2, 3 and 4.....	195
Figure 4.8. A graph demonstrating the clear effect of mol% (blue) on the conversions (red) of the DA reaction between cinnamaldehyde and cyclopentadiene catalyzed by nanogels N 4.1 – N 4.6 at various mol%, in water (maintaining a volume of 2 mL).	197
Figure 4.9. Conversion against time for the DA reaction between cyclopentadiene and cinnamaldehyde catalyzed by N 4.5 in 2 mL giving 9.8 mol% loading.	198
Figure 4.10. The conversion against time of M 3.1 (blue line) in 100 μ L H ₂ O and N 4.5 (red line) in 1.02 mL H ₂ O.	211
Figure 4.11. Number (blue line), Volume (red line) and Intensity (green line) DLS traces for the nanogels synthesized in this work.....	215
Figure 4.12. TEM image and frequency count of the SN 4.1 – SN 4.3 incorporating the MacMillan catalyst. TEM samples were prepared by drop deposition of a 0.1 mg mL ⁻¹ polymer solution in water onto copper/carbon grids that had been pre-treated with oxygen plasma and analyzed by using a JEOL TEM-2100 microscope operating at 200 kV.....	216
Figure 4.13. A schematic representation of the changeable nature of the shell characteristic at low temperatures (a hydrophilic fully extended polymer) or high temperatures (a hydrophobic collapsed polymer).	217

Figure 4.14. Change in particle size with temperature, as determined by DLS for SN 4.1 (blue line), SN 4.2 (red line) and N 4.5 (purple line).....	218
Figure 5.1. A reproduction of the 3D representation of Snase, the L-tryptophan moiety highlighted in purple is the last residue to exhibit order.....	232
Figure 5.2. A reproduction of the excitation (red line) and emission (purple line) spectra of phenylalanine, tyrosine and tryptophan in an aqueous pH 7 solution.	233
Figure 5.3. A reproduction of a figure which demonstrates how the influence of packing parameters can affect the self-assembled structure.	235
Figure 5.5. ¹ H NMR (300 MHz) spectrum of M 5.1 in CDCl ₃	242
Figure 5.6. ¹³ C NMR (75 MHz) spectrum of M 5.1 in CDCl ₃ , expanded parts of the spectrum are inserted where two peaks have very similar shifts.	242
Figure 5.7. Structures of the CTA 5.1 and 5.2 used in the polymerization of M 5.1 , detailed in Table 5.1.....	244
Figure 5.8. ¹ H NMR (300 MHz) spectrum of the conversion of M 5.1 in CDCl ₃ with polymeric peaks highlighted and observed monomeric peaks labelled. The conversion was calculated by subtracting the monomer peaks and CDCl ₃ peak from the integral and comparing the value to the quantity of monomer still left. e.g. $((15.28-0.79-5)/5) \times (1/(1.898+1))*100\% = 65\%$	245
Figure 5.9. A plot of $\ln(M)_0/(M)_t$ against time for the polymerization of P 5.1 , entry 1 in Table 5.1.....	246
Figure 5.10. SEC trace of P 5.1 (red line) and the chain extension (blue line) (DMF, PMMA calibration).	247
Figure 5.11. Conversions of the monomers in the nanogel with EMA (blue) (relative conversion) and M 5.1 (red). The integration of monomer: polymer for M 5.1 was used to determine conversion. As EMA monomer has been removed on removal of	

THF, the final ^1H NMR spectrum (24 h) was taken to be 100% conversion for EMA and the relative integration of EMA polymer to **M 5.1** polymer was used to determine the conversion of EMA.250

Figure 5.13. SEC trace showing the RI (blue line) and UV 309 nm trace (red line) (DMAC, PMMA calibration).251

Figure 5.14. PDA analysis from THF SEC showing monomer (top) and nanogel copolymer (bottom). Left hand axis shows elution time (min), right hand axis shows wavelength (nm) and the vertical axis shows intensity.252

Figure 5.15. A plot of decay time against scattering vector squared for **N 5.3c**. The resulting gradient is the diffusion coefficient of the particles.254

Figure 5.16. Representative TEM images of the synthesized nanogels, which demonstrates the spherical nature of the synthesized particles - scale bar is 100 nm. TEM samples were prepared by drop deposition of a 0.1 mg mL^{-1} polymer solution in water onto copper/carbon grids that had been pre-treated with oxygen plasma and analyzed by using a JEOL TEM-2100 microscope operating at 200 kV.256

Figure 5.17. The fluorescence spectra ($\lambda_{\text{ex}} = 380 \text{ nm}$, slit width = 10 nm) of **M 5.1** (blue line) and **P 5.1** (red line) in THF at 1 mg mL^{-1} , Rayleigh scattering $\lambda = 380 \text{ nm}$258

Figure 5.18. Fluorescence spectrum of **N 5.1** ($\lambda_{\text{ex}} = 280 \text{ nm}$, slit width = 2.5 nm), which equates to $0.0006 \text{ mg mL}^{-1}$ **M 5.1** in H_2O , Rayleigh scattering $\lambda = 280 \text{ nm}$, Raman Scattering $\lambda = 560 \text{ nm}$ in H_2O259

Figure 5.19. Possible photoproducts of L-tryptophan.260

Figure 5.20. The increase of intensity at $\lambda_{\text{em}} = 500 \text{ nm}$ of **N 5.3** exciting at either $\lambda_{\text{ex}} = 280 \text{ nm}$ (red line), 270 nm (blue line), 260 nm (green line) and 225 nm (purple

line) every 5 min (slit width = 2.5 nm). The intensities have been normalized to start at zero to provide a clearer visual comparison.....	261
Figure 5.21. The excitation and emission fluorescence spectra of DNSA encapsulated into an unfunctionalized EMA nanogel. The excitation spectrum (red line) is based on emission at $\lambda_{em} = 470$ nm (Rayleigh scattering $\lambda = 470$ nm, Raman scattering $\lambda = 235$ nm) and the emission spectrum (purple line) was excited at $\lambda_{ex} = 350$ nm (Rayleigh scattering $\lambda = 470$ nm), slit width = 5 nm.	263
Figure 5.22. Fluorescence spectrum showing N 5.3 after purging with N ₂ with $\lambda_{ex} = 225$ nm recorded every 5 min after addition of DNSA.....	265
Figure 5.23. A graph showing the decrease in fluorescence intensity of L-tryptophan with time, on addition of DNSA exciting at $\lambda_{ex} = 225$ nm every 5 min, and the trendlines that have been used to calculate specific times within the graph.....	266
Figure 5.24. The fluorescence intensity of DNSA excited at $\lambda_{ex} = 350$ nm for 1 mg mL ⁻¹ (red line), 5 mg mL ⁻¹ (green line), 10 mg mL ⁻¹ (purple line), 20 mg mL ⁻¹ (blue line), in THF (Rayleigh scattering $\lambda = 350$ nm).....	267
Figure 5.25. The fluorescence intensity of DNSA excited at $\lambda_{ex} = 380$ nm for 1 mg mL ⁻¹ (red line), 5 mg mL ⁻¹ (green line), 10 mg mL ⁻¹ (purple line), 20 mg mL ⁻¹ (blue line), in THF (Rayleigh scattering $\lambda = 380$ nm).....	267
Figure 5.26. A typical DNSA fluorescence emission intensity against time plot. Addition of 5 μ L of 2 mg mL ⁻¹ THF solution to 200 μ L of N 5.1 irradiated at $\lambda_{ex} = 225$ nm every 5 min.....	268
Figure 5.27. Representative TEM images of SN 5.1 – SN 5.5 which demonstrates the spherical nature of the synthesized particles - scale bar is 100 nm. TEM samples were prepared by drop deposition of a 0.1 mg mL ⁻¹ polymer solution in water onto	

copper/carbon grids that had been pre-treated with oxygen plasma and analyzed by using a JEOL TEM-2100 microscope operating at 200 kV.....	274
Scheme 1.1. A schematic representation of the steps of initiation, propagation and termination. I ₂ is the initiator and M the monomer.....	3
Scheme 1.2. A representation of the ATRP process using a transition metal complex (M _T) with a halide (X).....	4
Scheme 1.3. A schematic representation of the generic synthesis of monomeric versions of amino acids.....	13
Scheme 1.4. A modified table of contents graphic demonstrating how the phenolic protons of (<i>rac</i>)-BINOL are influenced by the presence of poly(L-tryptophan).....	22
Scheme 1.5. A schematic representation of how a thermally responsive polymer can be reclaimed and used for catalysis depending on the temperature of the system. ¹⁰⁵	27
Scheme 1.6. A schematic representation of iminium catalysis and the electrophilic sites that are formed.....	34
Scheme 2.1. Generic route for the synthesis of amino acid monomers with (meth)acryloyl chloride.....	57
Scheme 2.2. A schematic representation of how chiral structures are potentially able to deliver enriched solutions.....	60
Scheme 2.3. Synthetic route to L- M 2.1	64
Scheme 2.4. The potential mechanism of cyclization for M 2.1 when exposed to a radical flux and the suggested structures from either forming a) 7 member or b) 6 member ring.....	70
Scheme 2.5. The synthetic route to M 2.2	71
Scheme 2.6. Schematic overview of the synthesis of poly(M 2.1).....	74

Scheme 2.7. Synthetic route for M 2.3	75
Scheme 2.8. A schematic representation for the synthesis of L- M 2.4 and poly(L- M 2.4).	82
Scheme 2.9. The synthetic route to M 2.4-OH	98
Scheme 2.10. The synthetic route to a chiral APCN including the synthesis of the cross-linker.	100
Scheme 3.1. The mechanism of the MacMillan catalyst for the DA reaction. The formation of the imine transition state (1) from the reaction of the α,β -unsaturated aldehydes and the amine is crucial to lower the LUMO of the dienophile.	124
Scheme 3.2. The synthesis of (<i>S</i>)-MacMillan functionalized monomer (M 3.1) from the amino acid (<i>S</i>) – tyrosine methyl ester.	130
Scheme 3.3. Polymerization scheme of M 3.1 and DEGMA <i>via</i> RAFT polymerization and the structure of the resulting polymer.	133
Scheme 3.4. Model DA reaction, where R = C ₃ H ₇ and where there are four possible products: the <i>endo</i> and <i>exo</i> products of both enantiomers.	147
Scheme 3.5. A schematic of the DA reaction between cyclopentadiene and <i>trans</i> -hexen-1-al giving the conditions of the reaction.	149
Scheme 3.6. A schematic representation of the loss of the TFA salt.	151
Scheme 3.7 A schematic to demonstrate the <i>pseudo</i> -continuous process.	160
Scheme 4.1. A schematic from Cotanada <i>et al.</i> 's paper which demonstrates how their DMAP loaded micelle has molecular recognition properties.	179
Scheme 4.2. A schematic representation of the synthesis of a cross-linked nanogel from the monomers EMA and M 3.1 with a cross-linker EGDMA stabilized by SDS.	183

Scheme 4.3. A reaction scheme between cyclopentadiene and cinnamaldehyde and the four possible products, the favoured enantiomers according to the mechanism laid out by MacMillan is the (*R*)-enantiomer. The reaction between cyclopentadiene and cinnamaldehyde produces almost equal amounts of *exo* and *endo* products. ... 193

Scheme 4.4. A schematic representation of the addition of a shell to a nanogel seed molecule, the synthesis requires addition of a thermo-responsive monomer and a small amount of additional SDS along with initiator. 213

Scheme 5.1. A schematic representation of the measurement of CMC with an amphiphilic polymer and a fluorescent marker, in this case pyrene. Below the CMC pyrene is located in the continuous phase whereas above the CMC it is located in the hydrophobic cavity of the assembled structure. 234

Scheme 5.2. A representative scheme of the FRET process. The donor absorbs radiation and fluoresces at a wavelength which excites the acceptor that in turn emits at a different wavelength. 237

Scheme 5.3. The synthetic route to the L-tryptophan-containing monomer **M 5.1**. 241

Scheme 5.4. A schematic representation of the emulsion polymerization process used in the synthesis of **M 5.1** decorated cross-linked polymeric nanogels stabilized by SDS and cross-linked with EGDMA. 248

Scheme 5.5. A Schematic to represent the FRET interaction between the L-tryptophan-containing nanogel, A, and a FRET pair that is loaded into the nanogel. 262

Scheme 5.6. A schematic representation of the FRET experimental procedure. At $t = 0$ the DNSA is added to the fluorometer cell that already contains the nanogel solution which is immediately irradiated with light and the spectrum recorded. The fluorescence cell is left in position and irradiated at 5 min intervals and the spectra

recorded. Over time the spectra changed giving a lower emission of tryptophan and an increased emission for DNSA.	264
Scheme 5.7. A schematic representation of the structures synthesized through the addition of polymeric shells to a L-tryptophan containing core.	272
Table 2.1. Conditions used for the attempted polymerization of M 2.1 , varying the CTA, solvent, temperature, time, concentration and equivalents of monomer, the initiator and its equivalents.	67
Table 2.2. The conditions for the cyclization experiments conducted for M 2.2	72
Table 2.3. The results of the ratio of (<i>S</i>)-BINOL to (<i>R</i>)-BINOL in various samples before exposure to the chiral APCN and at extractions afterwards.	102
Table 3.1. The initial feed ratio, final catalyst incorporation, molecular weights and molecular weight distribution for P 3.1 – P 3.7	135
Table 3.2. The measured T_g values for the series of co-polymers P 3.1 – P 3.7	141
Table 3.3. The DA reaction at rt for 4 h catalyzed by M 3.1 and MacMillan catalyst, compared with reported literature values at 5 mol%.	150
Table 3.4. Kinetic data for the DA reaction of <i>trans</i> -hexen-1-al and cyclopentadiene catalyzed by P 3.2 and P 3.6 The reactions were carried out in H ₂ O, conversions measured by ¹ H NMR spectroscopy and enantioselectivity by GC analysis.	154
Table 3.5. DA reaction of <i>trans</i> -hexen-1-al and cyclopentadiene catalyzed by P 3.6 with and without RAFT end group. The data for the reaction without end group is the average of 2 repeats.	157
Table 3.6 Recycling data for the DA reaction catalyzed by P 3.6 where the polymer was recovered through dialysis followed by freeze-drying.	159

Table 3.7. <i>Pseudo</i> continuous recycling data for the DA reaction between cyclopentadiene and <i>trans</i> -hexen-1-al at 5 mol% after 4 h reactions, catalyzed by P 3.6 where additional TFA is added along with the solvents for each cycle.....	160
Table 3.8. The DA reaction cyclopentadiene and <i>trans</i> -hexen-1-al with 1 eq. of TFA for 4 h in H ₂ O.....	161
Table 3.9. The conversions and selectivities of the DA reaction between cyclopentadiene and <i>trans</i> -hexen-1-al with P 3.2 at 5 mol% used in a <i>pseudo</i> -continuous process with no further addition of TFA in each cycle.	162
Table 4.1. The synthesized nanogels N 4.1 – N 4.9 detailing the DoF (wt%) and co-monomer. The hydrodynamic size (nm) and dispersity (measured by DLS) and average diameter (nm) obtained from TEM.....	185
Table 4.2. The conversions of DA reaction between cinnamaldehyde and cyclopentadiene catalyzed by nanogels N 4.1 – N 4.6 at various mol%, in water (maintaining a volume of 2 mL).	196
Table 4.3. The conversions and selectivities for the DA reaction between cyclopentadiene and cinnamaldehyde catalyzed by N 4.5 in 2 mL giving 9.8 mol% loading.....	198
Table 4.4. Conversion of the DA reaction between cinnamaldehyde and cyclopentadiene catalyzed by N 4.3 – N 4.6 at 5 mol%, determined after 24 h.	199
Table 4.5. The conversions of the DA reaction after 24 h between cinnamaldehyde and cyclopentadiene conducted with the nanogels N 4.4 – N 4.6 at 5 mol% in the same volume of 1.365 mL. The volume was kept the same by the addition of water to N 4.5 and N 4.6	200
Table 4.6. Conversion of DA reaction between cinnamaldehyde and cyclopentadiene catalyzed by N 4.4 – N 4.6 at 1 mol%, determined after 24 h.	201

Table 4.7. The conversions and turnover number (TON) of the DA reaction after 24 h between cinnamaldehyde and cyclopentadiene conducted with the nanogels N 4.5 and N 4.6 at various mol%. The changing mol% has been achieved using two different methods either varying the amount of substrate added to a fixed volume of nanogel or by varying the amount of nanogel added to a fixed amount of substrate.	202
Table 4.8. The selectivities of the DA reaction after 24 h between cinnamaldehyde and cyclopentadiene. Catalysed by N 4.4 to which the sets of catalysis are compared. Entries 1 and 2 are the small molecule reaction, entries 3,4 and 5 different co-monomer nanogel, entries 3, 6 and 7 different mol % reaction, entries 3 and 8 different DoF nanogel and entries 3, 9 and 10 different DoF nanogel with the same volume resulting in different mol%.	204
Table 4.9. The reported T_g values for the homopolymers of poly(MMA), poly(EMA) and poly(<i>n</i> BuMA).	206
Table 4.10. Conversions of DA reaction between cinnamaldehyde and cyclopentadiene catalyzed by M 3.1 , N 4.4 and N 4.9 under different conditions, determined after 24 h.	210
Table 4.11. The synthesized nanogels SN 4.1 – SN 4.3 detailing the shell monomer, hydrodynamic size (nm) and dispersity (measured by DLS) and average diameter (nm) obtained from TEM.	214
Table 4.12. Conversion of DA reaction between cinnamaldehyde and cyclopentadiene catalyzed by SN 4.1 , SN 4.2 and the more concentrated SN 4.1a and SN 4.2a at various mol% at rt.	219
Table 4.13. The selectivities of SN 4.1 and SN 4.2 for the DA reaction after 24 h between cinnamaldehyde and cyclopentadiene.	220

Table 4.14. The conversions of the DA reaction after 24 h between cinnamaldehyde and cyclopentadiene conducted with SN 4.1a and SN 4.2a at various temperatures.	221
Table 5.1. The range of conditions tested for the polymerization of M 5.1 , altering temperature, radical flux, CTA and monomer concentration, along with the conversion and <i>D</i> of the resulting polymers. The structures of CTA 1 and 2 can be seen in Figure 5.6.	243
Table 5.2. The details of the synthesized nanogels N 5.1 – N 5.8 including CLD, co-monomer and size.	253
Table 5.3. The 1 st and 2 nd IP and gradient of decrease of L-tryptophan emission for the addition of DNSA to the nanogels N 5.1 – N 5.8	270
Table 5.4. Details of synthesized nanogels SN 5.1 – SN 5.5 including parent core, shell monomer and shell CLD.....	273
Table 5.5. The 1 st IP results of SN 5.1-SN 5.3 with addition of DNSA. These nanogels have the same shell, EMA, but have increasing levels of CLD.....	275
Table 5.6. The 1 st IP results of SN 5.4, SN 5.2 and SN 5.5 with addition of DNSA. These nanogels have the same CLD of 0.5% but have a different shell monomer of either MMA, EMA or <i>n</i> BuMA.	276

Declaration of authorship

This thesis is submitted in to the University of Warwick in support of my application for the degree of Doctor of Philosophy. It has been composed by myself and has not been submitted in any previous application for any degree. The work presented has been carried out by the author. The nanogel synthesis in Chapters 4 and 5 was developed in collaboration with Miss Dafni Moatsou and Dr. Annhelen Lu; the corresponding TEM images were obtained by Miss Dafni Moatsou and the multi angle DLS data for some of the nanoparticles were obtained by Dr. Annhelen Lu.

Acknowledgements

Firstly I must thank Rachel for the support and encouragement she has given me throughout my PhD. It goes without saying that her help and advice have been invaluable. I am also grateful to the EPSRC for funding and the Department of Chemistry for their facilities.

This PhD journey would have been so much more treacherous and difficult if not for the company I've had in the lab, office and at the tea point. Being surrounded by friendly and helpful people, both current and former members of the group, has helped immensely and I feel confident that the friendships forged through polymer chemistry will last. Not least my car share and training buddies. I shall miss our commute, our shared exercise goals and our (treacherous) bicycle rides. In particular I have to specifically thank Dafni and Annie for their ideas and help in the work carried out in this thesis, two immensely clever, kind and helpful individuals.

The encouragement I have had off my family and friends not only for my PhD but the route to get to this point has been so important. Knowing that my parents would support me in my decisions and were so proud at every point during this chemistry journey has allowed me to get this far. Having a group of friends spanning the country and world that have put up with my visits has had a large impact on my enjoyment of the past few years and needs to be mentioned – thank you. I have massively enjoyed my PhD and would not change a single day of it and that is heavily down to the influences of people who have surrounded me.

List of Publications

- 1) B. L. Moore and R. K. O'Reilly, Preparation of chiral amino acid materials and the study of their interactions with 1'-bi-2-naphthol, *J. Polym. Sci. Part A*, 2012, 50, 3567-3574. DOI: 10.1002/pola.26141 (**Chapter 2**)
- 2) B. L. Moore, A. Lu, D. A. Longbottom and R. K. O'Reilly, Immobilization of MacMillan catalyst *via* Controlled Radical Polymerization: Catalytic Activity and Reuse, *Polym. Chem.* 2013, 4, 2304-2312, DOI: 10.1039/C3PY21125H (**Chapter 3**)
- 3) B. L. Moore, D. Moatsou, A. Lu, and R. K. O'Reilly, Studying the activity of the MacMillan catalyst embedded within hydrophobic crosslinked polymeric nanostructures, *Polym. Chem.* 2014, DOI:10.1039/C3PY01734F. (**Chapter 4**)
- 4) B. L. Moore, A. Lu, D. Moatsou and R. K. O'Reilly, The effect of polymer nanostructure on diffusion of small molecules using tryptophan as a FRET probe, *Eur. Polym. J.* 2014, submitted. (**Chapter 5**)

Abbreviations

δ	chemical shift
λ	Wavelength
1-EPHP	1-ethylpiperdine hypophosphite
AIBN	Azo-(<i>bis</i>)-isobutrylnitrile
Ar	Aromatic
ATRP	atom transfer radical polymerization
CLD	crosslinking density
CMC	critical micelle concentration
COSY	correlation spectroscopy
CRP	controlled radical polymerization
CTA	chain transfer agent
d	Doublet
Da	daltons (g mol^{-1})
DA	Diels-Alder
D_{av}	average diameter
DCM	Dichloromethane
DEGMA	diethylene glycol methylether methacrylate
D_{h}	hydrodynamic radius
DLS	dynamic light scattering
DMAC	N,N-dimethylacetamide
DMAP	Dimethylaminopyridine
DMF	dimethyl formamide
DMSO	dimethyl sulfoxide

DNSA	dansyl amide
DoF	degree of catalyst functionalization
DOX	Doxorubicin
DP	degree of polymerization
DSC	differential scanning calorimetry
ee	enantioselectivity
EGDMA	ethylene glycol dimethacrylate
EMA	ethyl methacrylate
eq	Equivalents
FRET	forster resonance energy transfer
GC	gas chromatography
h	Hour
HOMO	highest occupied molecular orbital
HPLC	high performance liquid chromatography
HR ESI-MS	high resolution electron spray ionization mass spectrometry
Hz	Hertz
IP	inflection point
IR	Infrared
J	coupling constant
KPS	potassium persulfate
LCST	lower critical solution temperature
LUMO	lowest occupied molecular orbital
m	Multiplet

MCF	mesocellular foam
MgSO ₄	magnesium sulphate
min	Minute
MMA	methyl methacrylate
M_n	number average molecular weight
\bar{D}	dispersity
mol%	mole percent
M_w	weight average molecular weight
MW	molecular weight
MWCO	molecular weight cut off
NaHCO ₃	sodium hydrogencarbonate
nBuMA	nbutyl methacrylate
NFK	N-formyl-kynurenine
NiPAM	N-isopropylacrylamide
nm	nanometer
NMP	nitoxide mediated polymerization
NMR	nuclear magnetic resonance
PAA	poly(acrylic acid)
PDA	photodiode array
PEG	poly(ethylene glycol)
PMMA	poly(methyl methacrylate)
PS	poly(styrene)
q	Quartet
RAFT	reversible addition fragmentation chain transfer

RI	refractive index
rpm	revolutions per minute
rt	room temperature
s	Singlet
SDS	sodium dodecyl sulfate
SEC	size exclusion chromatography
Snase	Staphylococcal
^t Bu	<i>tert</i> -butyl
TEA	Triethylamine
TEGMA	triethylene glycol methylether methacrylate
TEM	transmission electron microscopy
Temp	Temperature
TFA	trifluoroacetic acid
T_g	glass transition temperature
THF	Tetrahydrofuran
TON	turnover number
TTR	Transthyretin
UCST	upper critical solution temperature
UV	Ultraviolet

Thesis Summary

The general concepts of the thesis have been introduced in Chapter 1. These include the polymerization techniques that have been utilized and a background to each of the applications that have been targeted.

In Chapter 2 the synthesis of poly(tryptophan) through a polymeric scaffold synthesized *via* RAFT polymerization is investigated. Once synthesized, the monomer and polymer, along with previously synthesized poly(phenylalanine), are used for in the chiral resolution experiments of 1,1'-bi-2-naphthol.

Chapter 3 focuses on the synthesis of a novel monomer that contains the catalytically active MacMillan catalyst synthesized from L-tyrosine. This enabled immobilization of the MacMillan catalyst into polymers prepared *via* RAFT polymerization. The monomeric catalyst could then be incorporated into co-polymers at pre-determined specific loadings. These polymers were then used to catalyze the Diels-Alder reaction with great effect and had the ability to be used in a pseudo-continuous process.

Chapter 4 places the monomeric MacMillan catalyst into nanogels synthesized through emulsion polymerization. The effect of having the catalyst within this unique environment was studied both through conversion and selectivity. The relatively simple synthesis allowed for the bespoke environment to be readily changed altering the amount of catalyst and co-monomer of the nanogel.

In Chapter 5 a new polymerizable L-tryptophan monomer has been synthesized and incorporated into RAFT synthesized polymers and nanogels which were synthesized through emulsion polymerization. Both of these structures fluorescent properties have been investigated; in particular the nanogels ability to function as a FRET pair to the small molecule dansyl amide has been examined. This has allowed for the effect of the structure of the nanogel on small molecule diffusion to be probed.

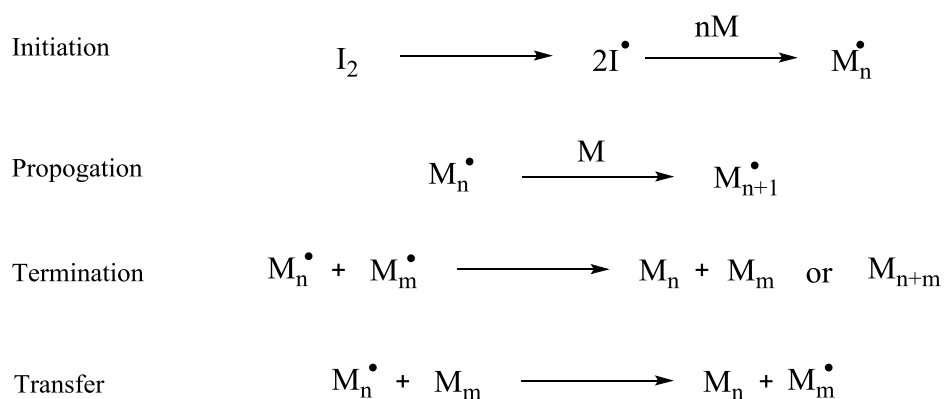
Chapter 1: Introduction

Polymerization Techniques

1.1.1 Reversible-Deactivation Radical Polymerization

A significant development in the synthesis of polymers was the introduction of reversible-deactivation radical polymerization (RDRP) techniques.^{1, 2} These methodologies have allowed for the control of polymer properties whilst using convenient procedures. Prior to the advent of these routes polymers were synthesized either by conventional free radical polymerization (CFRP) or living polymerization (LP).^{3, 4} CFRP can be used to polymerize most monomers in relatively mild conditions but permits no control over the polymer structure such as molecular weight (MW) or dispersity (D). LP gives a much greater handle on polymerization control with MW being controlled by stoichiometry and is capable of achieving low dispersities; however, LP requires highly stringent conditions in which no impurities can be present, including oxygen and water.

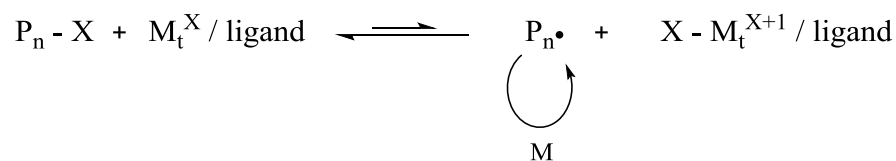
Whereas with the introduction of RDRP techniques it was possible to maintain the ease of a free radical synthesis with the control of a living polymerization process.³ These advances have allowed for synthesis of more complex polymeric structures with control over MW and dispersity.⁴ The three most common RDRP techniques are Atom Transfer Radical Polymerization (ATRP),^{5, 6} Nitroxide Mediated Polymerization (NMP)⁷⁻¹⁰ and Reversible Addition Fragmentation chain Transfer (RAFT)^{11, 12} polymerization. The steps common to all RDRP techniques are initiation, propagation, transfer and termination (Scheme 1.1).



Scheme 1.1. A schematic representation of the steps of initiation, propagation and termination. I_2 is the initiator and M the monomer.³

Both ATRP and NMP proceed by a reversible activation/deactivation equilibrium in which the equilibrium lies in favour of the dormant species, reducing the amount of radicals present and therefore the amount of termination. The use of stable radicals to control polymerization has its foundations in work by Rizzardo and Moad,⁸ which was further refined by Georges.¹³

The use of transition metals to provide the stable free radical was reported in 1995 by the groups of Sawamoto,¹⁴ Matyjaszewski^{15, 16} and Percec.¹⁷ ATRP requires a transition metal with a covalent bond capable of reversible fragmentation; commonly with a halide. The labile halide bond is the key to the process as it forms the dormant polymer species as demonstrated in Scheme 1.2.

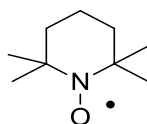


$P_n - X$	Halide capped polymer chain
M_t / ligand	Transition metal complex
$P_n \cdot$	Growing polymer chain
M	Monomer
$X - M_t / \text{ligand}$	Halide containing transition metal complex

Scheme 1.2. A representation of the ATRP process using a transition metal complex (M_t) with a halide (X).⁵

The reversible nature of the $P-X$ and the $X-M_t$ formation allows for the radical concentration to be kept low, reducing termination and slowing the growth resulting in well defined polymers.

NMP works on the same principle as ATRP but in this case an alkoxyamine initiator is responsible for the presence of dormant and active radicals. The most commonly used initiator is 2,2,6,6-tetramethylpiperidiny-1-oxy (TEMPO) (Figure 1.1) which forms an unstable carbon-oxygen bond with the growing polymer that will be cleaved thermally giving a radical terminated polymer that can propagate and a nitroxide free radical.^{9, 18} The growing polymer chain and the available TEMPO can recombine to produce the dormant polymer species again.

Figure 1.1. The structure of TEMPO, a common NMP initiator.¹⁸

The mechanism of RAFT differs from ATRP and NMP as it uses a degenerative chain transfer process, with the propagating chain in equilibrium with the dormant chain. At the same time that RAFT was reported by a group in Australia,¹¹ a similar polymerization technique was developed in France known as Macromolecular Design by Interchange of Xanthates (MADIX).¹⁹ The term RAFT is commonly used to describe these types of polymerization as MADIX limited itself to just the use of xanthates to control the polymerization whereas RAFT encompasses a range of chain transfer agents (CTAs). These CTAs are responsible for the control over the polymerization with equilibrium between propagating and dormant chains.²⁰⁻²² The generic families of CTA can be seen in Figure 1.2.

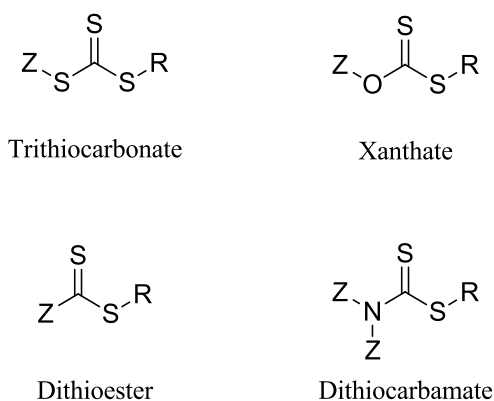


Figure 1.2. The structures of the different common types of CTA.

The choice of CTA is highly significant to achieve the successful polymerization of specific monomers. The differing Z and R groups of the CTA can have a significant impact on its reactivity and therefore need to be tuned to the monomer targeted for polymerization. The Z group affects the reactivity of the C=S bond towards radical addition and controls the stability of the fragmentation product²⁰ and the R group must be capable of forming a free radical leaving group but also to re-initiate polymerization.²¹ Therefore the radical formed on the CTA during the polymerization process must be matched to the reactivity of the radical formed on the growing polymer chain. Monomers can be split into the two groups of more activated monomer (MAMs) where the vinyl group is conjugated to a neighbouring functionality, such as a methacrylate or styrene, and less activated monomers (LAMs) where the vinyl group is adjacent to an electron rich atom, such as vinyl acetates (Figure 1.3).²³

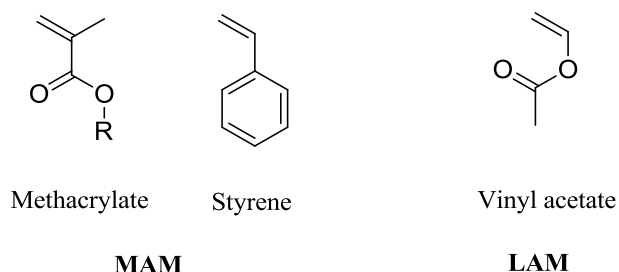


Figure 1.3. The structures of MAMs and LAMs.

LAMs form unstable and highly reactive propagating radicals, as they are not stabilized through resonance, and therefore the CTA must have a less reactive double bond to ensure propagation. This can be achieved by using xanthates and dithiocarbamates which form resonance structures (Figure 1.4) that can stabilize the radical produced. The other CTA families of dithioesters and trithiocarbonates are more suited to the less

reactive radicals formed on the MAMs as they have more reactive C=S bonds.²⁴⁻²⁶

Recently, there has been work to develop a universal CTA that is capable of polymerizing both MAMs and LAMs.^{23, 27, 28}

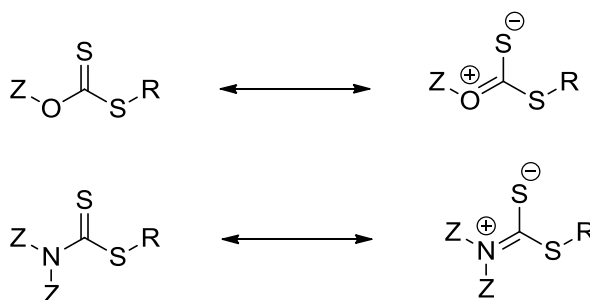
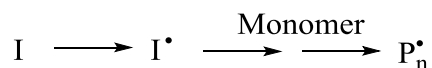


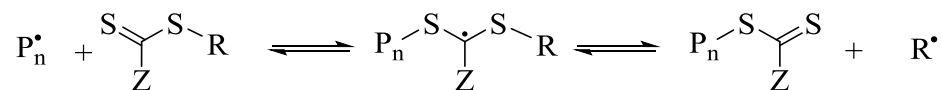
Figure 1.4. The resonance structures that can be formed by xanthates and dithiocarbamates which help to stabilize the radical.

The accepted basic RAFT mechanism can be seen in Figure 1.5. Present are the processes common to free radical polymerization: initiation, propagation and termination. However, there are two other important steps associated with RAFT polymerization – chain transfer and chain equilibrium.^{12, 29-31}

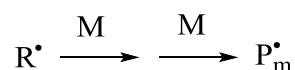
1) Initiation



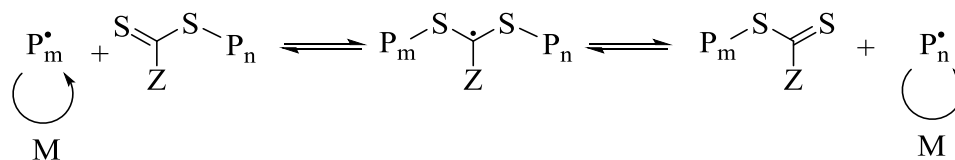
2) Chain Transfer



3) Propagation



4) Chain Equilibrium



5) Termination

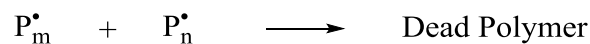


Figure 1.5. The generally accepted mechanism for RAFT polymerization.

Initiation is from an external source, typically azo-(*bis*)-isobutyronitrile (AIBN), the radicals of which will either react directly with a CTA or produce oligomers (P_n^\bullet) before then reacting with the CTA. Ideally, all the CTA will be consumed before propagation commences. The chain transfer step greatly affects the \bar{D} of the polymer and it is therefore essential that R^\bullet is a good homolytic leaving group with respect to P_n^\bullet to drive the chain equilibrium towards completion. The propagation step is coupled with the chain equilibrium so the CTA exchanges between growing polymer chains, keeping the active radical only present on a particular chain for a short period. The rapid exchange between active and dormant chains means that they all have an equal chance for growth

ensuring that chains grow at a similar rate and termination steps are minimized. RAFT is arguably the most versatile of these three RDRP techniques capable of polymerizing a wider range of monomers, in a variety of reaction media.³²⁻³⁵ One of the drawbacks of implementing RAFT is the coloured polymers that it produces but developments in the removal or functionalization of the end group can remove this colour if desired.³⁶⁻³⁸

1.1.2 Heterogeneous and emulsion polymerization

Heterogeneous polymerizations consist of two phases (oil-in-water or water-in-oil) and are named depending on the nature of the larger, continuous phase. These techniques are commonly used to prepare well defined polymeric particles.³⁹ There are a number of types of heterogeneous polymerizations including suspension, precipitation, dispersion and emulsion.⁴⁰ The characteristics of the polymerizations are usually identified by the solubility of the monomer, resulting polymer and initiator. With suspension polymerization, the monomer and initiator are insoluble within the continuous phase and monomer droplets are formed which are stabilized by a surfactant. Initiation occurs within the monomer droplet and the resulting polymer particle will have a particle size similar to that of the initial monomer droplet.⁴¹ Particles across a wide size spectrum from 20 μm to 2 mm have been synthesized using this technique. In both precipitation and dispersion polymerization, the initiator and monomer are soluble in the continuous phase with the resulting polymer insoluble.^{40, 42} They differ as the growing polymer particle is stabilized in a dispersion polymerization⁴³ whereas in the precipitation process the resulting polymer precipitates out of solution.³⁹ Both systems form much smaller particles compared to suspension polymerization with particles around 0.1 μm to 10 μm are readily synthesized.

With emulsion polymerization the initiator is soluble in the continuous phase, the monomer sparingly soluble and the resulting polymer insoluble.^{44, 45} Smith, Ewart and Harkins established a mechanism for emulsion polymerization in the 1940s, the steps of which can be seen in Figure 1.6.^{46, 47}

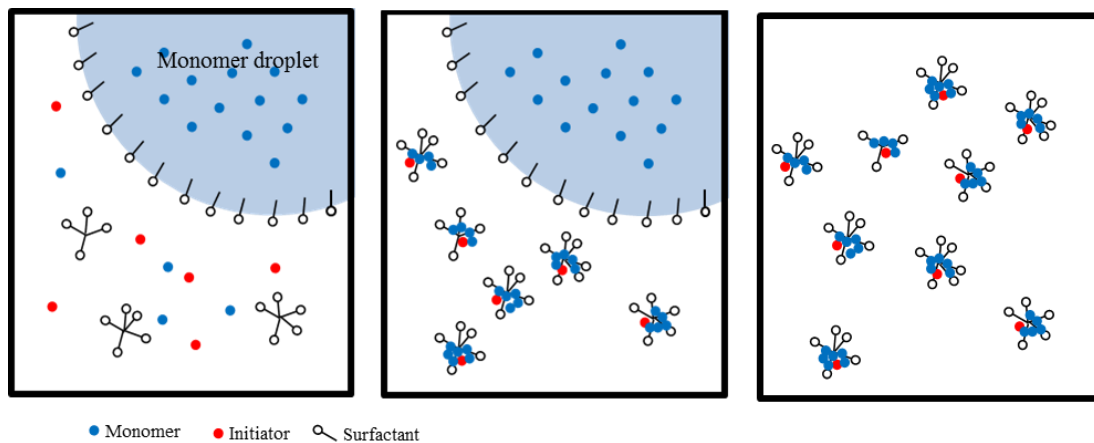


Figure 1.6. A representation of the synthetic process for emulsion polymerization.⁴⁰

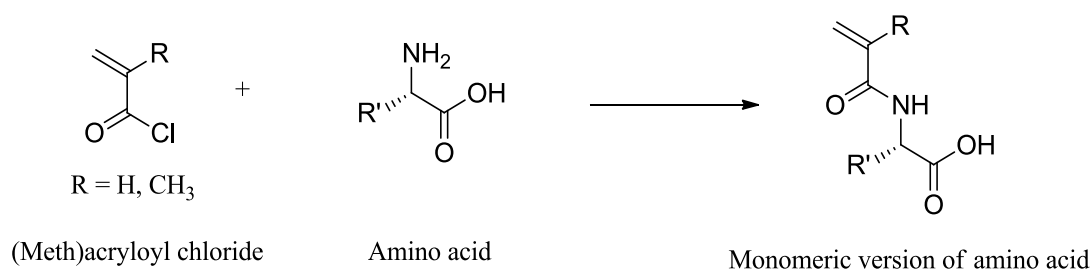
Initially the monomer forms large droplets stabilized by the surfactant in the aqueous phase. Additionally, excess surfactants will form micelles that may contain a few monomer units. Typically there are high numbers of surfactant micelles which are much smaller in size giving a high surface-to-volume ratio compared to the monomer droplets. As the initiator is soluble in the continuous phase, the polymerization is initiated here with the few monomer units present in the continuous phase. The polymer (or oligomer) chain grows until it becomes so hydrophobic that it must enter the surfactant micelle stabilizing it in the continuous phase. The polymer (or oligomer) continues to propagate within the surfactant micelle and additional monomer units from the monomer droplets will diffuse into the micelle and this process continues until the monomer droplet is completely depleted from monomer, resulting in high monomer conversions and thus

well-defined polymeric particles. The high conversion obtained by this polymerization is advantageous as removal of unreacted monomer is not required. However, excess surfactant not involved in particle stabilization may have to be removed. Additionally, cross-linker can be added to this polymerization producing more robust cross-linked particles which have improved stability to temperature, solvent and dilution compared to their non-cross-linked counterparts.^{40, 45}

1.2 Amino Acids in Polymers and Structures

1.1.2 Amino acid monomers

A variety of amino acids have been incorporated into polymers in recent years through the synthesis of bespoke monomers typically resulting in (meth)acrylamide monomers.⁴⁸⁻⁵⁰ Polymers incorporating amino acids in this way have received great interest due to their potential use in a range of applications given their bio-compatible and stimuli responsive nature.⁵¹⁻⁵⁴ The groups of Endo and Mori have led the research on the development of these monomers and incorporation into polymers, both through conventional and RDRP techniques.⁵⁰ The typical synthesis of amino acid containing monomers uses (meth)acryloyl chloride in a coupling reaction with the desired amino acid to yield the corresponding (meth)acrylamide monomer; this synthetic route can be seen in Scheme 1.3. Since the report by Sanda *et al.* in 1997 where this synthetic route was used to yield the monomeric equivalents of leucine, alanine, phenylalanine, glutamic acid, methionine and tyrosine⁵⁵ the same procedure has been used to synthesize other amino acid monomers including histidine,⁵⁶ proline^{57, 58} and tryptophan.⁵⁹⁻⁶²



Scheme 1.3. A schematic representation of the generic synthesis of monomeric versions of amino acids.

The synthesis of poly(amino acids) has not just been constrained to monomers synthesized *via* this route as illustrated in the review by Sanda and Endo.⁵⁰ Figure 1.7 is a reproduction from their review of the synthetic routes available to poly(amino acids) which includes ring opening polymerization and polycondensation along with the radical techniques utilized within this thesis.

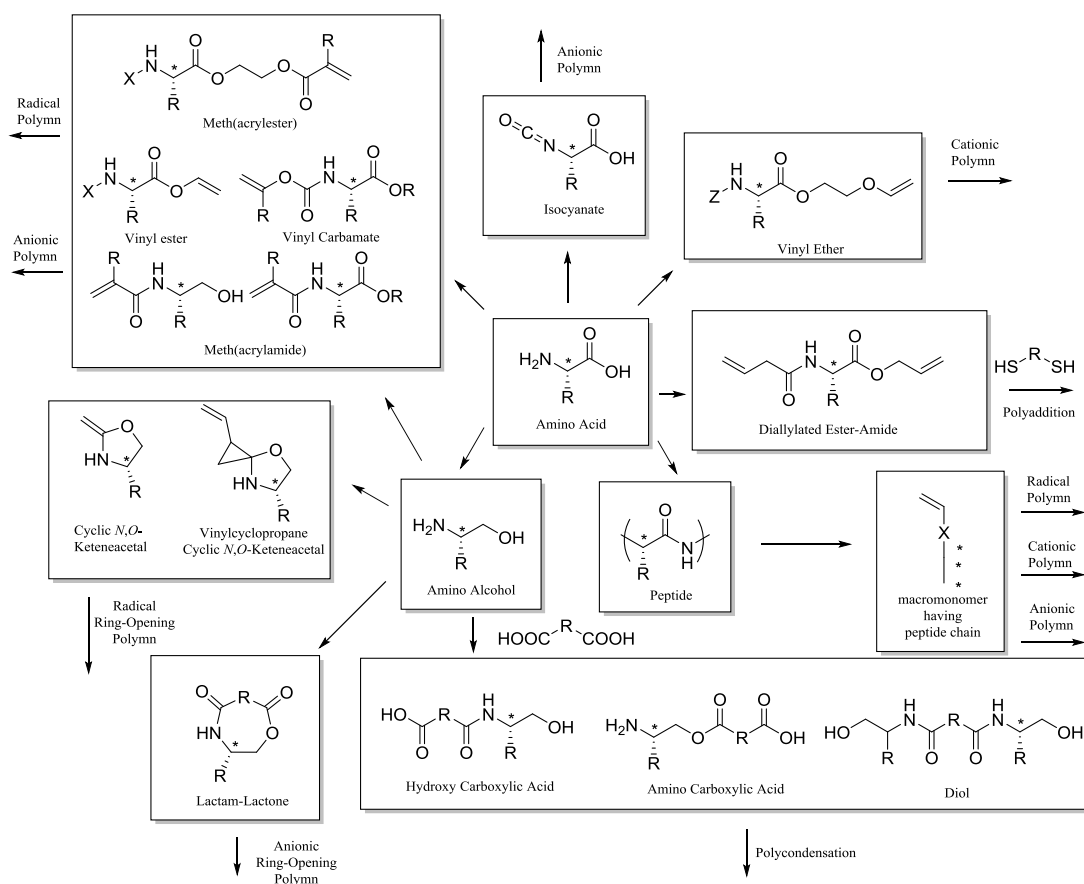


Figure 1.7. A reproduction of a the different synthetic routes available for the synthesis of poly(amino acids).⁵⁰

1.2.2 Polymeric structures incorporating amino acids

One of the primary reasons that amino acids are targeted as monomers is due to their natural chirality which, through incorporation into polymeric structures, can be exploited.⁴⁹ Chirality occurs when a molecule is asymmetric, which typically happens with the positioning of groups around a tetrahedral carbon atom. With reference to Figure 1.8 it is possible for two arrangements in a tetrahedral structure with four different groups; the two structures are mirror images and are non-superimposable, each possible formation is termed an enantiomer.⁶³ Enantiomers are indistinguishable, apart from their interactions with other chiral molecules and the direction they rotate plane polarized light.

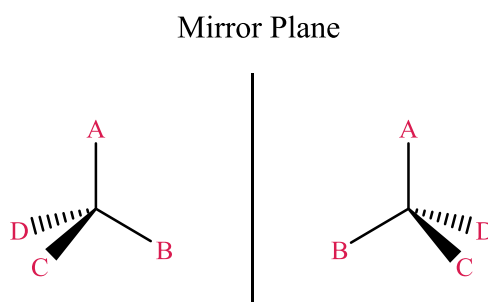


Figure 1.8. A representation of two enantiomers based on a tetrahedral carbon atom.

The different enantiomers of a chiral molecule are generally referred to as (*S*)- or (*R*)- which is based on the Cahn-Ingold-Prelog priority rules which label the groups in order of priority based on atomic weight.^{64,65} By placing the lowest priority group at the back, the other priorities will decrease in either a clockwise (*R*)- or anti-clockwise (*S*)- fashion. The labelling of (*R*)- and (*S*)- comes from the Latin terms for right and left (*rectus* and *sinister*).

Another labelling method is also available and particularly prevalent with amino acids, which is based on how the enantiomers rotate plane polarized light. As the light passes through a solution of one enantiomer it will either rotate the polarized light clockwise (*dextrorotary*) or anti-clockwise (*levorotary*) which gives rise to the terminology of D- and L- enantiomers. This terminology still predominates for amino acids with all naturally occurring amino acids present in the L- configuration. The two naming systems are not related with the labelling of (*R*)- and (*S*)- having no connection to the way an enantiomer will rotate the plane polarized light.

There are multiple examples of amino acid containing polymers that have been exploited for their properties, one of which is their inherent chirality. There have been several investigations on how this chirality is affected in the polymer. One such study utilized the enantiomers of the amino acid leucine to synthesize chiral micelle structures; formed from either a mixture of D and L leucine polymers or from single enantiomer polymers.⁶⁶ The micelles containing both enantiomers exhibited increased stability which was assigned to stereocomplexation within the core between the different enantiomers, this interaction has also been reported by Endo.⁶⁷ A representation of this work can be seen in Figure 1.9. Leucine's specific rotation has also been studied when it has been present in the polymeric form, Endo and co-workers noted that the specific rotation not only increased on polymerization but also inverted.⁶⁸

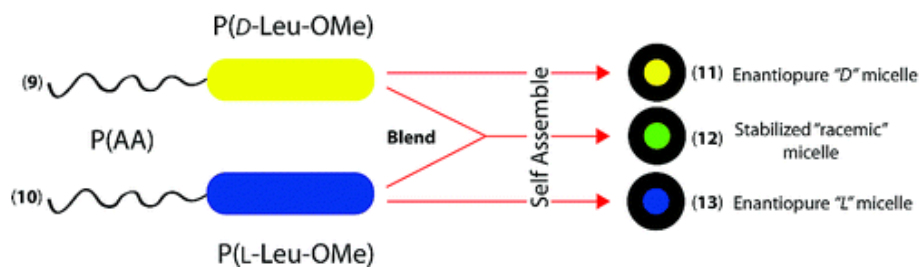


Figure 1.9. A reproduction of an overview of the differing stabilities afforded from mixtures of chiral leucine polymers.⁶⁶

The pH responsive nature of amino acids is another reason that they have been targeted for polymer incorporation.⁶⁹⁻⁷¹ Assembled structures based on phenylalanine have been shown to change morphology depending on the pH that they have been assembled at due to the differing ratio of hydrophobic to hydrophilic segments.⁷² The pH responsiveness of a tryptophan containing polymer has also been examined with polymers forming assembled structures at pH values of 6.0, but on reducing the pH to 4.0 only the corresponding unimers were present in solution.⁶⁰ The structure for this pH-responsive tryptophan polymer can be seen in Figure 1.10.

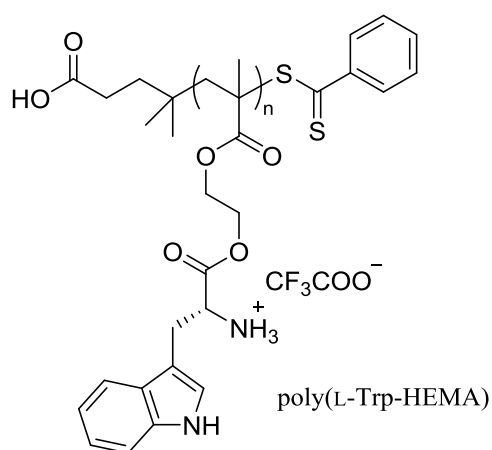


Figure 1.10. The structure of the pH-responsive tryptophan polymer.⁶⁰

This pH-responsiveness has sometimes also been coupled with the bio-compatibility of the poly(amino acids) as targets for drug carrying devices.⁷³ Both polymers of tryptophan and alanine have been investigated for their bio-compatibility.^{60,74} In Figure 1.11 the fluorescence microscopy images of HeLa cells in presence of a poly(tryptophan) can be seen; in the presence of the polymer the cells behave in a similar manner to the control sample and therefore the polymer has had a negligible cytotoxicity effect.⁶⁰

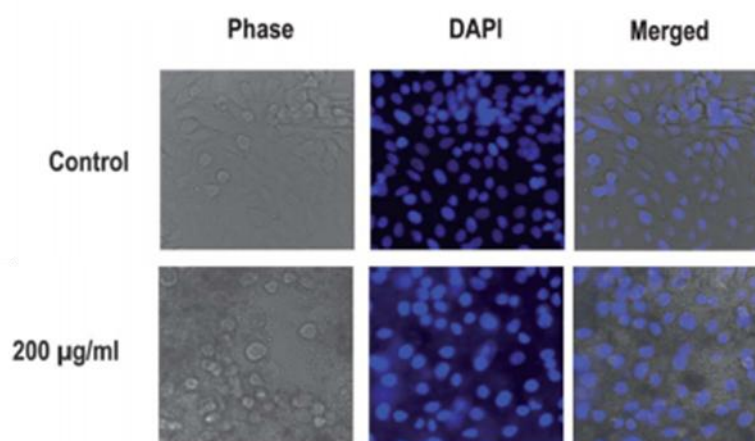


Figure 1.11. A reproduction of the fluorescence microscopy images that were used in alongside other data to demonstrate the negligible cytotoxicity effect of poly(tryptophan).⁶⁰

Other characteristics of amino acids have also been exploited with their incorporation into polymeric structures. It has often been noted that lower critical solution temperatures (LCSTs) can be altered through incorporation of amino acids.^{51, 75-77} Additionally tryptophan's fluorescent properties have often been targeted^{60,61} and have been the focus of research in Chapter 5. Their ability in enantiomer separations and chiral catalysis has also been extensively researched and will be discussed later.

1.3 Enantiomer Resolution

The chirality of a molecule has many implications and from an application point of view these are notable with interactions with any biological compounds. As amino acids and sugars are chiral the resulting higher order structures of peptides, proteins and polysaccharides share this chirality and therefore has to be a consideration in the development of drugs, agrochemicals, food additives, flavourings and fragrances.^{78, 79} As greater understanding of the role of chirality has been developed, the requirements for optically pure compounds has become more rigorous; for instance the US Food and Drug Administration (FDA) require the effects of both enantiomers and their mixtures before a patent for new drugs can be granted.^{78, 80} Therefore research into producing one enantiomer of a desired molecule has flourished but the need for chiral separation still remains. At early stages of development of new compounds with specific required characteristics the design and implementation of synthetic routes to achieve a single enantiomer could be costly and time consuming; one of the reasons that the research into chiral separation has continued.⁷⁸ There are two methods available for chiral separation: formation of chiral auxiliaries and separation based on non-covalent interactions. Chiral auxiliaries require the chemical modification of the enantiomers into diastereoisomers which can then be separated out based on their chemical or physical differences, such as through crystallization.⁸¹ The second method has a much wider scope with non-covalent diastereoisomers formed with a stationary phase through intermolecular interactions such as hydrogen bonding or $\pi - \pi$ stacking.⁷⁸ Molecularly imprinted polymers (MIP), chiral polymers, and cyclodextrins have been at the forefront of this research.

There has been extensive use of cyclodextrins for separation of compounds; both chiral and achiral. Their unique structure allows for the formation of inclusion compounds based on hydrophobicity, shape and size which are parameters that can be exploited for compound separation.⁸² Their frustum shape gives a hydrophobic interior whilst the compound itself is hydrophilic and chiral. The chemical structure of cyclodextrins and their unique 3D shape can be seen in Figure 1.12.⁸³

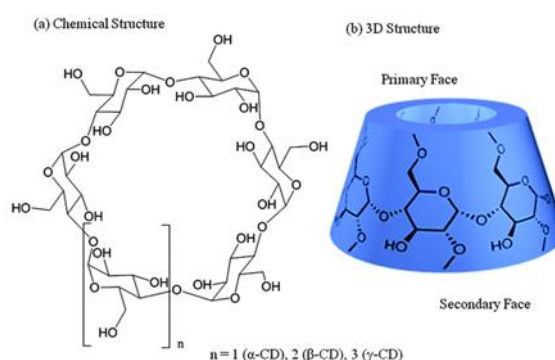


Figure 1.12. A reproduction of a representation of the chemical and 3D structure of cyclodextrins.⁸³

They have had success for chiral resolutions in both gas chromatography (GC) and high performance liquid chromatography (HPLC). One of the first reports of use of β -cyclodextrins for HPLC separation was in 1985 by Armstrong and co-workers.⁸⁴ They prepared an HPLC column by covalently attaching β -cyclodextrin to silica which was then able to resolve a range of molecules including derivatives of amino acids and barbiturates. In 1998 this group also demonstrated how a range of cyclodextrin based columns could resolve a variety of enantiomers and could detect as low as 0.1% enantiomer impurity using HPLC.⁸⁵ In 1988 Zukowski *et al.* demonstrated how immobilized and functionalized β -cyclodextrins could be used for chiral separation in a GC set up.⁸⁶

MIPs have also received attention for their ability to separate out enantiomers. These constructs are synthesized by templating a polymer around an enantiomer of interest which yields MIP with greater affinity for the template enantiomer over the other, enabling separation.⁸⁷ A typical route to the production of a MIP through a covalent imprinted approach can be seen in Figure 1.13. This methodology has been developed by Wulff who used species that contained both the template and the polymerizable group; after co-polymerization with a cross-linker the template is chemically removed leaving a cavity with a specific size and shape.⁸⁸ An overview of MIP materials used for resolution has been given in a review by Maier and Lindner.⁸⁷

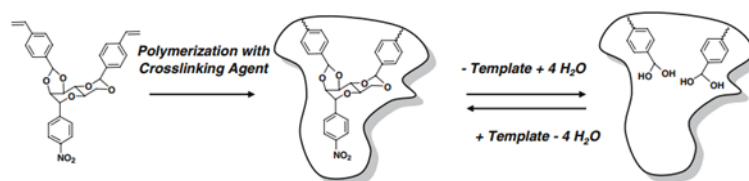
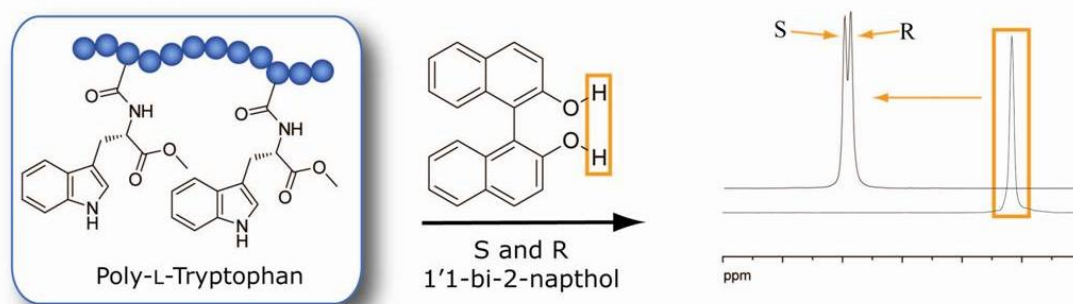


Figure 1.13. A reproduction of a representation of how templating is used to form MIPs.⁸⁷

MIPs have been used for a variety of chiral separations including chiral drugs such as β -blockers and anti-inflammatory drugs with high levels of success, these, along with others, have been outlined comprehensively in a review by Ansell.⁸⁹

Whilst these two previously mentioned routes have received the most attention, there have been reports of other chiral polymers that also exhibit enantiomer resolution type characteristics. These polymers include poly(amides), poly(urethanes) and poly(saccharides) and their ability to separate out enantiomers has been outlined by Okamoto and co-workers.⁹⁰ Through the preparation of chiral stationary phases from

these chiral polymers it has been possible to separate out enantiomers in HPLC set ups. Additionally chiral polymers synthesized from amino acids have also been used for enantiomer separation and resolution. For instance unique chiral hydrophobic domains have been prepared through the self-assembly of micelles based on an L-phenylalanine hydrophobic block.⁹¹ These constructs have shown some chiral resolution ability when incubated with a racemic solution of small molecule phenylalanine. Similarly, gel structures based on the amino acid L-alanine have also been shown to provide a route to enhanced enantiomer concentrations of the amino acid proline.⁹² Polymers containing the amino acid tryptophan have chiral recognition ability with the molecule 1, 1'-bi-2-naphthol (BINOL), an important chiral catalyst precursor, which is discussed in detail in Chapter 2.⁵⁹ A schematic demonstrating the change in the ¹H NMR spectrum of (*rac*)-BINOL on exposure to poly(L-tryptophan) can be seen in Scheme 1.4; the phenolic proton peaks are shifted downfield and split. This chiral resolution ability with BINOL was extended by De and co-workers as they examined a polymer of leucine in a similar fashion.⁹³



Scheme 1.4. A modified table of contents graphic demonstrating how the phenolic protons of (*rac*)-BINOL are influenced by the presence of poly(L-tryptophan).

1.4 Catalysis

1.4.1 Immobilized Catalysts

The immobilization of catalysts has received significant attention. Underlying the immobilization is the desire to reclaim and reuse the catalyst as they can often be difficult, expensive, toxic and time consuming to prepare.⁹⁴⁻⁹⁶ Therefore, being able to produce more products from the initial input is a desirable characteristic. Immobilizing catalysts can be seen as a way of bridging the gap between heterogeneous catalysts, which typically are easily removed from reactions, and homogeneous catalysts, which whilst normally less expensive and less toxic are difficult to retrieve.⁹⁷ Through immobilization it has been possible to carry out catalysis in the homogeneous phase but through exploitation of polymeric structures, the catalyst is easier to retrieve after catalysis.

Amino acids have also been targeted for their catalytic properties, both for when catalysis is carried out by the amino acid and when the amino acid acts as metal catalyst ligands. Proline has been immobilized into polymeric supports by a number of groups^{57, 58} and used for catalysis reactions which have given impressive results (low mol% loading, high selectivity) and with recycling potential.⁹⁸ One such immobilization was carried out by Kristensen *et al.* in which the catalyst proline was immobilized into either benzyl methacrylate or styrenic beads (Figure 1.14).⁵⁸ These were then used to catalyze the aldol reaction giving high yields (~80%) and ee (~98%).

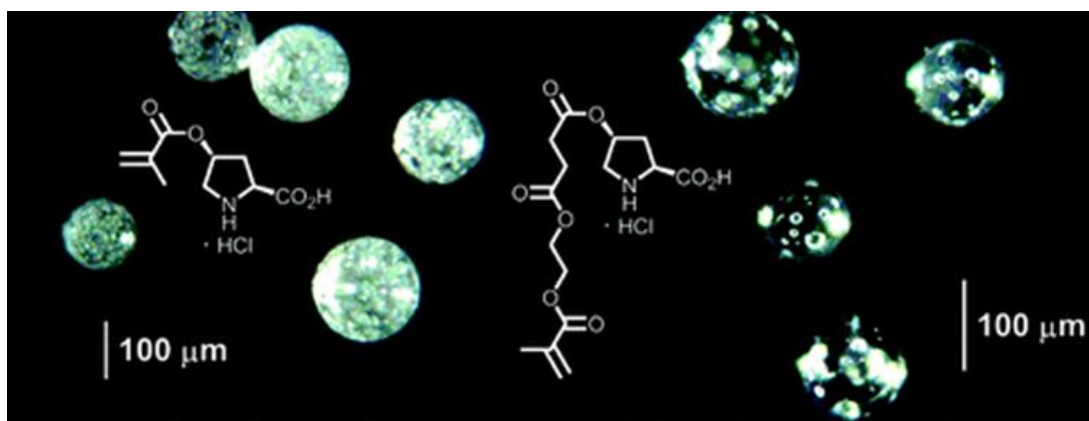


Figure 1.14. A reproduction of an overview of the work carried out by Kristensen *et al.*⁵⁸

Tyrosine has also found use as an immobilized catalyst, as starting material for the monomeric version of the MacMillan catalyst, which has given comparable catalytic results to the non-immobilized catalyst in Diels-Alder (DA) reactions (discussed further in Chapters 3 and 4).⁹⁹ Raja and co-workers have been able to support amino acids (L-proline, L-histidine and L-valine) in zeolite structures which have been used as ligands for transition metals such as iron and copper. These have been used as chiral catalysts in selective oxidation reactions.^{100, 101} Maurya *et al.* were able to immobilize the amino acid alanine as a ligand on a polystyrene support that was then used to complex either vanadium or copper.¹⁰² The catalysts were used successfully in the oxidation of cyclohexane and *p*-chlorotoluene reaching conversion up to 79% as measured by gas chromatography. The catalysts could be recovered and were analyzed by IR and electron paramagnetic resonance (EPR) spectroscopy and the vanadium species was shown to maintain its original state.

1.4.1.1 Polymeric Immobilization

There has been development of sophisticated systems that enable the recovery of the catalyst using properties built into the polymer. Bergbreiter and co-workers have

compiled many extensive and well-detailed reviews that focus on the recovery and reuse of polymers that allow for homogeneous catalysis and recovery through either solid/liquid or liquid/liquid separations.^{97, 103-105}

Many of these recovery techniques rely on a responsive system that enables the recovery; with the stimuli of temperature and pH having been the most explored. LCST polymers are commonly used to enable recovery of systems and is one example of a thermal stimulus.¹⁰⁶ The solubility of LCST polymers is greatly affected by temperature and as the system is heated, a critical temperature is reached when the polymer is no longer soluble in the surrounding media and precipitates, this temperature is known as the cloud point. The cloud point can be affected by concentration and therefore to determine the LCST of a polymer multiple concentrations have to be analyzed and a phase diagram produced which will provide a minimum point as shown in Figure 1.15. This lowest temperature for all concentrations is the LCST of the polymer. Due to polymer solubility the section of the phase diagram examined is low polymer composition levels.

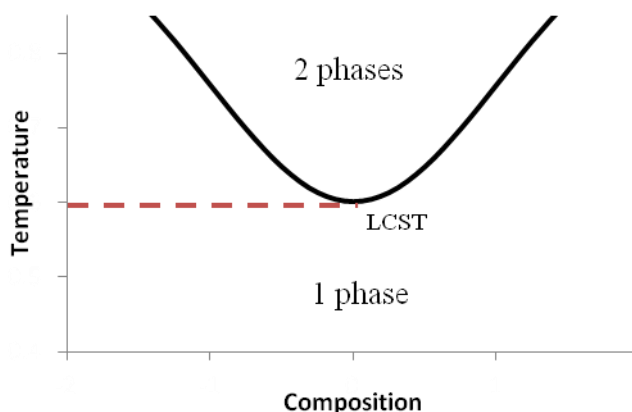
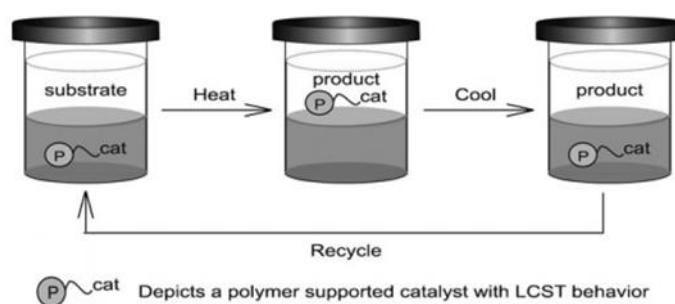


Figure 1.15. A representation of an LCST phase diagram showing the relationship between LCST cloud point and composition. The LCST is the minimum temperature.

By being able to manipulate the solubility of the polymer by a simple change in temperature can allow for easy polymer/catalyst separation from the reaction media.¹⁰⁷ There are multiple examples of how this route can enable polymer recovery.^{108, 109} For example, it has been used to great success by Shaw who used a poly(*N*-isopropylacrylamide) (poly(NiPAM)) system to immobilize a rhodium catalyst; the immobilized catalyst was capable of catalyzing hydrogenation reactions of methyl methacrylate at 26 °C and upon heating to 40 °C polymer precipitation occurred and the polymer could be recovered through filtration.¹¹⁰ On re-dispersion into water at a lower temperature, a second catalytic reaction of methyl methacrylate hydrogenation could be repeated, demonstrating the use of a polymer scaffold to enable the reclaim and reuse of the desired catalyst. This is an example of a thermomorphic system, a schematic demonstrating how this works can be seen in Scheme 1.5, which has been adapted from a review by Bergbreiter and co-workers.¹⁰⁵



Scheme 1.5. A schematic representation of how a thermally responsive polymer can be reclaimed and used for catalysis depending on the temperature of the system.¹⁰⁵

1.4.1.2 Nanoreactor Immobilization

The ability to immobilize the desired catalyst within a nanostructure has also led to high levels of control over the reactions catalyzed by the catalyst. With increasing levels of control over polymer design, it has been possible to synthesize structures that more resemble nature's catalyst: enzymes; which are well known for their excellent catalytic ability.¹¹¹⁻¹¹³ Micelles,¹¹⁴⁻¹¹⁶ dendrimers,¹¹⁷ star polymers¹¹⁸⁻¹²⁰ and nanogels^{98, 121-124} have all been exploited as scaffolds for catalyst immobilization and have shown great success in this aspect. A recent review by Sun and co-workers highlight how a range of polymeric systems have been exploited as recyclable catalyst supports.¹²⁵ A representation of catalyst immobilization within a cross-linked nanogel stabilized by a surfactant can be seen in Figure 1.16.

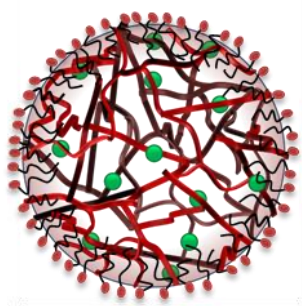


Figure 1.16. A representation of how a catalyst (green circles) could be immobilized into a cross-linked surfactant stabilized nanogel.

For instance, Patterson *et al.*¹²⁶ reported the successful immobilization of a palladium catalyst into the hydrophobic domain of a micelle formed through self-assembly. These constructs were synthesized through the use of a specially designed CTA that contained a hydrophobic SCS-pincer that was able to complex palladium and provide the hydrophobic driving force for assembly. Hydrophilic polymers were synthesized using this CTA by RAFT polymerization resulting in amphiphilic molecules due to the hydrophobic groups on the CTA. The self-assembly of these palladium decorated polymers placed the catalyst within the central hydrophobic cavity. The supported palladium was able to catalyze the reaction between vinyl epoxide and phenyl boronic acid; the rate of reaction was observed to increase by a factor of approximately 100 compared to a small molecule analogue. A reproduction of the comparison of the rates between the two systems can be seen in Figure 1.17; the reaction catalyzed by the micelle has reached 100% conversion in approximately 15 minutes whereas the unsupported palladium catalyst has reached only 80% conversion in 1750 minutes.

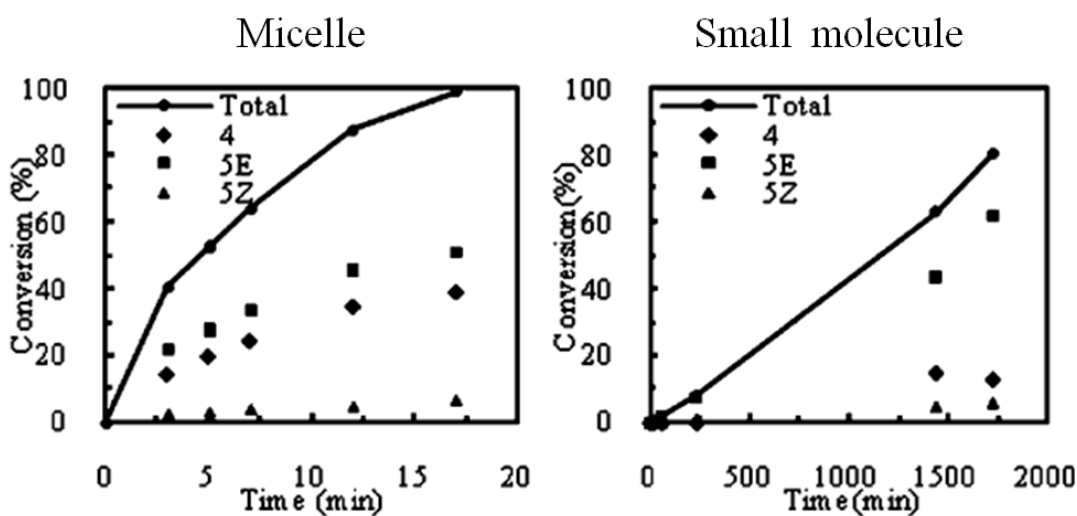


Figure 1.17. A reproduction of the conversion of the reaction between vinyl epoxide and phenyl boronic acid catalyzed by either palladium supported within a micelle or in a small molecule.¹²⁶

Similar results to this have been achieved for a plethora of catalysts including those developed within the group of L-proline,¹¹⁶ DMAP,¹²⁷ and the MacMillan catalyst¹²⁸ (discussed in Chapter 4) to name a few.

A key reason as to why these catalysts are more effective in these structures is due to the bespoke environment they have been placed within. The catalyst is often contained within a hydrophobic environment that is situated within an aqueous continuous phase. Hydrophobic reagents added to the system will concentrate in these small hydrophobic pockets which not only bring the reagents into close proximity to the catalyst but also create a high local concentration of the substrate(s). The reaction is therefore more comparable to being performed in a hydrophobic solvent at much higher concentrations. This phenomenon is referred to as the concentrator or hydrophobic effect and was first reported by Fréchet and co-workers using a dendrimer system.¹²⁹ Dendrimers have gone on to be used extensively for catalyst immobilization benefiting from this effect.¹¹⁷

The high level of control that polymer chemists have has enabled further complex structures to be developed to not just improve reactions compared to the non-supported catalyst; but to enable more complex reactions with incompatible functionalities. Fréchet and Hawker have developed a system that immobilized the catalysts DMAP and *para*-toluenesulfonic acid in separate star polymers. In the presence of each other these catalysts would deactivate one another, but kept in their isolated reaction space, a cascade reaction was successfully carried out, a reproduction of this impressive catalytic system can be seen in Figure 1.18.¹³⁰ The system was used to carry out an acid catalyzed acetal hydrolysis followed by an amine catalyzed Baylis-Hilman reaction in the same pot. The yield of the reaction was 65%, a highly impressive result especially when compared to permutations of the reaction when either the acid or amine was not supported which achieved 0% of the desired product.

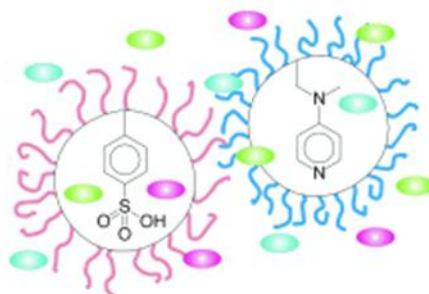


Figure 1.18. A reproduction of an overview of the compartmentalized catalysts used in a cascade reaction.¹³⁰

The group of Meijer has also been able to demonstrate how the high level of control of polymer design can be utilized for catalysis. The group has done extensive work with single chain polymeric nanoparticles (SCPN)¹³¹⁻¹³⁵ and have been able to immobilize the catalyst L-proline into a SCPN and as a result have significant control over the catalysis. When the polymer is in its fully extended state, proline is unable to catalyze

the reaction but when the nanoparticles were formed, the proline resided within the resulting hydrophobic environment and was then able to catalyze the aldol reaction.¹³⁶ A reproduction of an overview of this work can be seen in Figure 1.19.

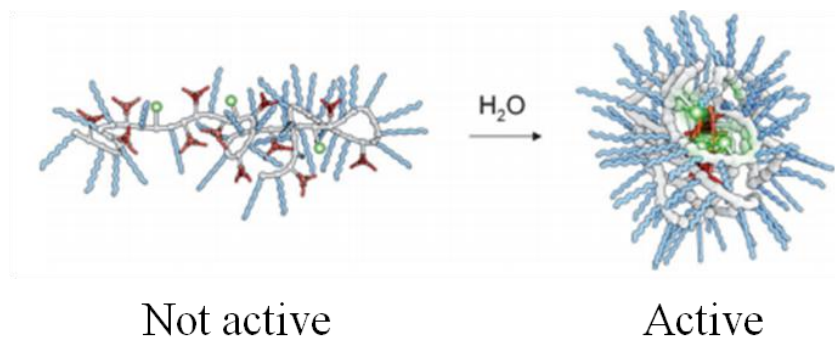
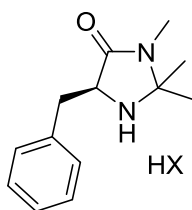


Figure 1.19. A reproduction of an overview of how the proline moieties (depicted in red) are in different environments dependent on the structure of the polymer.¹³⁶

1.4.2 MacMillan Catalysis

The originally reported MacMillan catalyst was derived from the amino acid phenylalanine.¹³⁷ Since the time of its inception, the MacMillan catalyst has been used extensively in a wide range of reactions. After its initial success in 2000 with the DA reactions of α,β -unsaturated aldehydes¹³⁷ the work was extended to the DA of α,β -unsaturated ketones in 2002.¹³⁸ The catalyst has also been used for Mukaiyama-Michael,¹³⁹ Friedel-Crafts alkylation,¹⁴⁰ cascade reactions,¹⁴¹ and hydride reductions.^{142, 143} The structure of the MacMillan catalyst and the reaction schemes for these reactions can be seen in Figure 1.20 and Figure 1.21 respectively.



MacMillan Catalyst

Figure 1.20. The structure of the MacMillan catalyst.

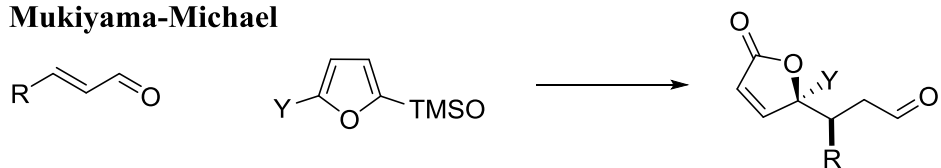
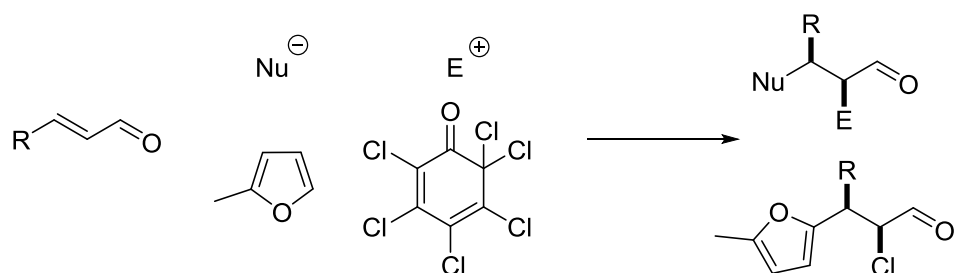
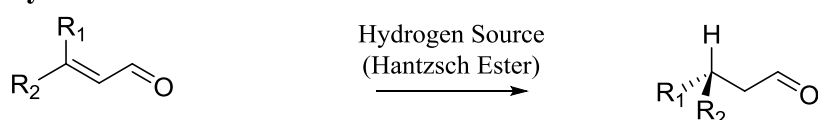
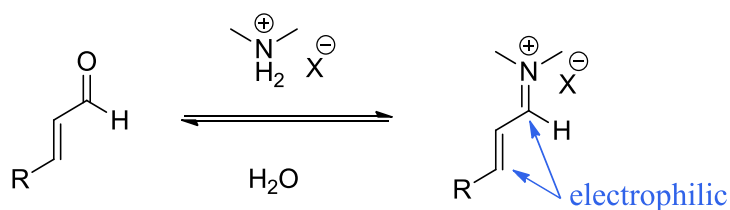
Mukaiyama-Michael**Friedel-Crafts****Cascade Reaction****Hydride Reduction**

Figure 1.21. A schematic representation of the reactions that the MacMillan catalyst has successfully catalyzed.

The MacMillan catalyst functions as an iminium catalyst; therefore the substrates used in the reactions must be capable of forming an imine on exposure to the catalyst and therefore aldehydes are commonly used (Figure 1.21) as substrates.¹⁴⁴ Through this process the electronic properties of the dieneophile are altered producing more reactive electrophilic centres, this can be seen in Scheme 1.6. This process is central to how the MacMillan catalyst operates.



Scheme 1.6. A schematic representation of iminium catalysis and the electrophilic sites that are formed.¹⁴⁴

Figure 1.22 illustrates how the MacMillan catalyst uses steric control to alter the selectivity of the DA reaction. The enantioselectivity is affected by the approach of the diene to the catalytic transition state. As shown in Figure 1.22 the diene is approaching from underneath (the *re*-face). This approach is favoured due to the large steric benzyl group on the top face (the *si*-face).

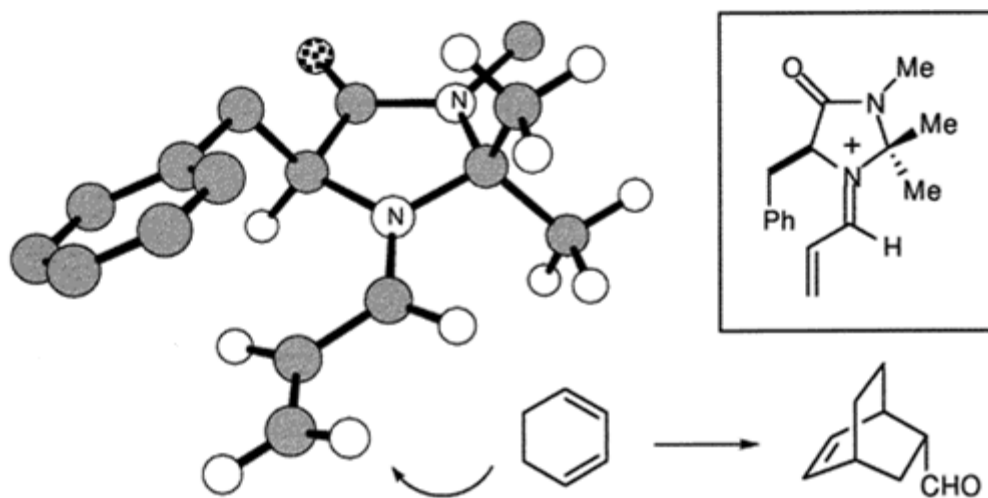


Figure 1.22. A 3D representation of the transition state reproduced from MacMillan's paper.¹³⁷ In this depiction the benzyl group is shielding the top side of the dieneophile from attack.

In 2002 MacMillan reported a design tweak in the catalyst replacing the methyl groups with a *tert*-butyl (*t*Bu) group that had multiple advantages.¹⁴⁵ Firstly, with regards to the rate of reaction, both the formation of the imine and the carbon-carbon bond steps had

been shown to contribute to the overall rate. With regards to the imine formation the replacement of the methyl groups with a ^tBu group removed the interaction between the lone pair of the imine forming nitrogen and one of the methyl groups, making the lone pair more accessible. One of the methyl groups also slightly obscured the *re*-face, which inhibited the approach of the diene; with replacement with the ^tBu group this steric hindrance was removed. This new design therefore takes into account steps to help improve the rate. Additionally, the ^tBu group is now much more prominent on the *si*-face of the molecule, which in conjugation with the benzyl group provides high levels of shielding. These effects can be observed more clearly in Figure 1.23. This new design has subsequently been referred to as the 2nd generation MacMillan catalyst.

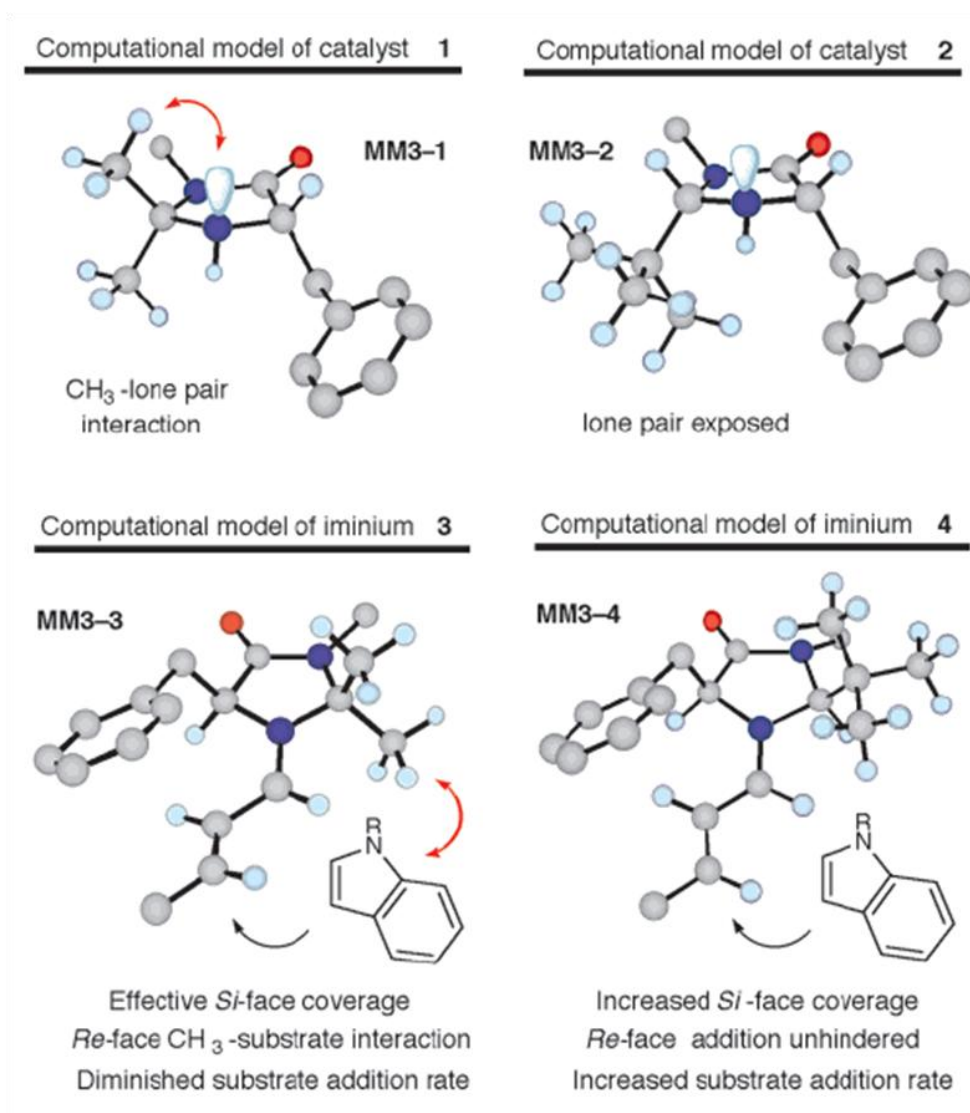


Figure 1.23. A schematic illustrating the advantages of the 2nd generation MacMillan catalyst reproduced from MacMillan's paper.¹⁴⁵ Here the catalyst is being used for indole alkylations which uses the same catalytic control as the DA reaction. The nitrogen lone pair is more exposed, the top face (*si*-face) is more covered and the *re*-face is more accessible. Models 1 and 2 show the differing lone pair accessibility of both catalysts: model 1 shows the interaction between the CH₃ group and the lone pair which has been removed in model 2 of the 2nd generation MacMillan catalyst, which makes the lone pair more exposed. Models 3 and 4 illustrate the difference in *re*-face coverage with model 3 having some steric hindrance on the *re*-face which is not the case for the 2nd generation catalyst in model 4.

The commercial availability of the catalyst reflects the importance and its wide spread use.¹⁴⁶ As a powerful organic catalyst there have been several attempts to immobilize the MacMillan catalyst;^{99, 147-155} many have been covered in the 2010 review by Hansen.¹⁵⁶ Further immobilizations in the past couple of years have implemented different technologies which have proved effective. Bengalia and co-workers have developed a flow system using a ‘homemade’ HPLC set up attaching the MacMillan catalyst to a silica particle and performing the DA reaction between cyclopentadiene and cinnamaldehyde for a continuous 150 hour period, which could be doubled on a regeneration of the column through washes with aqueous acetonitrile and solutions of HBF_4 .¹⁴⁷ They were able to achieve 95% yield and *endo* ee% of 83%. Whilst they admit that the system is far from perfect with issues relating to the packing of the column and reaction rates, they have achieved promising results. A schematic overview of this work can be seen in Figure 1.24.

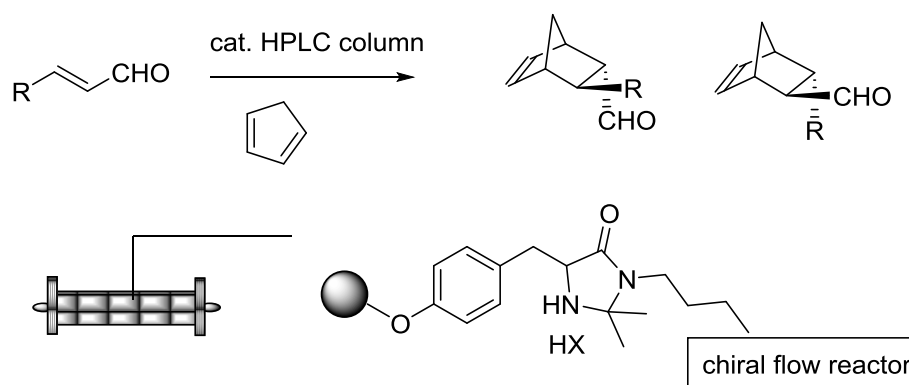


Figure 1.24. A reproduction of an overview of the immobilized MacMillan catalyst being used in a flow set-up for the catalysis of the DA reaction.

The group of Pericàs has utilized magnetism to reclaim the MacMillan catalyst through Fe_3O_4 particles.¹⁵¹ These were used for the catalysis of the Friedel-Crafts reaction for 6 runs which maintained its selectivity across all runs (~70% ee) and retained its initial activity (~50% yield) for 5 runs but only dropping to 40% yield in the final run. Using magnetism has enabled the quantitative recovery of the MacMillan catalyst and therefore offers a promising route for further immobilization studies.

1.5 Fluorescence

In most cases, on excitation, a molecule will lose the gained energy into its surroundings by vibration. However, in certain cases a radiative process occurs which removes the energy in the form of a photon as the electron quickly relaxes to a lower energy orbital, the release of this photon is termed luminescence.^{157, 158} There are two types of these processes: fluorescence and phosphorescence. Phosphorescence requires the presence of a triplet state and is not the focus of this work. In Figure 1.25 a Jablonski diagram illustrating the process of fluorescence can be seen. A molecule absorbs energy and is promoted into its excited state, where it will undergo vibrational relaxation and then fluorescence, emitting a photon to return to its ground state. The loss of energy through vibration results in the photon released having less energy than the initial photon and so fluorescence emission is observed at a higher wavelength than the excitation wavelength.

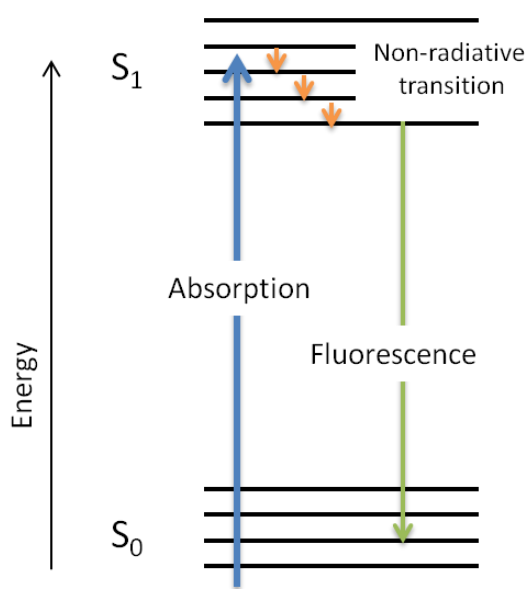


Figure 1.25. Jablonski diagram illustrating the process of fluorescence.

Fluorescence has been used extensively as a probe in order to increase the understanding of particular concepts. As fluorescence is highly dependent on environment, a slight change in its surroundings can be easily detected through a shift in wavelength of emission or a change in intensity.¹⁵⁹ For instance there has been significant work using fluorescence to monitor protein folding,¹⁶⁰ higher order structure assemblies¹⁶¹ and pH sensing within cells¹⁶² to name a few. A recent publication by Morris covers the benefit afforded by fluorescent biosensors.¹⁶³ These allow for biomolecules to be examined in the least intrusive way possible, giving insight into processes across a range of biological samples. The amino acid tryptophan is highly fluorescent and this characteristic has been exploited in many studies focussed on the folding of tryptophan containing peptides.¹⁶⁴⁻¹⁶⁶ Its use as a fluorescent probe has also found application away from biological compounds and this forms the basis of the research in Chapter 5.

1.5.1 Forster resonance energy transfer

One of the significant uses of fluorescence is Forster resonance energy transfer (FRET).¹⁵⁷ This is the non-radiative energy transfer from an excited chromophore (donor) to an acceptor through dipole-dipole interactions. In order for FRET to occur the two molecules must be in close proximity, typically less than 10 nm, and can therefore be used to indicate the locations of the two FRET pairs in solution. A common way of illustrating the FRET process is through a Jablonski diagram.

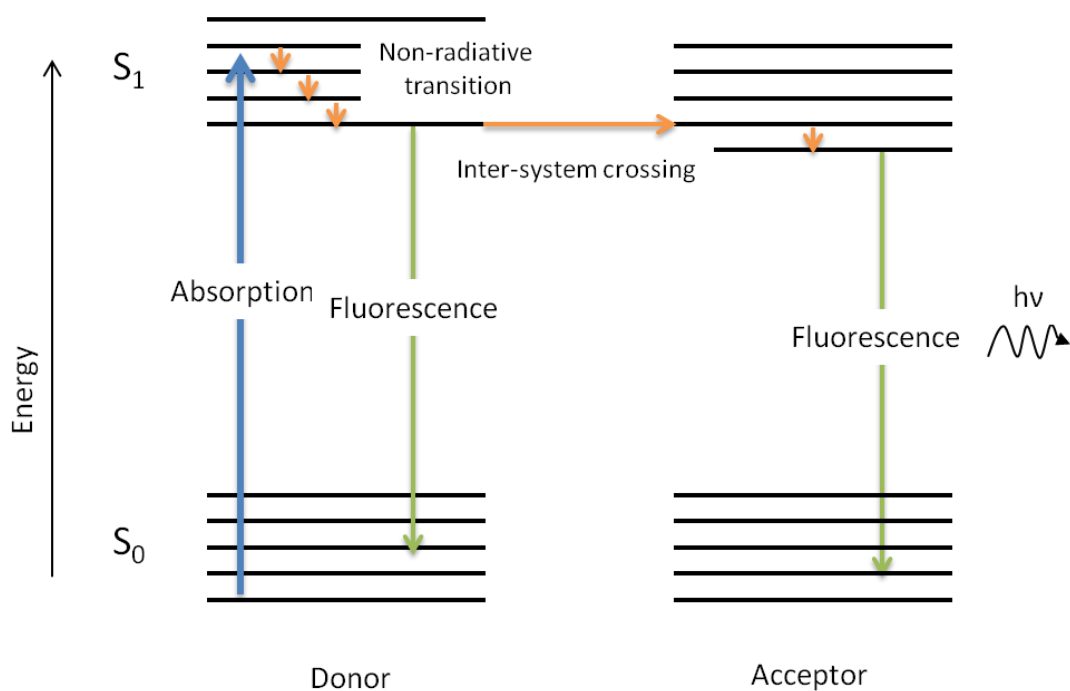


Figure 1.26. Jablonski diagram illustrating the process of fluorescence.

With reference to Figure 1.26, in its excited state a molecule can either undergo a radiative transition, fluorescence, to its ground state, or a non-radiative transition to an

acceptor molecule which places it into its excited state. After vibrational relaxation, this molecule will return to its ground state by fluorescence. The existence of FRET can therefore be observed by the decrease in fluorescence from the donor molecule and an increase in fluorescence from the acceptor molecule.

The use of FRET has been used extensively to study changes in structure. For instance Brewer and co-workers have used FRET between tryptophan and unnatural amino acids to study the disruption of the protein core on protein unfolding.¹⁶⁷ The methods they report have general applicability in the study of conformational changes in proteins after the incorporation of unnatural amino acids which act as a FRET pair. Through incorporation of these fluorescent unnatural amino acids at specific sites, they were placed in close proximity to the tryptophan residues when the protein was folded. On exposure to urea the protein was denatured and the distance between the residues increased as noted by the decrease in their FRET efficiency.

Tor and co-workers have also used FRET studies with tryptophan alongside a fluorescent ribonucleoside.¹⁶⁸ By monitoring the fluorescence of native tryptophan units in a protein at 350 nm and the fluorescent ribonucleoside at 440 nm they studied protein-RNA interactions (Figure 1.27). Through use of a FRET titration study they found that at an equimolar amount of the RNA and protein, the FRET pairs were $18 (\pm 3)$ Å apart, which was in good agreement with the estimated distance. Tryptophan residues are commonly found at or near the RNA recognition sites and therefore this fluorescent ribonucleoside could be used alongside other proteins for similar studies of their interactions.

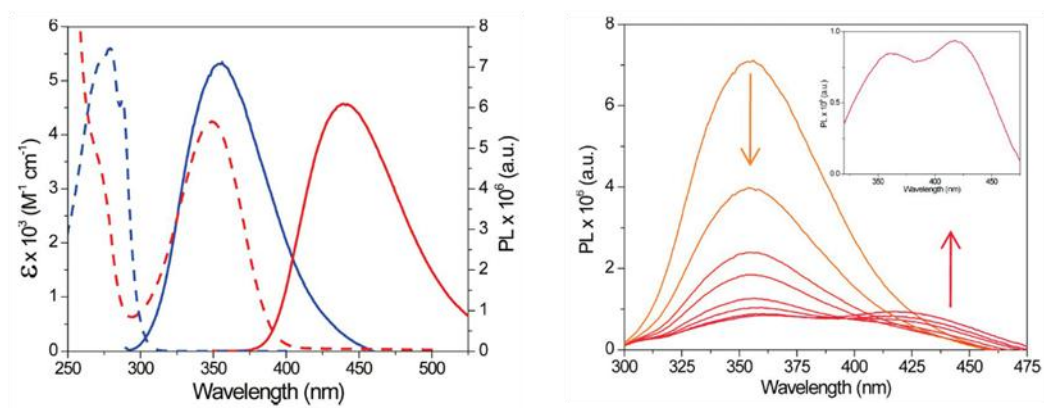


Figure 1.27. A reproduction of the fluorescence emission spectrum of tryptophan and the ribonucleoside FRET pair. The left hand spectra shows the emission (solid line) and absorption spectra (dashed line) of the tryptophan (blue) and the ribonucleoside FRET pair (red). The right hand spectra show that the tryptophan emission is decreasing and ribonucleoside emission increasing with increased concentrations of the ribonucleoside. The inset shows the emission spectrum at saturation.¹⁶⁸

1.6 Summary

Amino acids have been investigated as a synthetically viable route for the introduction of chirality into the pendent side chains of a polymer. This thesis focuses on the synthesis of polymerizable monomers of the amino acids L-tryptophan and L-tyrosine. Through the use of RAFT and emulsion polymerization the properties of the functionalized monomeric amino acids have then been explored. Specifically the roles of tryptophan in chiral separation and fluorescence, along with tyrosine's role as a precursor to a supported MacMillan catalyst, have been studied.

1.7 References

1. K. Matyjaszewski, *Curr. Opin. Solid State Mater. Sci.*, 1996, **1**, 769-776.
2. K. Matyjaszewski, in *Advances in Controlled/Living Radical Polymerization*, American Chemical Society, 2003, 2-9.
3. D. Colombani, *Prog. Polym. Sci.*, 1997, **22**, 1649-1720.
4. K. Matyjaszewski, *Prog. Polym. Sci.*, 2005, **30**, 858-875.
5. K. Matyjaszewski and J. Xia, *Chem. Rev.*, 2001, **101**, 2921-2990.
6. V. Coessens, T. Pintauer and K. Matyjaszewski, *Prog. Polym. Sci.*, 2001, **26**, 337-377.
7. E. Rizzardo and D. Solomon, *Polym. Bull.*, 1979, **1**, 529-534.
8. G. Moad, E. Rizzardo and D. H. Solomon, *Macromolecules*, 1982, **15**, 909-914.
9. C. J. Hawker, A. W. Bosman and E. Harth, *Chem. Rev.*, 2001, **101**, 3661-3688.
10. E. Rizzardo and D. H. Solomon, *Aust. J. Chem.*, 2013, **65**, 945-969.
11. J. Chiefari, Y. K. Chong, F. Ercole, J. Krstina, J. Jeffery, T. P. T. Le, R. T. A. Mayadunne, G. F. Meijs, C. L. Moad, G. Moad, E. Rizzardo and S. H. Thang, *Macromolecules*, 1998, **31**, 5559-5562.
12. G. Moad, E. Rizzardo and S. H. Thang, *Aust. J. Chem.*, 2005, **58**, 379-410.
13. M. K. Georges, R. P. N. Veregin, P. M. Kazmaier and G. K. Hamer, *Macromolecules*, 1993, **26**, 2987-2988.
14. M. Kato, M. Kamigaito, M. Sawamoto and T. Higashimura, *Macromolecules*, 1995, **28**, 1721-1723.
15. J.-S. Wang and K. Matyjaszewski, *Macromolecules*, 1995, **28**, 7901-7910.
16. J.-S. Wang and K. Matyjaszewski, *J. Am. Chem. Soc.*, 1995, **117**, 5614-5615.
17. V. Percec and B. Barboiu, *Macromolecules*, 1995, **28**, 7970-7972.

18. C. J. Hawker, *Acc. Chem. Res.*, 1997, **30**, 373-382.
19. R. Francis and A. Ajayaghosh, *Macromolecules*, 2000, **33**, 4699-4704.
20. J. Chiefari, R. T. A. Mayadunne, C. L. Moad, G. Moad, E. Rizzardo, A. Postma and S. H. Thang, *Macromolecules*, 2003, **36**, 2273-2283.
21. Y. K. Chong, J. Krstina, T. P. T. Le, G. Moad, A. Postma, E. Rizzardo and S. H. Thang, *Macromolecules*, 2003, **36**, 2256-2272.
22. D. J. Keddie, G. Moad, E. Rizzardo and S. H. Thang, *Macromolecules*, 2012, **45**, 5321-5342.
23. M. Benaglia, J. Chiefari, Y. K. Chong, G. Moad, E. Rizzardo and S. H. Thang, *J. Am. Chem. Soc.*, 2009, **131**, 6914-6915.
24. R. T. A. Mayadunne, E. Rizzardo, J. Chiefari, Y. K. Chong, G. Moad and S. H. Thang, *Macromolecules*, 1999, **32**, 6977-6980.
25. M. Destarac, W. Bzducha, D. Taton, I. Gauthier-Gillaizeau and S. Z. Zard, *Macromol. Rapid Commun.*, 2002, **23**, 1049-1054.
26. M. Destarac, D. Charmot, X. Franck and S. Z. Zard, *Macromol. Rapid Commun.*, 2000, **21**, 1035-1039.
27. M. Benaglia, M. Chen, Y. K. Chong, G. Moad, E. Rizzardo and S. H. Thang, *Macromolecules*, 2009, **42**, 9384-9386.
28. D. J. Keddie, C. Guerrero-Sanchez, G. Moad, R. J. Mulder, E. Rizzardo and S. H. Thang, *Macromolecules*, 2012, **45**, 4205-4215.
29. G. Moad, E. Rizzardo and S. H. Thang, *Aust. J. Chem.*, 2006, **59**, 669-692.
30. G. Moad, E. Rizzardo and S. H. Thang, *Aust. J. Chem.*, 2009, **62**, 1402-1472.
31. G. Moad, E. Rizzardo and S. H. Thang, *Aust. J. Chem.*, 2012, **65**, 985-1076.
32. D. J. Keddie, *Chem. Soc. Rev.*, 2013, **43**, 496-505.

33. B. V. K. J. Schmidt and C. Barner-Kowollik, *Nat Chem*, 2013, **5**, 990-992.
34. C. Barner-Kowollik and S. Perrier, *J. Polym. Sci., Part A: Polym. Chem.*, 2008, **46**, 5715-5723.
35. C. Barner-Kowollik, T. P. Davis, J. P. A. Heuts, M. H. Stenzel, P. Vana and M. Whittaker, *J. Polym. Sci., Part A: Polym. Chem.*, 2003, **41**, 365-375.
36. Y. K. Chong, G. Moad, E. Rizzardo and S. H. Thang, *Macromolecules*, 2007, **40**, 4446-4455.
37. H. Willcock and R. K. O'Reilly, *Polym. Chem.*, 2010, **1**, 149-157.
38. G. Moad, E. Rizzardo and S. H. Thang, *Polym. Int.*, 2011, **60**, 9-25.
39. A. Pich and W. Richtering, in *Polymer Science: A Comprehensive Reference*, eds. M. Moeller and K. Matyjaszewski, Elsevier, Amsterdam, London, 2012, 309 - 350.
40. R. Arshady, *Colloid. Polym. Sci.*, 1992, **270**, 717-732.
41. W. P. Hohenstein and H. Mark, *J. Polym. Sci.*, 1946, **1**, 127-145.
42. Y. Almog, S. Reich and M. Levy, *Brit. Polym. J.*, 1982, **14**, 131-136.
43. M. Okubo, S. Kawaguchi and K. Ito, in *Polymer Particles*, Springer Berlin Heidelberg, 2005, 299-328.
44. J. W. Vanderhoff, *J. Polym. Sci: Polym. Symp.*, 1985, **72**, 161-198.
45. C. S. Chern, *Prog. Polym. Sci.*, 2006, **31**, 443-486.
46. W. D. Harkins, *J. Am. Chem. Soc.*, 1947, **69**, 1428-1444.
47. W. V. Smith and R. H. Ewart, *J. Chem. Phys.*, 1948, **16**, 592-599.
48. H. Mori and T. Endo, *Macromol. Rapid Commun.*, 2012, **33**, 1090-1107.
49. R. K. O'Reilly, *Polym. Int.*, 2012, **59**, 568-573.
50. F. Sanda and T. Endo, *Macromol. Chem. Phys.*, 1999, **200**, 2651-2661.
51. M. Casolaro, *Macromolecules*, 1995, **28**, 2351-2358.

52. M. Yoshida, A. Safranj, H. Omichi and R. Katakai, *Macromolecules*, 1996, **29**, 2321-2323.
53. F. Bignotti, M. Penco, L. Sartore, I. Peroni, R. Mendichi, M. Casolaro and A. D'Amore, *Polymer*, 2000, **41**, 8247-8256.
54. A. Bentolila, I. Vlodayvsky, R. Ishai-Michaeli, O. Kovalchuk, C. Haloun and A. J. Domb, *J. Med. Chem.*, 2000, **43**, 2591-2600.
55. F. Sanda, T. Abe and T. Endo, *J. Polym. Sci., Part A: Polym. Chem.*, 1997, **35**, 2619-2629.
56. M. Casolaro, S. Bottari, A. Cappelli, R. Mendichi and Y. Ito, *Biomacromolecules*, 2004, **5**, 1325-1332.
57. A. C. Evans, J. Skey, M. Wright, W. Qu, C. Ondeck, D. A. Longbottom and R. K. O'Reilly, *J. Polym. Sci., Part A: Polym. Chem.*, 2009, **47**, 6814-6826.
58. T. E. Kristensen, K. Vestli, K. A. Fredriksen, F. K. Hansen and T. Hansen, *Org. Lett.*, 2009, **11**, 2968-2971.
59. B. L. Moore and R. K. O'Reilly, *J. Polym. Sci., Part A: Polym. Chem.*, 2012, **50**, 3567-3574.
60. S. G. Roy, R. Acharya, U. Chatterji and P. De, *Polym. Chem.*, 2012, **4**, 1141-1152.
61. H. Mori, E. Takahashi, A. Ishizuki and K. Nakabayashi, *Macromolecules*, 2013, **46**, 6451-6465.
62. P. Singh, A. Srivastava and R. Kumar, *Polym. Int.*, 2013, DOI: 10.1002/pi.4549.
63. IUPAC. Compendium of Chemical Terminology, 2nd ed. (the "Gold Book"). Compiled by A. D. McNaught and A. Wilkinson. Blackwell Scientific Publications, Oxford (1997).

64. R. S. Cahn, *J. Chem. Educ.*, 1964, **41**, 116.
65. R. S. Cahn, C. Ingold and V. Prelog, *Angew. Chem. Int. Ed.*, 1966, **5**, 385-415.
66. J. Skey, C. F. Hansell and R. K. O'Reilly, *Macromolecules*, 2010, **43**, 1309-1318.
67. F. Sanda, M. Nakamura and T. Endo, *Macromolecules*, 1996, **29**, 8064-8068.
68. F. Sanda, M. Nakamura, T. Endo, T. Takata and H. Handa, *Macromolecules*, 1994, **27**, 7928-7929.
69. J. Morcellet-Sauvage, M. Morcellet and C. Loucheux, *Macromolecules*, 1983, **16**, 1564-1570.
70. H. Mori, M. Matsuyama and T. Endo, *Macromol. Chem. Phys.*, 2008, **209**, 2100-2112.
71. H. Mori, M. Matsuyama and T. Endo, *Macromol. Chem. Phys.*, 2009, **210**, 217-229.
72. J. Du and R. K. O'Reilly, *Macromol. Chem. Phys.*, 2010, **211**, 1530-1537.
73. S. Yamada, S. Atsushi, M. Goto and T. Endo, *J. Polym. Sci., Part A: Polym. Chem.*, 2013, **51**, 4565-4571.
74. B. S. Lokitz, J. E. Stempka, A. W. York, Y. Li, H. K. Goel, G. R. Bishop and C. L. McCormick, *Aust. J. Chem.*, 2006, **59**, 749-754.
75. H. Mori, I. Kato and T. Endo, *Macromolecules*, 2009, **42**, 4985-4992.
76. H. Mori, I. Kato, M. Matsuyama and T. Endo, *Macromolecules*, 2008, **41**, 5604-5615.
77. H. Mori, H. Iwaya, A. Nagai and T. Endo, *Chem. Commun.*, 2005, 4872-4874.
78. N. M. Maier, P. Franco and W. Lindner, *J. Chromatogr. A*, 2001, **906**, 3-33.
79. M. Wills, *Science*, 2006, **311**, 619-620.

80. W. H. De Camp, *J. Pharm. Biomed. Anal.*, 1993, **11**, 1167-1172.
81. J. K. Whitesell, *Chem. Rev.*, 1989, **89**, 1581-1590.
82. E. Schneiderman and A. M. Stalcup, *J. Chromatogr. B*, 2000, **745**, 83-102.
83. J. Zhou and H. Ritter, *Polym. Chem.*, 2010, **1**, 1552-1559.
84. W. L. Hinze, T. E. Riehl, D. W. Armstrong, W. DeMond, A. Alak and T. Ward, *Anal. Chem.*, 1985, **57**, 237-242.
85. D. W. Armstrong, J. T. Lee and L. W. Chang, *Tetrahedron: Asymmetry*, 1998, **9**, 2043-2064.
86. J. Zukowski, D. Sybilska, J. Bojarski and J. Szejtli, *J. Chromatogr. A*, 1988, **436**, 381-390.
87. N. Maier and W. Lindner, *Anal. Bioanal. Chem.*, 2007, **389**, 377-397.
88. G. Wulff, *Angew. Chem. Int. Ed.*, 1995, **34**, 1812-1832.
89. R. J. Ansell, *Adv. Drug Del. Rev.*, 2005, **57**, 1809-1835.
90. C. Yamamoto and Y. Okamoto, *Bull. Chem. Soc. Jpn.*, 2004, **77**, 227-257.
91. J. Skey, H. Willcock, M. Lammens, F. Du Prez and R. K. O'Reilly, *Macromolecules*, 2010, **43**, 5949-5955.
92. L. Shi, P. Xie, Z. Li, Y. Wu and J. Deng, *Macromol. Chem. Phys.*, 2013, **214**, 1375-1383.
93. K. Bauri, S. Pant, S. G. Roy and P. De, *Polym. Chem.*, 2013, **4**, 4052-4060.
94. E. Bayer and V. Schurig, *Angew. Chem. Int. Ed.*, 1975, **14**, 493-494.
95. E. Bayer and W. Schumann, *J. Chem. Soc., Chem. Commun.*, 1986, 949-952.
96. D. P. Curran, *Angew. Chem. Int. Ed.*, 1998, **37**, 1174-1196.
97. D. E. Bergbreiter, *Catal. Today*, 1998, **42**, 389-397.

98. A. Lu, D. Moatsou, D. A. Longbottom and R. K. O'Reilly, *Chem. Sci.*, 2012, **4**, 965-969.
99. B. L. Moore, A. Lu, D. A. Longbottom and R. K. O'Reilly, *Polym. Chem.*, 2013, **4**, 2304-2312.
100. J. Dzierzak, M. Lefenfeld and R. Raja, *Top. Catal.*, 2009, **52**, 1669-1676.
101. J. Dzierzak, E. Bottinelli, G. Berlier, E. Gianotti, E. Stulz, R. M. Kowalczyk and R. Raja, *Chem. Commun.*, 2010, **46**, 2805-2807.
102. M. R. Maurya, M. Kumar, A. Kumar and J. Costa Pessoa, *Dalton Trans.*, 2008, 4220-4232.
103. D. E. Bergbreiter, *Chem. Rev.*, 2002, **102**, 3345-3384.
104. D. E. Bergbreiter, J. Tian and C. Hongfa, *Chem. Rev.*, 2009, **109**, 530-582.
105. D. E. Bergbreiter and S. D. Sung, *Adv. Synth. Catal.*, 2006, **348**, 1352-1366.
106. H. G. Schild, *Prog. Polym. Sci.*, 1992, **17**, 163-249.
107. D. E. Bergbreiter, B. L. Case, Y.-S. Liu and J. W. Caraway, *Macromolecules*, 1998, **31**, 6053-6062.
108. S. Wallyn, M. Lammens, R. K. O'Reilly and F. Du. Prez, *J. Polym. Sci., Part A: Polym. Chem.*, 2011, **49**, 2878-2885.
109. D. E. Bergbreiter, P. L. Osburn and J. D. Frels, *J. Am. Chem. Soc.*, 2001, **123**, 11105-11106.
110. W. J. Shaw, J. C. Linehan, A. Gutowska, D. Newell, T. Bitterwolf, J. L. Fulton, Y. Chen and C. F. Windisch, *Inorg. Chem. Commun.*, 2005, **8**, 894-896.
111. Y. Chi, S. T. Scroggins and J. M. J. Fréchet, *J. Am. Chem. Soc.*, 2008, **130**, 6322-6323.
112. H. Wei and E. Wang, *Chem. Soc. Rev.*, 2013, **42**, 6060-6093.

113. M. Raynal, P. Ballester, A. Vidal-Ferran and P. W. N. M. van Leeuwen, *Chem. Soc. Rev.*, 2014, DOI: 10.1039/C1033CS60037H
114. P. Cotanda and R. K. O'Reilly, *Chem. Commun.*, 2012, **48**, 10280-10282.
115. Z. Ge, D. Xie, D. Chen, X. Jiang, Y. Zhang, H. Liu and S. Liu, *Macromolecules*, 2007, **40**, 3538-3546.
116. A. Lu, P. Cotanda, J. P. Patterson, D. A. Longbottom and R. K. O'Reilly, *Chem. Commun.*, 2012, **48**, 9699-9701.
117. B. Helms and J. M. J. Fréchet, *Adv. Synth. Catal.*, 2006, **348**, 1125-1148.
118. A. W. Bosman, R. Vestberg, A. Heumann, J. M. J. Fréchet and C. J. Hawker, *J. Am. Chem. Soc.*, 2002, **125**, 715-728.
119. B. Helms, S. J. Guillaudeu, Y. Xie, M. McMurdo, C. J. Hawker and J. M. J. Fréchet, *Angew. Chem. Int. Ed.*, 2005, **44**, 6384-6387.
120. T. Terashima, M. Kamigaito, K.-Y. Baek, T. Ando and M. Sawamoto, *J. Am. Chem. Soc.*, 2003, **125**, 5288-5289.
121. T. Terashima, A. Nomura, M. Ito, M. Ouchi and M. Sawamoto, *Angew. Chem. Int. Ed.*, 2011, **50**, 7892-7895.
122. M. Yan, J. Ge, Z. Liu and P. Ouyang, *J. Am. Chem. Soc.*, 2006, **128**, 11008-11009.
123. Z. Chen, Z.-M. Cui, C.-Y. Cao, W.-D. He, L. Jiang and W.-G. Song, *Langmuir*, 2012, **28**, 13452-13458.
124. X. Huang, Y. Yin, Y. Tang, X. Bai, Z. Zhang, J. Xu, J. Liu and J. Shen, *Soft Matter*, 2009, **5**, 1905-1911.
125. J. Zhang, M. Zhang, K. Tang, F. Verpoort and T. Sun, *Small*, 2014, **10**, 32-46.

126. J. P. Patterson, P. Cotanda, E. G. Kelley, A. O. Moughton, A. Lu, T. H. Epps III and R. K. O'Reilly, *Polym. Chem.*, 2013, **4**, 2033-2039.
127. P. Cotanda, A. Lu, J. P. Patterson, N. Petzetakis and R. K. O'Reilly, *Macromolecules*, 2012, **45**, 2377-2384.
128. B. L. Moore, D. Moatsou, A. Lu and R. K. O'Reilly, *Polym. Chem.*, 2014.
129. B. Helms, C. O. Liang, C. J. Hawker and J. M. J. Fréchet, *Macromolecules*, 2005, **38**, 5411-5415.
130. B. Helms, S. J. Guillaudeu, Y. Xie, M. McMurdo, C. J. Hawker and J. M. J. Fréchet, *Angew. Chem. Int. Ed.*, 2005, **44**, 6384-6387.
131. M. Artar, T. Terashima, M. Sawamoto, E. W. Meijer and A. R. A. Palmans, *J. Polym. Sci., Part A: Polym. Chem.*, 2013, **52**, 12-20.
132. M. A. J. Gillissen, I. K. Voets, E. W. Meijer and A. R. A. Palmans, *Polym. Chem.*, 2012, **3**, 3166-3174.
133. N. Hosono, M. A. J. Gillissen, Y. Li, S. S. Sheiko, A. R. A. Palmans and E. W. Meijer, *J. Am. Chem. Soc.*, 2013, **135**, 501-510.
134. T. Mes, R. van der Weegen, A. R. A. Palmans and E. W. Meijer, *Angew. Chem. Int. Ed.*, 2011, **50**, 5085-5089.
135. P. J. M. Stals, M. A. J. Gillissen, R. Nicolay, A. R. A. Palmans and E. W. Meijer, *Polym. Chem.*, 2013, **4**, 2584-2597.
136. E. Huerta, P. J. M. Stals, E. W. Meijer and A. R. A. Palmans, *Angew. Chem. Int. Ed.*, 2012, **52**, 2906-2910.
137. K. A. Ahrendt, C. J. Borths and D. W. C. MacMillan, *J. Am. Chem. Soc.*, 2000, **122**, 4243-4244.

138. A. B. Northrup and D. W. C. MacMillan, *J. Am. Chem. Soc.*, 2002, **124**, 2458-2460.
139. S. P. Brown, N. C. Goodwin and D. W. C. MacMillan, *J. Am. Chem. Soc.*, 2003, **125**, 1192-1194.
140. N. A. Paras and D. W. C. MacMillan, *J. Am. Chem. Soc.*, 2001, **123**, 4370-4371.
141. Y. Huang, A. M. Walji, C. H. Larsen and D. W. C. MacMillan, *J. Am. Chem. Soc.*, 2005, **127**, 15051-15053.
142. S. G. Ouellet, J. B. Tuttle and D. W. C. MacMillan, *J. Am. Chem. Soc.*, 2004, **127**, 32-33.
143. J. B. Tuttle, S. G. Ouellet and D. W. C. MacMillan, *J. Am. Chem. Soc.*, 2006, **128**, 12662-12663.
144. Larsen, C. H.-M. 2006, *Investigating Imidazolidinone Catalysts*. California Institute of Technology, California.
145. J. F. Austin and D. W. C. MacMillan, *J. Am. Chem. Soc.*, 2002, **124**, 1172-1173.
146. <http://www.sigmaaldrich.com/catalog/product/aldrich/674575?lang=en®ion=GB>
147. A. Puglisi, M. Benaglia, R. Annunziata, V. Chiroli, R. Porta and A. Gervasini, *J. Org. Chem.*, 2013, **78**, 11326-11334.
148. C. A. Wang, Y. Zhang, J. Y. Shi and W. Wang, *Chem. Asian J.*, 2013, **8**, 1110-1114.
149. N. Haraguchi, Y. Takemura and S. Itsuno, *Tetrahedron Lett.*, 2010, **51**, 1205-1208.
150. T. E. Kristensen, K. Vestli, M. G. Jakobsen, F. K. Hansen and T. Hansen, *J. Org. Chem.*, 2010, **75**, 1620-1629.

151. P. Riente, J. Yadav and M. A. Pericas, *Org. Lett.*, 2012, **14**, 3668-3671.
152. S. A. Selkälä, J. Tois, P. M. Pihko and A. M. P. Koskinen, *Adv. Synth. Catal.*, 2002, **344**, 941-945.
153. Y. Zhang, L. Zhao, S. S. Lee and J. Y. Ying, *Adv. Synth. Catal.*, 2006, **348**, 2027-2032.
154. S. Pagoti, D. Dutta and J. Dash, *Adv. Synth. Catal.*, 2013, **355**, 3532-3538.
155. B. P. Mason, A. R. Bogdan, A. Goswami and D. T. McQuade, *Org. Lett.*, 2007, **9**, 3449-3451.
156. T. E. Kristensen and T. Hansen, *Eur. J. Org. Chem.*, 2010, **2010**, 3179-3204.
157. J. Lakowicz, *Principles of fluorescence spectroscopy*, Springer, New York, 2006.
158. B. Valeur, *Molecular Fluorescence Principles and Applications*, Wiley, Weinheim, 2002.
159. S. You, Q. Cai, K. Mullen, W. Yang and M. Yin, *Chem. Commun.*, 2014, **50**, 823-825.
160. X. Michalet, S. Weiss and M. Jager, *Chem. Rev.*, 2006, **106**, 1785-1813.
161. M. Wilhelm, C. L. Zhao, Y. Wang, R. Xu, M. A. Winnik, J. L. Mura, G. Riess and M. D. Croucher, *Macromolecules*, 1991, **24**, 1033-1040.
162. J. Han and K. Burgess, *Chem. Rev.*, 2009, **110**, 2709-2728.
163. M. C. Morris, *ACS Med. Chem. Lett.*, 2014, DOI 10.1021/ml400472e.
164. P. R. Callis and T. Liu, *J. Phys. Chem. B*, 2004, **108**, 4248-4259.
165. Y. Chen and M. D. Barkley, *Biochemistry*, 1998, **37**, 9976-9982.
166. J. T. Vivian and P. R. Callis, *Biophys. J.*, 2001, **80**, 2093-2109.

167. S. J. Miyake-Stoner, A. M. Miller, J. T. Hammill, J. C. Peeler, K. R. Hess, R. A. Mehl and S. H. Brewer, *Biochemistry*, 2009, **48**, 5953-5962.

168. Y. Xie, T. Maxson and Y. Tor, *J. Am. Chem. Soc.*, 2010, **132**, 11896-11897.

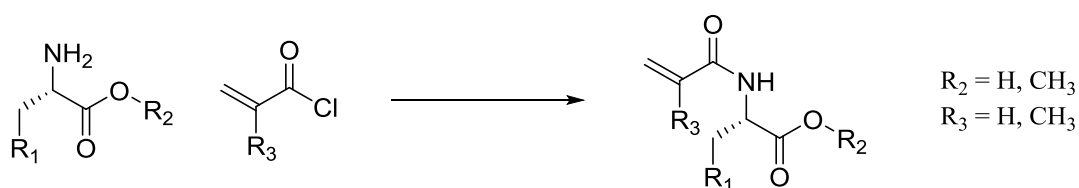
Chapter 2: The synthesis of poly(L-tryptophan) and its interactions with
1,1'-bi-2-naphthol

2.1 Abstract

Poly(L-tryptophan methyl ester) (poly(**M2.1**)) has been synthesized in this first instance by employing a post-polymerization functionalization strategy using poly(pentafluorophenyl) as the scaffold. Substitution of this scaffold with L-tryptophan methyl ester yielded the desired polymer. Both the D- and L-acrylamide monomers have been synthesized but attempts to polymerize these *via* RAFT have proved to be unfruitful. The chiral interactions of the new monomers and polymer, along with previously reported phenylalanine methyl ester monomers and polymers, have been studied by monitoring the interactions with 1,1'-bi-2-naphthol. The results indicate that there is a stronger interaction with tryptophan over phenylalanine, as well as favorable interactions of (*S*)-BINOL with the L-amino acids and (*R*)-BINOL with the D-amino acids.

2.2 Introduction

Readily available chiral starting materials such as amino acids have been the focus for the synthesis of polymers containing pendent chiral groups. Amino acids including leucine,¹⁻³ proline,⁴⁻⁶ phenylalanine,⁷ alanine,⁸ and histidine⁹ have been converted into monomers that have subsequently been incorporated into polymeric structures using a range of reversible-deactivation radical polymerization (RDRP) techniques. These polymers have been used in variety of applications including catalysis,⁶ enantiomer separation¹⁰ and investigation into the tertiary structures that they form.³ The bifunctionality of amino acids lends itself to easy functionalization into monomers, work that has been pioneered by Endo and co-workers.^{1, 5, 7, 11} Simple chemistry using the amino functionality with either acryloyl or methacryloyl chloride will yield monomers capable of undergoing polymerization using a range of techniques. A generic synthesis is presented in Scheme 2.1. It is only with the advances in polymerization technology that well-defined polymers of these amino acids have been able to be produced.



Scheme 2.1. Generic route for the synthesis of amino acid monomers with (meth)acryloyl chloride.

The work carried out in this Chapter highlights the difficulty of polymerizing an acrylamide tryptophan monomer and how the use of a modifiable polymeric scaffold enabled the first synthesis of poly(L-tryptophan). The polymer was then used to

investigate the possibility of chiral recognition.¹² Since the synthesis of poly(L-tryptophan) was first reported by post-polymerization, the direct polymerization of tryptophan monomers has been published by several groups, with their monomers differing from ours.¹³⁻¹⁵ De *et al.*¹³ reported the first direct polymerization of tryptophan using reversible addition-fragmentation chain transfer (RAFT) polymerization with an *N*-Boc protected tryptophan where functionalization with 2-hydroxyethyl methacrylate (HEMA) was accomplished using the carboxylic acid functionality of tryptophan. After a deprotection step the polymer was found to be pH-responsive, where precipitation occurred upon increasing the pH. They also demonstrated that their polymers were fluorescent and had negligible cytotoxicity levels to HeLa cells and therefore have potential uses in imaging and drug delivery. A copy of an overview of their work can be seen in Figure 2.1.

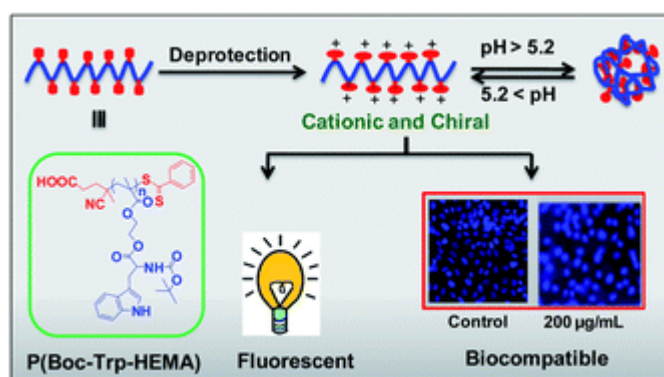


Figure 2.1. A reproduction of the table of contents figure for the work published by De *et al.*¹³

The second report sees Kumar *et al.*, again using RAFT, synthesize a nanoporous polymer that incorporates L-tryptophan.¹⁵ This tryptophan monomer was synthesized from the unfunctionalized amino acid with acryloyl chloride. Lastly Mori *et al.* used the same monomer as Kumar *et al.* and synthesized a block co-polymer *via* RAFT which

self-assembled into micelle constructs placing the tryptophan in the core. They then exploited the increased fluorescence of tryptophan in this environment (compared to the homo-polymer) as a sensor for fluoride ions, an important concept for the applications of drinking water analysis, detection of chemical warfare agents and refinement of uranium sources.¹⁴ Again a figure giving an overview of this work can be seen in Figure 2.2. Poly(L-tryptophan) has also been synthesized *via* a polycondensation of a urethane derivative.¹⁶

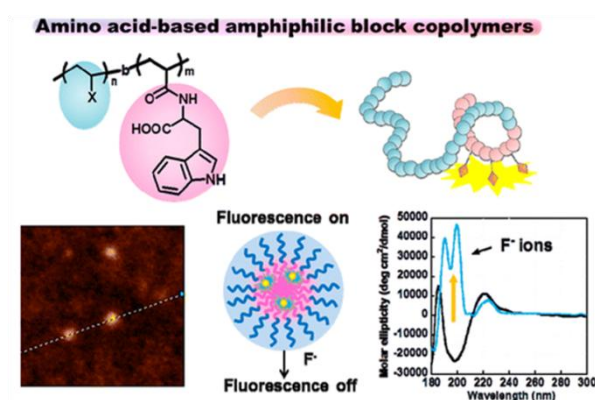
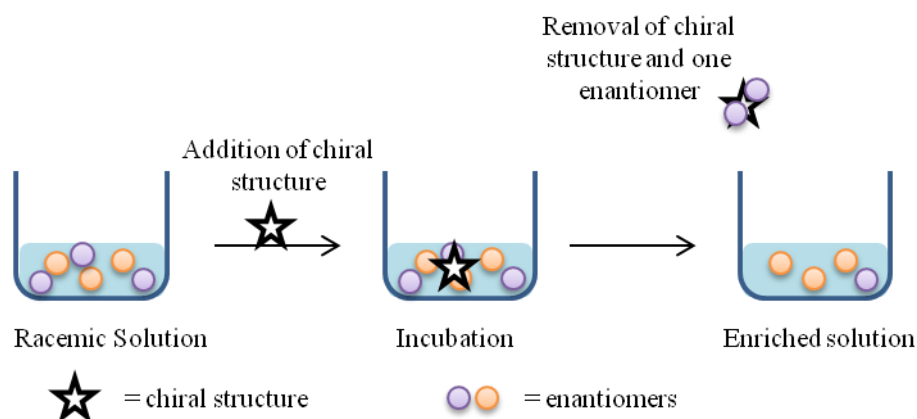


Figure 2.2. A reproduction of the table of contents figure for the work published by Mori *et al.*¹⁴

Enantiomer separation is an important area of research due to the significant effects that different enantiomers can have.¹⁷ Wang *et al.* have used a chiral glycopolymer to perform chiral resolution of enantiomers. On incubation of their novel polymer with tartaric acid or mandelic acid a difference in the specific rotation of the solution was observed which was attributed to the selective uptake of one enantiomer over the other.¹⁸ Previous work in the O'Reilly group using L-phenylalanine micelles successfully achieved specific enantiomer interactions. Micelles with a L-phenylalanine core were incubated with a racemic mixture of phenylalanine overnight. Analysis of the

surrounding solution by polarimetry demonstrated that it had become depleted of the D-isomer, highlighting a preferred affinity for the opposite enantiomer.¹⁰ This chiral recognition relied on the different strength of interactions between the ‘stationary’ and mobile enantiomers, allowing for the increased removal of one enantiomer from the solution to the core, thus leaving an enantiomerically enriched solution behind. A schematic demonstrating how these chiral structures are able to deliver enriched enantiomer solutions can be seen in Scheme 2.2. Nevertheless, chiral polymers are yet to achieve the superior ability of cyclodextrins for enantioseparations. Cyclodextrins are at the moment the most efficient way to separate enantiomers which has led to their extensive use in chiral chromatography techniques.¹⁹⁻²¹



Scheme 2.2. A schematic representation of how chiral structures are potentially able to deliver enriched solutions.

1,1'-Bi-2-naphthol (BINOL) has been extensively used in chiral recognition as a result of its importance as a chiral catalyst precursor²²⁻²⁵ and the ease of which the enantiomer effects can be observed by ¹H NMR spectroscopy. There have been many reports on using different types of polymers to induce a shift of the (*rac*)-BINOL phenolic proton

signals (highlighted in Figure 2.3) whilst simultaneously separating the signal, demonstrating different strength interactions between the enantiomers.

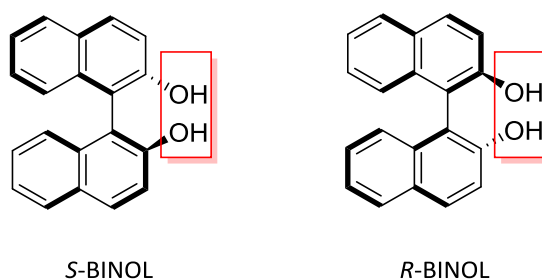


Figure 2.3. The structures of (*S*)- and (*R*)- BINOL with the phenolic protons highlighted which give rise to the trackable signal.

The polymers used have included a leucine based polymer,³ a methacrylamide microgel star polymer,²⁶ chiral poly((meth)acrylamides)^{27, 28} and poly(maleimides).²⁹ A reproduction of an image from the leucine based polymer separation is shown in Figure 2.4.³ The separation of the (*rac*)-BINOL peak into its constituent enantiomers has been highlighted in the red trace, which shows two peaks (one for each enantiomer) opposed to the single peak present in the blue trace.

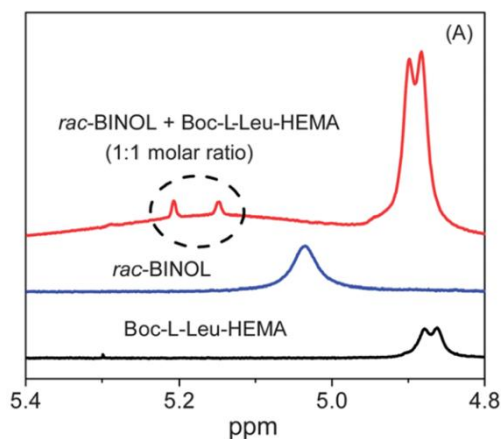


Figure 2.4. A reproduction of an image of the separation of (*rac*)-BINOL enantiomers in ^1H NMR spectroscopy caused by a leucine monomer.³

BINOL has also been used in order to determine enantiomeric excess.³⁰ A single enantiomer of BINOL induces a shift in the spectra of the substrate and the relative proportions can be used to calculate enantiomeric excess quickly and easily.³¹ Redando *et al.* used BINOL to highlight the ease of this process with omeprazole (a chiral drug). On incubation with (*S*)-BINOL the (*R*)- and (*S*)- enantiomers of omeprazole had different shifts in the ^1H NMR spectrum and therefore the relative amount could be easily calculated. An example of their ^1H NMR spectra for both omeprazole in the presence and absence of (*S*)-BINOL, along with the chemical structure of omeprazole highlighting the proton used to calculate the relative amounts, can be seen in Figure 2.5.

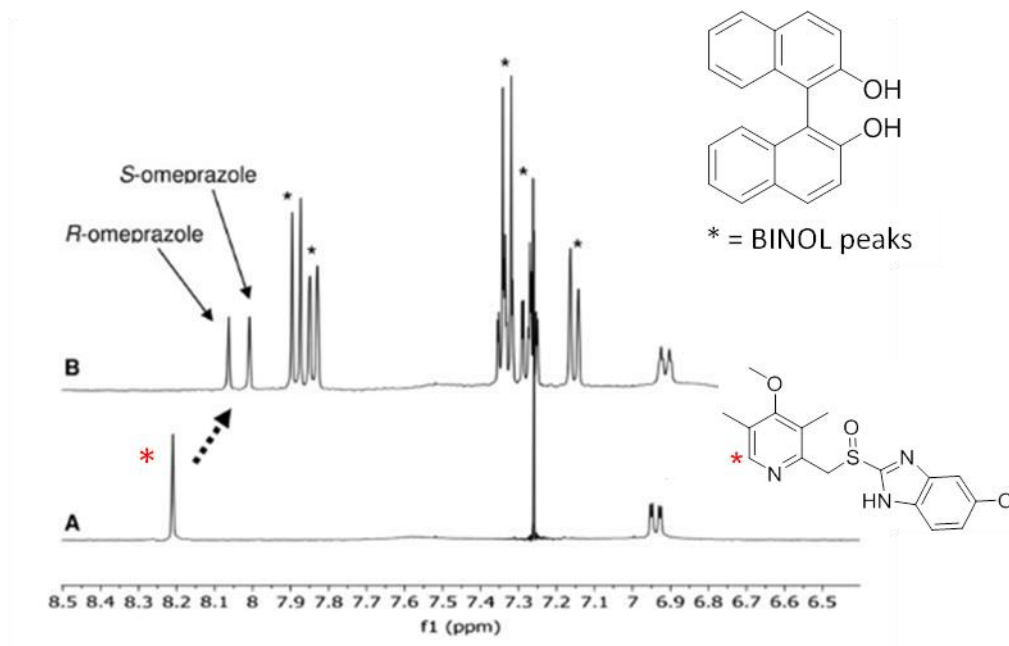


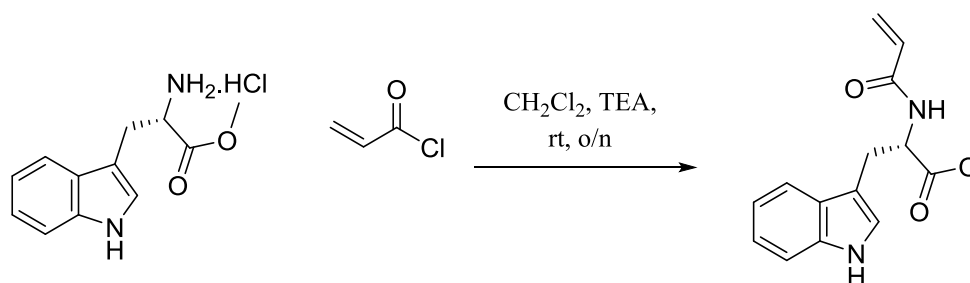
Figure 2.5. A reproduction of the ^1H NMR spectrum from the work conducted by Redando *et al.*³¹ The bottom spectrum shows a ^1H NMR spectrum of omeprazole on its own and the top spectrum a ^1H NMR spectrum of omeprazole in the presence of (*S*)-BINOL. The top spectrum shows how the proton, highlighted on the structure, has shifted and split into the two enantiomers. The other peaks marked with the black asterisk are due to the presence of BINOL.

This interaction with (*rac*)-BINOL has also been demonstrated in the work presented here and further investigation has shown that there is a like-for-like interaction between enantiomers.

2.3 Results and Discussion

2.3.1 Synthesis of Monomers

The acrylamide tryptophan monomer was prepared using a well-established coupling procedure between an acid chloride and a primary amine, widely used to prepare *N*-functionalized amino acid monomers.¹ The synthetic route to monomer **M 2.1** is detailed in Scheme 2.3.



Scheme 2.3. Synthetic route to L-M 2.1.

The monomer was synthesized in 53% yield and was neutralized by washing with base before being purified by column chromatography in ethyl acetate (EtOAc). **M 2.1** was characterized by ¹H and ¹³C NMR spectroscopy which can be seen in Figure 2.6 and Figure 2.7 respectively. The ¹H NMR spectrum showed the expected chemical shifts, integration and splitting. The protons on the indole ring (**j** – **m**) are coupled to each other giving two doublets (**j** and **m**), two triplets (**k** and **l**) and a singlet (**h**). The protons on the alkene have also coupled to each other in a typical acrylate splitting, the protons **a** and **b** have been split into doublets of doublets as they have coupled with each other and proton **c**. The geminal ²*J* coupling is small as expected at ²*J* = 1.5 Hz. The magnitude of the splitting with **c** is different depending on the relative positioning with

the *trans* $^3J_{a-c} = 17$ Hz and the *cis* $^3J_{b-c} = 9$ Hz. The difference in this magnitude is due to the differing orbital overlaps. Protons **e** and **f** have also been split by each other resulting in a doublet for proton **e** ($^3J = 5.1$ Hz) and a doublet of triplets for **f** as it has been further split by the amine, **d** ($^3J = 5.1, 8.1$ Hz). The optical rotation of the monomer was also measured by polarimetry confirming the presence of the chiral centre $[\alpha]_{298}^{20} = +0.72$.

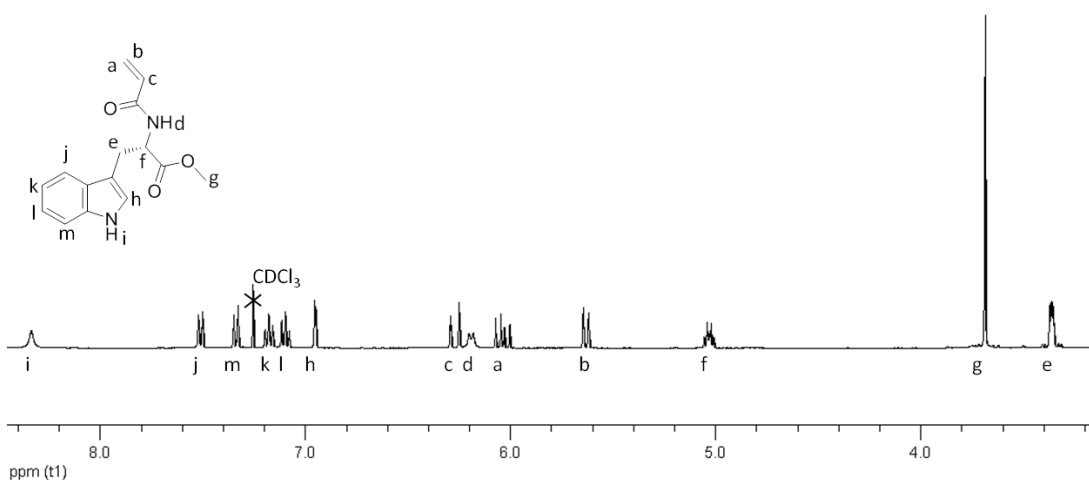


Figure 2.6. ^1H NMR (300 MHz) spectrum for L-M **2.1** in CDCl_3 .

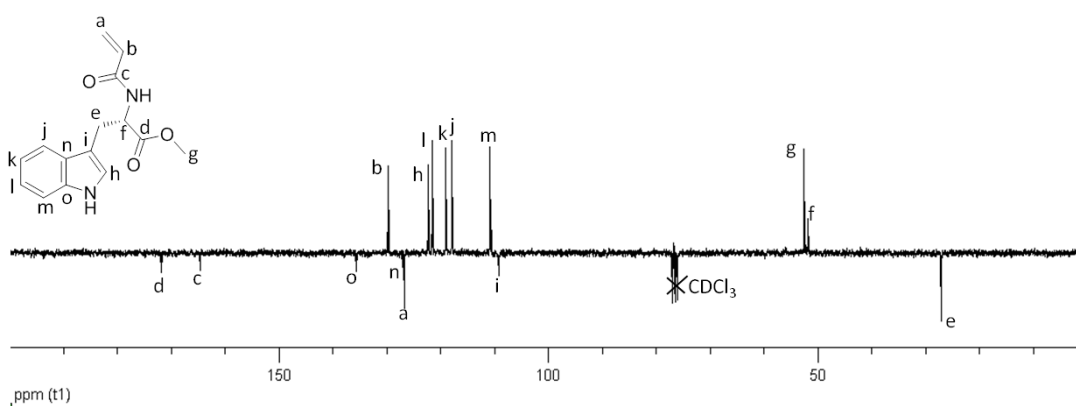


Figure 2.7. ^{13}C NMR (75 MHz) spectrum for L-M **2.1** in CDCl_3 .

2.3.2 Polymerization Investigation

A widespread investigation into the RAFT polymerization conditions for this monomer proved to be unsuccessful, despite similar conditions successfully polymerizing the previously reported phenylalanine monomer.³² By varying the chain transfer agent (CTA), solvent, temperature and monomer concentration, the optimum conditions for this polymerization was examined, as shown in Table 2.1 with selected SEC collected for polymerizations with promising conversions, which can be seen in Figure 2.4. Unfortunately, the investigation proved unsuccessful with no conditions found for reproducible controlled polymerization of the monomer; although some entries in the table did show promising results. Entries 1 and 3 have good levels of conversion but their \bar{D} values of 1.63 and 2.00 (Figure 2.8) are higher than ideal. Entries 23 and 25 have lower \bar{D} values of 1.27 and 1.29 but their conversions are low at 36% and 52%. The entries of 14 and 15 have the most promise, achieving 62% and 75% and \bar{D} values of 1.37 and 1.40 respectively.

Table 2.1. Conditions used for the attempted polymerization of **M 2.1**, varying the CTA, solvent, temperature, time, concentration and equivalents of monomer, the initiator and its equivalents.

Entry	CTA	Solvent	Temp (°C)	Time (h)	Concentration of monomer (g mL ⁻¹)	Equivalents of monomer	Initiator	Initiator equivalents	Conversion (%) ^a	<i>D</i> ^b
1	-	Dioxane	90	63	0.05	50	1	1	85	1.63
2	-	Dioxane	95	23	0.05	50	1	1	56	-
3	-	Dioxane	95	23	0.10	50	1	1	94	-
4	-	Dioxane	95	23	0.20	50	1	1	99	-
5	1	Dioxane	65	48	0.10	40	1	0.2	-	-
6	2	Dioxane	65	48	0.10	40	1	0.2	-	-
7	2	Dioxane	65	48	0.05	40	1	0.2	15	-
8	2	Dioxane	90	48	0.10	40	1	0.2	-	-
9	2	Dioxane	90	48	0.05	40	1	0.2	13	-
10	3	DMSO	65	22	0.17	50	1	0.2	-	-
11	4	Dioxane	65	31	0.10	100	1	0.3	-	-
12	4	Dioxane	70	28	0.10	50	1	0.3	16	-
13	4	Dioxane	80	28	0.10	50	1	0.3	14	-
14	4	Dioxane	90	63	0.05	100	1	0.2	62	1.37
15	4	Dioxane	90	30	0.05	100	1	0.3	75	1.40
16	4	Dioxane	90	11	0.05	100	1	0.3	27	-
17	4	Dioxane	90	24	0.05	200	1	0.2	-	-
18	4	Dioxane	95	23	0.04	50	1	0.3	23	-
19	4	Dioxane	95	23	0.05	50	1	0.3	29	-
20	4	Dioxane	95	23	0.10	50	1	0.3	26	-
21	4	DMF	80	20	0.10	50	1	0.3	35	-
22	5	Dioxane	65	18	0.10	50	1	0.2	-	-
23	6	Dioxane	90	48	0.10	50	1	0.3	36	1.24
24	6	Dioxane	90	64	0.10	50	1	0.3	30	1.24
25	6	Dioxane	90	48	0.10	50	2	0.3	52	1.21
26	6	DMF	90	43	0.10	50	2	0.3	27	-
27	6	DMSO	90	46	0.10	50	1	0.3	-	-
28	6	Toluene	100	40	0.10	50	1	0.3	-	-

^aDetermined by ¹H NMR spectroscopy

^bDetermined by THF SEC against PMMA standards

The structures of the CTAs used can be seen in Figure 2.8 along with the SEC traces for selected entries.

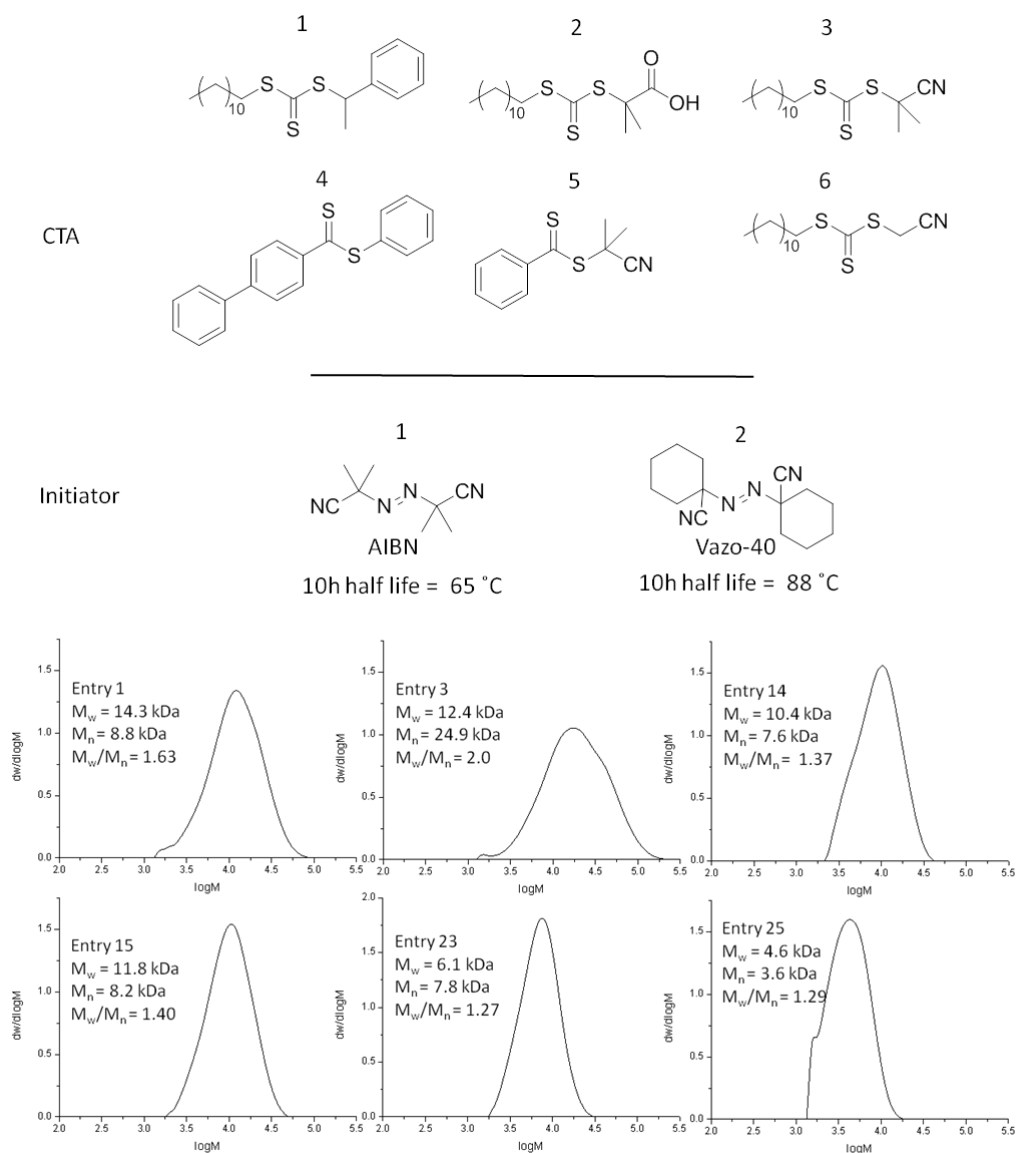


Figure 2.8. The CTAs used and a selection of SEC traces for entries 1, 3, 14, 15, 23 and 25 from Table 2.1.

Superior control over the polymerization is shown with a second L-tryptophan monomer (discussed in Chapter 5) with a longer linker between the polymerizable double bond and the tryptophan functionality.

Tryptophan monomers, structurally similar to **M 2.1** have been reported since our publication and have been polymerized using RAFT. However, crucially our monomer (Figure 2.9) is functionalized through the amino functionality whereas others have been functionalized through the carboxylic acid (De, Boc-L-Trp-HEMA)¹³ or with the carboxylic acid unprotected (Kumar, Mori, L-A-Trp-OH).^{14, 15} These slight differences are clearly significant as the synthesis of the monomer and polymer reported by Kumar and Mori was repeated. Their monomer (L-A-Trp-OH) was synthesized and successfully polymerized by RAFT (using the CTA 2-Cyano-2-propyl dodecyl trithiocarbonate (CTA 3, Figure 2.8) and DMSO at 150 mg mL⁻¹) to 72% conversion with *D* of 1.26. This suggests the methyl group on **M 2.1** is significant to the polymerization kinetics. Further modelling investigations could potentially provide greater insight into the electronic properties of the monomers.

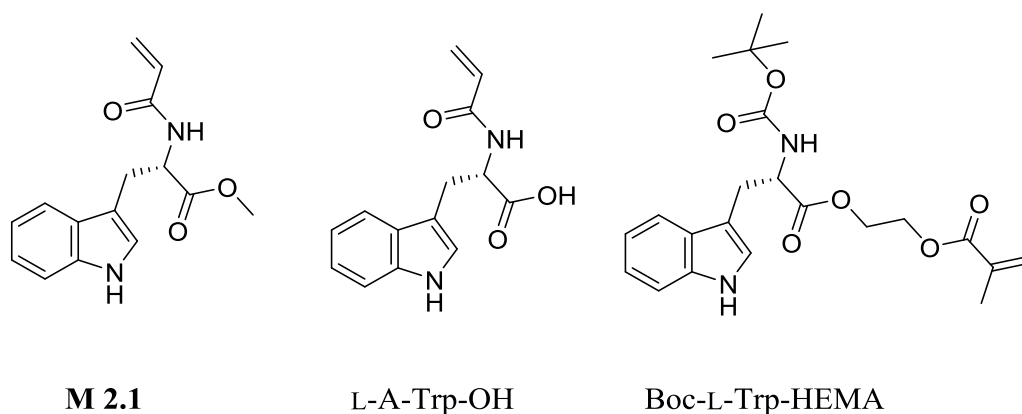
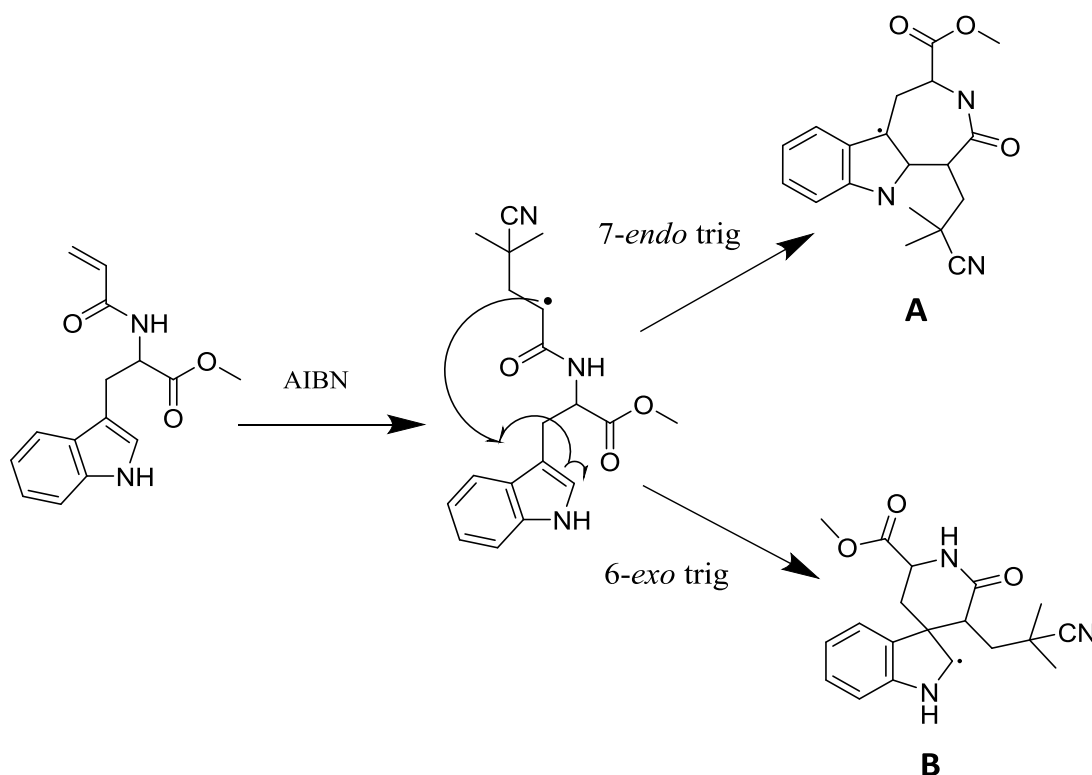


Figure 2.9. The structure of **M 2.1** and an acrylamide based monomer of tryptophan (L-A-Trp-OH) with a free carboxylic acid which is easily polymerized *via* RAFT synthesized by Kumar¹⁵ and Mori¹⁴ and a tryptophan monomer functionalized through the carboxylic acid synthesized by De (Boc-L-Trp-HEMA).¹³

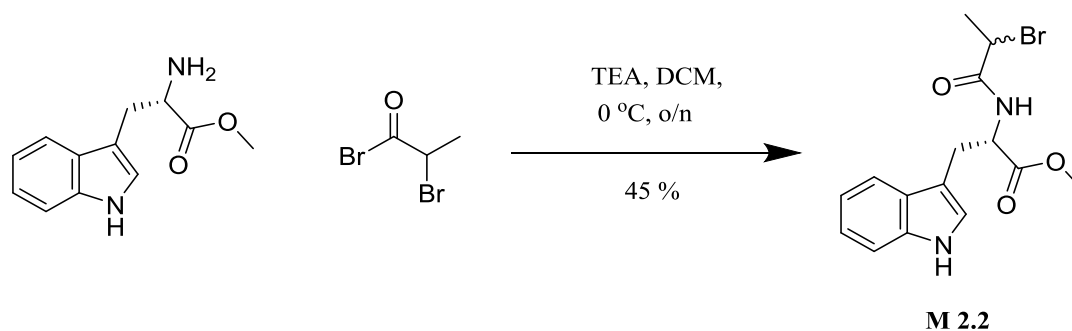
The possibility of the tryptophan undergoing a cyclization reaction rather than polymerizing was also investigated as a potential side reaction. The potential mechanism and structures of these scenarios are presented in Scheme 2.4. The two possible structures are the results of the formation of a 6 or 7 member ring. According to Baldwin's rules (which indicate that the ring closing mechanisms are favoured) either of these routes could be possible; with the classifications of these mechanisms being 6-*exo*-trig (**B**) and 7-*endo*-trig (**A**).³³

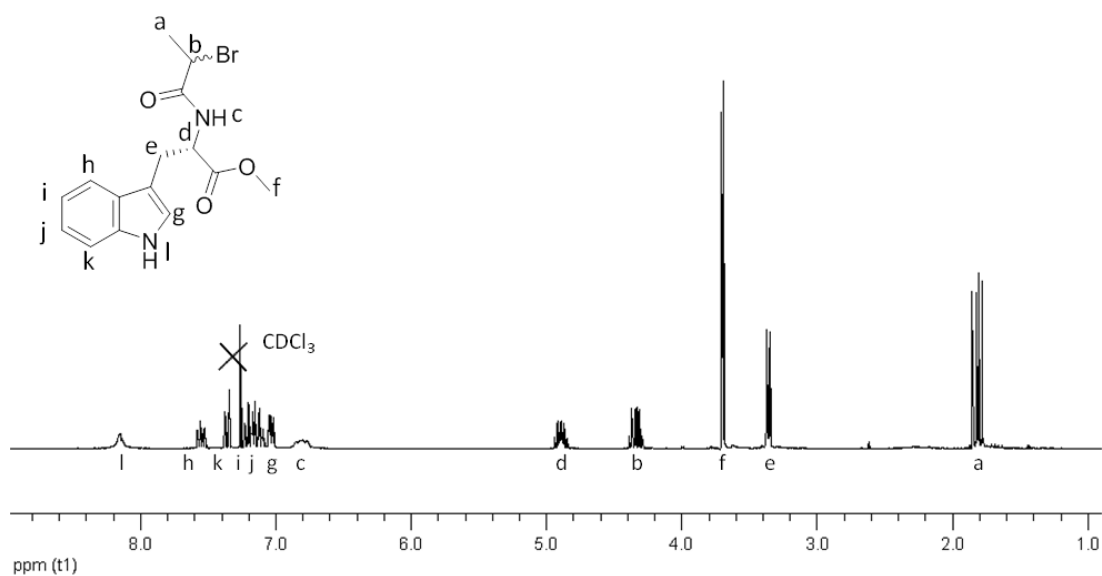


Scheme 2.4. The potential mechanism of cyclization for **M 2.1** when exposed to a radical flux and the suggested structures from either forming a) 7 member or b) 6 member ring.

In order to test this hypothesis, a tryptophan monomer analogue that cannot polymerize but can cyclize was synthesized (**M 2.2**) and exposed to the polymerization conditions

as well as typical cyclization conditions. The synthesis of the structure can be seen in Scheme 2.5. The product was purified by neutralization with base and column chromatography giving a yield of 45%. The ^1H NMR spectrum can be seen in Figure 2.10 and gave the expected chemical shifts and integration although a number of signals have given more complex splitting patterns than anticipated due to the presence of diastereoisomers. Proton **a** is present as two doublets ($^3J = 7.2$ Hz), proton **b** as two quartets ($^3J = 6.9$ Hz), proton **d** as two triplets ($^3J = 5.4, 6.8$ Hz) and the signal for **f** is also present as two singlets. Only the expected coupling between protons was confirmed by correlation (COSY) ^1H NMR spectroscopy. The potential presence of rotamers was also investigated by conducting ^1H NMR spectroscopy at an elevated temperature of 323 K; the ^1H NMR spectrum showed no change in peak shape making the presence of rotamers unlikely. Therefore the additional peaks have been assigned to the presence of diastereoisomers.

Scheme 2.5. The synthetic route to **M 2.2**.

Figure 2.10. ^1H NMR (300 MHz) of **M 2.2** in CDCl_3 .

The cyclization experiment was monitored by observing the proton adjacent to the bromine atom (δ 4.34 ppm) by ^1H NMR spectroscopy. If the cyclization reaction did take place, a significant shift in the signal was expected. The conditions used are detailed in Table 2.2.

Table 2.2. The conditions for the cyclization experiments conducted for **M 2.2**.

Reaction	[M 2.2] (g mL^{-1})	Initiator equivalents	Time (h)	Temperature ($^{\circ}\text{C}$)
A ^a	0.1	0.5	6	90
B ^a	0.1	0.02	6	90
C ^a	0.03	0.6	20	90
D ^b	0.04	0	25	120

^a **M 2.2** was exposed to AIBN and heated akin to the polymerization conditions

^b The conditions for a cyclization was followed using CuBr/TPA conditions³⁴

The ^1H NMR spectra for these reactions can be seen in Figure 2.11 with the proton under observation highlighted on the structure in red. The labelling A-D refers to the reaction conditions outlined in Table 2.2. The presence of the peak indicates that cyclization has not taken place as the loss of the bromine atom would cause a significant shift in ppm upfield, as it will no longer be adjacent to the bromine. However, the possibility of cyclization occurring during polymerization cannot be ruled out as the polymer grows and becomes more sterically hindered, even though it is not favourable for the monomer.

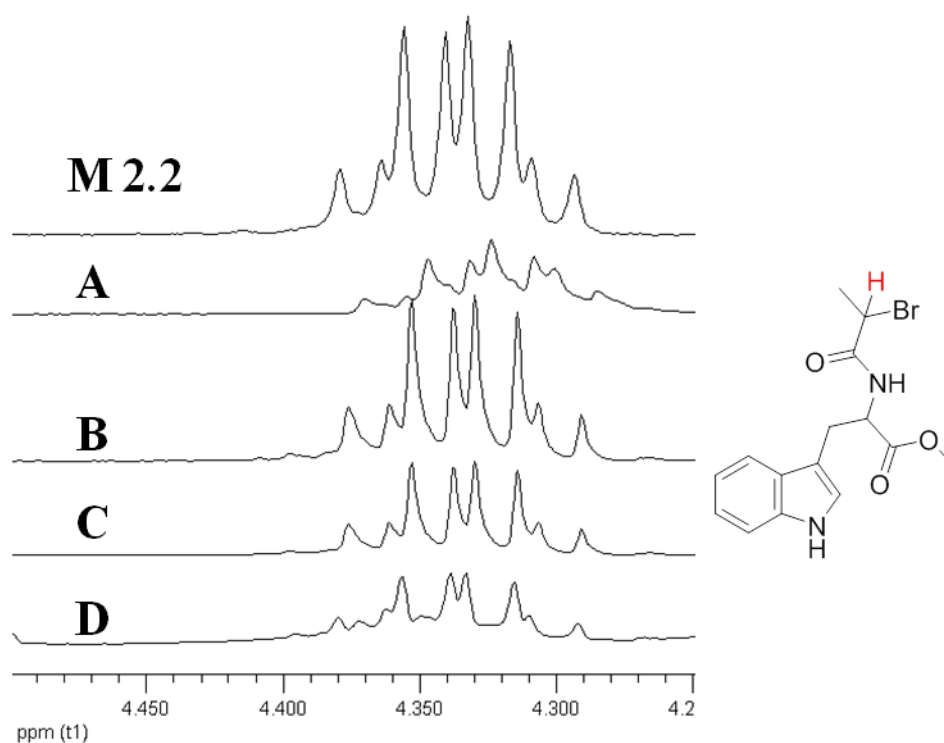
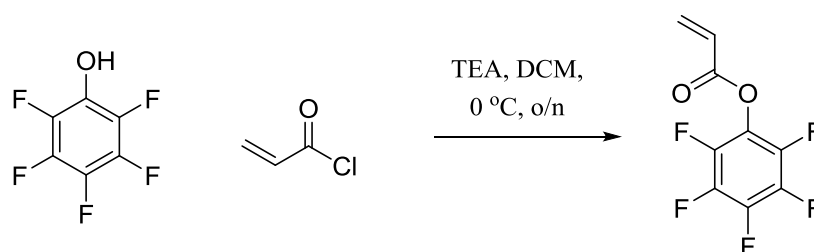


Figure 2.11. ^1H NMR (300 MHz) spectrum in CDCl_3 of the original **M 2.2** and the end product of the four reactions outlined in Table 2.2 focussing on the proton signal for the proton adjacent to the bromine. The integration of the peak remained constant with respect to the aromatic peaks of the monomer.

The pentafluorophenyl acrylate monomer, **M 2.3**, was synthesized through coupling of pentafluorophenol to acryloyl chloride (Scheme 2.7) following literature precedent.³⁶ The monomer was purified by column chromatography in petroleum ether to give a 47% yield. The ¹H and ¹⁹F NMR spectra can be seen in Figure 2.12. The ¹H NMR spectrum showed the expected chemical shifts, integration and splitting as previously reported.³⁶ The ¹⁹F NMR spectrum also showed the expected splitting with a coupling constant of ³J = 18.4 Hz.



Scheme 2.7. Synthetic route for **M 2.3**.³⁶

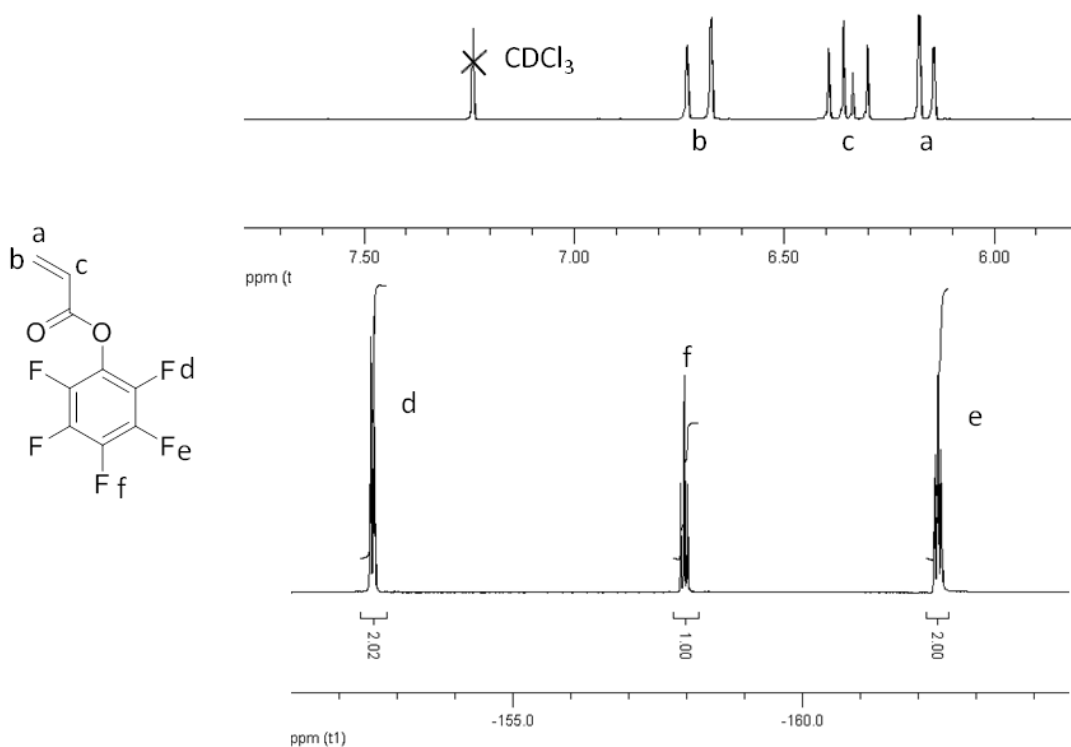


Figure 2.12. ^1H NMR (300 MHz) spectrum (top) and ^{19}F NMR (282 MHz) spectrum (bottom) of **M 2.3** in CDCl_3 .

Initially **M 2.3** was polymerized *via* RAFT with good control, $M_{n(\text{NMR})}$ 4.5 kDa $D_{(\text{SEC})}$ 1.09. The CTA used for the polymerization was 2-(dodecylthiocarbonothioylthio)-2-methylpropionic acid (DDMAT) with 0.1 equivalents of AIBN, in dioxane at a monomer concentration of 1 g mL^{-1} . The polymerization was heated at $80 \text{ }^\circ\text{C}$ for 2 hours to give 83% conversion by ^1H NMR spectroscopy. The ^{19}F NMR spectrum of **M 2.3** and poly(**M 2.3**) can be seen in Figure 2.13, where the slight shifts and broadening of the fluorine signals are indicative of polymer formation.

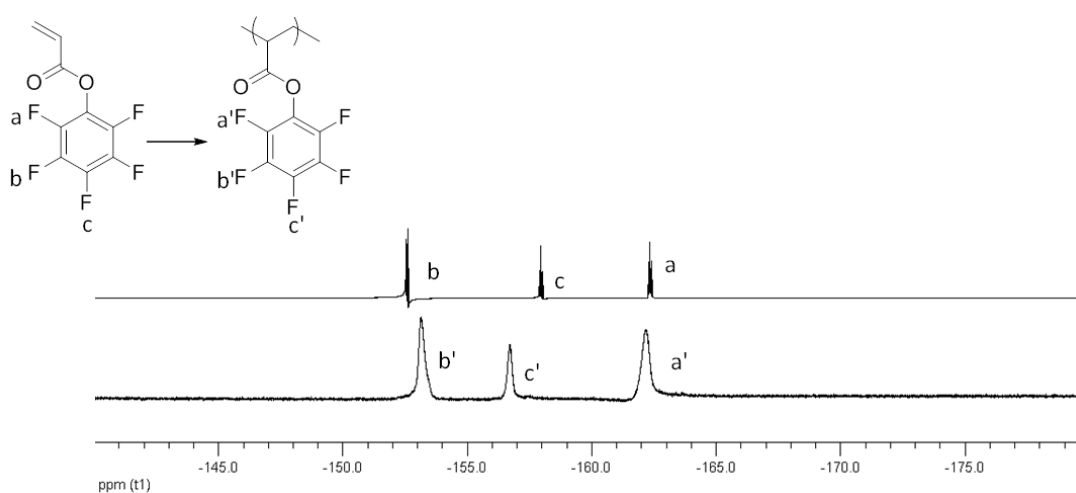


Figure 2.13. ^{19}F NMR (375 MHz) spectrum of **M 2.3** (top) and poly(**M 2.3**) (bottom) in CDCl_3 .

On exposure to nucleophiles (such as amines), the pentafluorophenol group can be substituted to give pentafluorophenol and a polymer with the desired, substituted functionality. Therefore, the primary amine of tryptophan (and indeed all amino acids) can be used in this substitution. By stirring the poly(**M 2.3**) scaffold overnight in THF with L-tryptophan methyl ester poly(**M 2.1**) was synthesized. The reaction was monitored by ^{19}F NMR spectroscopy which confirmed 100% substitution to poly(**M 2.1**). The starting and final ^{19}F NMR spectra for this reaction can be seen in Figure 2.14, the absence of polymer signals in the ^{19}F NMR spectrum indicate that no poly(**M 2.3**) remained. The ^1H NMR of the synthesized poly(**M 2.1**) can be seen in Figure 2.15, the broad signals correspond to those of tryptophan.

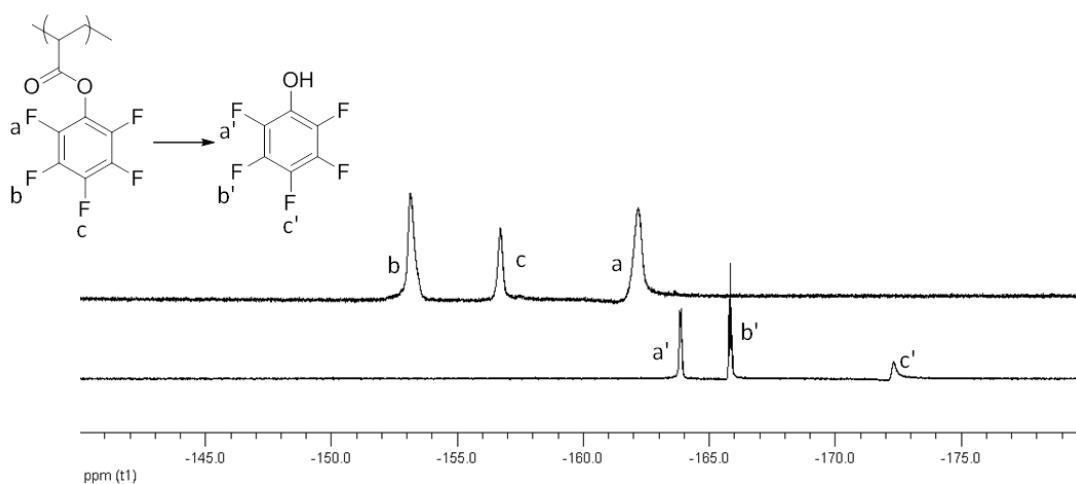


Figure 2.14. ^{19}F NMR (375 MHz) spectra of poly(**M 2.3**) before (top) and after substitution (bottom) in CDCl_3 .

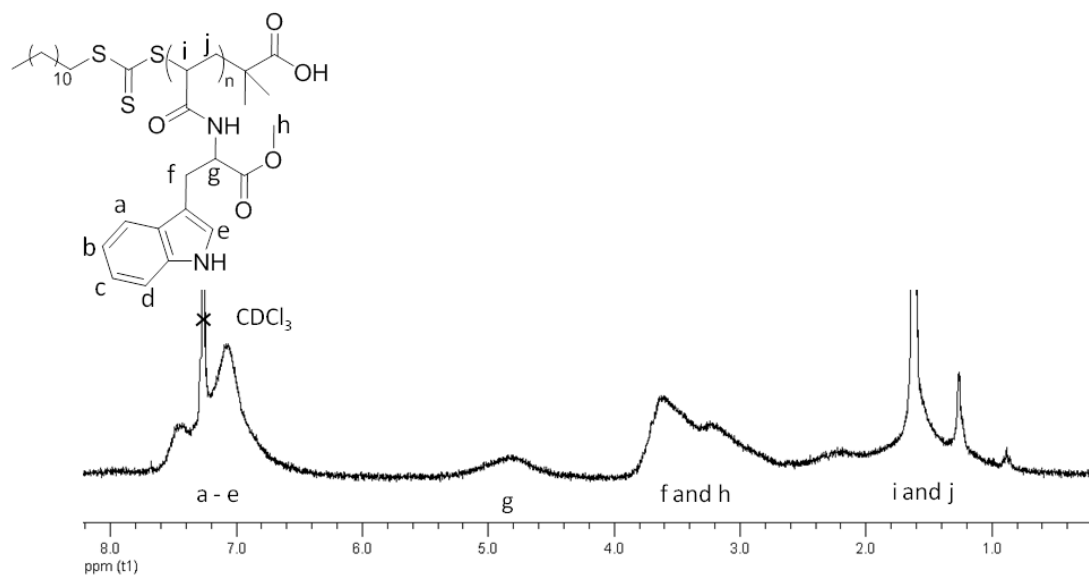


Figure 2.15. ^1H NMR (300 MHz) spectrum of poly(**M 2.1**) in CDCl_3

The SEC traces of poly(**M 2.3**) ($M_{n(\text{SEC})} = 2.5$ kDa, $D = 1.09$) and poly(**M 2.1**) ($M_{n(\text{SEC})} = 4.9$ kDa, $D = 1.11$) can be seen in Figure 2.16. Both show a narrow molecular weight distribution, although the two polymers were characterized using two different SEC set-ups due to the difference in solubility, poly(**M 2.3**) in CHCl_3 and poly(**M 2.1**) in DMF.

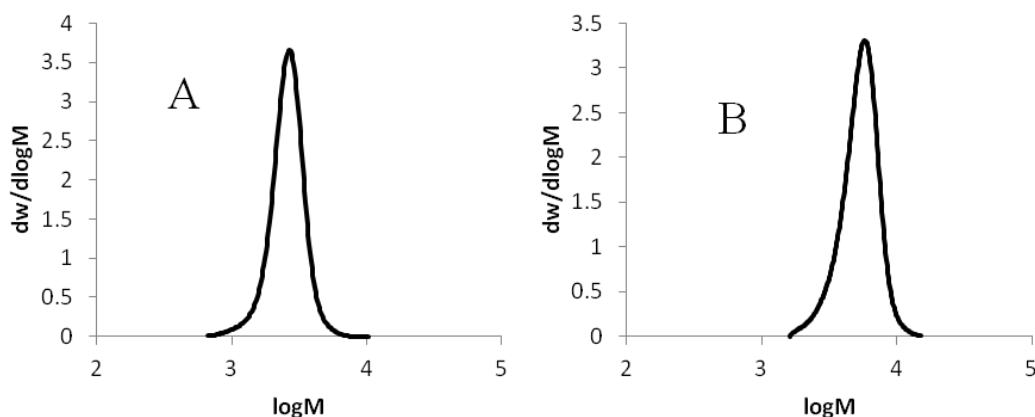


Figure 2.16. SEC traces of a) poly(**M 2.3**) in CHCl_3 and b) poly(**M 2.1**) in DMF.

Matrix-assisted laser desorption/ionization-time of flight (MALDI-ToF) analysis was used to confirm the successful substitution from poly(**M 2.3**) to the desired and well-defined poly(**M 2.1**) (Figure 2.17). Spectrum 1 in Figure 2.17 shows the anticipated spacing for a repeat unit of tryptophan and the other two spectra are the two main isotope patterns observed, here focused on DP 9. In all cases the RAFT end group was lost which has previously been observed. Müller *et al.* analyzed RAFT synthesized poly(*N*-isopropylamine) by MALDI-TOF, and whilst they observed the expected masses for retention of the RAFT end group, they also had disproportionation and transfer products.³⁷ Favier *et al.* also observed the C-S bond fragmentation within the spectrometer in their study of *N*-acryloylmorpholine polymers.³⁸ Spectrum 2 shows the main isotope pattern and corresponds to termination by a proton after the loss of the RAFT end group, structure B. Also observable in this spectrum is a small population caused by structure A. The other main isotope population can be seen in spectrum 3 and this is caused by structure C, a disproportionation product.

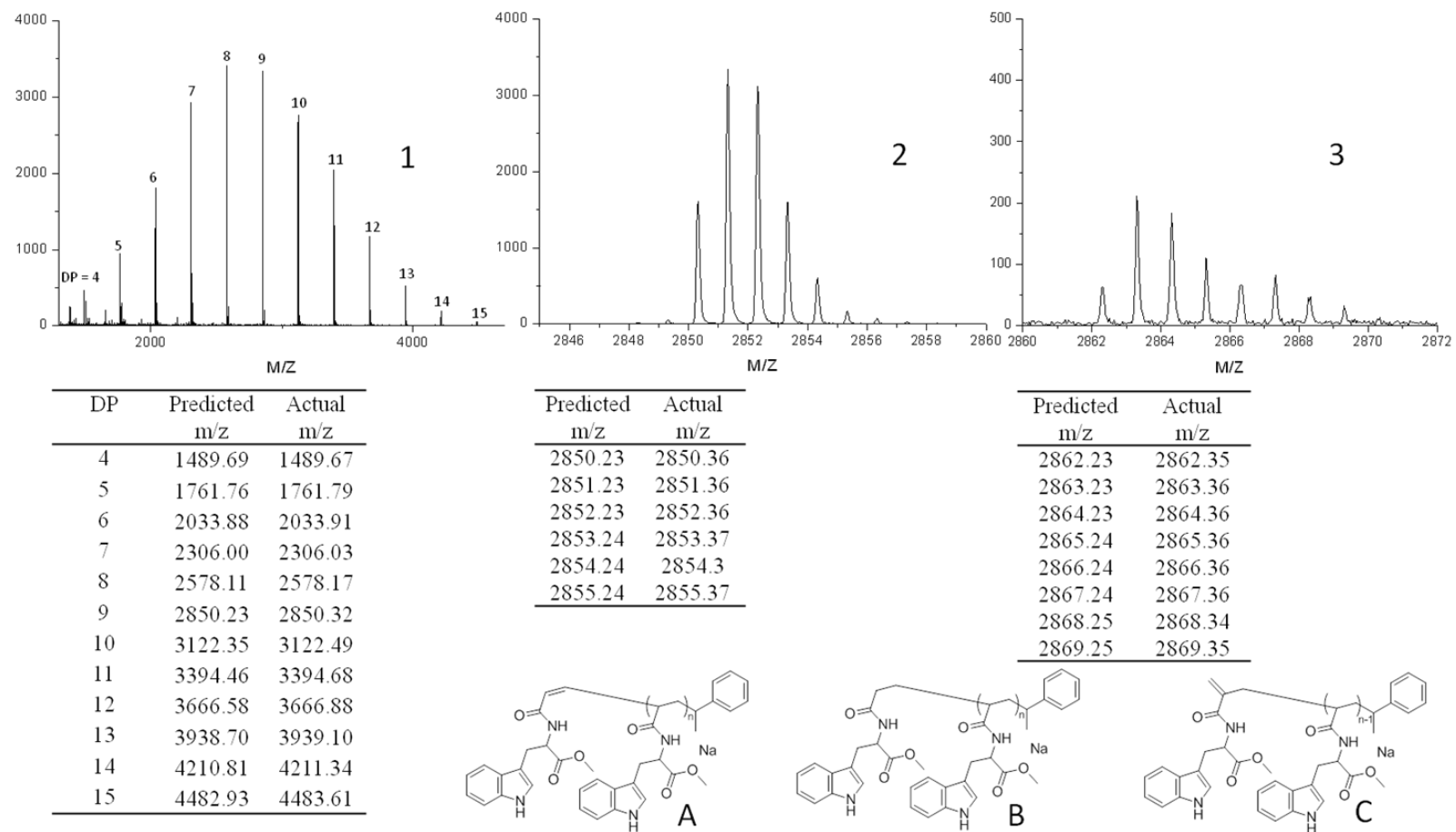


Figure 2.17. MALDI-TOF spectra of poly(M 2.1). MALDI-ToF was collected on poly(M 2.1) of DP 18 calculated from the ¹H NMR spectrum, using dithranol as a matrix and NaTFA as the cationizing agent.

The IR spectrum of the resulting polymer was also measured to rule out the possibility of the formation of poly(acrylic acid) (PAA) from reactions with water. This can be seen, along with poly(**M 2.3**) and **M 2.1**, in Figure 2.18. This would result in a strong peak around 1700 cm^{-1} , indicative of a carboxylic acid, which should be absent from the IR spectrum of **M 2.1**. The absence of such peaks confirms that PAA had not been synthesized. The IR spectrum of **M 2.3** shows the presence of an ester with the C=O and C-O at 1780 cm^{-1} and 1500 cm^{-1} respectively, these peaks are absent from the other two spectra. In poly(**M 2.1**) stretches for the C=O bond for both the amide (1660 cm^{-1}) and ester (1730 cm^{-1}) are present which match the stretches for these bonds in the monomer **M 2.1**. The formation of these new amide and ester peaks which are also seen in the monomer further confirms the successful synthesis.

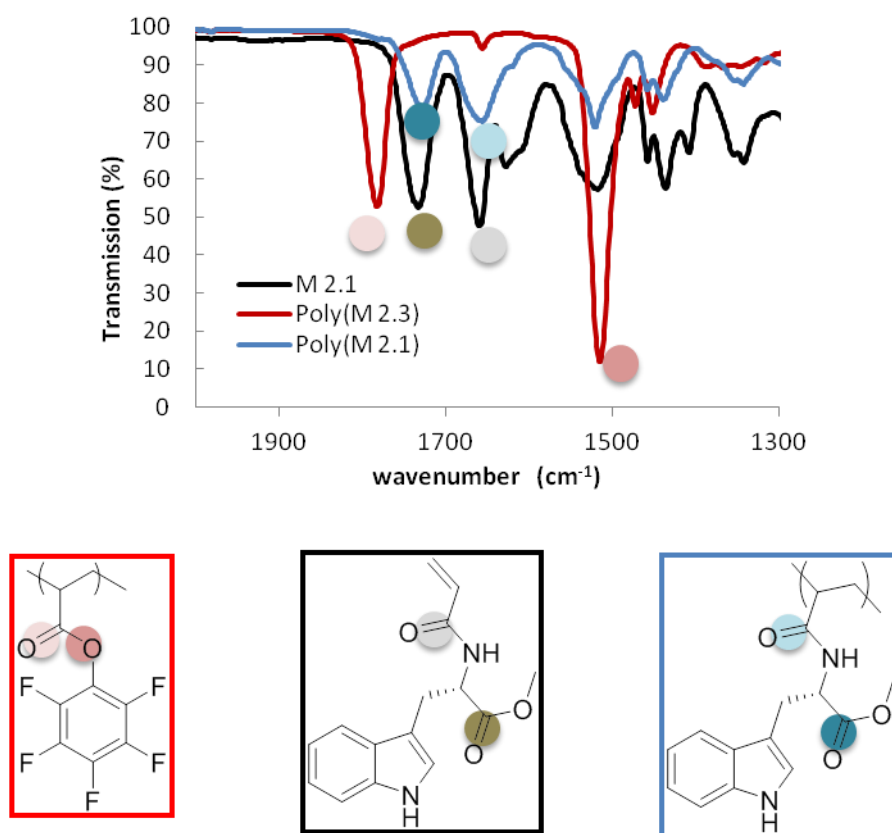
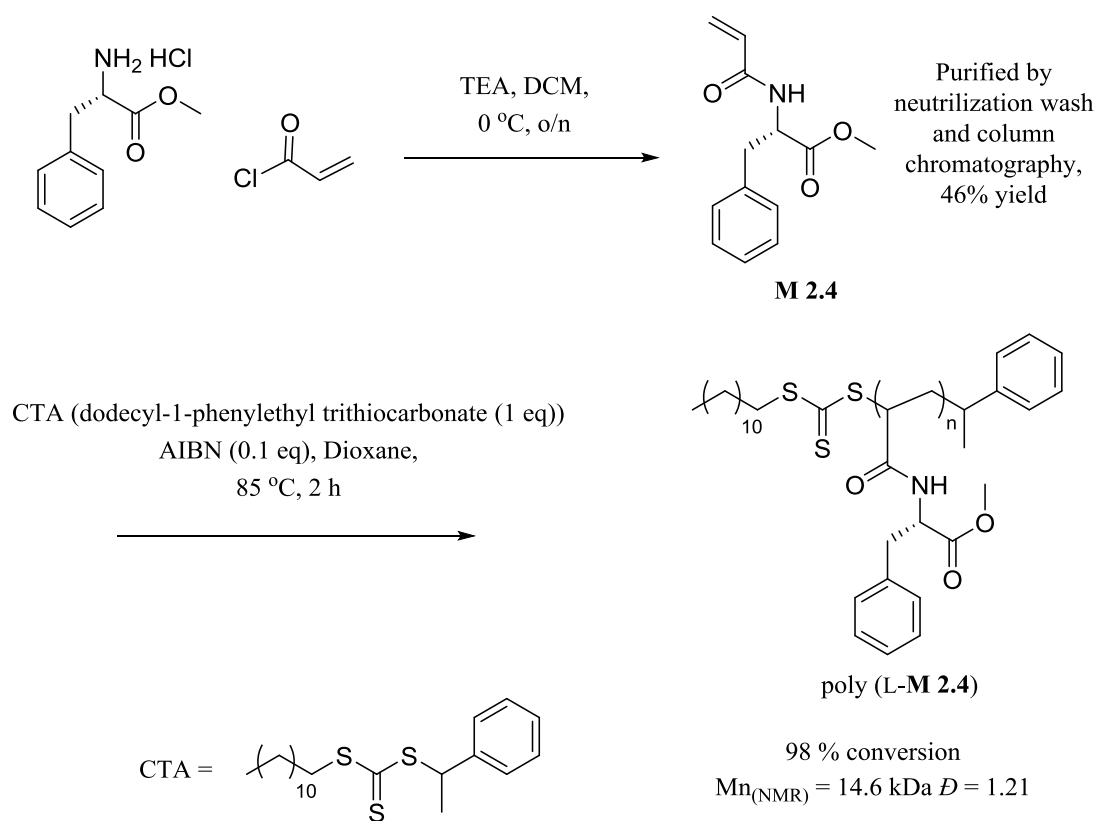


Figure 2.18. IR of **M 2.1**, poly(**M 2.3**), and poly(**M 2.1**).

2.3.4 Interaction between chiral monomers and BINOL

Utilizing the newly synthesized enantiomers of **M 2.1** and poly(**M 2.1**), the chiral interactions with BINOL have been investigated. For comparison the enantiomers of the monomer and polymer of the previously reported phenylalanine has also been investigated.³⁹ The L-phenylalanine monomer (**M 2.4**) and its corresponding polymer (poly(L-**M 2.4**)) were prepared using literature precedent as depicted in Scheme 2.8.³⁹ The monomer is prepared in a similar way to **M 2.1** and standard RAFT polymerization conditions used for the synthesis of the polymer.



Scheme 2.8. A schematic representation for the synthesis of L-**M 2.4** and poly(L-**M 2.4**).

The ^1H NMR spectrum of **M 2.4** can be seen in Figure 2.19 and gave the expected integration and chemical shifts. However, signals for proton **f** and proton **e** do not have the expected splitting of a doublet and triplet but rather appear as a triplet ($^3J = 5.5$ Hz) and a doublet of triplets ($^3J = 5.5$ Hz). This splitting has been rationalized as due to the chiral nature of the molecule protons **f** are diastereotopic.

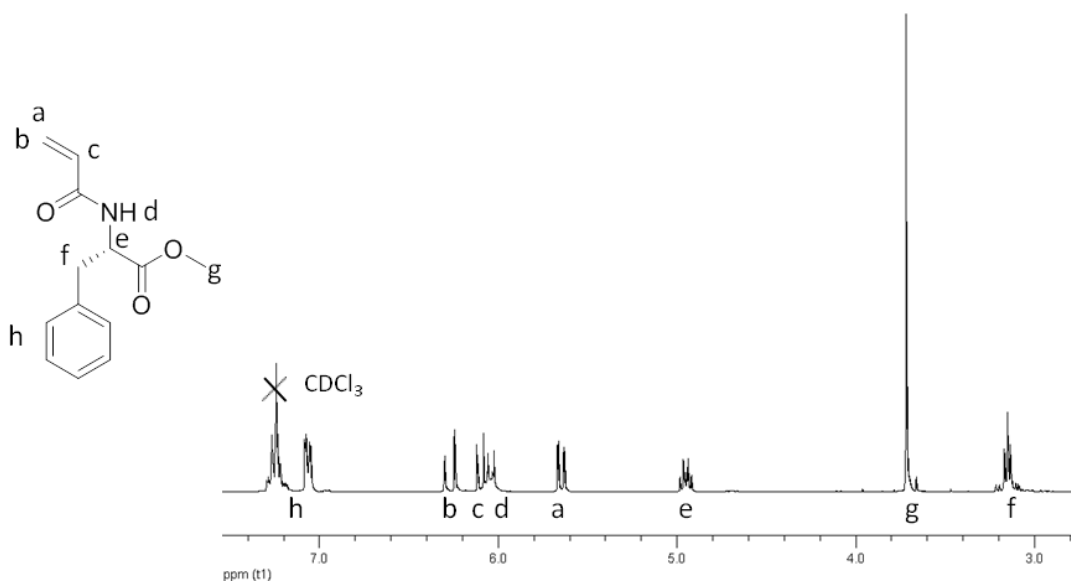


Figure 2.19. ^1H NMR (300 MHz) spectrum of L-**M 2.4** in CDCl_3 .

The interactions between BINOL and the enantiomers of **M 2.1** and **M 2.4** along with poly(L-**M 2.1**) and poly(L-**M 2.4**) have been investigated to determine if these chiral molecules exhibit preferential enantiomer interactions. The monomers, as opposed to the unmodified amino acids, were used to give a direct comparison to the polymers. A schematic of the various combinations can be seen in Figure 2.20.

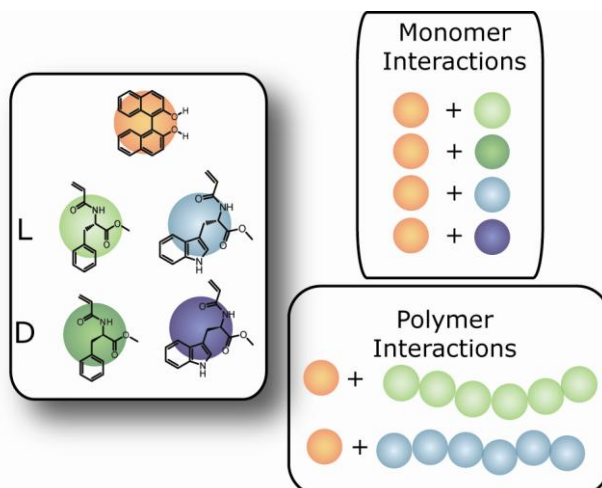


Figure 2.20. The monomers, polymers and their combinations with (*rac*)-BINOL.

The interactions have been studied using ^1H NMR spectroscopy (Figure 2.22) focussing on the phenolic peaks of (*rac*)-BINOL highlighted in Figure 2.21. All ^1H NMR spectroscopy experiments were conducted with 0.7 mL of CDCl_3 and 10 mg of (*rac*)-BINOL with the chiral substrates varied in order to achieve the desired loadings; typically at 1.0:1.0 mol ratio of monomer to polymer 9.5 mg of **M 2.1** and 8.5 mg **M 2.4** were required.

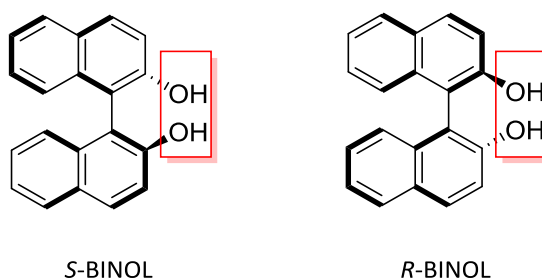


Figure 2.21. The chemical structure of the two enantiomers of (*rac*)-BINOL. The protons highlighted in the box are those used to examine the interactions.

Spectrum **A** (Figure 2.22) shows a ^1H NMR spectrum of (*rac*)-BINOL in CDCl_3 . There is a singlet peak at δ 4.90 ppm which corresponds to the phenolic protons. Spectra **B-E** are the various combinations with the enantiomers of **M 2.1** and **M 2.4**; the phenolic protons have been shifted downfield from 4.92 ppm to approximately 5.05 ppm and split in all four cases. The shift downfield indicates that there are intermolecular interactions between the monomers and the (*rac*)-BINOL. The magnitude of this shift differs between the two amino acids, with tryptophan (spectra **D** and **E**) shifting the peak *ca.* 0.04 ppm further compared to phenylalanine (spectra **B** and **C**) which has shifted the peak *ca.* 0.14 ppm from its initial position. The greater shift indicates a stronger interaction for tryptophan compared to phenylalanine.⁴⁰ Although the difference between the two amino acids is small compared to the amount that the BINOL peak has been shifted from its initial position. The other peak that can be seen in spectra **B – E** is a proton from the monomer which is highlighted within Figure 2.22.

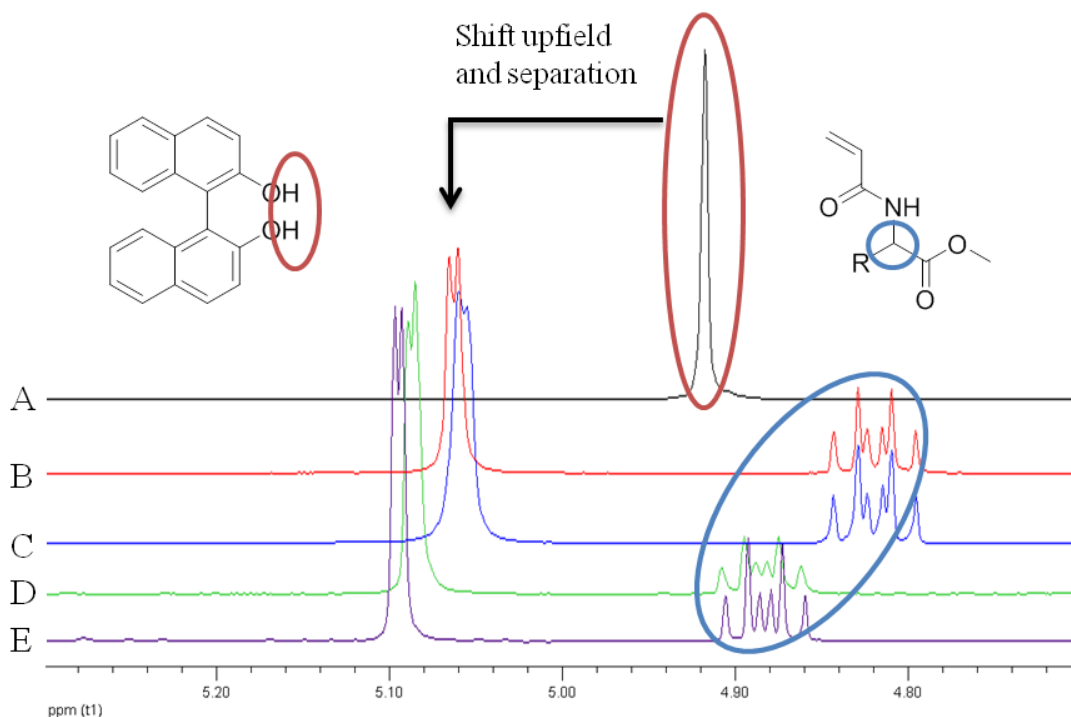


Figure 2.22. ^1H NMR (300 MHz) spectrum showing the interaction of the four monomers with (*rac*)-BINOL. a) (*rac*)-BINOL with no monomers; b) (*rac*)-BINOL + L-M **2.4**; c) (*rac*)-BINOL + D-M **2.4**; d) (*rac*)-BINOL + L-M **2.1** and e) (*rac*)-BINOL + D-M **2.1**. At 1.0:1.0 molar ratio of (*rac*)-BINOL:monomer in CDCl_3 .

Lu *et al.*²⁷ observed a similar ^1H NMR spectroscopic shift of the (*rac*)-BINOL signals between 0.15 and 0.25 ppm upon interaction with poly(acrylamides). Xu *et al.*⁴¹ also reported shifts of the (*rac*)-BINOL signals upon interaction with derivatives of the amino acids phenylalanine and alanine; although the shifts were slightly larger (between 0.17 and 0.35 ppm). The magnitude of the shift for **M 2.1** is of similar magnitude to those previously reported. The (*rac*)-BINOL peak has also been shifted 0.3 ppm on interaction with the monomer *N,N*-dimethylacrylamide at a 1.0:1.0 molar ratio. It is likely, therefore, that the acrylamide functionality is involved; however, the differing magnitudes of the shift when exposed to either phenylalanine or tryptophan indicate that the effect is not solely based on the acrylamide functionality.

The shift downfield is also coupled with a splitting of the (*rac*)-BINOL peak. This is attributed to the different enantiomers of (*rac*)-BINOL having different affinities to the chiral amino acid monomers. Further experiments with L-**M 2.4** highlighted that the molar ratio of (*rac*)-BINOL to the monomer (1.0:0.6-2.4) in the mixture was crucial in order to get clear separation between the two enantiomers (Figure 2.23).

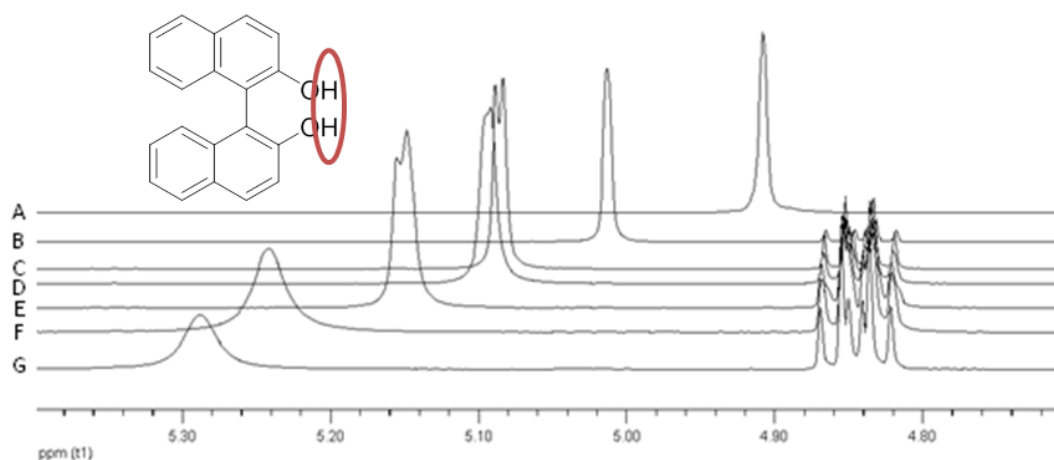


Figure 2.23. ^1H NMR (300 MHz) spectrum showing the effect of altering the molar ratios of (*rac*)-BINOL and L-**M 2.4**. a) (*rac*)-BINOL with no added monomer; b) (*rac*)-BINOL: L-**M 2.4** 1.0:0.6; c) 1.0:1.0; d) 1.0:1.2; e) 1.0:1.5; f) 1.0:1.9 and g) 1.0:2.4 in CDCl_3 .

When (*rac*)-BINOL is in higher concentration (2.0:1.0 (*rac*)-BINOL: monomer, spectrum **B** in Figure 2.23), no splitting of the phenolic signals is observed. Where the amount of monomer exceeds (*rac*)-BINOL by either a small amount (**D**) or a much larger amount (**E**) the splitting is evidenced as a shoulder peak. The highest degree of splitting can be seen when the ratio is close to 1.0:1.0, spectrum **C**. As more monomer is added, the (*rac*)-BINOL-OH peak is shifted further downfield but the splitting becomes unobservable as the peak broadens.

To investigate the relationship between the enantiomers of the amino acids and (*rac*)-BINOL a racemic mixture comprised of partially deuterated (*R*)-BINOL was used. This was synthesized by dissolving (*R*)-BINOL in CHCl_3 and stirring vigorously with D_2O before removing the solvents; repeating this process three times gave a sample with 20% deuteration compared to a non-deuterated sample. This was measured by comparing the relative integration of the phenolic protons to the aromatic group which can be seen in Figure 2.24; the presence of deuterium instead of hydrogen on the phenol groups of BINOL will lead to a decrease in signal intensity in the ^1H NMR spectrum for the same mass.

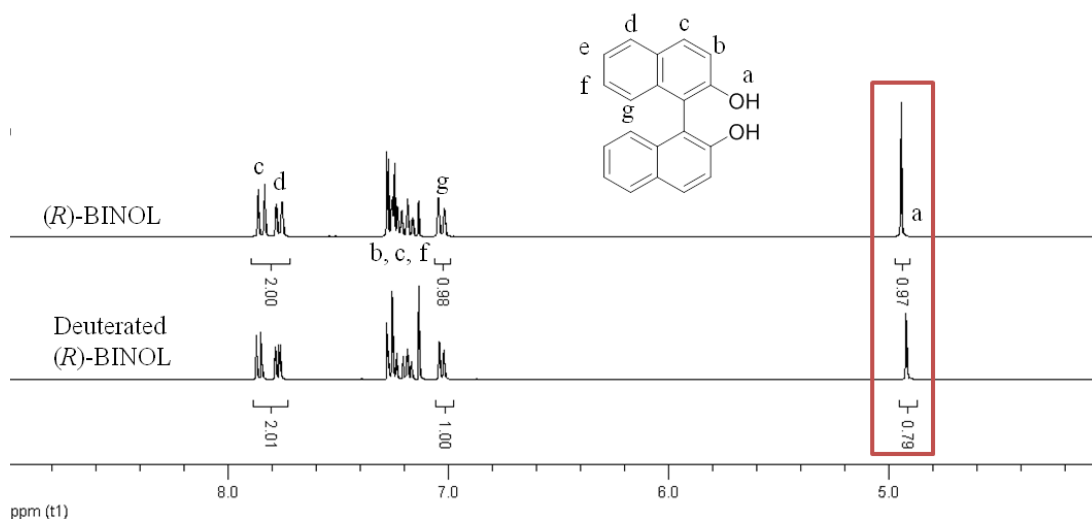


Figure 2.24. ^1H NMR (300 MHz) spectrum of (*R*)-BINOL before and post exposure to D_2O in CDCl_3 . The phenolic peaks have been highlighted with the relative integration falling from 0.97 in the (*R*)-BINOL ^1H NMR spectrum to 0.79 in the deuterated (*R*)-BINOL ^1H NMR spectrum.

A (*rac*)-BINOL sample was then prepared using equal amounts of non deuterated (*S*)-BINOL and the part deuterated (*R*)-BINOL. The experiments previously described were then repeated using this new (*rac*)-BINOL mixture (Figure 2.25). Once again the

splitting of the peaks were observed across the series of spectra; however, as the two separated peaks are unequal in size due to the deuterated (*R*)-BINOL the (*rac*)-BINOL enantiomers can be determined. There is a clear trend in the positioning of the (*rac*)-BINOL enantiomers: the L- amino acids (spectra **A** and **C**) have caused a greater shift for (*S*)-BINOL, with the reverse being true for the D- amino acids (spectra **B** and **D**): a clear demonstration that different sets of enantiomers have different strength interactions.

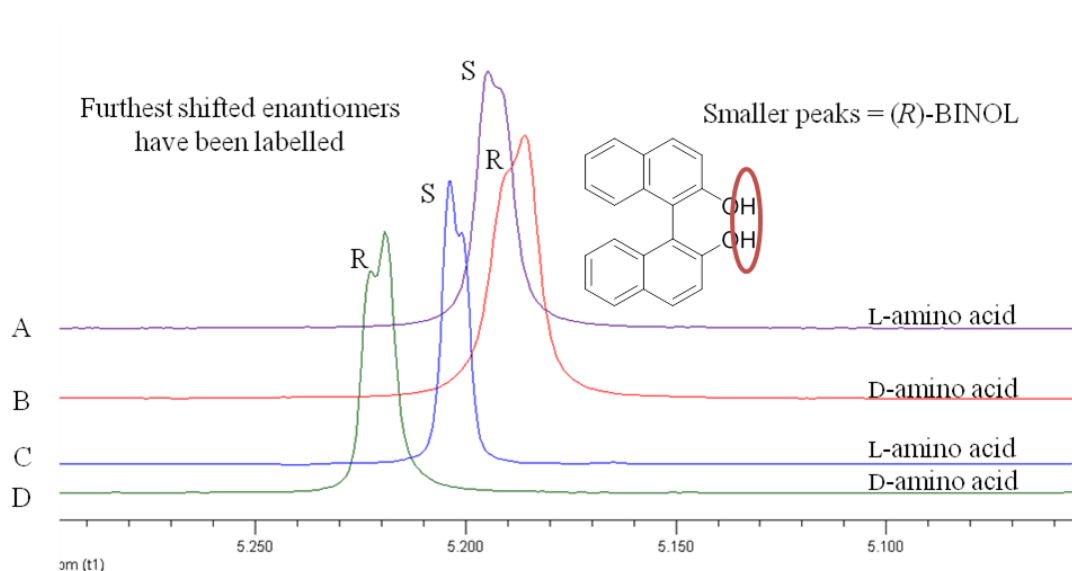


Figure 2.25. ^1H NMR (300 MHz) spectrum showing the interaction of (*rac*)-BINOL with part deuterated (*R*)-BINOL with (A) L-**M 2.4**; (B) D- **M 2.4**; (C) L-**M 2.1** and (D) D- **M 2.4** in CDCl_3 . The furthest shifted enantiomer has been labelled as either (*R*)- or (*S*)- BINOL and the spectra have been labelled to indicate if the monomer is either L- or D-.

Mikhalev *et al.* have performed similar interaction studies using (*S*)-BINOL. They did not focus on the shift of the (*S*)-BINOL but rather on the additive; using (*S*)-BINOL and a racemic mixture of substrate it was possible to determine enantiomeric excess.⁴² They were able to perform this for a range of substrates including pantalactone.

Hence the racemic monomers of phenylalanine were investigated with either (*S*)- or (*R*)-BINOL at a molar ratio of 2.0:1.0 ((*rac*)-**M 2.4**: BINOL) (Figure 2.26), which is the ratio used in the report by Mikhalev. This then gives a ratio of 1 BINOL molecule to 1 L- **M 2.4** to 1 D- **M 2.4**.⁴² It appears that two doublets of triplets are formed at the CH chiral centre in the monomer and both have shifted slightly upfield by *ca.* 0.003 ppm on mixing with either (*R*)-BINOL, spectrum B, or (*S*)-BINOL, spectrum C. This peak has been separated out into its two constituent peaks demonstrating that different interactions are occurring between the L- and D- enantiomers of **M 2.4** and the enantiomers of BINOL. The peak is split into two triplets as it couples to the diastereotopic CH₂ protons. On separation these two triplets are effectively being split into four triplets producing a complicated signal. That the peak is being separated makes it apparent that (*S*)-BINOL is interacting to different extents with the L-**M 2.4** and D-**M 2.4** monomers.

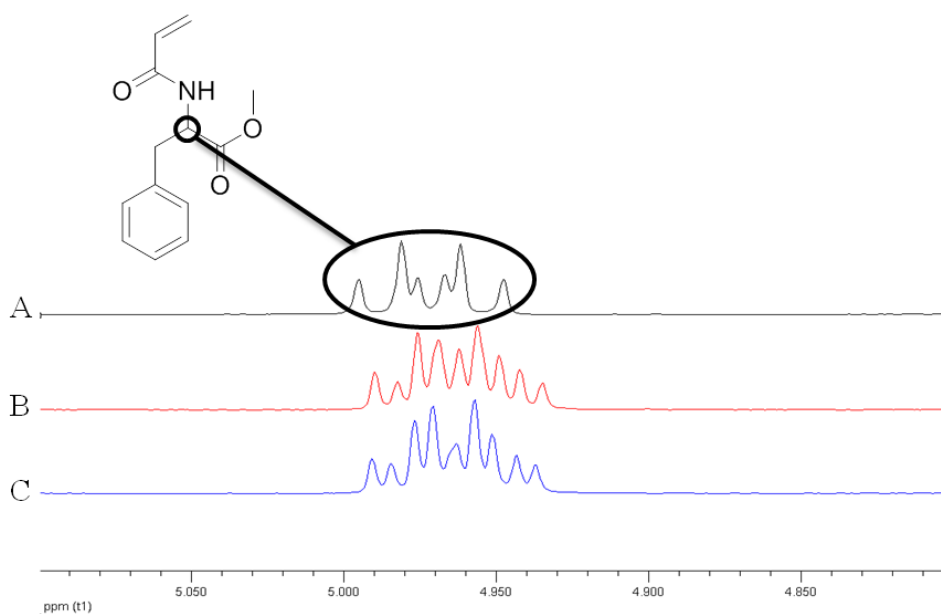


Figure 2.26. ¹H NMR (300 MHz) spectrum of a racemic mixture of **M 2.4** with a) no added BINOL b) (*R*)-BINOL added and c) (*S*)-BINOL added at a molar ratio of 2:1 aligned to CDCl₃.

Each of the doublets of triplets were then assigned by examining (*S*)-BINOL with each of the enantiomers of phenylalanine separately at a 1.0:1.0 molar ratio. A dichloromethane (CH_2Cl_2) spike was used as an internal standard in these experiments to confirm the assignments (Figure 2.27).

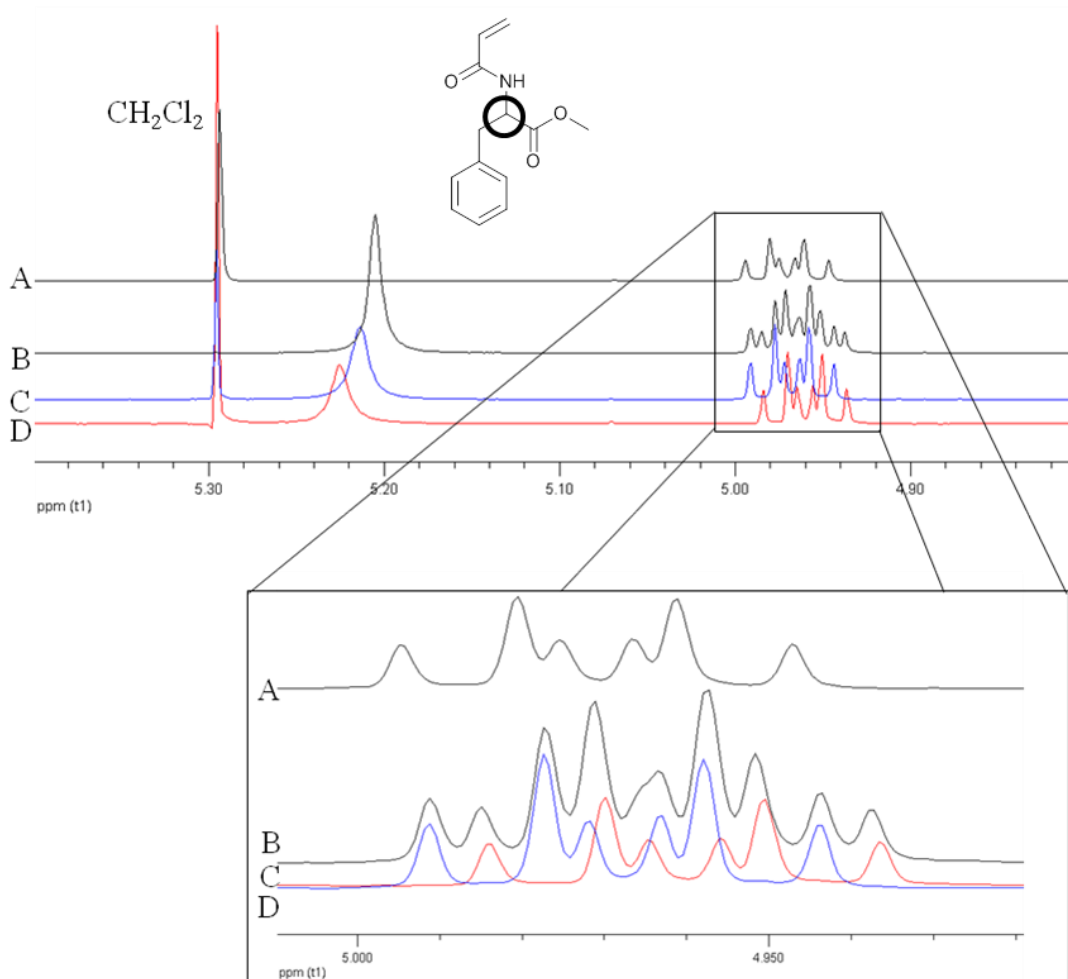


Figure 2.27. ^1H NMR (300 MHz) spectra of (*S*)-BINOL with b) racemic **M 2.4** c) D-**M 2.4** (blue line) d) L-**M 2.4** (red line) all with CH_2Cl_2 as an internal standard and a) racemic **M 2.4** as a standard in CDCl_3 .

With comparison to the racemate (Figure 2.27, spectrum A) the CH signal from the monomer has been shifted upfield (by *ca.* 0.003 ppm), with the L-**M 2.4** being shifted upfield by the greatest amount (spectrum D). This suggests that L-**M 2.4** has the

strongest interaction. Once again evidence that different sets of enantiomers are interacting with different strengths. Both experiments have shown that (*S*)-BINOL has a stronger interaction with the L- amino acids over the D- amino acids.

L-tryptophan and L-phenylalanine are the (*S*)-enantiomers and therefore in this work there is a preference for like-for-like chiral interactions with (*rac*)-BINOL. Interestingly, upon comparison with the literature there seems to be a trend as to which enantiomers are likely to have the preferred interactions. Lu *et al.*,²⁷ Redondo *et al.*³¹ and Mikhalev *et al.*⁴² all observe a like-for-like interaction with BINOL and a different enantiomeric pair; the preferred interaction being determined by noting which enantiomer has shifted the greatest extent in the ¹H NMR spectrum. Whereas Skey *et al.*,¹⁰ who studied the same enantiomers (L-phenylalanine to resolve L- and D-phenylalanine) observed the opposite enantiomer interaction with L- and D- having the greatest affinity.

2.3.5 Interactions between chiral polymers and BINOL

Having studied the interactions between the L-tryptophan containing monomer (**M 2.1**) and the L-phenylalanine containing monomer (**M 2.4**) their corresponding polymers were also examined, in the same manner, with (*rac*)-BINOL. The ^1H NMR spectra of this study can be seen in Figure 2.28.

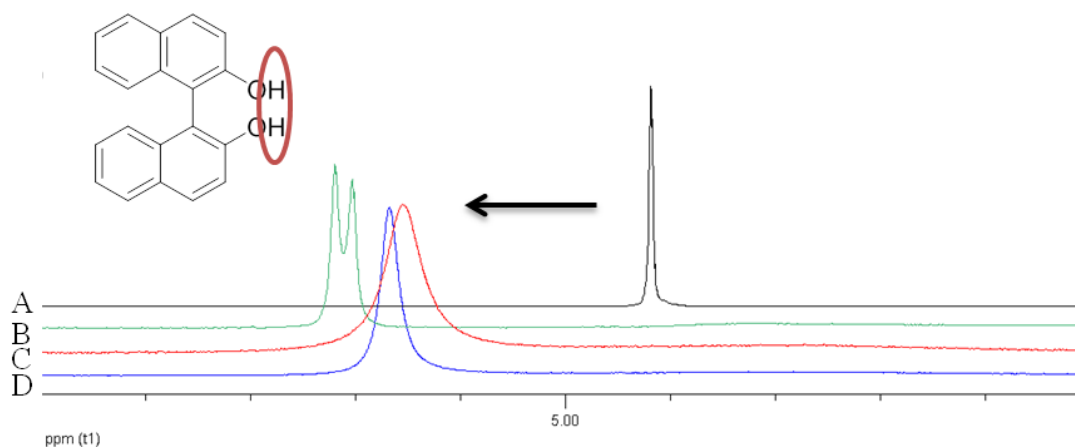


Figure 2.28. ^1H NMR (300 MHz) spectra of a) (*rac*)-BINOL at a 1.0:1.0 ratio of (*rac*)-BINOL to residues with polymers with b) poly(L-**M 2.4**)(DP 38) and c) poly(L-**M 2.1**) (DP 150) and d) poly(L-**M 2.1**) (DP 66) in CDCl_3 .

These ^1H NMR spectra confirm that the (*rac*)-BINOL-amino acid interaction is also observed with the polymeric systems as the (*rac*)-BINOL peak is shifted downfield by around 0.15 ppm. The different strength interactions between enantiomers is observed for the poly(L-**M 2.4**) (**B**) but is absent for the poly(L-**M 2.1**) (**C-D**). It is likely that this still exists, however, but as was shown with the monomer, in order to observe clear splitting the ratio has to be close to 1.0:1.0, which is more difficult to calculate for the polymers due to not having an absolute molecular weight and dispersity. This problem has also been noted in work conducted since by De *et al.* who synthesized a polymer

from the amino acid L-leucine and examined its effects with (*rac*)-BINOL.³ They too noted a difficulty in observing the separation when the ratio was not exactly 1.0:1.0, a difficult achievement with polymeric samples. This separation may potentially be improved by conducting the experiments on an NMR instrument with a stronger magnetic field.

The ratio of polymer to (*rac*)-BINOL was also altered (1.0:0.8-1.1) (Figure 2.29) in order to try and separate out the (*rac*)-BINOL peak. Unfortunately this was unsuccessful with the (*rac*)-BINOL peak shifting to a higher ppm (4.92 ppm to approximately 5.05) but remaining as one peak.

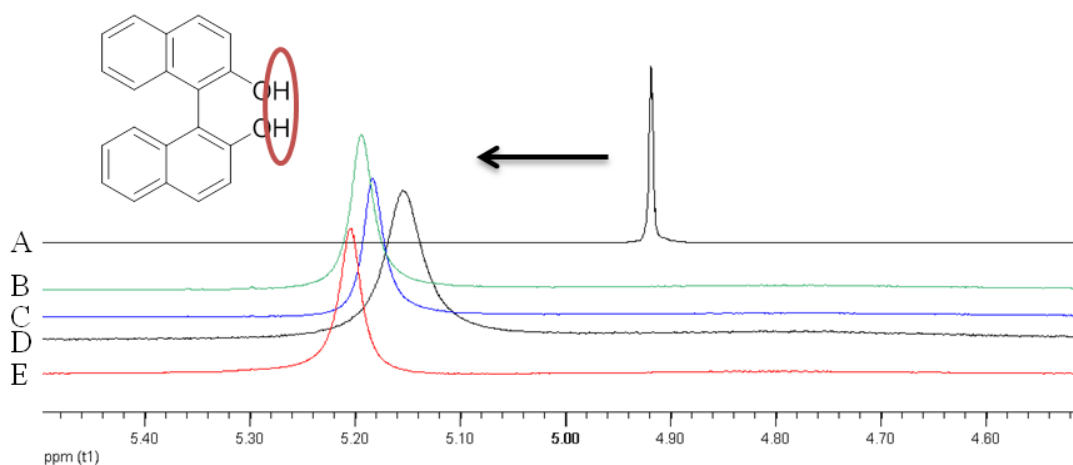


Figure 2.29. ¹H NMR (300 MHz) spectra of a) (*rac*)-BINOL and poly(L-**M 2.1**) (DP 150) polymer at varying ratios of residue: (*rac*)-BINOL of b) 1.0:0.8, c) 1.0:0.9 d) 1.0:1.0 and e) 1.0:1.1 in CDCl₃.

The interaction has also been studied with variable temperatures (198 – 318 K) (Figure 2.30) again monitoring the phenolic (*rac*)-BINOL protons with poly(L-**M 2.4**). At lower temperatures (198 K) the interaction is the strongest with the peak being shifted the

furthest from 4.92 ppm to 5.17 ppm; an anticipated result as with increasing temperature the molecule motion begins to overcome the intermolecular interactions.

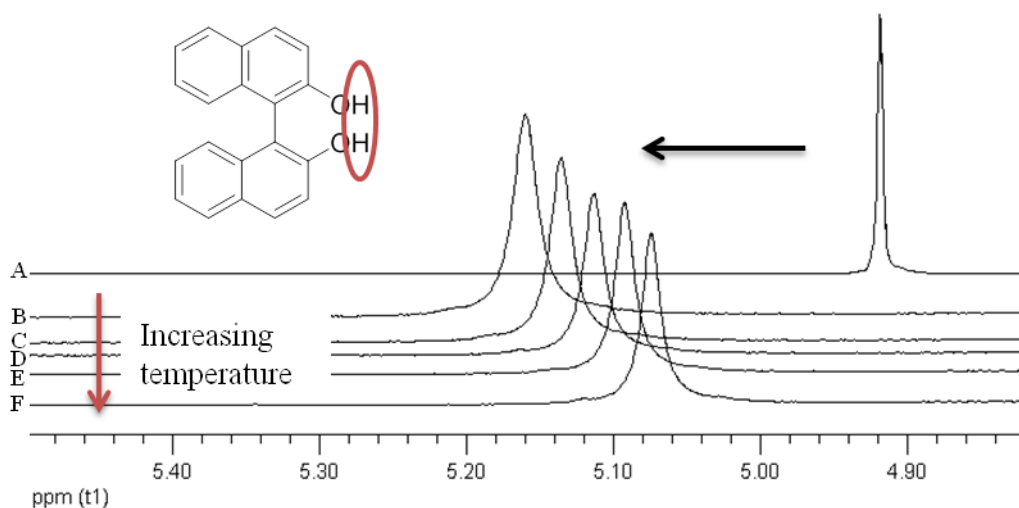


Figure 2.30. ^1H NMR (300 MHz) spectrum of a) (*rac*)-BINOL and the spectra showing the interactions of (*rac*)-BINOL with poly(L-M **2.4**) varies with temperature b) 198 K c) 303 K d) 308 K e) 313 K f) 318 K in CDCl_3 .

The polymers in solution were studied by circular dichroism (CD) analysis. The CD of poly(L-M **2.4**) has previously been studied.¹⁰ The CD of poly(L-M **2.1**) can be seen in Figure 2.31, demonstrating that the polymer has chiral properties as an absorbance was observed. The CD spectrum has similar characteristics to that reported by Mori in the range that was recorded.¹⁴ The peak observed at 230 nm can be attributed to the $\pi_1 \rightarrow \pi^*$ transition of the amide chromophore.

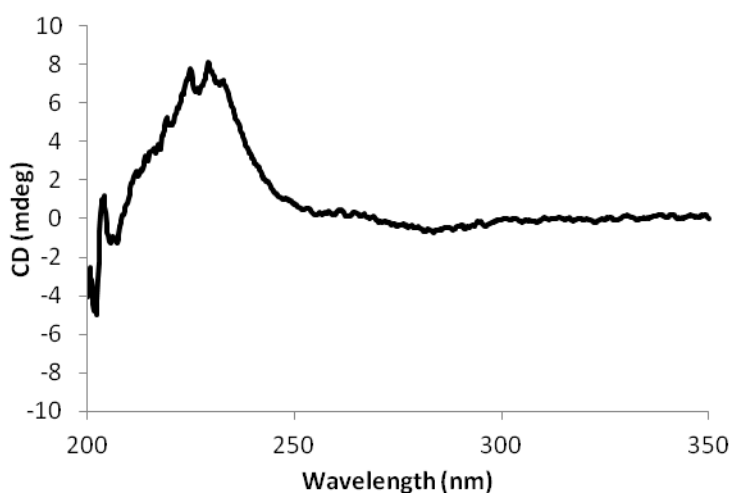


Figure 2.31. CD spectrum of poly(**M 2.1**) at 1 mg mL^{-1} in dioxane measured in a 0.1 mm cell.

CD analysis has also been used to confirm the interactions between (*rac*)-BINOL and the monomers. On addition of (*rac*)-BINOL to **M 2.1** there is a decrease in intensity and a shift to a higher wavelength, which demonstrates that there is an interaction involving the amide altering its absorbance profile.⁴³

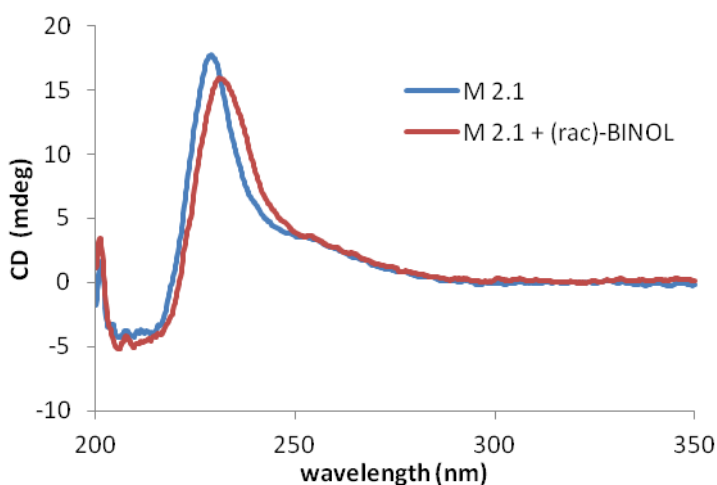


Figure 2.32. CD spectra of 1 mg mL^{-1} **M 2.1** in 0.1 mm cell in dioxane (blue line) and the same sample with 0.01 mL of 1 mg mL^{-1} (*rac*)-BINOL in dioxane (red line).

2.3.6 Physical Separation

Whilst it has been demonstrated that the enantiomers of (*rac*)-BINOL have different strength interactions with the enantiomers of the amino acids phenylalanine and tryptophan, it has not been possible to physically separate out the enantiomers. A report by Deng *et al.* in 2013 demonstrated how a chiral amphiphilic polymer co-network (APCN) that incorporated an amino acid monomer (not dissimilar to those used here) was able to provide enriched solutions of the enantiomers of proline.⁴⁴ To achieve these enriched solutions both enantiomers were absorbed into the chiral-APCN and then soaked in ethanol (EtOH) to draw the enantiomers out. The EtOH solution was tested periodically with polarimetry to determine the relative amounts of enantiomer. A reproduction of an overview of their work along with the data of the proline enantiomer release can be seen in Figure 2.33.

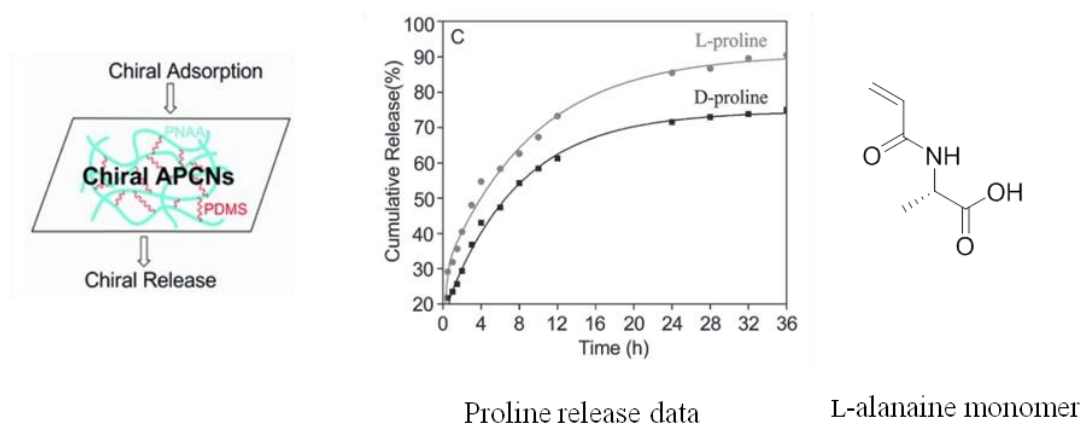
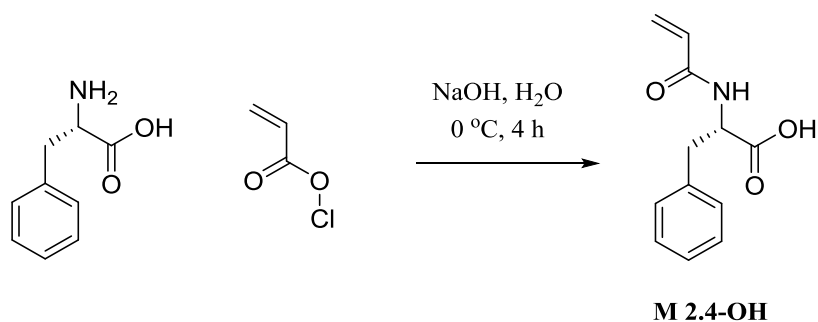


Figure 2.33. A reproduction of the TOC of Deng *et al.* work along with the release data for the proline enantiomers from their chiral-APCN and the structure of the L-alanine monomer used in this work.

Their chiral-APCN was synthesized from a monomeric version of the amino acid L-alanine and a modified poly(dimethyl siloxane) (**M-PDMS**) monomer. With reference

to Figure 2.33 the release data from this chiral-APCN shows greater expulsion of the L-proline enantiomer compared to D-proline over time as measured by polarimetry; the slower clearance of the D-enantiomer suggests a stronger interaction with the L-alanine incorporated into the chiral-APCN.

Therefore this system was investigated as a potential route to provide enriched solutions of (*rac*)-BINOL by immobilizing a monomeric version of the amino acid phenylalanine into an APCN. The phenylalanine monomer used here is very close to the monomer used previously (**M 2.4**) but in order to try and repeat Deng *et al*'s work as closely as possible a monomeric version that retained the free carboxylic acid was synthesized (**M 2.4-OH**). The synthetic route can be seen in Figure 2.9, the monomer was isolated by acidification of the solution resulting in a white precipitate which was collected to give a 69% yield.



Scheme 2.9. The synthetic route to **M 2.4-OH**.

The ^1H NMR spectrum of **M 2.4-OH** can be seen in Figure 2.34 which gave expected integration and chemical shift. However, signals for proton **e** and proton **g** do not have the expected splitting of a doublet and triplet but rather appear as a multiplet and two

doublet of doublets ($^3J = 3.6, 10.8$ Hz). This splitting has been rationalized as due to the chiral nature of the molecule proton **g** is diastereotopic resulting in two signals and a more complex splitting pattern; as **g** couples to both proton **e** and the other CH₂ proton and **e** couples to both the diastereotopic **g** protons with different coupling constants.

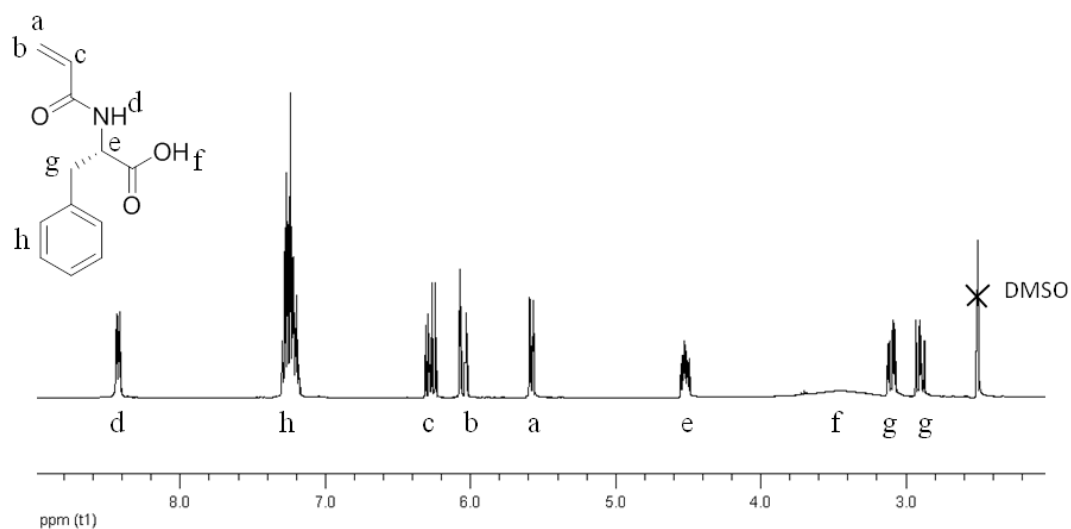
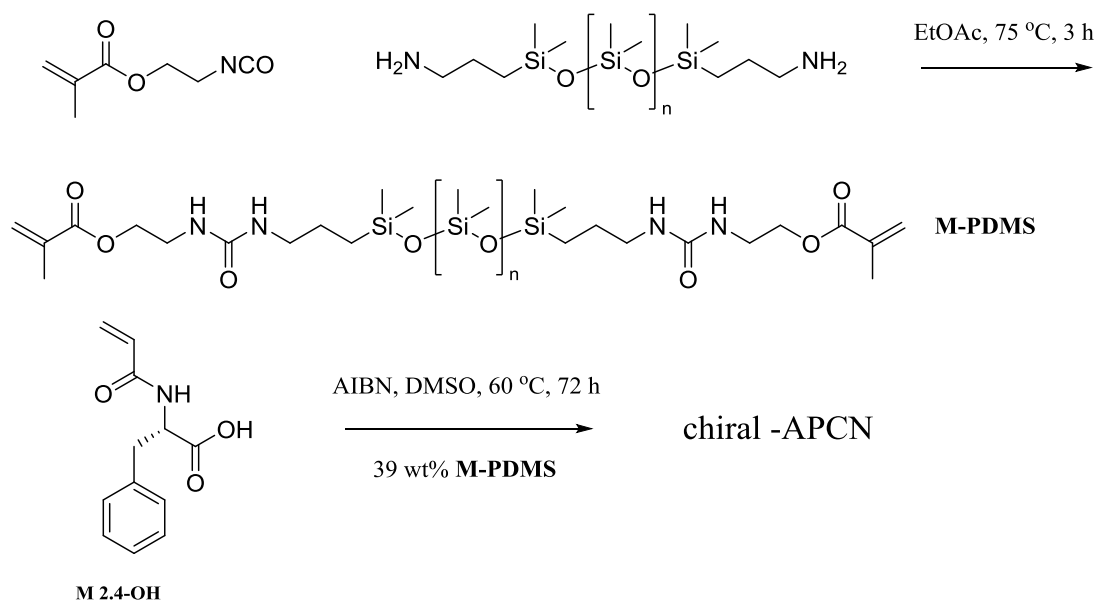


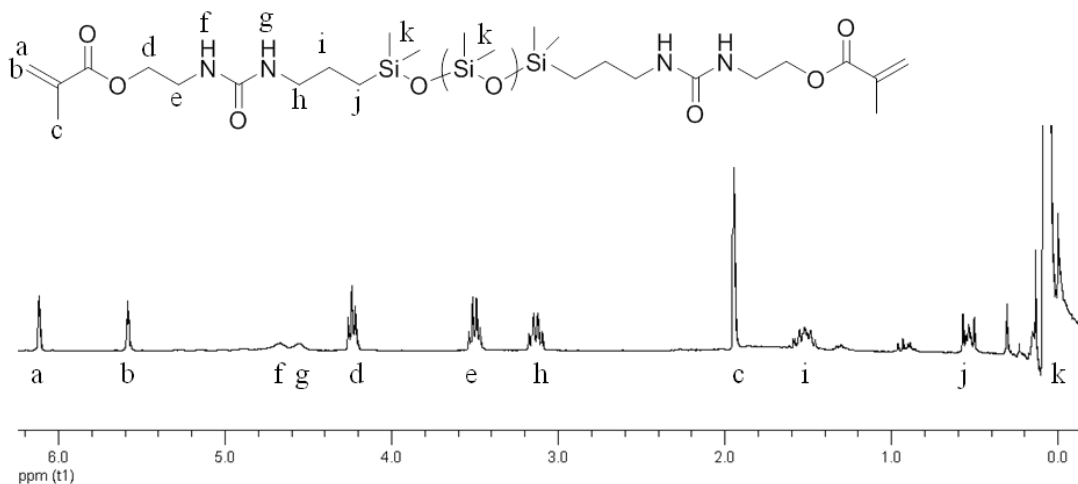
Figure 2.34. ¹H NMR spectrum (300 MHz) of **M 2.4-OH** in DMSO.

The synthesis of the cross-linking monomer **M-PDMS** and the chiral-APCN can be seen in Scheme 2.10.



Scheme 2.10. The synthetic route to a chiral APCN including the synthesis of the cross-linker.

The ^1H NMR spectrum for the synthesized **M-PDMS** can be seen in Figure 2.35 which gave expected chemical shifts, integration and splitting.

Figure 2.35 ^1H NMR (300 MHz) spectrum for the synthesized monomer **M-PDMS** in CDCl_3 .

The synthesized chiral-APCN was purified by washing with THF and water to remove any unreacted monomer before drying under vacuum and then analyzed by IR (Figure 2.36). The IR spectrum is dominated by the strong peaks arising from the silicon backbone of the **M-PDMS** at 1259 cm^{-1} , 1018 cm^{-1} and 794 cm^{-1} . The carbonyl region ($1750\text{ cm}^{-1} - 1400\text{ cm}^{-1}$) has multiple overlapping absorptions from the amides, esters and carboxylic acids from the monomers. A faint OH stretch can be seen (2529 cm^{-1}) arising from the **M 2.4-OH** monomer, and NH stretches from the amides can be seen at 3356 cm^{-1} .

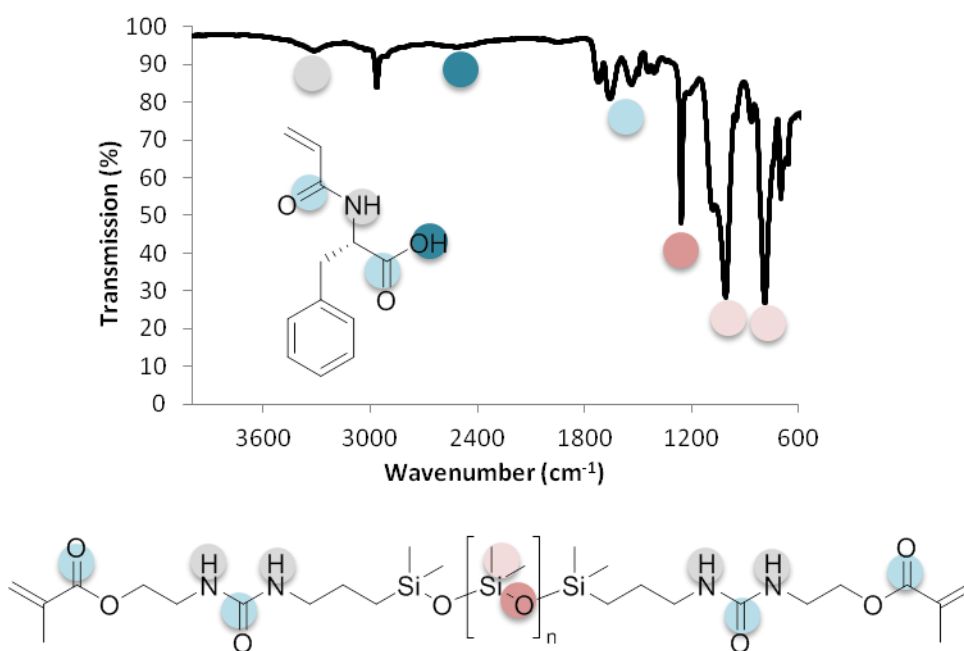


Figure 2.36. IR of the chiral-APCN with peaks from the two monomers highlighted.

The synthesized chiral-APCN (61 wt% **M 2.4-OH**, assuming 100% conversion of monomer) was then saturated with a (*rac*)-BINOL solution in THF at a molar ratio of 1.0:1.0 (*rac*)-BINOL to **M 2.4-OH**. After the majority of the THF solution had been

absorbed, further THF was added in order to extract the (*rac*)-BINOL in a washing process. The results of the experiment can be seen in Table 2.3.

With reference to Table 2.3, the ratio of (*S*)-BINOL in the starting material was found to be 46% by chiral-HPLC. The remaining (*rac*)-BINOL THF solution that was not absorbed by the chiral-APCN was analyzed to ascertain if unequal amounts of enantiomers were absorbed by the chiral-APCN (THF after absorption). This value, along with the starting value of 46% (*S*)-BINOL was then used to calculate the amount of (*S*)-BINOL within the chiral-APCN (ratio inside chiral-APCN).

Table 2.3. The results of the ratio of (*S*)-BINOL to (*R*)-BINOL in various samples before exposure to the chiral APCN and at extractions afterwards.

Sample	(<i>S</i>)-BINOL (%)^a run 1	(<i>S</i>)-BINOL (%)^a run 2
(<i>rac</i>)-BINOL	46	46
THF after absorption	48	45
Ratio inside chiral-APCN	44	47
1st extraction	48	49
2nd extraction	49	48
3rd extraction	55	49

^aDetermined by chiral HPLC

For these experiments chiral HPLC was used to determine the relative ratios of (*rac*)-BINOL in solution whereas the previous worked relied on a polarimeter. Unfortunately,

the significance of these results is very low with the percentage changes very small and within error. These could not be improved upon with changing the molar ratios between (*rac*)-BINOL and the stationary chiral phase. As from the ^1H NMR spectroscopy experiments the interactions of the enantiomers are very similar in strength and therefore perhaps unsurprising that they were unable to be separated out in this manner. Further studies in this area could concentrate on altering the solvents for loading and release, studying the effect of pH and changing the loading of chirality within the APCN.

2.4 Conclusions

The acrylamide monomer of tryptophan has been synthesized following literature precedent for previous amino acids. The use of RAFT proved unsuccessful in the polymerization of this new monomer. Therefore, poly(tryptophan) was synthesized through a post-polymerization route utilizing a polymer scaffold of poly(pentafluorophenol).

The new monomer, along with previously reported phenylalanine monomers, and their corresponding polymers have been investigated for their chiral interaction properties with the chiral catalyst precursor BINOL. It has been shown that (*rac*)-BINOL has a like-for-like enantiomer preference with the amino acids investigated here and that tryptophan has an increased interaction compared to phenylalanine. Therefore all poly(amino acids), which can be easily synthesized following the route established here, are an accessible range of chiral poly(acrylamides). These poly(acrylamides) could potentially have greater chiral resolution power than that demonstrated with these materials.

2.5 Experimental

2.5.1 Instrumentation

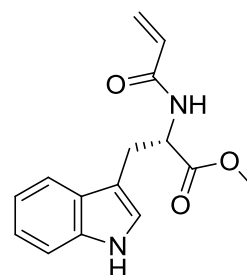
^1H , ^{13}C and ^{19}F NMR spectra were recorded on a 300 or 400 MHz NMR and polymer ^{13}C NMR spectra were recorded on a 700 MHz NMR on a Bruker DPX FT-NMR spectrometer using deuterated solvents. Chemical shifts are reported as δ in parts per million (ppm) relative to the deuterated solvent used. Size exclusion chromatography (SEC) data were obtained either using dimethylformamide (DMF) or chloroform (CHCl_3) with a flow rate of 1.0 mL min^{-1} using $2 \times \text{PLgel } 5 \mu\text{m Mixed-D}$ columns, plus one guard column or dimethylacetamide (DMAC) with LiBr (1 mg mL^{-1}) as eluent, with a flow rate of 1.0 mL min^{-1} at $50 \text{ }^\circ\text{C}$ $2 \times \text{PLgel } 5 \mu\text{m mixed-C}$ columns, plus one guard column. The data was analyzed using Cirrus SEC software based on poly(methymethacrylate) (PMMA) standards. Absolute rotations were measured on a Greenford 52580 polarimeter using a sodium lamp at 589 nm in a 0.25 dm path length cell in chloroform. Matrix-assisted laser desorption and ionization time of flight (MALDI-ToF) was conducted by Dr. Claire Hansell and measured on a Bruker Daltonics Ultraflex II MALDI-ToF mass spectrometer using SpheriCal (purchased from Polymer Factory) standards. The sample (10 mg mL^{-1}) and the matrix (dithranol) (7 mg mL^{-1}) were dissolved in CHCl_3 . Twice the volume of matrix to sample were then added together and spotted onto the plate, allowed to dry and then 1.5 times the volume of cationizing agent (NaTFA, 1 mg mL^{-1}) was spotted.⁴⁵ The spectra were collected in linear mode and as an accumulation of 2000 laser shots. High performance liquid chromatography (HPLC) analysis on a Shimadzu Prominence HPLC with a Chiracel OD-H column $250 \text{ mm} \times 4.6 \text{ mm} \times 5 \mu\text{m}$, with guard column ($5 \mu\text{m}$).

2.5.2 Methods and Techniques

Azo-(*bis*)-isobutyronitrile (AIBN) was recrystallized from methanol and stored in the dark at 4 °C. The acrylamide amino acid methyl esters,^{7, 11, 14} chain transfer agent (CTA), dodecyl-1-phenylethyl trithiocarbonate,^{46,47} pentafluorophenyl acrylate³⁶, poly (acrylamide) amino acids,¹⁰ **M-PDMS**⁴⁴ and the chiral-APCN⁴⁴ were synthesized using modified literature reports. L-tryptophan methyl ester was prepared from L-tryptophan methyl ester hydrochloride by dissolving in NaHCO₃ and extracting into CH₂Cl₂. The initiator Vazo-40 was purchased from Wako. All other chemicals were purchased from Sigma-Aldrich and used without further purification.

2.5.2.1 Synthesis of Small Molecules

M 2.1: L-tryptophan methyl ester hydrochloride (5.00 g, 2.32×10^{-2} mol) was dissolved in CH₂Cl₂ (50 mL), and to this solution triethylamine (7.90 mL, 5.70×10^{-2} mol) was added. Acryloyl chloride (2.24 mL, 2.75×10^{-2} mol) was added dropwise at 0 °C



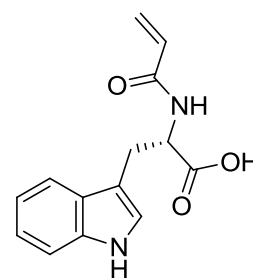
with stirring under nitrogen and the solution stirred overnight at room temperature. The reaction mixture was washed with 2×50 mL HCl, 50 mL NaHCO₃ and 50 mL NaCl. The organic layer was dried over MgSO₄ then the solvent removed under vacuum. Column chromatography was used to purify the yellow oil using ethyl acetate as the eluent. Yield: 3.30 g, 53%. ¹H NMR (400 MHz, CDCl₃): δ 3.13 (2H, d, ³J = 5.1 Hz, CH₂-Ph), 3.34 (3H, s, CO₂CH₃), 4.59 (1H, dd, ³J = 5.1, 8.1 Hz, CH), 5.61 (1H, dd, ²J = 1.5, ³J = 9 Hz, CHH=CH-), 6.07 (1H, dd, ³J = 9, 17 Hz, CHH=CH-), 6.30 (1H, dd, ²J = 1.5, ³J = 17 Hz, CHH=CH-), 6.95 (1H, s, CCHNH, -Ar), 7.10 (1H, d, ³J = 5.7 Hz, CHCHCHCHCNH₂, -Ar), 7.17 (1H, d, ³J = 5.4 Hz, CHCHCHCHCNH₂, -Ar), 7.33 (1H,

t, $^3J = 6$ Hz, CHCHCHCHCNH₂, -Ar), 7.51 (1H, t, $^3J = 6$ Hz, CHCHCHCHCNH₂, -Ar), 8.56 (1H, br d, $^3J = 10$ Hz, -CONH-), 10.87 (1H, br s, Ar-NH); ¹³C NMR (400 MHz, CDCl₃): δ 27.0 (Ar-CH₂), 51.8 (CH₂-CH-(NH)-COOCH₃), 52.5 (COOCH₃), 110.8-135.5 (Ar), 164.3 (NHC=O), 171.8 (COOMe) Figure 2.6 and Figure 2.7; HR ESI-MS found 295.1053 m/z [M+Na]⁺ expected 295.1059; $[\alpha]_D^{25} = +72$

D-M 2.1: Yield: 42% ¹H NMR (400 MHz, CDCl₃): δ 3.28 (2H, m, CH₂-Ph), 3.70 (3H, s, CO₂CH₃), 5.04 (1H, dt, $^3J = 8.0, 5.0$ Hz, CH), 5.61 (1H, d, $^3J = 10$ Hz, CHH=CH-), 6.07 (1H, dd, $^3J = 10, 17$ Hz, CHH=CH-), 6.15 (1H, br d, $^3J = 8$ Hz, -CONH-), 6.28 (1H, d, $^3J = 17$ Hz, CHH=CH-), 6.95 (1H, s, CCHNH, -Ar), 7.10 (1H, d, $^3J = 5.7$ Hz, CHCHCHCHCNH₂, -Ar), 7.17 (1H, d, $^3J = 5.4$ Hz, CHCHCHCHCNH₂, -Ar), 7.33 (1H, t, $^3J = 6$ Hz, CHCHCHCHCNH₂, -Ar), 7.51 (1H, t, $^3J = 6$ Hz, CHCHCHCHCNH₂, -Ar), 8.25 (1H, br s, Ar-NH); HR ESI-MS found 295.1051 m/z [M+Na]⁺ expected 295.1059; $[\alpha]_D^{25} = -76$.

L-A-Trp-OH: was synthesized according to literature precedent.¹⁴

Yield 61%. ¹H NMR (300 MHz, DMSO): δ 3.12 (2H, dd, $^3J = 5.1$ Hz, 14.7 Hz, CH₂-Ph), 4.56 (1H, t, $^3J = 8.4$ Hz, CH), 5.58 (1H, dd, $^2J = 2.4$ Hz, $^3J = 10.2$ Hz, CHH=CH-), 6.05 (1H, dd, $^2J = 2.1$ Hz, $^3J = 17.1$ Hz, CHH=CH-), 6.31 (1H, dd, $^3J = 10.2, 17.1$ Hz, CHH=CH-), 6.95-7.55 (5H, m, -Ar), 8.41 (1H, br d, $^3J = 7.8$ Hz, -CONH-), 10.85 (1H, br s, Ar-NH), 12.71 (1H, bs, COOH). $[\alpha]_D^{25} = +169$.



M 2.4: was synthesized according to literature precedent.¹⁰ ¹H NMR

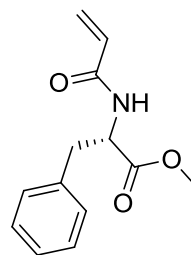
(CDCl₃, 300 MHz) δ: 3.15 (2H, t, ³J = 5.5 Hz, Ar-CH₂), 3.72 (3H, s,

C(O)OCH₃), 4.95 (1H, t, ³J = 5.5 Hz, Ar-CH₂-CH), 5.65 (1H, dd, ²J

= 1.2 Hz, ³J = 10.2 Hz, CHH=CH), 6.00 (1H, NH), 6.06 (1H, dd, ³J =

10.2 Hz, ³J = 17.1 Hz, CHH=CH), 6.26 (1H, dd, ²J = 1.5 Hz, ³J = 17.1 Hz, CHH=CH),

7.15 (5H, m, Ar-H).



M 2.2: the synthesis followed that of **M 2.1** substituting acryloyl

chloride for 2-bromopropionyl bromide. ¹H NMR (300 MHz,

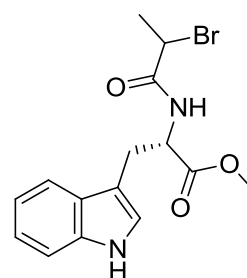
CDCl₃): δ 1.79 (3H, s, CH₃-CHBr), 3.36 (2H, d, ³J = 5.4 Hz,

CH₂-Ph), 3.70 (3H, s, CO₂CH₃), 4.34 (1H, q, ³J = 6.9 Hz, CH₃-

CHBr), 5.89 (1H, t, ³J = 6.8 Hz, CH), 6.78 (1H, d, ³J = 7.8 Hz, -CONH-), 7.02-7.57

(5H, m, -Ar), 8.12 (1H, br s, Ar-NH); HR ESI-MS found 375.0311 m/z [M+Na]⁺

expected 375.0320.



M 2.3: was synthesized according to literature precedent.³⁶ Yield 47 %.

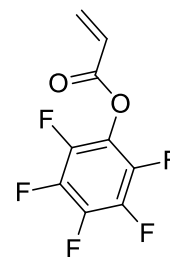
¹H NMR (CDCl₃, 300 MHz) δ: 6.15 (1H, dd, ²J = 0.9 Hz, ³J = 10.5 Hz,

CHH=CH), 6.34 (1H, dd, ³J = 10.5 Hz, 17.4 Hz, CHH=CH), 6.70 (1H,

dd, ²J = 0.6 Hz, ³J = 17.1 Hz, CHH=CH). ¹⁹F NMR (CDCl₃, 282 MHz)

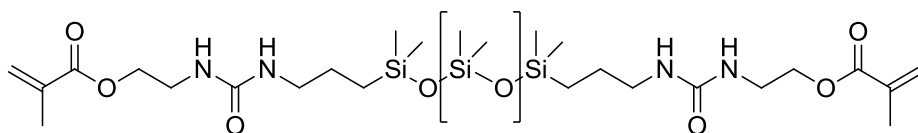
δ: -152.5 (2H, d, ³J = 18.4 Hz, *o*-C₅F₅), -157.9 (1H, t, ³J = 18.4 Hz, *p*-C₅F₅), -162.3 (2H,

t, ³J = 18.4 Hz, *m*-C₅F₅).



M-PDMS:

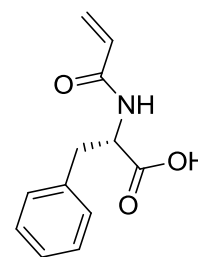
was



synthesized according to literature precedent.⁴⁴ Yield 77%. ¹H NMR (250 MHz, CDCl₃): δ 0.07 (Si-CH₃ backbone), 0.54 (2H, m, ³J = 6.7 Hz, Si-CH₂), 1.52 (2H, quin, ³J = 6.7 Hz, Si-CH₂-CH₂), 1.95 (3H, s, CHH=C(CH₃)), 3.13 (2H, q, ³J = 6.7 Hz, Si-CH₂-CH₂-CH₂), 3.50 (2H, q, ³J = 5.5 Hz, C(O)O-CH₂-CH₂), 4.24 (2H, t, ³J = 5.5 Hz, C(O)O-CH₂-CH₂), 4.55 (1H, s, Si-CH₂-CH₂-CH₂-NH), 4.66 (1H, s, C(O)O-CH₂-CH₂-NH), 5.58 (1H, s, CHH=C(CH₃)), 6.12 (1H, s, CHH=C(CH₃))

M 2.4-OH: was synthesized according to literature precedent.¹¹ Yield

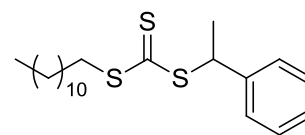
69%. ¹H NMR (DMSO, 300 MHz) δ: 3.00 (2H, dd, ³J = 3.6 Hz, 10.8 Hz, Ar-CH₂), 3.44 (1H, bs, C(O)OH), 4.52 (1H, m, Ar-CH₂-CH), 5.58 (1H, dd, ²J = 1.5 Hz, ³J = 7.5 Hz, CHH=CH), 6.04 (1H, dd, ²J =



1.5 Hz, ³J = 12.6 Hz, CHH=CH), 6.27 (1H, dd, ³J = 7.5 Hz, 12.6 Hz, CHH=CH), 7.24 (5H, m, Ar-H), 8.42 (1H, d, ³J = 6 Hz, NH).

CTA (dodecyl-1-phenylethyl trithiocarbonate): was

synthesized according to literature precedent^{46,47} 51% yield.



¹H NMR (CDCl₃, 300 MHz) δ: 0.80 (3H, t, ³J = 6.3 Hz, CH₃-(CH₂)₉), 1.17 (18H, bs, (CH₂)₉), 1.62 (2H, quin, ³J = 7.8 Hz, CH₃-(CH₂)₉-CH₂), 1.66 (3H, d, ³J = 7.2 Hz, Ar-CH(CH₃)), 3.24 (2H, t, ³J = 7.2 Hz, CH₂-SC(S)S), 5.25 (1H, q, ³J = 7.2 Hz, Ar-CH(CH₃)), 7.24 (5H, m, Ar-H).

2.5.2.2. Synthesis of polymers

Synthesis of poly(M 2.1) via RAFT: **M 2.1** (0.5 g, 2.15×10^{-3} mol), dodecyl-1-phenylethyl trithiocarbonate (0.016 g, 4.29×10^{-5} mol), AIBN (from a stock solution, 0.0007 g, 4.29×10^{-6} mol) and 1,4-dioxane (2 mL) were added together in an oven dried ampoule. The solution was degassed by $3 \times$ freeze pump thaw cycles, backfilled with nitrogen and placed in a pre-heated oil bath at 85 °C for 1.5 h. The polymer was precipitated into cold, stirring diethyl ether, filtered and dried under vacuum. ^1H NMR (300 MHz, CDCl_3): δ 1.34-1.75 (2H, br, CH_2 backbone) 2.13-2.47 (1H, br, CH backbone), 2.66-3.17 (2H, br, CH_2Ph), 3.36-3.68 (3H, br, CO_2CH_3), 4.33-5.00 (1H, br, CH_2CH), 6.97-7.36 (5H, br, C_6H_5), 7.63-8.23 (1H, br, NH) Conversion by ^1H NMR spectroscopy, 88%. M_n (^1H NMR in CDCl_3) = 8.4 kDa, M_n (SEC, DMF, PMMA calibration) = 6.8 kDa, $D = 1.19$.

Synthesis of poly(L-Trp-OH): The monomer (0.1 g, 3.80×10^{-4} mol), 2-cyano-2-propyl dodecyl trithiocarbonate (0.001 g, 3.80×10^{-6} mol), AIBN (from a stock solution, 0.00006 g, 3.80×10^{-7} mol) and DMSO (0.6 mL) were added together in an oven dried ampoule. The solution was degassed by $3 \times$ freeze pump thaw cycles, backfilled with nitrogen and placed in a pre-heated oil bath at 70 °C for 10 h. Conversion by ^1H NMR spectroscopy, 72%. M_n (SEC, DMAC, PMMA calibration) = 35 kDa, $D = 1.25$.

Synthesis of poly(M 2.3): In a typical synthesis **M 2.3** (1.0 g, 4.19×10^{-3} mol), S-dodecyl-S'-(α - α' -dimethyl- α'' -acetic acid) trithiocarbonate (DDMAT) (0.034 g, 9.33×10^{-5} mol), AIBN (from stock solution, 0.0015 g, 9.33×10^{-6} mol) and dioxane (1.0 mL) were weighed into an oven dried ampoule. This was degassed by $3 \times$ freeze pump thaw

cycles, was backfilled with nitrogen and placed into a pre-heated oil bath at 80 °C for 2 h. ^1H NMR (300 MHz, CDCl_3) δ 1.88-3.26 (3H, polymer backbone); ^{19}F NMR (282 MHz, CDCl_3) -162.5 (2H, br s, *o*- C_5F_5), -156.8 (1H, br s, *p*- C_5F_5), -153.4 (2H, br s, *m*- C_5F_5). Conversion by ^{19}F NMR spectroscopy, 83%; M_n (^1H NMR in CDCl_3) = 4.5 kDa, M_n (SEC, CHCl_3 , PMMA calibration) = 2.5 kDa, $D = 1.09$.

ATRC for M 2.2: Cu(I)Br (0.012 g, 8.52×10^{-5} mol) and TPA (0.025 g, 8.52×10^{-5} mol) were placed in an oven dried ampoule sealed with a suba seal and degassed by 3 x evacuate and refill cycles. In another ampoule the solvent (2.36 mL) and **M 2.2** (0.100 g, 2.84×10^{-4} mol) was degassed by 3 x freeze pump thaw cycles. The liquid was then added to the solid under inert conditions and heated to 125 °C for 25 h. ^1H NMR spectra resembled that of **M 2.2**, no reaction had occurred.

Synthesis of poly(M 2.4): were synthesized according to literature precedent.¹⁰ ^1H NMR spectroscopy gave 98% conversion. M_n (^1H NMR in CDCl_3) = 14.6 kDa, M_n (SEC, THF, PMMA calibration) = 8.7 kDa, $D = 1.21$.

Synthesis of Chiral-APCN: A modified literature precedent was used substituting a chiral monomer for **M 2.4-OH**.⁴⁴ IR: 794, 1018, 1259, 1521, 1527, 1647, 1729, 2529, 3356 cm^{-1} .

2.5.2.3 Conversion of poly(M 2.3) to poly(M 2.1)

Poly(**M 2.3**) (0.113 g, 1.13×10^{-5} mol) and L-tryptophan methyl ester (0.15 g, 6.78×10^{-4} mol) prepared from the hydrochloride salt were dissolved in THF (~5 mL) and stirred overnight. The conversion by ^{19}F NMR was 100%. The polymer was precipitated into

hexane and then dialyzed against distilled H₂O (MWCO = 3.5 kDa) to remove excess L-tryptophan methyl ester. ¹H NMR (400 MHz, CDCl₃) δ 1.40-3.73 (8H, **CHCH**₂ polymer backbone and **CH**₂Ar and CO₂**CH**₃), 4.35-5.10 (1H, br **CH**₂**CH**), 6.44-7.53 (5H, br, Ar-**H**), 8.32-9.64 (1H, br, **NH**). *M_n* (¹H NMR in CDCl₃) = 4.6 kDa, *M_n* (SEC, DMF, PMMA calibration) = 4.9 kDa, *D* = 1.11.

2.5.2.4 A typical ¹H NMR spectroscopy study of 1,1-Bi-2-naphthol (*rac*)-BINOL

(*rac*)-BINOL (0.01 g, 3.50 × 10⁻⁵ mol) and L-**M 2.4** (0.008 g, 3.42 × 10⁻⁵ mol) were weighed into a vial, dissolved in CDCl₃ (0.7 mL) and then transferred to an NMR tube. A typical ¹H NMR spectroscopy assignment, ¹H NMR (400 MHz, CDCl₃): δ 3.35 (**CHCH**₂, monomer), 3.68 (CO₂**CH**₃, monomer), 5.08 (**CHCH**₂, monomer), 5.21 (**OH**, BINOL), 6.11 (**NH**, monomer), 5.61-6.28 (vinyl peaks from monomer), 6.93-7.97 (Ar-**H** of BINOL and monomer).

2.5.2.5 Preparation of deuterated (*R*)-BINOL

A portion of (*R*)-BINOL was dissolved in the minimum amount of CHCl₃ and then stirred vigorously for approximately 10 min with an excess of D₂O. CHCl₃ was removed under vacuum and D₂O by freeze drying. The process was repeated 3 times to give BINOL with 20% deuterated phenolic groups. This was then used with (*S*)-BINOL to create a racemic mixture by weighing out equal parts of (*S*)-BINOL and (*R*)-BINOL and grinding the two powders together.

2.5.2.6 Chiral separation experiment

The synthesized chiral-APCN (25 mg) was weighed into a vial. (*rac*)-BINOL (20 mg) was dissolved in THF (400 μL) and added to the chiral-APCN. This was left overnight the majority of the THF had been absorbed into the gel. The remaining THF was tested

for the enantiomer proportions to determine the proportions within the chiral-APCN. THF (~200 μL) was then added to the gel and shook vigorously for 15 s before being removed and analysed. This removal process was repeated a number of times.

2.6 References

1. F. Sanda, M. Nakamura, T. Endo, T. Takata and H. Handa, *Macromolecules*, 1994, **27**, 7928-7929.
2. J. Skey, C. F. Hansell and R. K. O'Reilly, *Macromolecules*, 2010, **43**, 1309-1318.
3. K. Bauri, S. Pant, S. G. Roy and P. De, *Polym. Chem.*, 2013, **4**, 4052-4060.
4. A. C. Evans, J. Skey, M. Wright, W. Qu, C. Ondeck, D. A. Longbottom and R. K. O'Reilly, *J. Polym. Sci., Part A: Polym. Chem.*, 2009, **47**, 6814-6826.
5. H. Mori, H. Iwaya, A. Nagai and T. Endo, *Chem. Commun.*, 2005, 4872-4874.
6. A. Lu, T. P. Smart, T. H. Epps III, D. A. Longbottom and R. K. O'Reilly, *Macromolecules*, 2011, **44**, 7233-7241.
7. H. Mori, K. Sutoh and T. Endo, *Macromolecules*, 2005, **38**, 9055-9065.
8. I.-D. Chung, P. Britt, D. Xie, E. Harth and J. Mays, *Chem. Commun.*, 2005, 1046-1048.
9. M. Casolaro, S. Bottari, A. Cappelli, R. Mendichi and Y. Ito, *Biomacromolecules*, 2004, **5**, 1325-1332.
10. J. Skey, H. Willcock, M. Lammens, F. Du Prez and R. K. O'Reilly, *Macromolecules*, 2010, **43**, 5949-5955.
11. H. Mori, M. Matsuyama, K. Sutoh and T. Endo, *Macromolecules*, 2006, **39**, 4351-4360.
12. B. L. Moore and R. K. O'Reilly, *J. Polym. Sci., Part A: Polym. Chem.*, 2012, **50**, 3567-3574.
13. S. G. Roy, R. Acharya, U. Chatterji and P. De, *Polym. Chem.*, 2012, **4**, 1141-1152.

14. H. Mori, E. Takahashi, A. Ishizuki and K. Nakabayashi, *Macromolecules*, 2013, **46**, 6451-6465.
15. P. Singh, A. Srivastava and R. Kumar, *Polym. Int.*, 2013, DOI: 10.1002/pi.4549.
16. S. Yamada, S. Atsushi, M. Goto and T. Endo, *J. Polym. Sci., Part A: Polym. Chem.*, 2013, **51**, 4565-4571.
17. N. M. Maier, P. Franco and W. Lindner, *J. Chromatogr. A*, 2001, **906**, 3-33.
18. J. Wang, X. Zhu, Z. Cheng, Z. Zhang and J. Zhu, *J. Polym. Sci., Part A: Polym. Chem.*, 2007, **45**, 3788-3797.
19. S. Gingter, E. Bezdushna and H. Ritter, *Macromolecules*, 2010, **43**, 3128-3131.
20. N. Maier and W. Lindner, *Anal. Bioanal. Chem.*, 2007, **389**, 377-397.
21. Y.-F. Poon, I. W. Muderawan and S.-C. Ng, *J. Chromatogr. A*, 2006, **1101**, 185-197.
22. S. Matsunaga, T. Ohshima and M. Shibasaki, *Adv. Synth. Catal.*, 2002, **344**, 3-15.
23. X. Li, J. B. Hewgley, C. A. Mulrooney, J. Yang and M. C. Kozlowski, *J. Org. Chem.*, 2003, **68**, 5500-5511.
24. M. Rueping, E. Sugiono and S. A. Moreth, *Adv. Synth. Catal.*, 2007, **349**, 759-764.
25. M. Shibasaki, M. Kanai, S. Matsunaga and N. Kumagai, *Acc. Chem. Res.*, 2009, **42**, 1117-1127.
26. M. S. Isonaga, K.; Kamigaito, M.; Okamoto, *Polym. Prepr.*, 2005, **46**, 401.
27. W. Lu, L. Lou, F. Hu, L. Jiang and Z. Shen, *J. Polym. Sci. Part A: Polym. Chem.*, 2010, **48**, 5411-5418.
28. K. Morioka, Y. Isobe, S. Habaue and Y. Okamoto, *Polym. J.*, 2005, **37**, 299-308.

29. T. Oishi, Y. Isobe, K. Onimura and H. Tsutsumi, *Polym. J.*, 2003, **35**, 245.
30. T. P. Quinn, P. D. Atwood, J. M. Tanski, T. F. Moore and J. F. Folmer-Andersen, *J. Org. Chem.*, 2011, **76**, 10020-10030.
31. J. Redondo, A. Capdevila and I. Latorre, *Chirality*, 2009, **22**, 472-478.
32. J. Skey and R. K. O'Reilly, *J. Polym. Sci., Part A: Polym. Chem.*, 2008, **46**, 3690-3702.
33. J. Clayden, N. Greeves, S. Warren and P. Wothers, *Organic Chemistry*, Oxford University Press, Oxford, 2001.
34. A. J. Clark, J. V. Geden, S. Thom and P. Wilson, *J. Org. Chem.*, 2007, **72**, 5923-5926.
35. M. Eberhardt, R. Mruk, R. Zentel and P. Theato, *Eur. Polym. J.*, 2005, **41**, 1569-1575.
36. F. D. Jochum and P. Theato, *Macromolecules*, 2009, **42**, 5941-5945.
37. C. Schilli, M. G. Lanzendorfer and A. H. E. Muller, *Macromolecules*, 2002, **35**, 6819-6827.
38. A. Favier, C. Ladavière, M.-T. Charreyre and C. Pichot, *Macromolecules*, 2004, **37**, 2026-2034.
39. F. Sanda, T. Abe and T. Endo, *J. Polym. Sci., Part A: Polym. Chem.*, 1997, **35**, 2619-2629.
40. M. de Loos, J. van Esch, R. M. Kellogg and B. L. Feringa, *Angew. Chem. Int. Ed.*, 2001, **40**, 613-616.
41. K.-X. Xu, P.-F. Cheng, J. Zhao and C.-J. Wang, *J. Fluoresc.*, 2009, **21**, 991-1000.

42. O. V. Mikhalev, O. R. Malyshev, M. G. Vinogradov, G. V. Chel'tsova-Bebutova and A. V. Ignatenko, *Russ. Chem. Bull.*, 1995, **44**, 873-877.
43. Y. Chen and B. A. Wallace, *Biophys. Chem.*, 1997, **65**, 65-74.
44. L. Shi, P. Xie, Z. Li, Y. Wu and J. Deng, *Macromol. Chem. Phys.*, 2013, **214**, 1375-1383.
45. K. T. Wiss and P. Theato, *J. Polym. Sci., Part A: Polym. Chem.*, 2010, **48**, 4758-4767.
46. J. Skey and R. K. O'Reilly, *Chem. Commun.*, 2008, 4183-4185.
47. A. Lu, T. P. Smart, T. H. Epps III, D. A. Longbottom and R. K. O'Reilly, *Macromolecules*, 2011, **44**, 7233-7241.

Chapter 3: The immobilization of the MacMillan catalyst into co-polymers
via RAFT and their use in the Diels-Alder reaction

3.1 Abstract

Co-polymers incorporating the MacMillan organocatalyst have been synthesized *via* RAFT polymerization. The immobilization of catalysts in general has been extensively studied, primarily in order to enhance the recyclability and reusability of the immobilized catalyst. Through the synthesis of a novel monomer which contains both the catalytic MacMillan functionality and a polymerizable methacrylate group the easy incorporation of the MacMillan catalyst into polymers has been achieved.

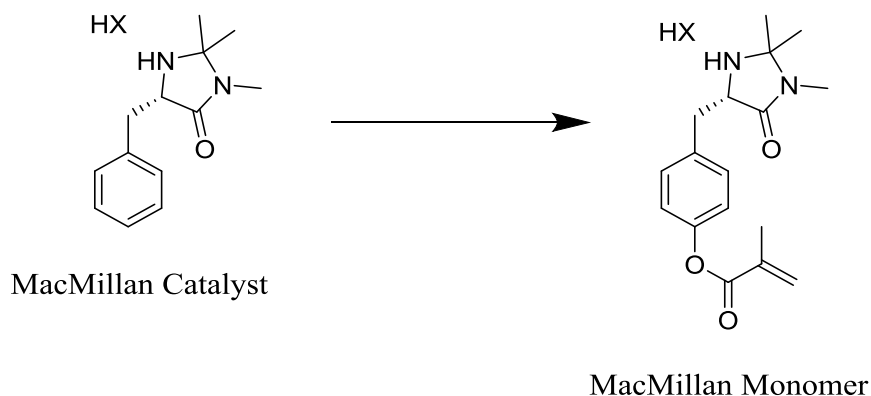


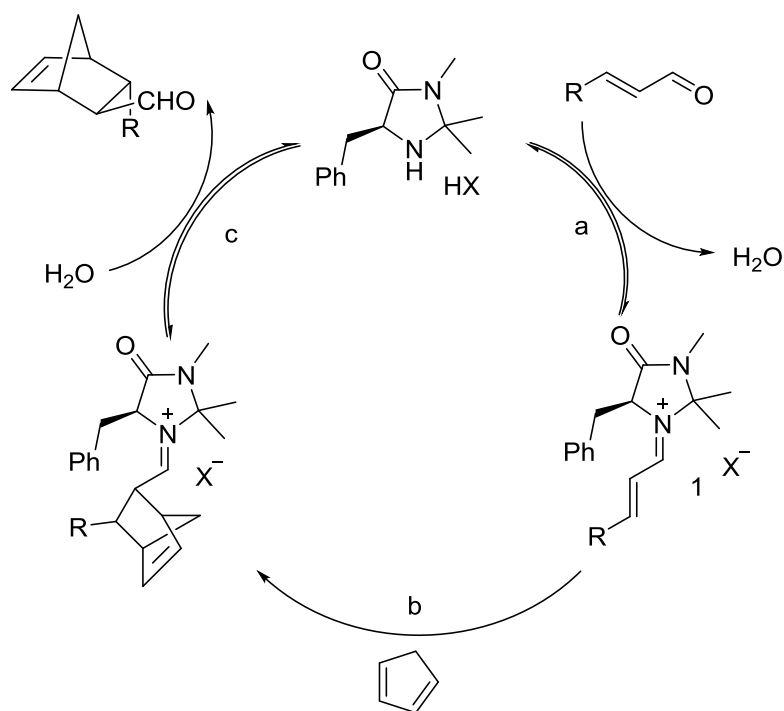
Figure 3.1. The chemical structures of the MacMillan catalyst and the newly synthesized MacMillan monomer, where HX is an acid salt.

The loading of the catalyst within the co-polymers can be easily controlled by altering the feed ratio of the MacMillan monomer and the co-monomer diethylene glycol methyl ether methacrylate (DEGMA). The use of RAFT enables the synthesis of these well-defined polymers allowing control over molecular weight and catalyst incorporation. The synthesized polymers have different physical properties with the lower critical solution temperature (LCST) and the glass transition temperature (T_g) both dependent on the catalyst incorporation. The catalytic activity of the co-polymers has been

explored using the Diels-Alder (DA) reaction between cyclopentadiene and *trans*-hexen-1-al and shows enantioselectivity close to that previously reported by MacMillan. The polymers have been shown to be reusable in a *pseudo* continuous process with conversions and enantioselectivities maintained over 4 cycles.

3.2 Introduction

The MacMillan catalyst is a very powerful organic catalyst capable of catalyzing a wide range of organic reactions.¹⁻⁷ It was first reported in 2000 as an organocatalyst for a highly enantioselective DA reaction.¹ The structure has been developed as an organic alternative to Lewis acid catalysis. Therefore, the reversible formation of iminium ions from α,β -unsaturated aldehydes and amines was targeted as a way to emulate how Lewis acids are able to lower the lowest occupied molecular orbital (LUMO) of dienophiles in the DA reaction. The success of this design gave the desired results for the enantioselective catalysis of the DA reaction. The mechanistic route for the catalyst can be seen in Scheme 3.1.⁸ The α,β -unsaturated aldehydes react with the catalyst at the amine site and form an imine; which is then susceptible to attack from the diene.



Scheme 3.1. The mechanism of the MacMillan catalyst for the DA reaction. The formation of the imine transition state (1) from the reaction of the α,β -unsaturated aldehydes and the amine is crucial to lower the LUMO of the dienophile.

The DA reaction requires the overlap of the highest occupied molecular orbital (HOMO) of the diene and the LUMO of the dienophile. This is illustrated in Figure 3.2; during the formation of the imine (Scheme 3.1) the LUMO of the dienophile is lowered allowing for stronger overlap between the requisite orbitals.

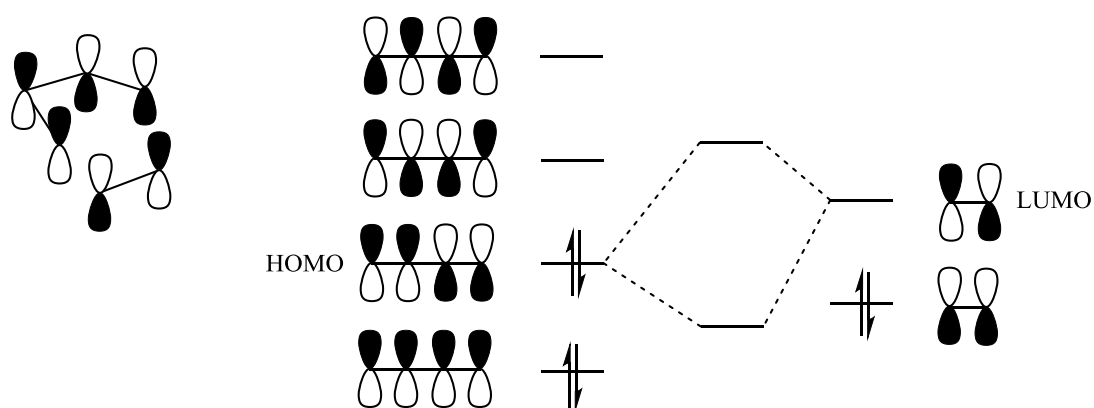


Figure 3.2. A representative of the energy overlap of the p orbital of the DA reaction highlighting the symmetry and energy overlap of the HOMO of the diene and LUMO of the dienophile.

The MacMillan catalyst is able to control the selectivity of the reaction due to steric hindrance imposed upon the substrates. The catalytic transition state of the MacMillan catalyzed DA reaction between acrolein and 1,3-cyclohexadiene can be seen in Figure 3.3. The diastereoselectivity (*exo:endo* ratio) is caused during the formation of the catalytic transition state. The favoured structure is depicted in Figure 3.3 where the alkene of the dienophile is separated from the methyl groups on the catalyst. The enantioselectivity is controlled through the approach of the diene, in this case 1,3-cyclohexadiene. The diene can either attack from above (the *si*-face) or from below (the *re*-face). Approach from the *re*-face is significantly favoured due to the large benzyl group covering the top *si*-face.

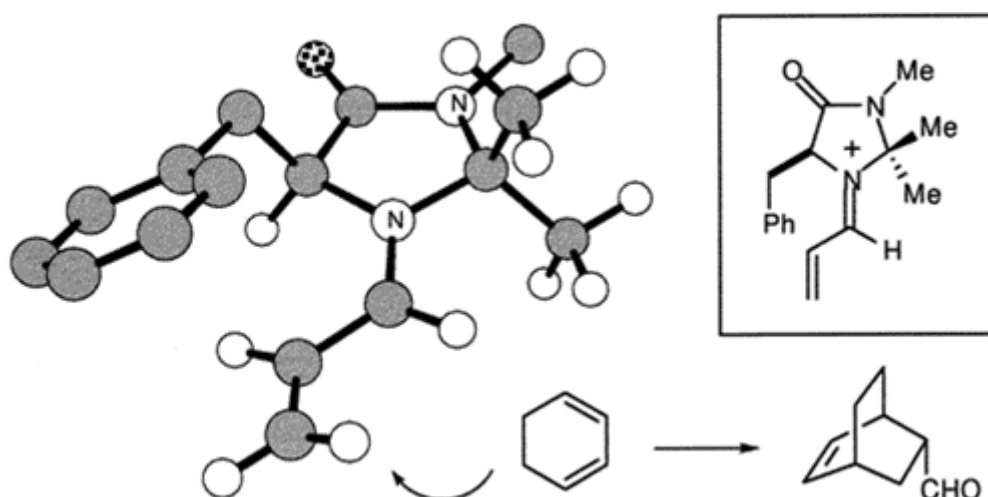


Figure 3.3. A 3D representation of the transition state reproduced from MacMillans paper.¹ In this depiction the benzyl group is shielding the top side of the dienophile from attack.

There have been several attempts to immobilize this powerful catalyst, often with recovery and reuse in mind, which has been well reviewed by Kristensen and Hansen in 2010.⁹ Most of the methods had hitherto revolved around random attachment of the catalyst to various supports, usually pre-formed ones. The first report in 2002 was using a PEG support which showed some recycling ability and selectivities comparable to those initially reported by MacMillan.¹⁰ The supported catalyst was used to perform the DA reaction between acrolein and 1,3-cyclohexadiene achieving up to 92% *endo* ee compared to 94% *endo* ee reported by MacMillan. Other supports have included JandaJelTM,¹¹ mesocellular foams,¹² sulfonated poly(styrene),¹³ silica particles,¹⁴ silica polymer,¹⁵ superparamagnetic Fe₃O₄ particles,^{16, 17} and the use of a flow system.¹⁸ In 2010 Kristensen *et al.* developed a methacrylic polymerizable monomer (as shown in Figure 3.4) with the MacMillan catalytic functionality incorporated and co-polymerized it in a suspension polymerization with PEG 400 methyl ether methacrylate and PEG 600 dimethacrylate.¹⁹

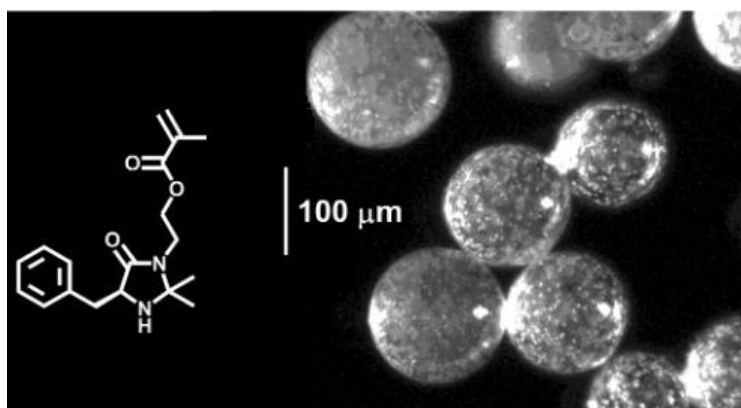


Figure 3.4. The structure of the methacrylic MacMillan monomer used by Kristensen *et al.* and the resulting cross-linked polymer beads.¹⁹

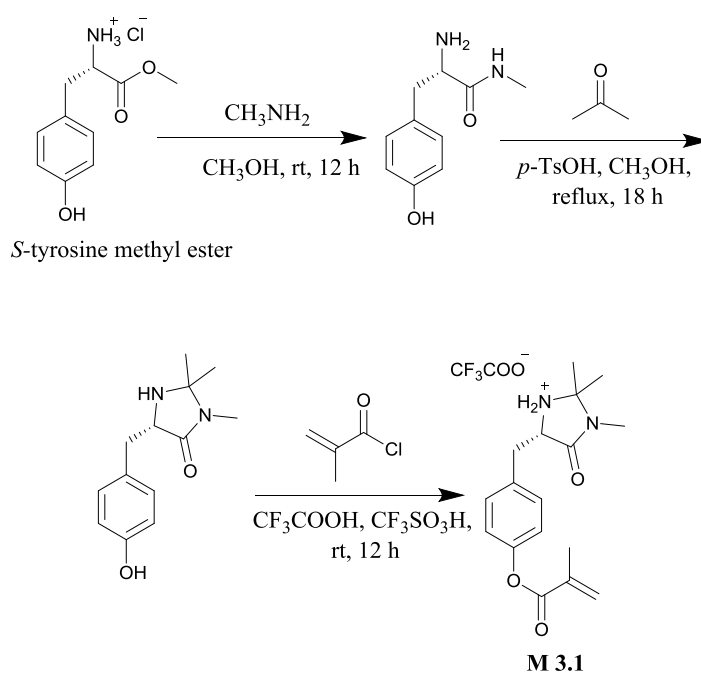
This immobilization technique is the closest to the route employed by ourselves as it focuses on a bottom-up approach; giving more control over the environment and degree of incorporation of the catalyst as opposed to the post-modification approach. Kristensen *et al.* had success with this work; having immobilized the catalyst they could use it in the DA reaction between cyclopentadiene and 4-nitrocinnamaldehyde. They did however observe a degradation of the catalyst's selectivity and were limited to three cycles before they observed a decrease in selectivity from *endo* ee% of 81% in the first cycle to 62% in the third, which fell again on the fourth re-use to 51%.

The advent of reversible-deactivation radical polymerizations (RDRP) techniques that are tolerant to functional groups has made it possible to polymerize complex monomers without adversely affecting the polymer kinetics. In particular, RAFT has been shown to be tolerant to a range of monomer functionalities and reaction conditions and was used in this work to synthesize our MacMillan-containing polymers *via* RAFT.²⁰⁻²³

3.3 Results and discussion

3.3.1 Monomer Synthesis

In order to control the incorporation and environment that the MacMillan catalyst was placed in, a new polymerizable monomer was synthesized where the catalytic functionality was retained. The new monomer was synthesized from the amino acid (*S*)-tyrosine and thus a natural source of chirality. The original MacMillan synthesis was carried out using another amino acid, phenylalanine. However, by using tyrosine, an additional phenol group is available which can be used to introduce a polymerizable group. A representation of the synthetic route is shown in Scheme 3.2. The first two steps were carried out following the synthesis of the original MacMillan catalyst where the first step was the reaction of (*S*)-tyrosine methyl ester with methyl amine through a nucleophilic substitution reaction, resulting in the first intermediate. The intermediate was then dissolved in acetone and refluxed to achieve the ring formation. The final step was the coupling with methacryloyl chloride, based on well-known chemistries. The resulting product was a white powder, obtained in excellent overall yield and synthesized on a multi-gram scale producing 33 g (87% yield) of the product in one batch of **M 3.1**.



Scheme 3.2. The synthesis of (*S*)-MacMillan functionalized monomer (**M 3.1**) from the amino acid (*S*) – tyrosine methyl ester.

The new monomer was characterized through ^1H NMR (Figure 3.5) and ^{13}C NMR (Figure 3.6) spectroscopy, IR (Figure 3.7) and high resolution mass spectrometry where a mass of 303.1698 m/z for $[\text{M} + \text{H}]^+$ was found, correlating well with the expected mass of 303.1709 m/z for the desired product. The ^1H NMR spectrum showed expected chemical shifts and integration. Protons **e** are diastereotopic causing them to have different shifts in the ^1H NMR spectrum. They have then been split into a doublet of doublets (δ 2.94 ppm, $^3J = 10.5$ Hz, 15 Hz) and (δ 3.48 ppm, $^3J = 3.6$ Hz, 15 Hz) with a geminal 2J coupling between the protons of magnitude $J = 15$ Hz and a coupling to the proton on the chiral centre, **f**. Proton **f** is a doublet of doublets ($^3J = 3.6$ Hz, 10.5 Hz) as it couples to both the diastereotopic protons labelled **e**.

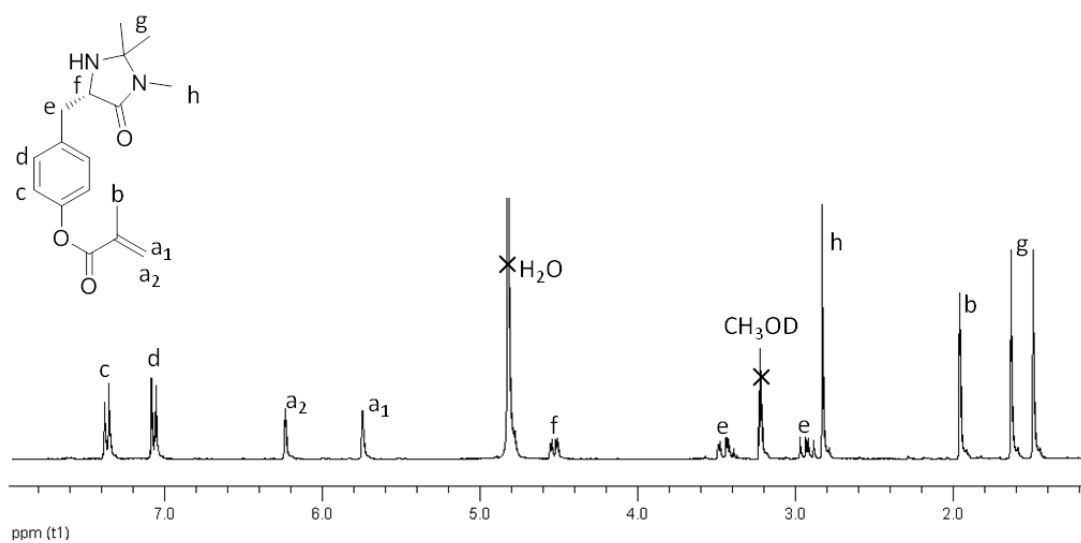


Figure 3.5. ¹H NMR (300 MHz) spectrum of **M 3.1** in CD₃OD.

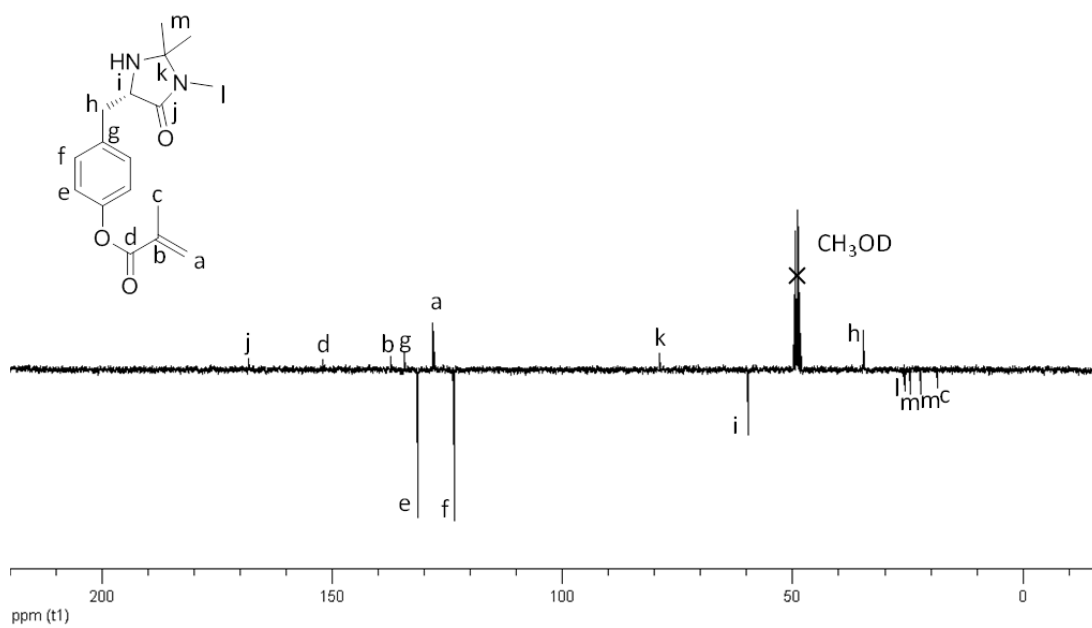


Figure 3.6. ¹³C NMR (75 MHz) spectrum of **M 3.1** in CD₃OD.

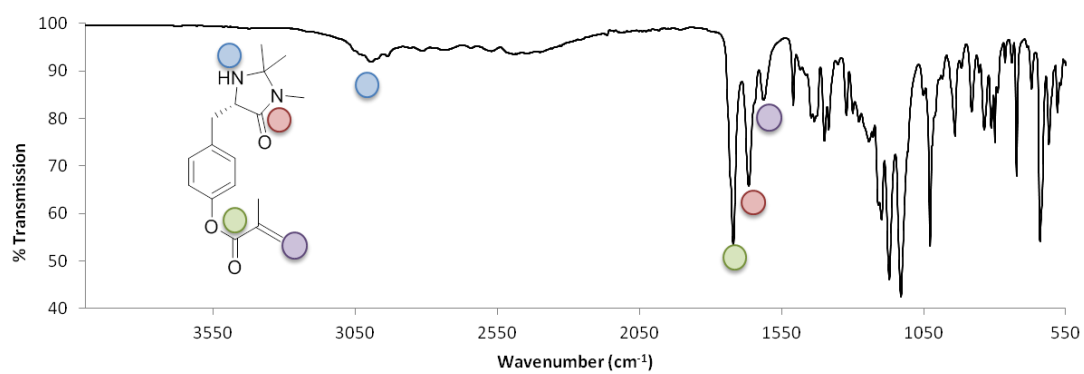
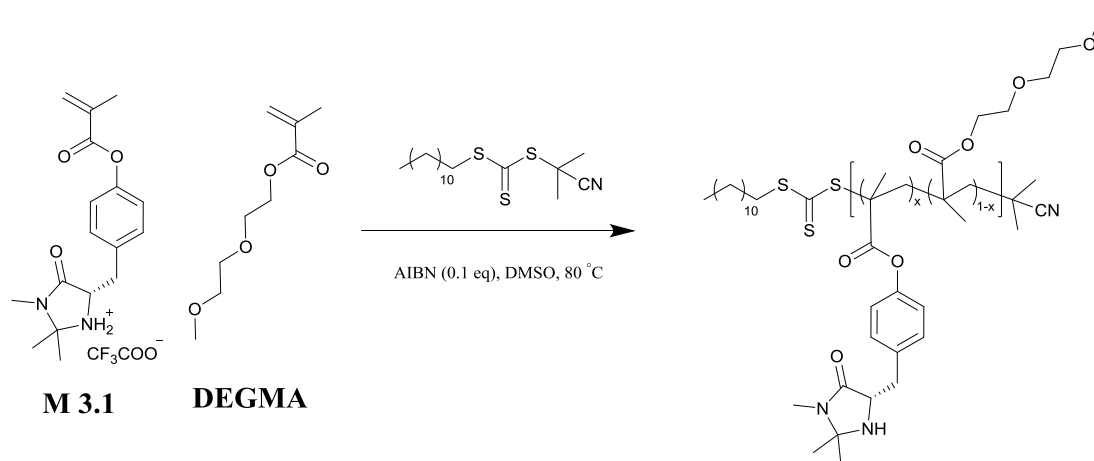


Figure 3.7. IR spectrum of **M 3.1** indicating the presence of a secondary amine, carbonyl groups and carbon-carbon double bond. Other significant absorptions around 1130 cm^{-1} are attributed to C-O bonds and 1030 cm^{-1} to C-N bonds.

3.3.2 Polymer Synthesis

Co-polymers were synthesized with a range of **M 3.1** loadings with the co-monomer diethylene glycol methyl ether methacrylate (DEGMA). This monomer was chosen as the reactions of the MacMillan catalyst are typically carried out in polar solvents and therefore the polymer would have to be soluble in these conditions. Additionally exposed functionality within the monomer was avoided in case of interference with the catalysis reaction, a longer chain methyl ether methacrylate was also not selected to minimize the chance of steric interference with the catalysis. The RAFT conditions were adapted from previous successful RAFT polymerizations targeting a DP of 100 with a radical flux of 0.1 equivalents.²⁴ The synthesis and structures of the polymers can be seen in Scheme 3.3 and a typical ¹H NMR spectrum for the synthesized polymers in Figure 3.8.



Scheme 3.3. Polymerization scheme of **M 3.1** and DEGMA *via* RAFT polymerization and the structure of the resulting polymer.

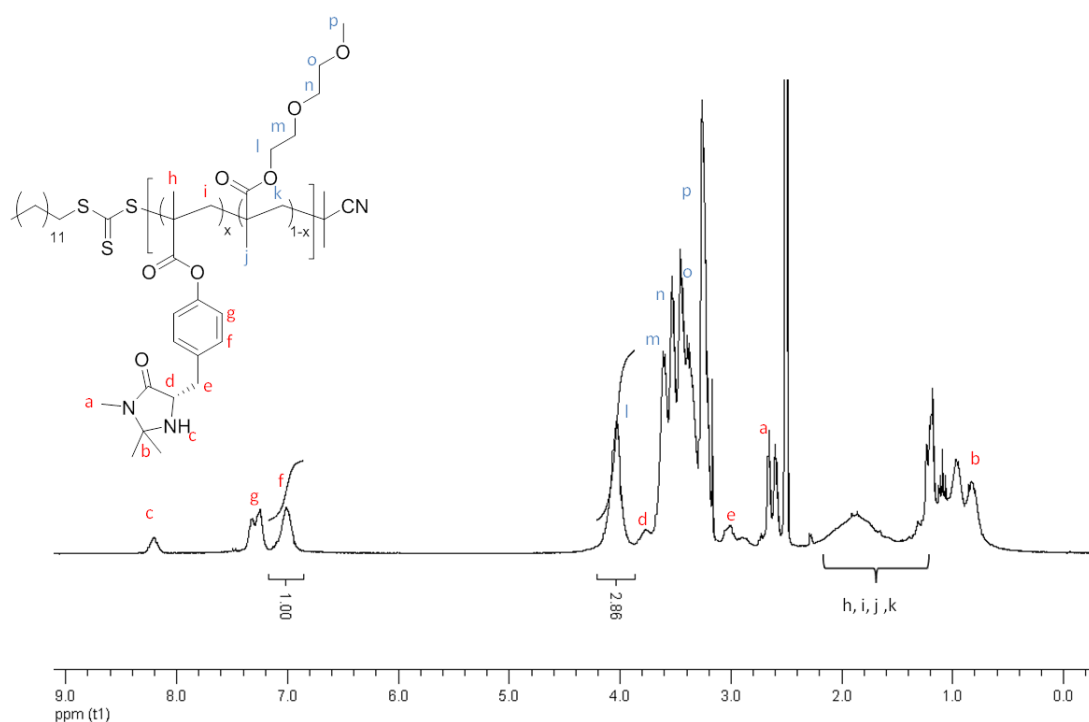


Figure 3.8. A representative ^1H NMR spectrum (300 MHz) in CD_3OD of the synthesized functional copolymers; polymer presented is **P 3.2**. The relative incorporation of the two monomers was determined from the signals of **g** and **l**, here integrated to 1.00 and 2.86. ($1.00/3.86 \times 100\% = 26\%$)

The co-polymers were synthesized using RAFT which allowed for control over molecular weight, molecular weight distribution and catalyst incorporation. The dispersities of the polymers are slightly larger than ideal which has been attributed to potential interaction and therefore broadening on the SEC column. The amount of **M 3.1** catalyst incorporated into the co-polymers was varied from 6 – 100%. The RAFT end group signals from the co-polymers could not be seen in the ^1H NMR spectrum as they were obscured by signals from the polymer; therefore M_n obtained from SEC was used, data detailed in Table 3.1. The synthesized polymers all have similar molecular weights but the amount of catalyst incorporation has been altered giving a range of polymers.

Table 3.1. The initial feed ratio, final catalyst incorporation, molecular weights and molecular weight distribution for **P 3.1** – **P 3.7**.

Polymer	Feed Ratio (DEGMA:M 3.1)	$M_{n, th}$ (kDa)	M_n (kDa) ^a	\mathcal{D}^a	Catalyst incorporation (%) ^b
P 3.1	92:8	17.0	11.8	1.35	6
P 3.2	76:24	21.7	11.6	1.39	26
P 3.3	69:31	20.7	11.8	1.33	33
P 3.4	58:42	23.3	12.0	1.39	38
P 3.5	37:63	22.7	11.5	1.47	57
P 3.6	13:87	26.8	11.4	1.46	73
P 3.7	0:100	27.8	5.8	1.31	100

^aDetermined by SEC (THF, PMMA calibration)

^bDetermined by comparing ratio of DEGMA to **M 3.1** from a ¹H NMR spectrum

3.3.2.1 Racemization

To ensure the enantiomeric purity of the monomer was retained during the polymerization process, which is vital to retain the maximum catalytic activity of the catalyst, the original (*S*)-MacMillan catalyst was synthesized. This catalyst was subjected to the same polymerization conditions as **M 3.1** to confirm no racemization of the catalyst had occurred. The catalyst was then recovered from the polymerization mixture and analyzed by chiral-HPLC (Figure 3.9).

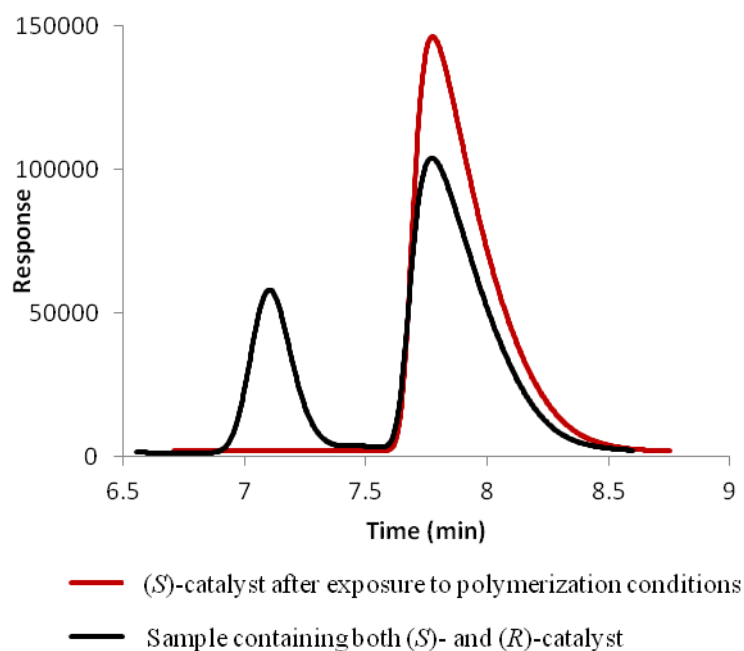


Figure 3.9. HPLC chromatogram of a sample containing both (*S*)- and (*R*)-MacMillan catalyst (black line) and recovered *S*-MacMillan catalyst after exposure to polymerization conditions (red line). Only the (*S*)-catalyst is detected after exposure to the polymerization conditions.

The recovered (*S*)-MacMillan catalyst showed no sign of racemization to the (*R*)-MacMillan catalyst. Based on this result, it was proposed that **M 3.1** is likely to behave in a similar fashion with no racemization occurring during polymerization. Thus, only the (*S*)-enantiomer is expected to be incorporated into the co-polymer.

3.3.2.2 Reactivity Ratios

The reactivity ratios of **M 3.1** and DEGMA in their co-polymerization were investigated next to elucidate the co-polymer microstructure, i.e. determine if the catalyst functionality is randomly distributed along the polymer chain or if an alternating/block co-polymer will result. In a co-polymerization with two monomers (M_1 and M_2), the growing polymer chain can either be capped with M_1 or M_2 both of which can

polymerize with either M_1 or M_2 , with the two monomers being present in different concentrations (illustrated in Figure 3.10).



Figure 3.10. A schematic illustration of the different reactions that can take place during co-polymerization of two different monomers.

The reactivity ratios are defined as the relative rates of reaction of each monomer adding to the end of the polymer as described in Equation 3.1. From these values it is possible to ascertain information about the likely nature of the resulting polymer.

$$r_1 = \frac{k_{11}}{k_{12}} \quad r_2 = \frac{k_{22}}{k_{21}} \quad (3.1)$$

If r_1 and r_2 are both much higher than 1, co-polymerization is unlikely and two homopolymers will instead be synthesized. If they are slightly larger than 1, homopolymerization is still preferred but cross polymerization can happen compared to the previous system, which would result in the formation of a multi block co-polymer. When r_1 and r_2 are both approximately equal to 1 then M_1 is just as likely to react with M_1 as with M_2 and a random co-polymer will be synthesized. If both r_1 and r_2 are instead equal to 0, co-polymerization is much preferred resulting in an alternating co-polymer. If one reactivity ratio is much lower than 1 and the other much higher, a

polymer with a compositional drift will result as one monomer will react much quicker with itself and when this monomer is depleted from the polymerization, the second monomer will start to get incorporated. These scenarios are depicted in Figure 3.11.

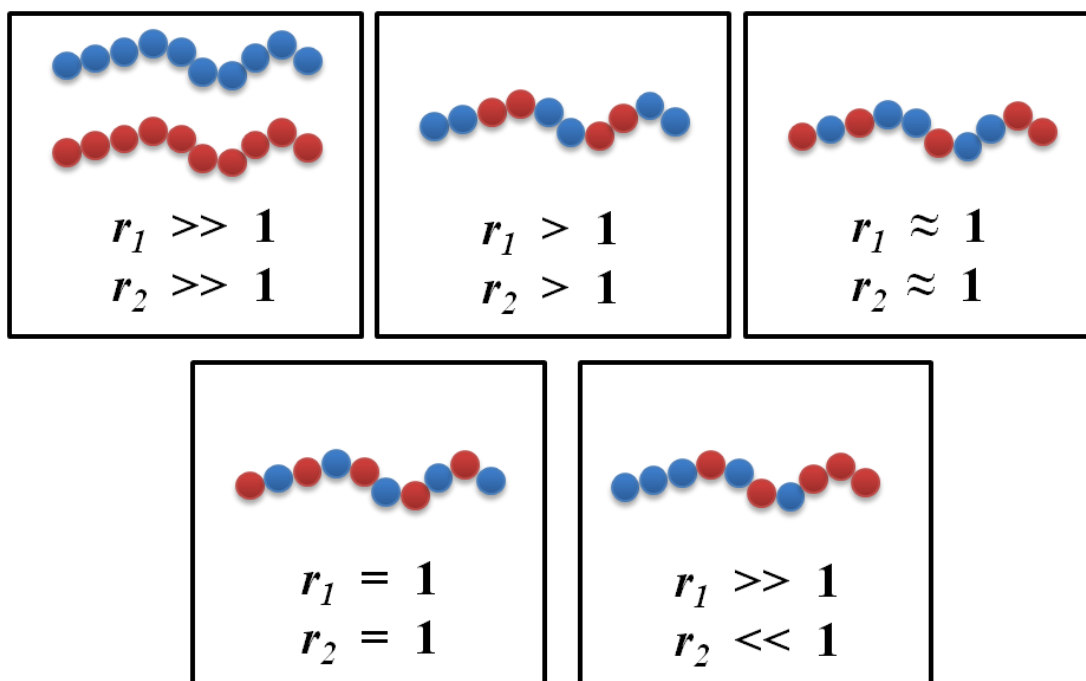


Figure 3.11. A representation of the different polymer structures that can be synthesized depending on the reactivity ratios of the co-monomers.

In order to determine the reactivity ratios a series of co-polymerizations were carried out with different starting feed ratios of **M 3.1** to DEGMA (90:10, 70:30, 50:50, 30:70, 10:90). Conversions of both monomers were kept low (5 – 15%) in order to eliminate any effect of diffusion or accessibility of the growing polymer chain. The conversions were determined by ^1H NMR spectroscopy. The molar fractions of the two monomers in the starting feed and the final polymer were calculated using ^1H NMR spectroscopy and analyzed by the computer program Contour, developed by van Herk.²⁵ The monomer incorporations can be seen in Figure 3.12.

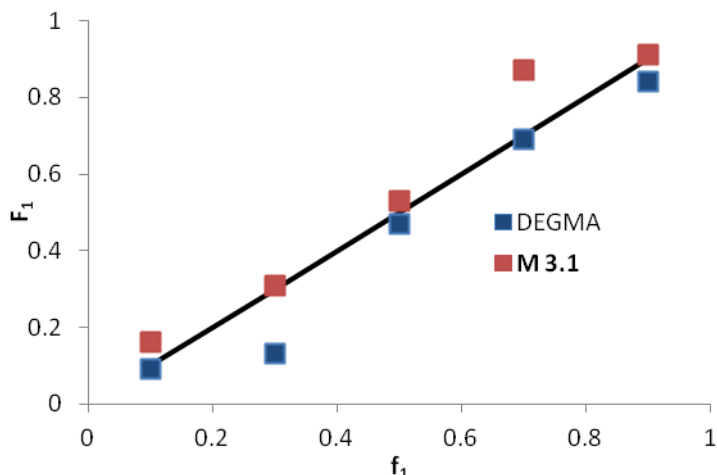


Figure 3.12. Plot of monomer fraction in the initial feed and in resulting co-polymer of **M 3.1** and DEGMA, used to determine reactivity ratios.

The reactivity ratios were determined as follows for $r_{\text{M 3.1}} = 0.892$ and $r_{\text{DEGMA}} = 0.575$. Both monomers are near to the ideal kinetics and are likely to react with each other as well as themselves, most likely yielding a random co-polymer. Therefore, the co-polymers synthesized within this series can be considered as random co-polymers with the catalytic functionalities distributed randomly along the polymer backbone. However, as the kinetics deviate from ideal the azeotropic copolymer composition needs to be considered. This is the point at which the composition of the polymer is constant and equal to the starting feed ratio and calculated according to Equation 3.2, for this system f_{1c} is equal to 0.8.²⁶

$$f_{1c} = \frac{(1 - r_2)}{2 - (r_1 + r_2)} \quad (3.2)$$

3.3.3 Polymer properties

3.3.3.1 Glass transition temperature

The glass transition temperature (T_g) is the temperature at which the polymer stops behaving like a crystalline glass and starts to behave like a rubber. The T_g can be influenced by a number of variables including chain stiffness. This is influenced by the chemical nature of the polymer backbone and pendent side groups. A more rigid structure will give higher T_g . The presence of intermolecular interactions such as dipole-dipole interactions, hydrogen bonding, ionic interactions or even covalent bonding will also affect the T_g .

The T_g was measured by Differential Scanning Calorimetry (DSC) which measures the change in heat as a function of temperature. The process of going through the T_g is endothermic and is therefore detected as a change in heat flow at a given temperature which is measured against an empty holder as a reference. Above the T_g the polymer has turned from a glassy material to a rubber like state.

The synthesized co-polymers have significant differences in their physical properties with low incorporation of **M 3.1** giving rubbery polymers and high incorporation giving glassy solids as depicted in the photo of the samples in Figure 3.13. The colour of the RAFT end group is less apparent in the higher catalyst incorporation polymers, which has been attributed to a dominating effect from the higher incorporation of **M 3.1** which is a white solid. The T_g of the polymer series was measured confirming these observations where higher incorporation of the catalyst increases the T_g . The results can be seen in Table 3.2.

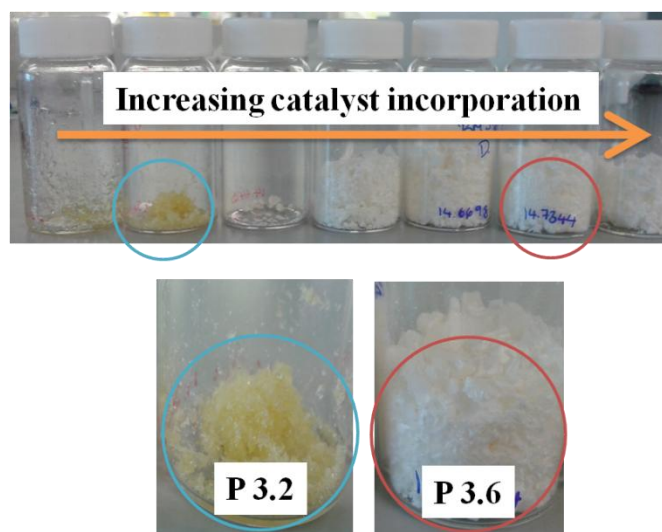


Figure 3.13. A photo of the polymer **P 3.1** – **P 3.7**, as the catalyst incorporation increases the polymers' physical appearance changes from a yellow sticky solid to a white fluffy solid.

Table 3.2. The measured T_g values for the series of co-polymers **P 3.1** – **P 3.7**

Polymer	Catalyst incorporation (%) ^a	T_g (onset) ^b	T_g (midpoint) ^b
P 3.1	6	15.0	23.1
P 3.2	26	21.1	36.1
P 3.3	33	39.1	45.6
P 3.4	38	58.4	67.7
P 3.5	57	100.6	101.2
P 3.6	73	128.0	134.0
P 3.7	100	134.0	140.0

^aDetermined by comparing ratio of DEGMA to **M 3.1** in ¹H NMR spectrum

^bDetermined by DSC using an aluminium sample holder recording between 0 and 150 °C over two cycles with a scan rate of 5 °C min⁻¹.

The T_g midpoint varied from 23 °C for **P 3.1** (the lowest incorporation of **M 3.1**, 6%) up to 140 °C for **P 3.7** (highest incorporation of **M 3.1**, 100%). The dramatic change in T_g can be explained by the changing structure of the polymer with increasing incorporation of **M 3.1**. **M 3.1** has a more rigid structure than DEGMA and thus at higher incorporation, a higher T_g was observed. More rigid structures will yield higher T_g 's as more energy is required to mobilize the monomer units. **M 3.1** has the potential for more intermolecular interactions than DEGMA as it can form hydrogen bonds and also has the potential for π -stacking; thus, increasing the rigidity of the chain and contributing to an increase in T_g .

3.3.3.2 Lower critical solution temperature

The co-monomer DEGMA is known to exhibit a lower critical solution temperature (LCST). This is a property of the polymer solubility in solution with respect to temperature. An LCST polymer is soluble at temperatures below its LCST and insoluble above. In order to measure the LCST multiple concentration solutions need to be analyzed in order to find the temperature minima across all concentrations as seen in Figure 3.14. This minima is the LCST temperature, at a given concentration the LCST cloud point is measured. There are other systems that display the opposite behaviour known as upper critical solution temperatures (UCST).

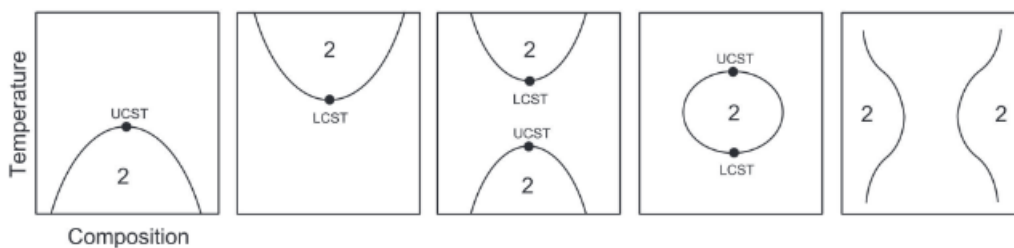


Figure 3.14. A reproduction of graphs highlighting the dependence of temperature on composition for both LCST and UCST systems.²⁷

This LCST effect is caused by the preferred interactions of the polymer with either itself or the solvent, which is most commonly water. LCST polymers will form hydrogen bonds with water but not with themselves, creating a loss in entropy but a gain in enthalpy from the bond formation; the Gibbs free energy equation must therefore be considered (Equation 3.3).

$$\Delta G = \Delta H - T\Delta S \quad (3.3)$$

The spontaneous mixing below the LCST cloud point (where ΔG is below zero) is driven by the formation of hydrogen bonds between the polymer and solvent. At elevated temperatures the entropic loss from the formation of these structures becomes more significant and eventually outweighs the enthalpy gain causing the polymer to precipitate.

The co-polymers synthesized in this work exhibit LCST cloud point behaviour which was found to be dependent on catalyst incorporation and polymer concentration. The

results can be seen in Figure 3.15 and have been compared to a homopolymer of DEGMA (poly(DEGMA)).

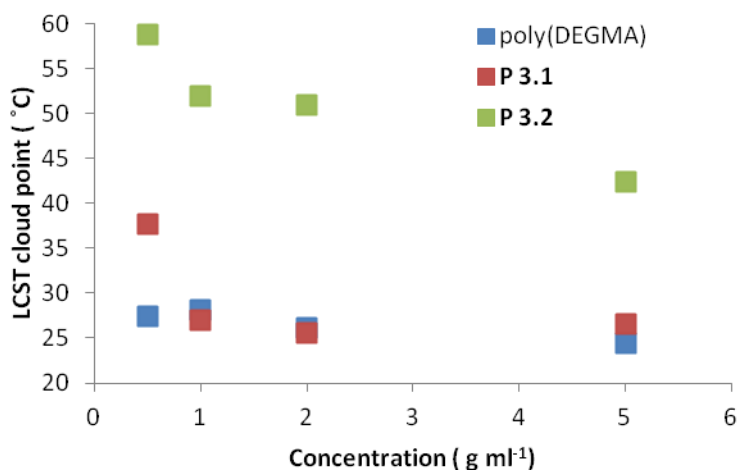


Figure 3.15. Cloud point data for poly(DEGMA), **P 3.1** and **P 3.2** across a range of concentrations in water. The data was recorded at 500 nm with a heating/cooling rate of 1 °C min⁻¹. The cloud point was taken at the temperature when the absorbance equalled 0.5 after the data had been normalized between 0 and 1 absorbance units.

At higher loadings of **M 3.1** in the polymer the LCST cloud point increases. The poly(DEGMA) ($M_{n(\text{NMR})} = 16.7$ kDa) has an LCST cloud point at 0.5 mg mL⁻¹ of 27 °C which increased to 38 °C for **P 3.1** (6% loading of **M 3.1**) and was increased for **P 3.2** (26% loading of **M 3.1**) to 59 °C. The LCST of the poly(DEGMA) compares well to literature values of 26 °C at 1 mg mL⁻¹ with the synthesized polymer in this work having an LCST of 28 °C at 1 mg mL⁻¹.²⁸ Analysis of polymers at higher loadings was inconclusive as their cloud points fell out of the measurable range of the instrument. As LCST is measured in water the highest temperature feasible is 100 °C but at temperatures lower than this factors such as bubbles and condensation can affect the

results along with the instrument set up unable to reliably heat past 90 °C. This increase in LCST cloud point with increasing **M 3.1** loading is explained by the ability of **M 3.1** to form hydrogen bonds to itself and not only with water creating more enthalpy in the system. Thus, a higher temperature is required for the entropic loss to cause unfavourable mixing. The LCST cloud point traces for poly(DEGMA), **P 3.1** and **P 3.2** can be seen in Figure 3.16.

The cloud point is affected by the concentration of polymer as shown in the phase diagram in Figure 3.14: at low concentrations the cloud point falls with increasing concentration and at higher concentrations the cloud point increases alongside concentration. The data in Figure 3.15 shows that these concentrations are in the first regime with the LCST cloud point of poly(DEGMA) falling from 27.4 °C at 0.5 mg mL⁻¹ to 24.4 °C at 5.0 mg mL⁻¹. The cloud point is affected by the changing concentration due to the relationship between the entropy and enthalpy of the system as previously discussed. At very low concentrations there is minimal loss of entropy as there are only a few polymer-water interactions and therefore a higher temperature has to be reached before precipitation occurs. As polymer concentration increases, the amount of polymer-water interactions increases causing a larger ΔS term and therefore a lower cloud point. This continues until a minimum is reached, the LCST, before the cloud point begins to increase. Here, further addition of polymer allows the increase of polymer-polymer interactions creating a larger ΔH which is not matched in growth by the ΔS term and therefore higher cloud point temperatures are observed.

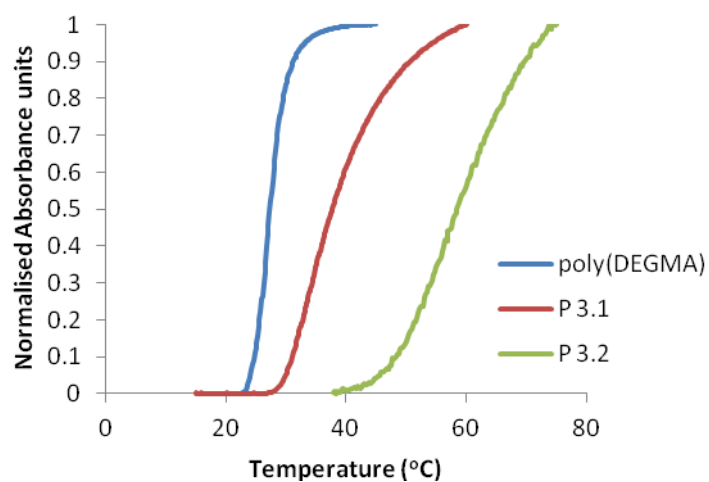
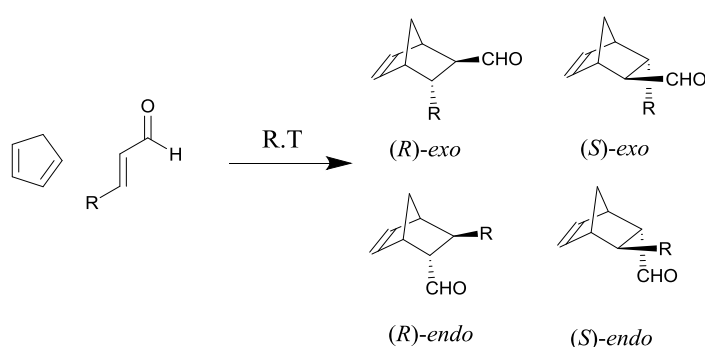


Figure 3.16. LCST cloud point measurements traces taken at 0.5 mg mL^{-1} and measured at 500 nm with the temperature taken at 0.5 absorbance units after the data had been normalized between 0 and 1 for a) poly(DEGMA) (blue line) b) **P 3.1** (red line) and c) **P 3.2** (green line).

3.3.4 Diels-Alder Catalysis

The catalytic efficiency of the co-polymers was investigated using a benchmark reaction: the Diels-Alder (DA) reaction between cyclopentadiene and *trans*-hexen-1-al. This reaction has previously been used to demonstrate the capability of the MacMillan catalyst and was therefore selected as the model reaction. In the first report of the catalyst these were one pair of substrates chosen to demonstrate the catalyst capabilities, the reaction took place with 5 mol% of catalyst in MeOH:H₂O (95:5 v/v%) at 23 °C for 14 hours which gave 92% yield *exo:endo* 1.0:1.0 86% *exo* ee and 90% *endo* ee. This reaction has four possible products and these can be seen below in Scheme 3.4.



Scheme 3.4. Model DA reaction, where R = C₃H₇ and where there are four possible products: the *endo* and *exo* products of both enantiomers.

According to the mechanistic procedure laid out by MacMillan the favoured enantiomer is the (*S*)- product, which is the enantiomer that MacMillan reported was in excess. The reaction conversions were measured using ¹H NMR spectroscopy; a typical ¹H NMR spectrum for the resulting products can be seen in Figure 3.17. The enantioselectivities were measured by chiral-GC and a typical spectrum with the four products resolved and assigned can be seen in Figure 3.18.

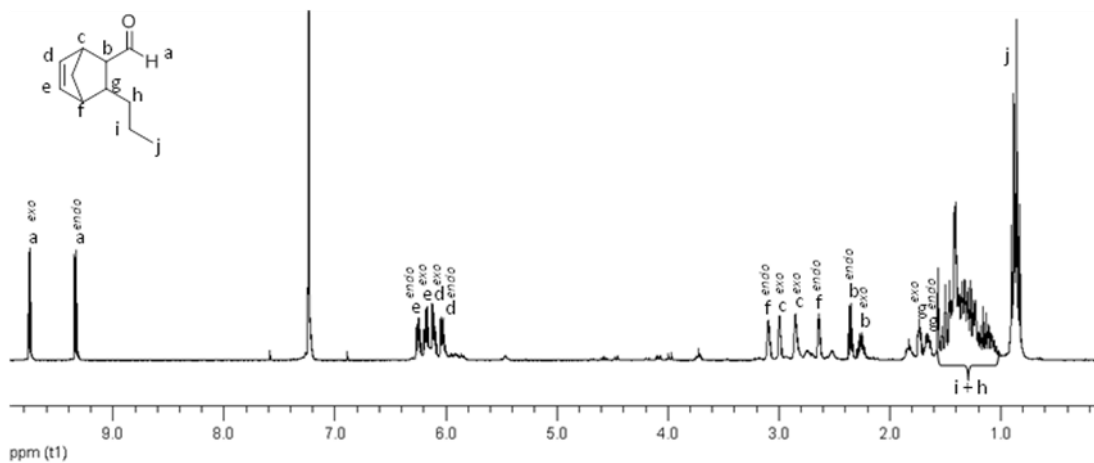


Figure 3.17. A representative ¹H NMR (300 MHz) spectrum in CDCl₃ of the DA products.

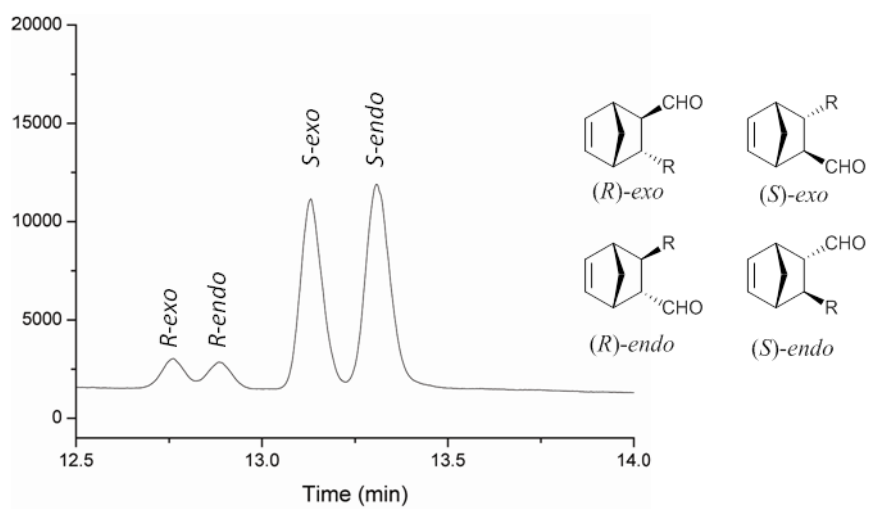


Figure 3.18. A representative GC chromatogram of the DA products.

3.3.4.1 Monomer

Initially, the reaction was carried out with **M 3.1** and the non-polymerizable monomer (discussed above), their structures can be seen in Figure 3.19. The results can be seen in Table 3.3 and a scheme highlighting the reaction conditions can be seen in Scheme 3.5.

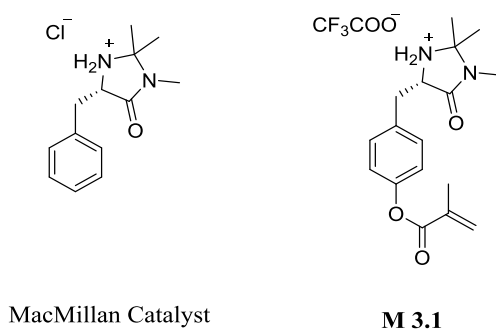
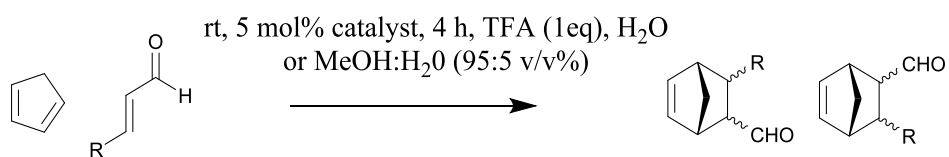


Figure 3.19 The structures of **M 3.1** and the MacMillan catalyst.



Scheme 3.5. A schematic of the DA reaction between cyclopentadiene and *trans*-hexen-1-al giving the conditions of the reaction.

Table 3.3. The DA reaction at rt for 4 h catalyzed by **M 3.1** and MacMillan catalyst, compared with reported literature values at 5 mol%.

Catalyst	Solvent	Conversion ^a (%)	<i>exo:endo</i> ^b	<i>exo</i> ee% ^c	<i>endo</i> ee% ^c
MacMillan (reported)	CH ₃ OH:H ₂ O ^d	92	1.0:1.0	84	93
MacMillan (synthesized)	CH ₃ OH:H ₂ O ^d	95	1.0:0.8	89	93
M 3.1	CH ₃ OH:H ₂ O ^d	84	1.0:1.0	79	88
M 3.1	H ₂ O	94	1.0:1.1	73	88

^aDetermined by ¹H NMR spectroscopy through comparison of the *trans*-hexen-1-al aldehyde proton ($\delta = 9.45$ ppm) and the product aldehyde protons ($\delta = 9.33$ ppm and 9.75 ppm)

^bDetermined by ¹H NMR spectroscopy through comparison the product aldehyde protons ($\delta = 9.33$ ppm (*exo*) and 9.75 ppm(*endo*))

^cDetermined by chiral GC analysis

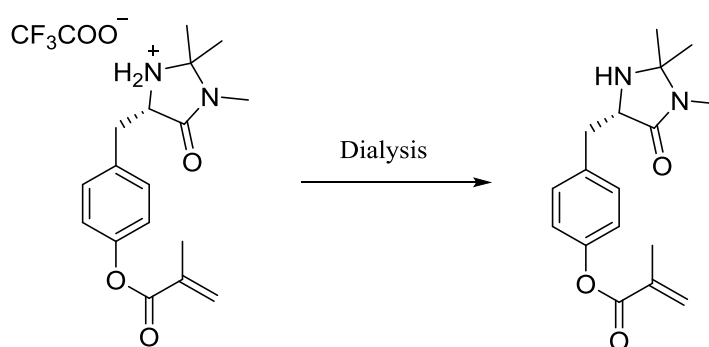
^dMeOH:H₂O 95:5 v/v%

The results of the small molecule catalysis demonstrate that the synthesized MacMillan catalyst and monomer **M 3.1** perform in a similar fashion. However, with reference to Figure 3.19 there is a subtle but crucial difference in the structure of the monomer to the catalyst. The monomer has a TFA salt whereas the catalyst has an HCl salt. The salt acts as a co-catalyst and is important in the rate of the iminium formation; the effect of the acidity of the catalyst has been noted by Larsen.² More acidic co-catalysts (pKa HCl = -8.0, pKa TFA = -0.25) provide higher reactivity and improve enantioselectivity. Therefore, the slight fall in conversion from the reported MacMillan catalyst of 92% and to 84% and 93% to 88% *endo* ee for **M 3.1** is not surprising. However, when

incorporated into the polymer the reactivity of **M 3.1** compares well to the unsupported monomer.

3.3.4.2 Functionalized co-polymers

The functionalized co-polymers were then used to perform the same DA reaction (5 mol% in either H₂O or MeOH:H₂O 95:5 v/v%). These results can be seen in Figure 3.20. The first attempt at utilizing these polymers to catalyze the DA reaction under the same conditions was unsuccessful. Dialysis against nanopure water was used to purify the polymers in order to remove any remaining water soluble monomers. Unfortunately, this process removed the TFA salt that **M 3.1** had been synthesized with and is crucial for catalysis (Scheme 3.6).



Scheme 3.6. A schematic representation of the loss of the TFA salt.

Therefore the reactions with the polymers required addition of the acid co-catalyst. Therefore 1 equivalent of TFA was added to the reaction in order to activate the *trans*-hexen-1-al. At equal equivalents to the monomer (0.05 equivalents) the reaction was still unsuccessful and consequently an increased amount was utilized to ensure

activation of all the aldehyde substrate. TFA was chosen in order to make the catalysis comparable to the monomer.

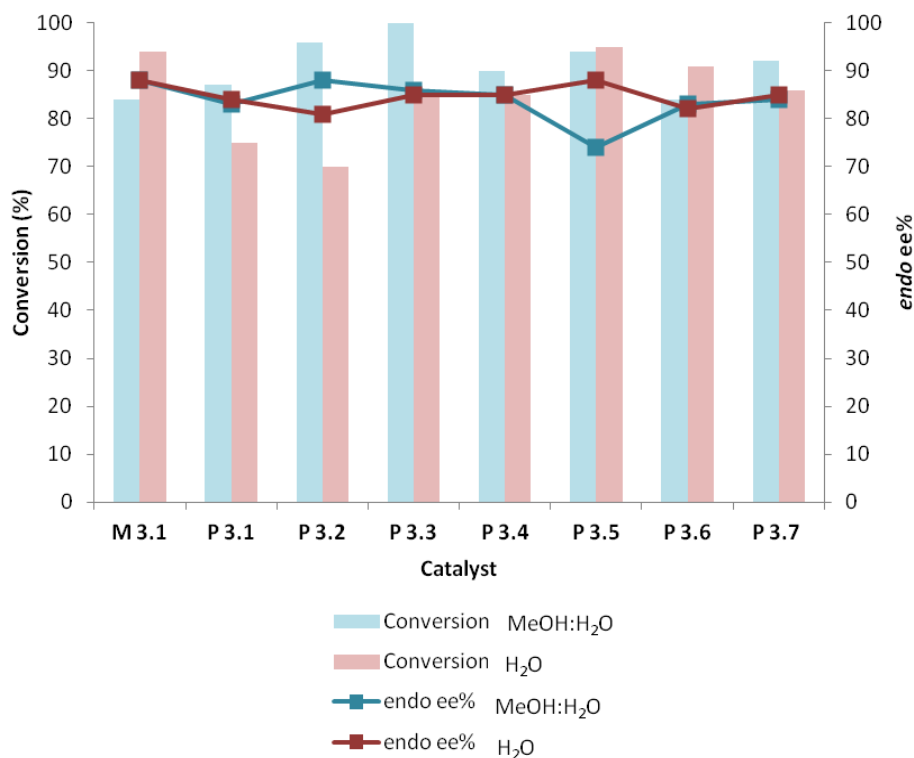


Figure 3.20. The conversions and selectivities of the data highlighting the similarity between the two solvent systems.

Indeed high catalytic activity was observed for the co-polymers in the DA reaction. The *exo:endo* ratios were similar across all the reactions (1.0:0.6-1.1) and the *ee*'s comparable but uniformly slightly lower than those reported in the literature for both *endo* and *exo* products. Moreover, changing the reaction solvent from CH₃OH:H₂O (95:5 v/v%) to pure H₂O appears to have little effect on the reaction conversion and enantioselectivity. All the reactions have been conducted at 5 mol% achieved by adding different amounts of polymer based on the loadings. Therefore the reactions have

different concentration of polymer, but not catalyst. At the scale these reactions were performed at there was no noticeable change in viscosity of the solution which could be caused by the variation in polymer quantity.

3.3.4.2.1 DA kinetics

It has been previously reported that the space around the catalyst or catalyst isolation can have a dramatic effect on the activity of the catalyst.^{29,30} It was therefore anticipated that varying the loading of catalyst on the polymer and therefore the relative space around the catalyst may have a significant effect on its catalytic activity.

Therefore, the kinetics of the reaction catalyzed by co-polymers **P 3.2** (26%) and **P 3.6** (73%) were investigated to determine if the loading affected the rate of reaction. The plots of conversion with time for **P 3.2** and **P 3.6** are shown below in Figure 3.21 and further details of the reaction in Table 3.4.

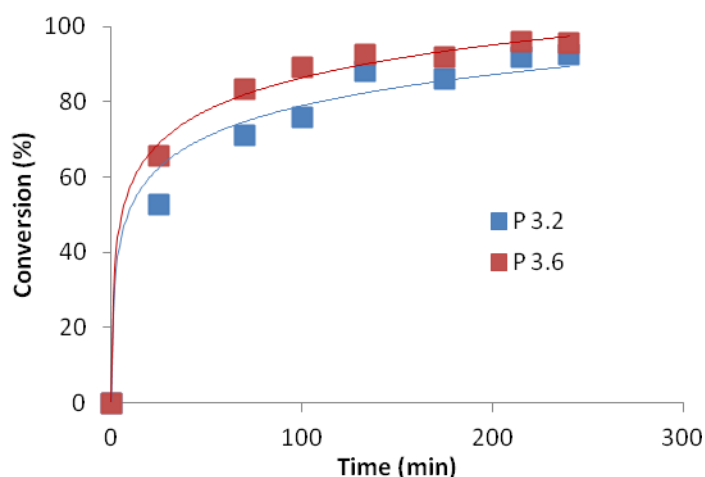


Figure 3.21. Kinetic plots for the DA reaction between cyclopentadiene and *trans*-hexen-1-al catalyzed by **P 3.6** and **P 3.2** fitted to a logarithmic trendline.

Table 3.4. Kinetic data for the DA reaction of *trans*-hexen-1-al and cyclopentadiene catalyzed by **P 3.2** and **P 3.6**. The reactions were carried out in H₂O, conversions measured by ¹H NMR spectroscopy and enantioselectivity by GC analysis.

Material	Time (min)	Conversion ^a (%)	<i>exo:endo</i> ^b	<i>exo</i> ee% ^c	<i>endo</i> ee% ^c
P 3.2 (26%)	25	53	1.0:1.2	70	78
	70	71	1.0:1.1	69	77
	100	76	1.0:1.1	70	75
	133	88	1.0:1.1	68	74
	175	86	1.0:1.1	68	76
	215	92	1.0:1.1	68	77
	240	93	1.0:1.1	69	80
P 3.6 (73%)	25	66	1.0:1.2	70	79
	70	83	1.0:1.1	69	75
	100	89	1.0:1.1	70	75
	133	93	1.0:1.1	98	73
	175	92	1.0:1.2	68	74
	215	96	1.0:1.1	68	74
	240	96	1.0:1.1	67	76

^aDetermined by ¹H NMR spectroscopy through comparison of the *trans*-hexen-1-al aldehyde proton ($\delta = 9.45$ ppm) and the product aldehyde protons ($\delta = 9.33$ ppm and 9.75 ppm)

^bDetermined by ¹H NMR spectroscopy through comparison the product aldehyde protons ($\delta = 9.33$ ppm (*exo*) and 9.75 ppm(*endo*))

^cDetermined by chiral GC

A similar rate of catalysis was observed for the two co-polymers. The enantioselectivities of the two polymers at different time points in the reaction were also found to be comparable. For this system, therefore, it seems that the catalyst loading has

little to no effect on the efficiency of the catalyst. As the reactions were both carried out at 5 mol% a different amount of each polymer was added to the reaction (7 mg for **P 3.2** and 3 mg for **P 3.6** in 100 μ L of H₂O) but there was no noticeable effect on solution viscosity at the scale the reactions were performed on.

The effect of temperature has also been investigated for **M 3.1**, **P 3.2** (26%) and **P 3.7** (100%). As anticipated, the reaction activity increased with temperature but to the expense of the enantioselectivity. There is no deviance away from this trend with regards to different catalytic loadings suggesting that the catalyst is operating in the same fashion regardless of loading and the associated rigidity of the polymer.

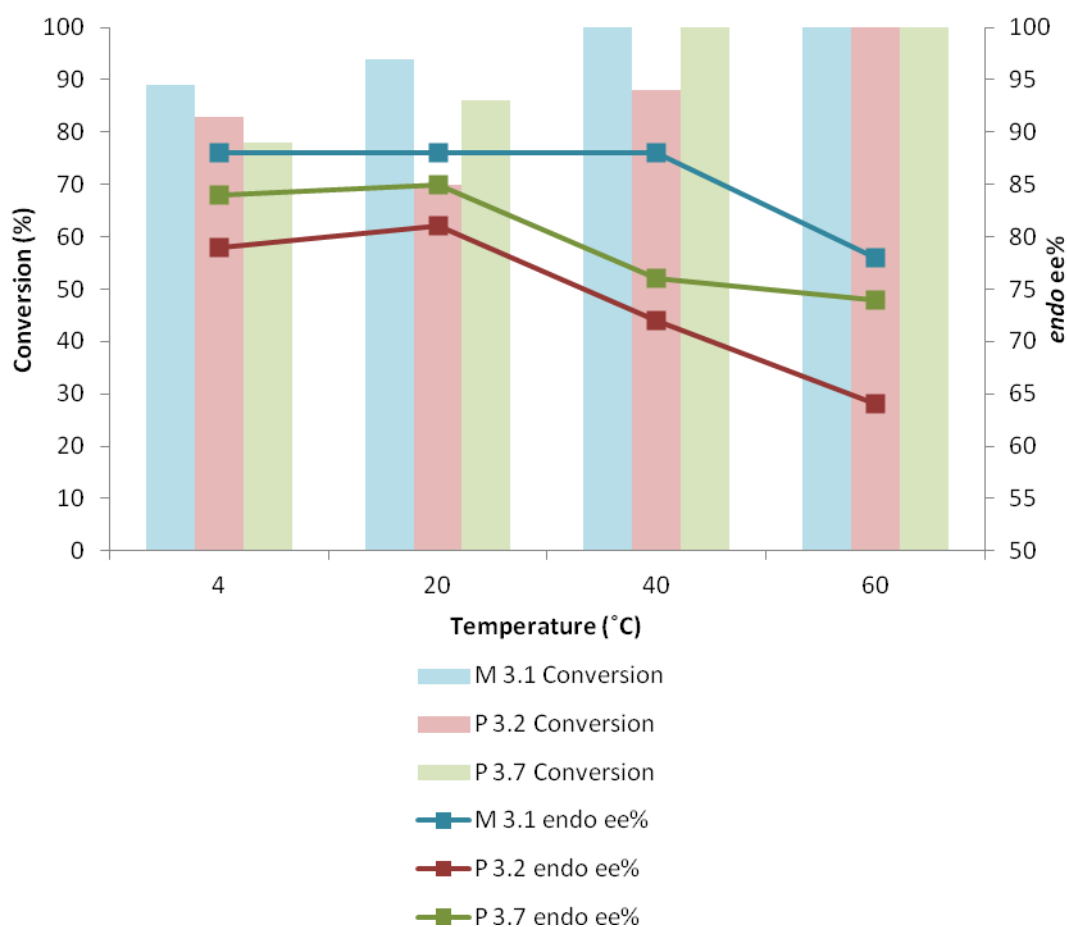


Figure 3.22. The conversions and selectivities for the DA reaction between cyclopentadiene and *trans*-hexen-1-ol after 4 h for **M 3.1**, **P 3.2** and **P 3.7** at different temperatures (4, 20, 40 and 60 °C) at 5 mol%.

It is possible that the RAFT end group still present on the co-polymers may interfere with the reaction. In order to determine the impact of the RAFT end group, it was removed using established chemistries.³¹ This was carried out using a radical induced method and with 1-ethylpiperidine hypophosphite (1-EHP) as a proton donor, leaving the co-polymer with a proton replacing the end group. The successful removal of the end group was confirmed by the loss of the characteristic UV trace in the SEC at 309 nm (Figure 3.23). The resulting DA data for this end group removed polymer can also be seen in Table 3.5. The catalytic activity of the polymer before and after end group

removal was comparable, both achieving 91% conversion. The enantioselectivity of 82% pre and 75% post *endo* ee was also comparable suggesting that the presence of the end group, and the route for its removal had negligible effects on the reaction.

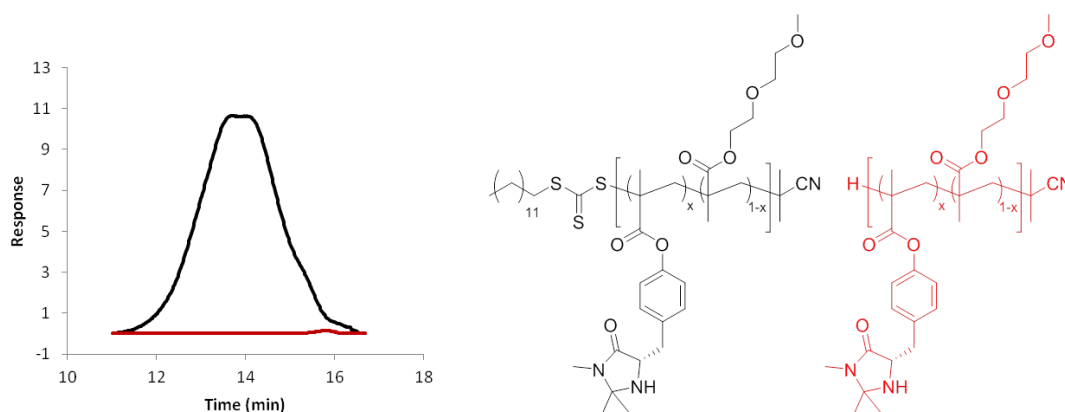


Figure 3.23. THF SEC UV 309 nm trace of **P 3.6** before (black line) and after end group removal (red line), along with the structures of the two polymers.

Table 3.5. DA reaction of *trans*-hexen-1-al and cyclopentadiene catalyzed by **P 3.6** with and without RAFT end group. The data for the reaction without end group is the average of 2 repeats.

End group	Conversion ^a (%)	<i>exo:endo</i> ^b	<i>exo</i> ee% ^c	<i>endo</i> ee% ^c
With	91	1.0:1.1	74	82
Without	91	1.0:1.0	70	75

^aDetermined by ¹H NMR spectroscopy through comparison of the *trans*-hexen-1-al aldehyde proton ($\delta = 9.45$ ppm) and the product aldehyde protons ($\delta = 9.33$ ppm and 9.75 ppm)

^bDetermined by ¹H NMR spectroscopy through comparison the product aldehyde protons ($\delta = 9.33$ ppm (*exo*) and 9.75 ppm(*endo*))

^cDetermined by chiral GC

3.3.5 Polymer recycling

As the polymers exhibit LCST behaviour it was envisaged that this property could be exploited to assist in reclaiming the polymer and therefore the catalyst. Unfortunately, the reagents had a solubilising effect on the polymer system raising their LCST and making this route unviable.

3.3.5.1 Recycling through polymer reclaim

Initial attempts to recycle the catalyst were made by trying to reclaim the polymer through conventional polymer handling techniques, i.e. through precipitation, dialysis or freeze drying. One of the advantages of catalyst immobilization onto polymers is that their solubility is often very different from small molecules. This makes it possible to use precipitation methods to separate polymers from monomers. Catalyst recovery and re-use using the dialysis/freeze-drying method is detailed in Table 3.6. The physical loss of polymer in each recovery step, having carried out the reaction on a small scale, was highly significant and made this method inappropriate with only 10% total recovery of polymer after 4 cycles. A loss in conversion and a slight loss in selectivity has been observed. As the recovery was through dialysis, it was presumed that the TFA would be lost again and additional TFA was added along with the reagents in each re-use.

Table 3.6 Recycling data for the DA reaction catalyzed by **P 3.6** where the polymer was recovered through dialysis followed by freeze-drying.

Cycle	Conversion ^a (%)	<i>exo:endo</i> ^b	<i>exo</i> ee% ^c	<i>endo</i> ee% ^c	Recovery (%)
1	86	1.0:1.3	67	61	60
2	85	1.0:1.2	65	65	49
3	46	1.0:1.4	59	52	13
4	70	1.0:1.4	56	50	10

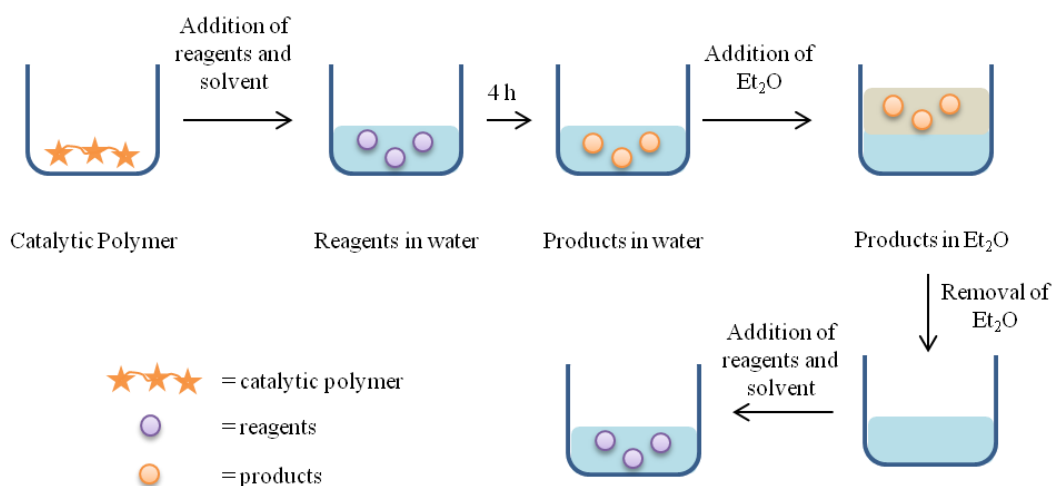
^aDetermined by ¹H NMR spectroscopy through comparison of the *trans*-hexen-1-al aldehyde proton ($\delta = 9.45$ ppm) and the product aldehyde protons ($\delta = 9.33$ ppm and 9.75 ppm)

^bDetermined by ¹H NMR spectroscopy through comparison the product aldehyde protons ($\delta = 9.33$ ppm (*exo*) and 9.75 ppm(*endo*))

^cDetermined by chiral GC

3.3.6.2 Pseudo-continuous recycling

As the starting materials, products and polymer differ in their solubility it was envisaged that everything but the polymer could be removed by a simple extraction method. Thus, after the 4 hour reaction, a diethyl ether wash was performed, leaving the polymer in the aqueous layer and the substrates/products in the organic layer. A schematic of this process can be seen in Scheme 3.7.

Scheme 3.7 A schematic to demonstrate the *pseudo*-continuous process.

Upon addition of new starting materials (including TFA), the reaction proceeded to high conversion but with a drop in selectivity from 75% *endo* ee to 57% *endo* ee after 2 cycles (Table 3.7).

Table 3.7. *Pseudo* continuous recycling data for the DA reaction between cyclopentadiene and *trans*-hexen-1-al at 5 mol% after 4 h reactions, catalyzed by **P 3.6** where additional TFA is added along with the solvents for each cycle.

Cycle	Conversion ^a (%)	<i>exo:endo</i> ^b	<i>exo</i> ee% ^c	<i>endo</i> ee% ^c
1	72	1.0:1.0	64	75
2	95	1.0:1.1	58	72
3	94	1.0:1.4	35	57

^aDetermined by ¹H NMR spectroscopy through comparison of the *trans*-hexen-1-al aldehyde proton ($\delta = 9.45$ ppm) and the product aldehyde protons ($\delta = 9.33$ ppm and 9.75 ppm)

^bDetermined by ¹H NMR spectroscopy through comparison the product aldehyde protons ($\delta = 9.33$ ppm (*exo*) and 9.75 ppm(*endo*))

^cDetermined by chiral GC

The drop in enantioselectivity could be related to the addition of new TFA in each cycle, as TFA itself can catalyze the reaction, the results of which can be seen in Table 3.8. With 1 equivalent of TFA for 4 hours in H₂O the reaction has reached 45% conversion but with no obvious control over selectivity. There is a preference for the *endo* product but no significant enantioselective control.

Table 3.8. The DA reaction cyclopentadiene and *trans*-hexen-1-al with 1 eq. of TFA for 4 h in H₂O.

Catalyst	Conversion ^a (%)	<i>exo:endo</i> ^b	<i>exo</i> ee% ^c	<i>endo</i> ee% ^c
TFA	45	1.0:3.8	1.6	11

^aDetermined by ¹H NMR spectroscopy through comparison of the *trans*-hexen-1-al aldehyde proton ($\delta = 9.45$ ppm) and the product aldehyde protons ($\delta = 9.33$ ppm and 9.75 ppm)

^bDetermined by ¹H NMR spectroscopy through comparison the product aldehyde protons ($\delta = 9.33$ ppm (*exo*) and 9.75 ppm(*endo*))

^cDetermined by chiral GC

Thus, the reactions were repeated but this time omitting the addition of TFA for each cycle. Interestingly, the reaction proceeded with good conversion and selectivity. Therefore it has been hypothesized that the diethyl ether wash does not remove all the TFA, negating the need for an additional amount.

Table 3.9. The conversions and selectivities of the DA reaction between cyclopentadiene and *trans*-hexen-1-al with **P 3.2** at 5 mol% used in a *pseudo*- continuous process with no further addition of TFA in each cycle.

Cycle	Conversion ^a (%)	<i>exo:endo</i> ^b	<i>exo</i> ee% ^c	<i>endo</i> ee% ^c
1	95	1.0:1.3	75	79
2	99	1.0:1.1	79	86
3	87	1.0:1.1	84	88
4	70	1.0:1.0	81	87

^aDetermined by ¹H NMR spectroscopy through comparison of the *trans*-hexen-1-al aldehyde proton ($\delta = 9.45$ ppm) and the product aldehyde protons ($\delta = 9.33$ ppm and 9.75 ppm)

^b Determined by ¹H NMR spectroscopy through comparison the product aldehyde protons ($\delta = 9.33$ ppm (*exo*) and 9.75 ppm(*endo*))

^cDetermined by chiral GC

After four cycles, a drop in conversion and a slight rise in selectivity were observed which have been attributed to a change in concentration of TFA in solution. If any TFA is being lost in the diethyl ether wash this would reduce its concentration; consequently this would reduce the rate, which could also lead to improved selectivity.

This catalyst has been a challenging target for recovery and recycling in previous work due to the catalyst's unstable nature,¹⁹ although there has been no indication of how the catalyst is actually unstable. Most likely the degradation of the ring system and the subsequent loss of the catalytic site is responsible. However, there has recently been progress towards a facile recovery system using magnetism¹⁶ and a flow system.¹⁸

3.4 Conclusions

A novel monomer containing a polymerizable methacrylate group and the catalytic MacMillan moiety has been synthesized in good yield. The monomer has been homo- and co-polymerized with DEGMA using RAFT polymerization to yield well-defined polymers containing varying amounts of the catalytic monomer.

Both the monomer and series of polymers were tested for their catalytic ability in the DA reaction between cyclopentadiene and *trans*-hexen-1-al. Comparable conversions and selectivities were achieved to the reported MacMillan catalyst.

The polymer properties of cloud point and T_g have also been analyzed for the range of co-polymers and the incorporation of **M 3.1** was found to affect both properties where higher catalyst incorporations resulted in an increase of cloud point and T_g .

The catalytic polymers were also used in a *pseudo*-continuous recycling process by removing starting materials and end products based on the different solubility between the small molecular materials and the polymer. The re-use cycles showed limited degradation of the catalyst and are a significant step towards the controlled immobilization and the re-use of the MacMillan catalyst.

3.5 Experimental

3.5.1 Instrumentation

Both ^1H and ^{13}C NMR spectra were recorded on a 300 or 400 MHz Bruker DPX FT-NMR spectrometer using deuterated solvents. Chemical shifts are reported as δ in parts per million relative to the solvent used. Size exclusion chromatography/gel permeation chromatography (SEC/GPC) data were obtained using PLgel 5 μm mixed-D columns, plus one guard column and tetrahydrofuran (THF) with 2% triethylamine (TEA) as eluent, with a flow rate of 1.0 mL min^{-1} . The data was analyzed using Cirrus GPC software and compared to poly(methylmethacrylate) (PMMA) standards. Lower critical solution temperature (LCST) measurements were performed on a Perkin Elmer UV/Vis spectrometer (Lambda 35) equipped with a Peltier temperature controller at 500 nm with a constant heating/cooling rate of $1\text{ }^\circ\text{C min}^{-1}$. Enantiomeric excess (ee%) was measured by gas chromatography (GC) on a Varian 450-GC with a 25 m chirasil-Dex chiral column or by high performance liquid chromatography (HPLC) analysis on a Shimadzu Prominence HPLC with a Chiracel OD-H column $250\text{ mm} \times 4.6\text{ mm} \times 5\text{ }\mu\text{m}$, with guard column (5 μm). The centrifuge used to reclaim the MacMillan monomer was a Sigma 2-16 P centrifuge operated at 7000 rpm. Glass transition temperatures (T_g) were determined using a Mettler Toledo DSC1-STAR. Differential scanning calorimetry (DSC) was carried out on the sample (2 - 10 mg) in an aluminium sample holder where an empty holder was used as the reference. Changes in heat flow were recorded between $0\text{ }^\circ\text{C}$ and $150\text{ }^\circ\text{C}$ over two cycles with a scan rate of $5\text{ }^\circ\text{C min}^{-1}$, under a nitrogen stream (50 mL min^{-1}). The instrument was calibrated using indium metal standards supplied by

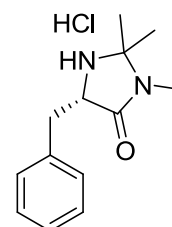
Mettler Toledo and the data was analyzed using STARe software package (version 9.30).

3.5.2 Methods and Techniques

Azo-(*bis*)-isobutyronitrile (AIBN) was purchased from Sigma-Aldrich, recrystallized from methanol and stored in the dark at 4 °C. DEGMA was purchased from Sigma-Aldrich, filtered through an aluminium oxide column and stored at 4 °C before use. Cyclopentadiene was prepared by cracking dicyclopentadiene purchased from Sigma-Aldrich. All other chemicals were purchased from Sigma-Aldrich and used without further purification.

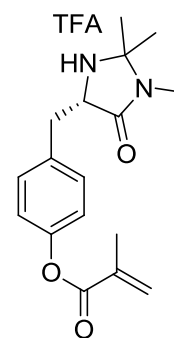
3.5.2.1 Synthesis of small molecules

Synthesis of the MacMillan catalyst: In order to determine if racemization of the catalyst stereocenter had occurred under the polymerization conditions, non-polymerizable MacMillan catalysts (both *S* and *R* versions) were synthesized from *S*- and *R*-phenylalanine.



HPLC analysis (hexane:propan-2-ol, 90:10 using a Chiracel OD-H column 250 mm × 4.6 mm × 5 μm, with guard column (5 μm)) showed the following retention times: (*S*)-enantiomer, $t_R = 7.9$ min and (*R*)-enantiomer, $t_R = 7.2$ min.

M 3.1: (*S*)-Tyrosine methyl ester hydrochloride (25 g, 0.128 mol) was dissolved in a solution of methylamine in ethanol (33 wt%, 81 mL, 0.64 mol) and stirred overnight. The resulting solution was diluted with diethyl ether (~ 100 mL) and the solvent removed *in vacuo*. This process was repeated multiple times (~ 5) until all excess amine had



been removed. The resulting sticky yellow solid was dissolved in methanol (150 mL) and acetone (47 mL, 0.643 mol) and *para*-toluene sulfonic acid (0.22g, 0.128 mol) was then added. The solution was stirred under reflux for 18 h. Excess reagents and solvents were removed *in vacuo*. Care was taken to remove the methanol as remaining traces of the solvent affect the final crystallization step, due to the high solubility of the product in this solvent. Trifluoroacetic acid (30 mL) was added carefully to the resulting orange solid at 0 °C. The reaction was left to stir until the solid was dissolved. Trifluoromethanesulfonic acid (2.83 mL, 0.032 mol) was then added slowly and allowed to stir for 10 min before methacryloyl chloride (25 mL, 0.256 mol) was added slowly.³² The reaction mixture was then allowed to warm to room temperature and stirred overnight. Excess solvents and acids were removed by air flow and the resulting product thoroughly dried under vacuum with a sintered attachment to prevent loss of any solids. A sticky yellow solid resulted and to this, diethyl ether (300 mL) was added, resulting in a white precipitate which was collected, further washed with diethyl ether (~ 100 mL) and dried *in vacuo* to give the desired MacMillan functionalized monomer **M 3.1** as an amorphous white solid (33.4 g, 87%). ¹H NMR (300 MHz, CD₃OD): δ 1.51 (3H, s, -NH-C(CH₃)₂-N(CH₃)-), 1.65 (3H, s, -NH-C(CH₃)₂-N(CH₃)-), 1.97 (3H, s, C(CH₃)=CH₂), 2.85 (3H, s, N(CH₃)), 2.94 (1H, dd, ³J = 10.5 Hz, 15 Hz, Ar-CHH-CH-), 3.48 (1H, dd, ³J = 3.6 Hz, 15 Hz, Ar-CHH-CH-), 4.55 (1H, dd, ³J = 3.6 Hz, 10.5 Hz,

Ar-CHH-CH-), 5.76 (1H, s, C(CH₃)=CHH-), 6.25 (1H, s, C(CH₃)=CHH-), 7.09 (2H, d, ³J = 8.4 Hz, Ar), 7.39 (2H, d, ³J = 8.4 Hz, Ar). ¹³C NMR (75 MHz, CD₃OD): δ 18.5 (CH(CH₃)=CH₂), 22.2 (C(CH₃)₂), 24.5 (C(CH₃)₂), 25.7 (N(CH₃)), 34.7 (Ar-CH₂), 59.7 (Ar-CH₂-CH), 78.9 (C(CH₃)₂), 123.5 (Ar), 128.1 (CH(CH₃)=CH₂), 131.4 (Ar), 134.3 (Ar), 137.2 (CH(CH₃)=CH₂), 151.9 (C(O)-CH(CH₃)=CH₂), 168.1 (N(CH₃)-C(O)). HR ESI-MS: found 303.1698 m/z [M+H]⁺, expected 303.1709. IR: 3006, 1718, 1663, 1617, 1199, 1171, 1130, 1027 cm⁻¹. [α]_D²⁵ = + 7.5.

3.5.2.2 Synthesis of Polymers

Co-polymerization of M 3.1 and DEGMA: A typical polymerization was carried out as follows: to an oven-dried ampoule, **M 3.1** (0.087 g, 10 eq, 0.28 mmol), DEGMA (0.490 g, 90 eq, 2.6 mmol), azo-(*bis*)-isobutyronitrile (0.4 mg, 0.1 eq, 2.9 × 10⁻³ mmol), 2-cyano-2-propyl dodecyl trithiocarbonate (0.01g, 1 eq, 2.9 × 10⁻² mmol) and DMSO (1 mL) were added. The mixture was degassed *via* three freeze-pump-thaw cycles and backfilled with nitrogen, before being placed in a pre-heated oil bath at 80 °C. After 6 hours, the reaction was quenched by rapid cooling in liquid nitrogen and exposure to oxygen. The polymer was then extensively dialyzed against deionized water (MWCO = 3500 Da) before being freeze-dried. ¹H NMR (300 MHz, DMSO): δ 0.8-2.1 (CH₂ and CH₃ polymer backbone), 3.2-3.7 (br m, DEGMA CH₂ and CH₃), 4.1 (br, C(O)O-CH₂-CH₂-O, DEGMA), 6.8-7.3 (br, Ar-MacMillan). Conversion by ¹H NMR spectroscopy: **M 3.1**, 93% and DEGMA, 84%. *M_n* (SEC, THF, PMMA calibration) = 11.8 kDa, *D* = 1.35.

Synthesis of poly(DEGMA): DEGMA (0.5 g, 100 eq, 2.6 mmol), 2-cyano-2-propyl dodecyl trithiocarbonate (9.2 mg, 1 eq, 2.7×10^{-2} mmol), AIBN (0.4 mg, 0.1 eq, 2.7×10^{-3} mmol) and dioxane (0.5 mL) were weighed into an oven-dried ampoule and degassed *via* three freeze-pump-thaw cycles, backfilled with nitrogen and heated at 70 °C. After 6 hours, the reaction was quenched by rapid cooling in liquid nitrogen and exposure to oxygen. The polymer was then dialyzed extensively against deionized water (MWCO = 3500 Da) before being freeze-dried. ^1H NMR (300 MHz, CDCl_3): δ 0.8-1.1 (3H, br, CH_3 polymer backbone), 1.7-2.0 (2H, br, CH_2 , polymer backbone), 3.41 (3H, br s, $-\text{O}-\text{CH}_3$), 3.55 (2, br s, $-\text{O}-\text{CH}_2-\text{CH}_2-\text{O}-\text{CH}_3$), 3.61 (2H, br s, $-\text{O}-\text{CH}_2-\text{CH}_2-\text{O}-\text{CH}_3$), 3.66 (2H, br s, $\text{C}(\text{O})\text{O}-\text{CH}_2-\text{CH}_2-$), 4.08 (2H, br s, $\text{C}(\text{O})\text{O}-\text{CH}_2-\text{CH}_2-$). Conversion by ^1H NMR spectroscopy: 95%, degree of polymerization (DP) = 89. M_n (^1H NMR) = 16.7 kDa. M_n (SEC, THF, PMMA calibration) = 13.8 kDa, $D = 1.36$.

3.5.2.3 Polymer end group removal

P 3.6 (50 mg, 1eq, 4.4×10^{-3} mmol), AIBN (0.4 mg, 0.5 eq, 2.2×10^{-3} mmol), 1-ethylpiperidine hypophosphite (1-EPHP) (4 mg, 5 eq, 2.2×10^{-2} mmol), toluene (1 mL) and DMSO (0.5 mL) were weighed into an oven-dried ampoule and degassed *via* three freeze pump-thaw cycles, backfilled with nitrogen and heated at 100 °C. After 2 hours, the toluene was removed under vacuum and the mixture dialyzed against deionized water (MWCO = 3.5 kDa). The polymer was then freeze-dried to yield a white solid. SEC analysis showed no absorbance in the UV-309 nm trace corresponding to the trithiocarbonate RAFT end group indicating that it was no longer present in significant quantities.

3.5.2.4 Polymer chirality retention test

By exposing the non-polymerizable (*S*)-MacMillan catalyst to the same polymerization conditions as **M 3.1**, possible racemization of the catalyst was investigated. The non-polymerizable (*S*)-MacMillan catalyst (0.250 g, 50 eq, 0.98 mmol), AIBN (0.3 mg, 0.1 eq, 2.0×10^{-3} mmol), CTA (2-cyano-2-propyl dodecyl trithiocarbonate, 6.8 mg, 1 eq, 2.0×10^{-2} mmol) and DMSO (0.5 mL) were weighed into an oven-dried ampoule and degassed *via* three freeze pump-thaw cycles before being back-filled with nitrogen and heated to 80 °C. After 6 h, the polymer was precipitated into cold stirring Et₂O, giving a cloudy solution and the polymer was collected by centrifugation. The resultant solid was analyzed by HPLC (hexane:propan-2-ol, 90:10 and showed only the presence of the (*S*)-enantiomer, $t_R = 7.9$ min ((*R*)-enantiomer, $t_R = 7.2$ min).

3.5.2.5 DA catalysis reaction

A typical DA reaction was carried out as follows: the catalytically active polymer was weighed into a vial (5 mol% catalyst loading) and dissolved in the appropriate solvent (water or water/methanol mixture, 0.09 M of catalyst). TFA (0.013 mL, 1 eq) was then added, followed by the dienophile (0.02 mL, 1 eq) and the solution allowed to stir for a few minutes before cyclopentadiene (0.015 mL, 1 eq) was added. Analysis of the reaction was carried out directly when it was performed in H₂O. pH of solvent system (100 μL H₂O + 13 μL of TFA) = 1.4. Additional work up was required when CH₃OH:H₂O (95:5 v/v%) was used a solvent (to remove acetal side-products). The aliquot (~ 0.1 mL) was stirred in H₂O:TFA:CHCl₃ (1:1:2) (~ 4mL) before being neutralized with NaHCO₃ (~ 2 mL) and then extracted into Et₂O (2 × ~ 5 mL). Conversion was determined by ¹H NMR spectroscopy and ee% measured by GC,

injection temperature 250 °C, column temperature 80 °C, ramp to 160 °C at 4.5 °C min⁻¹, *exo* isomers $t_R = 12.8$ and 13.2 min, *endo* isomers $t_R = 12.9$ and 13.4 min. ¹H NMR (300 MHz, CDCl₃): δ 9.33 (1H, d, ³J=3.0 Hz, C(O)H *exo*), 9.45 (1H, d, ³J=8.1 Hz, C(O)H starting material), 9.75 (1H, d, ³J=3.0 Hz, C(O)H *endo*). Data from **M 3.1** in H₂O: conversion 94% (¹H NMR spectroscopy), *exo:endo* ratio 1.00:1.05 (¹H NMR spectroscopy), 73% *exo* ee, 88% *endo* ee (GC analysis).

3.5.2.6 Polymer reuse

Through a freeze-dry method: **P 3.6** (75%) was weighed into a vial (30 mg, 0.05 eq of catalyst, 5 mol%) and dissolved in CH₃OH:H₂O (95:5 v/v%, 1 mL, 0.09 M). TFA (0.130 mL, 1 eq) and *trans*-hexen-1-al (0.200 mL, 1 eq) were added to the polymer solution and left to stir for 5 min before cyclopentadiene (0.300 mL, 2 eq) was added. After 4 h an aliquot was taken for analysis and the reaction mixture was washed with Et₂O (2 × ~ 10 mL) and CHCl₃ (2 × ~ 10 mL) removing the organic starting materials and products. The remaining aqueous layer was then diluted with DMSO. The water-DMSO solution containing the polymer was then dialyzed extensively against deionized water (MWCO = 3.5 kDa) and freeze-dried to give a white solid. The recovered polymer was weighed and reused in a second cycle.

Through a pseudo-continuous method: **P 3.6** (75%) was weighed into a vial (30 mg, 0.05 eq of catalyst, 5 mol%) and dissolved in CH₃OH:H₂O (95:5 v/v%, 1 mL, 0.09 M). TFA (0.13 mL, 1 eq) and *trans*-hexen-1-al (0.2 mL, 1 eq) were added to the polymer solution and left to stir for 5 min before cyclopentadiene (0.3 mL, 2 eq) was added. The reaction mixture was then left to stir for 4 hours at room temperature, at which point an

aliquot (0.1 mL) was taken and left to stir in a mixture of TFA:H₂O:CHCl₃ (1:1:2) (4 mL) for 2 hours before being neutralized with NaHCO₃ (2 mL) and extracted into Et₂O (2 × 5 mL). The remaining polymer solution was washed with hexane, extracting the starting materials and products leaving the polymer in the acidic CH₃OH:H₂O solution. To this solution, more reagents (*trans*-hexen-1-al and cyclopentadiene) were added and the catalysis/reuse process repeated.

3.6 References

1. K. A. Ahrendt, C. J. Borths and D. W. C. MacMillan, *J. Am. Chem. Soc.*, 2000, **122**, 4243-4244.
2. S. P. Brown, N. C. Goodwin and D. W. C. MacMillan, *J. Am. Chem. Soc.*, 2003, **125**, 1192-1194.
3. Y. Huang, A. M. Walji, C. H. Larsen and D. W. C. MacMillan, *J. Am. Chem. Soc.*, 2005, **127**, 15051-15053.
4. A. B. Northrup and D. W. C. MacMillan, *J. Am. Chem. Soc.*, 2002, **124**, 2458-2460.
5. S. G. Ouellet, J. B. Tuttle and D. W. C. MacMillan, *J. Am. Chem. Soc.*, 2004, **127**, 32-33.
6. N. A. Paras and D. W. C. MacMillan, *J. Am. Chem. Soc.*, 2001, **123**, 4370-4371.
7. J. B. Tuttle, S. G. Ouellet and D. W. C. MacMillan, *J. Am. Chem. Soc.*, 2006, **128**, 12662-12663.
8. Larsen, C. H.-M. 2006, *Investigating Imidazolidinone Catalysts*. California Institute of Technology, California.
9. T. E. Kristensen and T. Hansen, *Eur. J. Org. Chem.*, 2010, **2010**, 3179-3204.
10. M. Benaglia, G. Celentano, M. Cinquini, A. Puglisi and F. Cozzi, *Adv. Synth. Catal.*, 2002, **344**, 149-152.
11. S. A. Selkälä, J. Tois, P. M. Pihko and A. M. P. Koskinen, *Adv. Synth. Catal.*, 2002, **344**, 941-945.
12. Y. Zhang, L. Zhao, S. S. Lee and J. Y. Ying, *Adv. Synth. Catal.*, 2006, **348**, 2027-2032.

13. N. Haraguchi, Y. Takemura and S. Itsuno, *Tetrahedron Lett.*, 2010, **51**, 1205-1208.
14. A. Puglisi, M. Benaglia, R. Annunziata, V. Chiroli, R. Porta and A. Gervasini, *J. Org. Chem.*, 2013, **78**, 11326-11334.
15. C. A. Wang, Y. Zhang, J. Y. Shi and W. Wang, *Chem. Asian J.*, 2013, **8**, 1110-1114.
16. P. Riente, J. Yadav and M. A. Pericas, *Org. Lett.*, 2012, **14**, 3668-3671.
17. S. Pagoti, D. Dutta and J. Dash, *Adv. Synth. Catal.*, 2013, **355**, 3532-3538.
18. V. Chiroli, M. Benaglia, F. Cozzi, A. Puglisi, R. Annunziata and G. Celentano, *Org. Lett.*, 2013, **15**, 3590-3593.
19. T. E. Kristensen, K. Vestli, M. G. Jakobsen, F. K. Hansen and T. Hansen, *J. Org. Chem.*, 2010, **75**, 1620-1629.
20. J. Chiefari, Y. K. Chong, F. Ercole, J. Krstina, J. Jeffery, T. P. T. Le, R. T. A. Mayadunne, G. F. Meijs, C. L. Moad, G. Moad, E. Rizzardo and S. H. Thang, *Macromolecules*, 1998, **31**, 5559-5562.
21. G. Moad, E. Rizzardo and S. H. Thang, *Aust. J. Chem.*, 2005, **58**, 379-410.
22. G. Moad, E. Rizzardo and S. H. Thang, *Aust. J. Chem.*, 2006, **59**, 669-692.
23. J. Skey and R. K. O'Reilly, *Chem. Commun.*, 2008, 4183-4185.
24. J. Skey and R. K. O'Reilly, *J. Polym. Sci., Part A: Polym. Chem.*, 2008, **46**, 3690-3702.
25. A. M. van Herk, *J. Chem. Educ.*, 1995, **72**, 138.
26. J. M. G. Cowie, *Polymers: Chemistry and Physics of Modern Materials*, Nelson Thornes, Cheltenham, 1991.
27. J. Seuring and S. Agarwal, *Macromol. Rapid Commun.*, 2012, **33**, 1898-1920.

28. M. Luzon, C. Boyer, C. Peinado, T. Corrales, M. Whittaker, L. Tao and T. P. Davis, *J. Polym. Sci., Part A: Polym. Chem.*, 2010, **48**, 2783-2792.
29. J. Dzierzak, E. Bottinelli, G. Berlier, E. Gianotti, E. Stulz, R. M. Kowalczyk and R. Raja, *Chem. Commun.*, 2010, **46**, 2805-2807.
30. A. Lu, D. Moatsou, D. A. Longbottom and R. K. O'Reilly, *Chem. Sci.*, 2012, **4**, 965-969.
31. H. Willcock and R. K. O'Reilly, *Polym. Chem.*, 2010, **1**, 149-157.
32. T. E. Kristensen, K. Vestli, K. A. Fredriksen, F. K. Hansen and T. Hansen, *Org. Lett.*, 2009, **11**, 2968-2971.

Chapter 4: The immobilization of the MacMillan catalyst into a hydrophobic environment through the synthesis of nanogel structures

4.1 Abstract

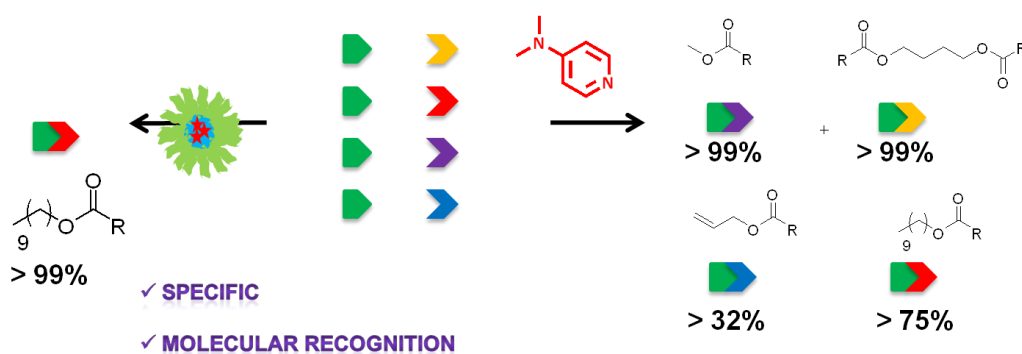
The polymerizable MacMillan containing monomer **M 3.1** has been incorporated into nanogels using an oil-in-water emulsion polymerization. This has enabled the containment of the catalyst **M 3.1** within a hydrophobic environment and the effects of this have been investigated using the Diels-Alder reaction between cyclopentadiene and cinnamaldehyde. In some of the polymer systems, conversions comparable to the unsupported catalyst were achieved. Nevertheless, a small loss in catalyst selectivity was observed upon functionalization onto the polymer support, with *endo* ee% around 80% compared to unsupported **M 3.1** achieving closer to 90%. The structures do, however, exhibit the concentrator effect with the catalyst able to perform as well as unsupported **M 3.1** in conditions 10 times more dilute. Similar structure with a permanent stabilizer which have potential use as recyclable entities have also been synthesized; but these has proved ineffective with reduced conversion and poor selectivity observed.

4.2 Introduction

Through the synthesis of a polymerizable MacMillan containing monomer (**M 3.1**) it has been possible to immobilize the catalyst into a range of polymeric nanostructures stabilized by SDS. This immobilization has been used to place the catalyst into a unique hydrophobic environment. There has been focus on placing catalysts into different environments for a plethora of reasons including exploiting the concentrator effect, allowing for improved rates of reaction, altering the selectivity of reactions, or performing traditionally organic reactions in the water phase.¹⁻⁸

The concentrator effect was a term coined by Fréchet in 2005 as they noted changes in catalytic ability as a result of the environment around the catalyst.⁹ This first foray focused on dendrimers of differing polarities and structures, which can be seen in Figure 4.1. Dendrimer 1 has a poly(benzyl ether) structure and dendrimer 2 a more hydrophilic poly(aliphatic ester) core, with the catalyst 4-(dialkylamino) pyridine (DMAP) located in the centre of both dendrimers. These structures were used for reactions with hydrophilic substrates that in the presence of a non-polar solvent congregate in the more hydrophilic interior. On the acylation of 1-methylcyclohexanol in hexane, dendrimer 2 clearly outperformed dendrimer 1 achieving approximately 45% conversion compared to 20% after 24 hours: a demonstration of the concentrator effect.

micelle was used in place of the free DMAP only the most hydrophobic alcohol product was detected; a clear demonstration of the power of hydrophobic confinement. A schematic reproduced from this report can be seen in Scheme 4.1. The power of selectivity of this reaction demonstrated impressive molecular recognition capabilities.



Scheme 4.1. A schematic from Cotanada *et al.*'s paper⁴ which demonstrates how their DMAP loaded micelle has molecular recognition properties.

Other surfactant based micelles,¹¹⁻¹³ and polymeric micelles^{3,4,14,15} have also been used to support catalysts in a similar manner and have been shown to benefit from these hydrophobic effects.

These structures, with their manipulation of catalytic environment, are a demonstration of enzyme mimics.^{16,17} Enzymes are well known for their immense catalytic ability both in regards of rate and selectivity, with enzymes burying their active site in a central hydrophobic area surrounded by a hydrophilic shell. Other examples that have been designed to mimic enzyme ability include star polymers,¹⁸⁻²⁰ and sophisticated folding polymers.²¹

The polymeric structures discussed here are cross-linked nanogels. These are related to polymeric micelles but have the advantage of a one-pot synthesis rather than a multi-step synthetic procedure and have increased stability (due to their cross-linking) with regards to temperature, concentration and solvent. These benefits make them an attractive target for catalyst immobilization that will allow for the exploitation of the concentrator effect. As previously discussed there have been attempts at immobilizing the MacMillan catalyst,²²⁻²⁹ but none so far have immobilized the catalyst in order to place it into a unique environment. There has been success using these type of nanogel structures for catalysis with the immobilization of metals³⁰ and enzymes.³¹ In particular the immobilization of the catalytic amino acid L-proline has inspired this work.³² Through the synthesis of an L-proline containing monomer, the catalyst was incorporated into PMMA nanogels and used for the aldol reaction between 4-nitobenzaldehyde and cyclohexanone. The catalytic ability of this system was shown to be affected by altering the core co-monomer, degree of catalyst functionalization (DoF) and the nanogel cross-linking density (CLD). Through the synthesis of a series of nanogels altering the co-monomer between different methacrylates the conversion of the aldol reaction was altered; with lauryl methacrylate, which has the longest carbon chain in the series, giving a significantly reduced conversion of 16% compared to the 99% achieved for the ethyl methacrylate system. On altering the CLD of the nanogel a general trend was observed with a fall in conversion observed with higher levels of cross-linking. Although this had a limited effect at the lower levels of CLD (0.5 wt% - 5 wt%) when the value was increased to 50 wt% the conversion of the system was reduced to 14%. The changing level of DoF within the nanogel returned interesting results with lower DoF 2 wt% nanogel giving a conversion of 73% whereas the higher

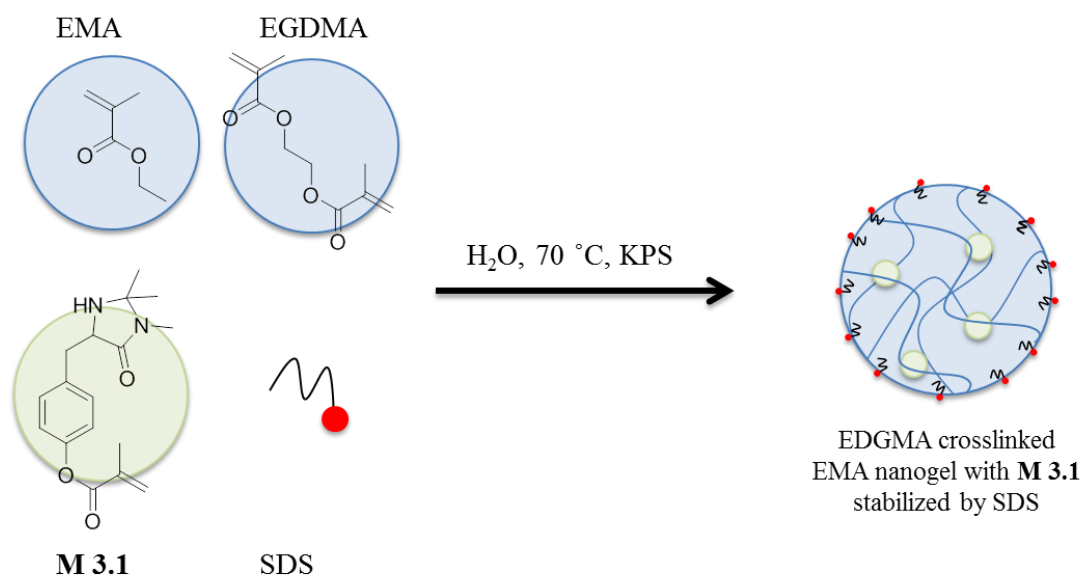
DoF 15 wt% nanogel only gave a conversion of 18%, which the authors have attributed to an increased ability of the catalyst due to site isolation. The system allowed for unprecedented low loadings of catalyst to be achieved which highlighted the role of hydrophobic effects.

Herein, the immobilization of the MacMillan catalyst into nanogels with variable DoF and co-monomer is reported. The catalytic ability of the resulting nanostructures were evaluated using the Diels-Alder (DA) reaction between cyclopentadiene and cinnamaldehyde;³³ the effects of conversion and selectivity were thoroughly investigated.

4.3 Results and Discussion

4.3.1 Nanogel Synthesis

The MacMillan containing monomer (**M 3.1**) has been incorporated into cross-linked hydrophobic polymeric particles, stabilized in an aqueous dispersion, which in this thesis shall be referred to as nanogels, following literature precedent laid out by Lu *et al.*³² The polymerizable nature of **M 3.1** allows for its incorporation into these structures, placing it in a hydrophobic environment. The functional monomer **M 3.1** was successfully co-polymerized with a co-monomer (which in the majority of this work has been ethyl methacrylate (EMA)) and the cross-linker ethylene glycol dimethacrylate (EGDMA). The co-polymerization was carried out in water and in the presence of a stabilizer, sodium dodecyl sulfate (SDS). SDS was required for the initial stabilization of the relatively large hydrophobic monomer droplets and subsequently for the stabilization of the smaller hydrophobic cross-linked polymer nanogels. A schematic of the synthesis can be seen in Scheme 4.2.



Scheme 4.2. A schematic representation of the synthesis of a cross-linked nanogel from the monomers EMA and **M 3.1** with a cross-linker EGDMA stabilized by SDS.

The polymerization has been analyzed by ¹H NMR spectroscopy to assess the kinetics of the **M 3.1** and EMA co-polymerization. In order to accurately analyze the synthesized polymer it was necessary to synthesize non-cross-linked particles in order to solubilize the resulting polymer in a solvent for ¹H NMR analysis. The conversions of the two monomers throughout the polymerization were measured by taking time-interval samples and disrupting the SDS stabilization through addition of an organic solvent, in this case THF was used. The solvents were then removed and conversion of **M 3.1** calculated by comparing the relative amounts of polymer and monomer present in the ¹H NMR spectrum. Conversions of EMA were calculated in a different manner as monomeric EMA was removed simultaneously with the solvent. As emulsion polymerizations typically go to high conversions the relative integration of EMA polymer to **M 3.1** polymer in a ¹H NMR spectrum of a final sample was taken as 100% EMA conversion. The relative integrations of **M 3.1** polymer to EMA polymer in

earlier samples as measured by ^1H NMR spectroscopy could then provide relative EMA conversion. The conversions of the two monomers can be seen in Figure 4.2. They proceed at similar rates suggesting that they are being incorporated evenly throughout the polymer structure. The data for the series of nanogels, **N 4.1** to **N 4.9**, have been detailed in Table 4.1.

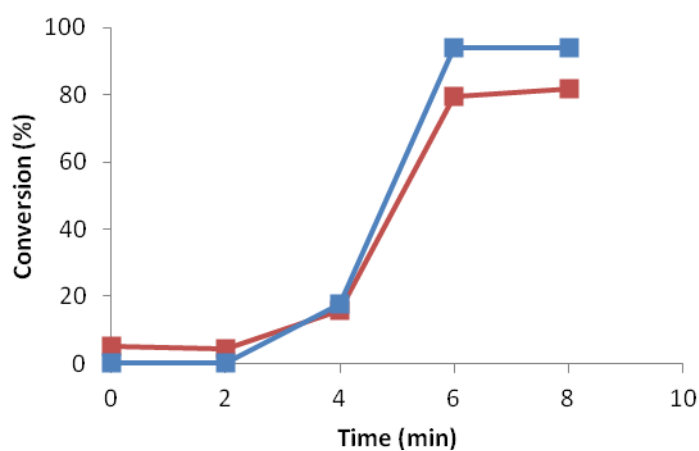


Figure 4.2. Conversions of the monomers in the nanogel with EMA (blue line) (relative conversion) and **M 3.1** (red line). The integration of monomer: polymer for **M 3.1** was used to determine conversion. As EMA monomer will have been removed on removal of THF, the final ^1H NMR spectrum was taken to be 100% conversion for EMA and the relative integration of EMA polymer to **M 3.1** polymer was used to determine the conversion of EMA.

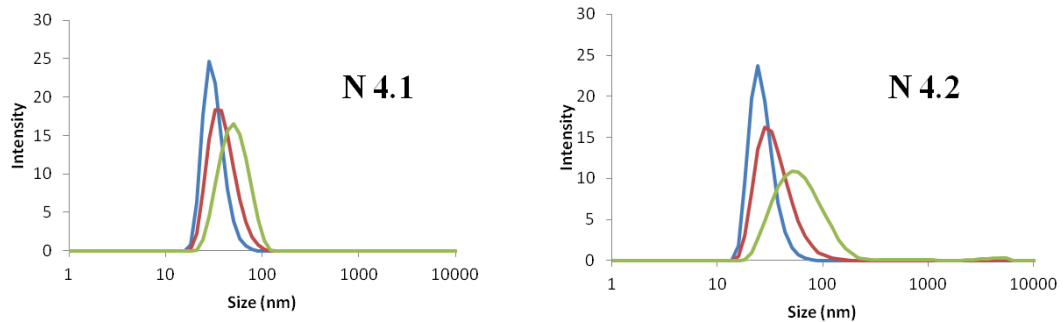
Table 4.1. The synthesized nanogels **N 4.1** – **N 4.9** detailing the DoF (wt%) and co-monomer. The hydrodynamic size (nm) and dispersity (measured by DLS) and average diameter (nm) obtained from TEM.

Nanogel	DoF (wt%)	Co-monomer	D_H (nm), (\mathcal{D})^a	D_{av} (nm)^b
N 4.1	0.5	EMA	48 (0.085)	42 ± 7
N 4.2	1	EMA	54 (0.213)	43 ± 9
N 4.3	2	EMA	48 (0.045)	45 ± 8
N 4.4	15	EMA	38 (0.219)	39 ± 8
N 4.5	20	EMA	35 (0.074)	40 ± 7
N 4.6	25	EMA	63 (0.081)	55 ± 10
N 4.7	15	MMA	33 (0.193)	23 ± 5
N 4.8	15	<i>n</i> BuMA	35 (0.252)	40 ± 9
N 4.9	0	EMA	35 (0.096)	35 ± 9

^aDetermined by DLS

^bDetermined by TEM

The number, volume and intensity traces from dynamic light scattering (DLS) for the synthesized nanoparticles can be seen in Figure 4.3. For all nanogels there is a good overlay of the three traces indicating that well-defined particles were synthesized with relatively low dispersity. The size data generated from DLS along with the calculated dispersity can be seen in Table 4.1. As is always the case the traces for number, volume and intensity do not directly overlay as the data represents different information. The intensity spectrum is the direct measurement that the DLS produces, as larger particles scatter light to a greater extent ($\text{intensity} \propto \text{radius}^6 \equiv I \propto r^6$) this needs to be accounted for which is done through application of Mie theory, which generates the volume distribution. This is then converted to the number distribution through standard geometry (volume of a sphere = $4/3\pi r^3$) to account for the different volumes that different size spheres take up. Therefore, the number distribution is used to determine the relative amounts of different size particles in solution. The number traces for all the DLS results here show one population.



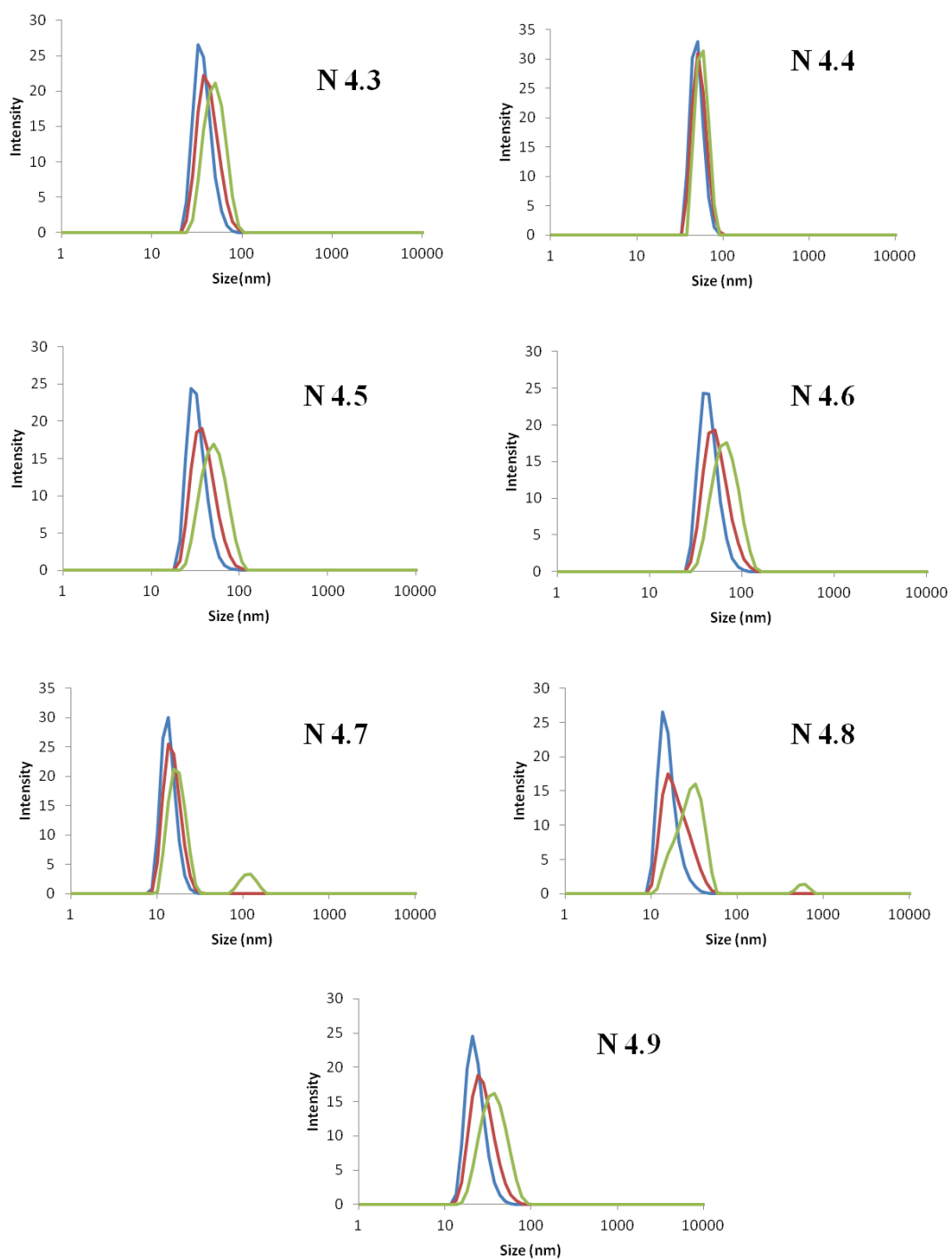


Figure 4.3. Number (blue line), Volume (red line) and Intensity (green line) DLS traces for the nanogels N 4.1 – N 4.9.

A representative correlogram for **N 4.4** can be seen in Figure 4.4. The smooth fall in correlation coefficient and the steady line after the coefficient has reached zero is indicative of a single population of nanostructures.

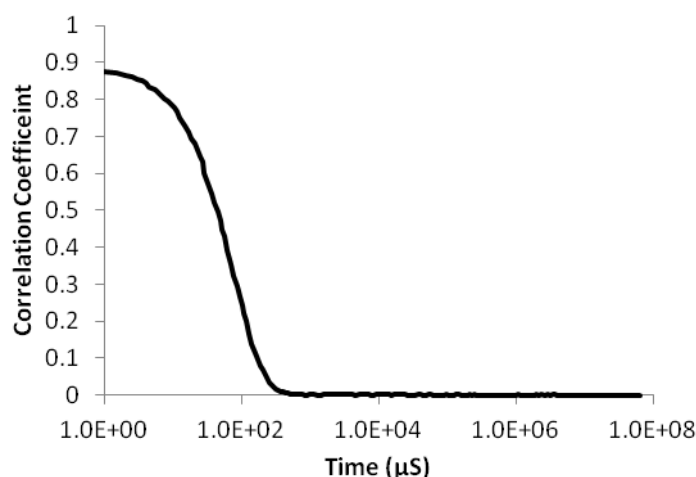
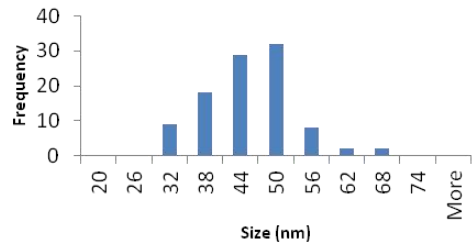
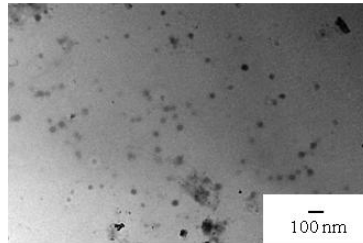


Figure 4.4. The correlation coefficient for the DLS measurement of **N 4.4**.

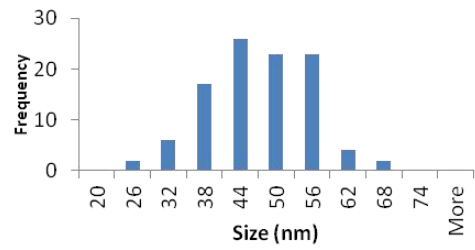
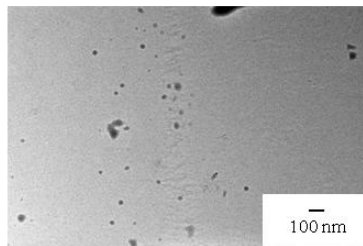
Whilst DLS is an excellent method to readily determine the presence of structures in solution, their size and dispersity, it cannot confirm their shape. For this purpose, transmission electron microscopy (TEM) has been used. A micrograph of each nanogel and a histogram of the size distribution obtained from counting particles are shown below. The TEM images indicate that the nanogels synthesized are mostly spherical in nature as anticipated. Some of the particles deviate from a perfect sphere which has been attributed to drying effects caused by TEM sample preparation. The size calculated from TEM with standard deviation error can be seen in Table 4.1. The average particle size obtained from TEM is often smaller than the size generated by DLS. This is a direct result of the nature of the two techniques with particles in a solvated state being

measured in DLS and a dried state in TEM, accounting for the difference in size observed.

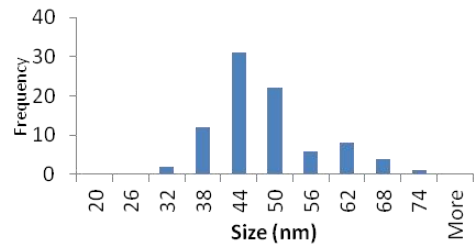
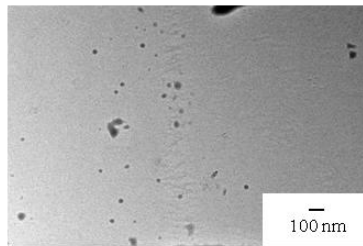
N 4.1



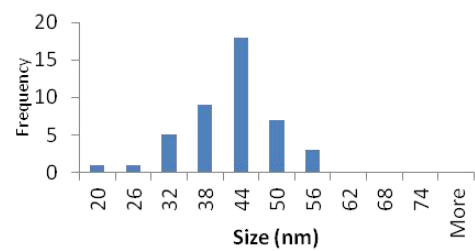
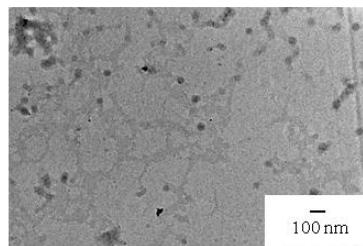
N 4.2



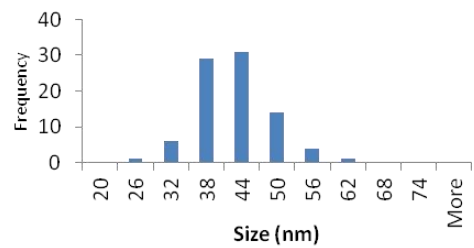
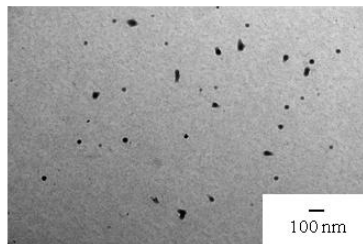
N 4.3



N 4.4



N 4.5



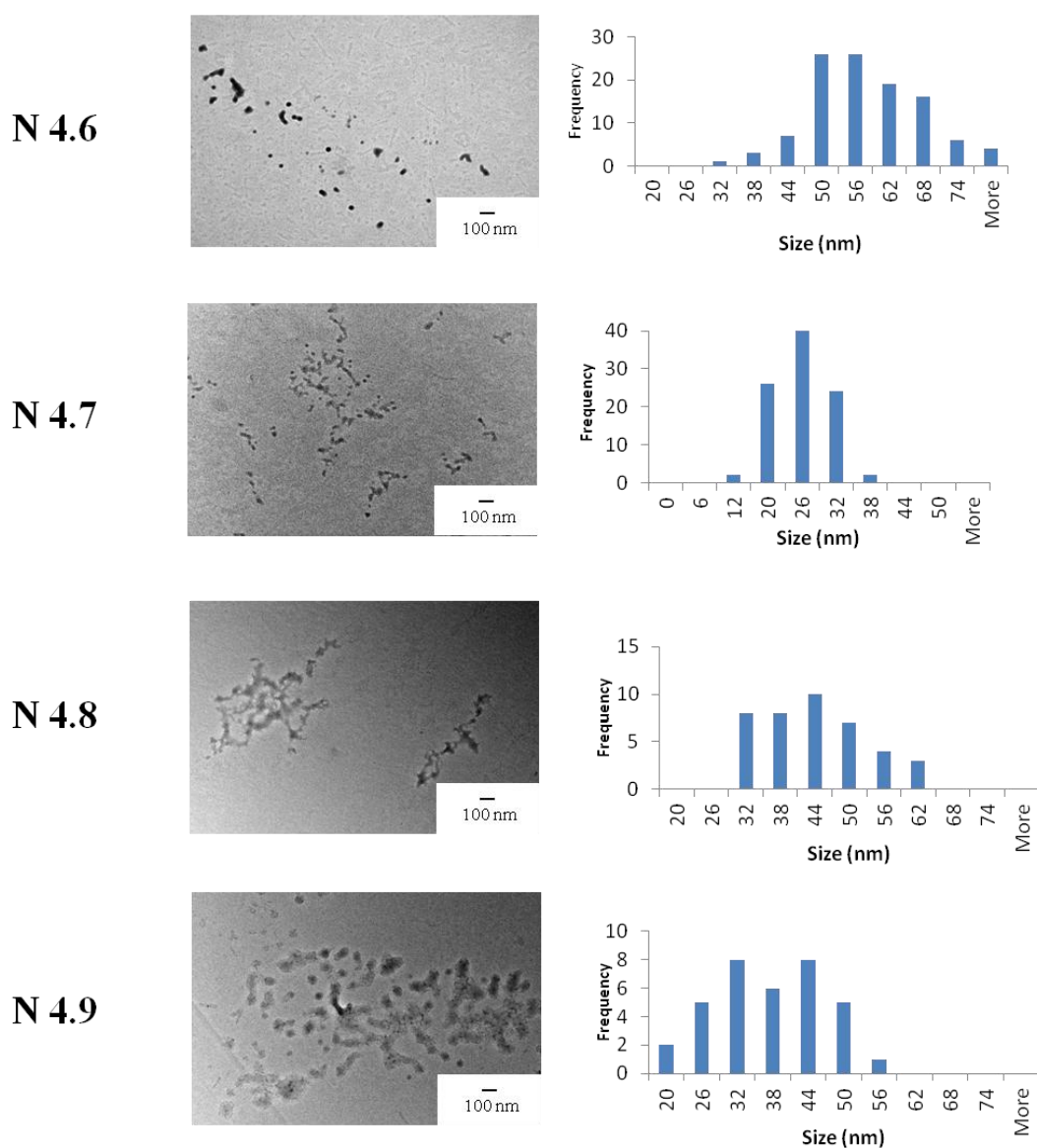


Figure 4.5. TEM image and frequency count of the nanogels incorporating the MacMillan catalyst. TEM samples were prepared by drop deposition of a 0.1 mg mL^{-1} polymer solution in water onto copper/carbon grids that had been pre-treated with oxygen plasma and analyzed by using a JEOL TEM-2100 microscope operating at 200 kV.

By altering the relative amount of **M 3.1** to the co-monomer it was possible to readily alter the nanogel DoF. By altering the DoF, the effect of catalyst concentration and nano-environment concentration on catalyst activity can be probed. Therefore, a range of nanogels have been synthesized varying the DoF from 0.5% (**N 4.1**) to 25% (**N 4.6**). The co-monomer has also been changed whilst keeping the DoF the same (15%)

yielding **N 4.7** with a methyl methacrylate (MMA) core, **N 4.4** with an EMA core and **N 4.8** with a *n*-butyl methacrylate (*n*BuMA) core. This range of co-monomers alters the hydrophobicity of the core and the level of steric hindrance as well as the glass transition temperature (T_g). The structure of these three different monomers can be seen in Figure 4.6. For comparison, an unfunctionalized nanogel, **N 4.9**, has also been synthesized with an EMA core. The details of these synthesized nanogels can be seen in Table 4.1.

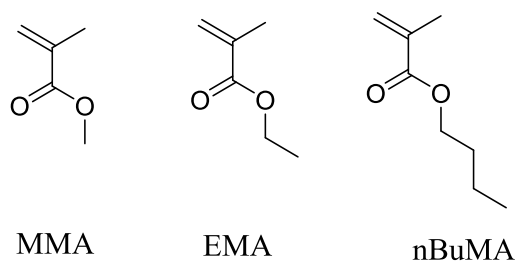
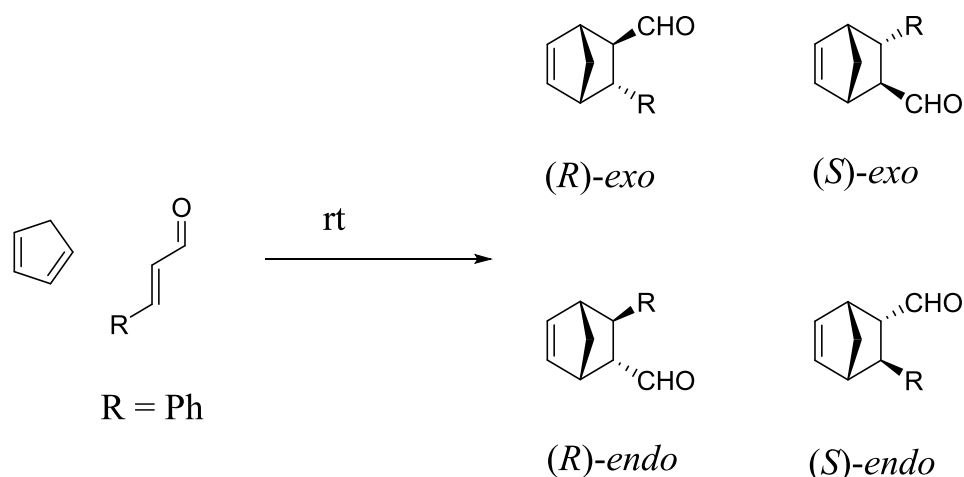


Figure 4.6. The structures of the co-monomers used in nanogel synthesis of methyl methacrylate (MMA), ethyl methacrylate (EMA) and *n*BuMA (butyl methacrylate).

4.3.2 Diels-Alder catalysis

The catalytic activity of the immobilized **M 3.1** has once again been probed by the DA reaction using the substrates cyclopentadiene and cinnamaldehyde. Initially the conversion of the DA reaction has been examined across the series of nanogels. The selectivity of the catalyst, which is also an important indicator of how successful the immobilization has been, is discussed in section 4.3.3. It was necessary to move away from *trans*-hexen-1-al (used in Chapter 3) due its lower boiling point: *trans*-hexen-1-al has a boiling point of 47 °C compared to cinnamaldehyde which has a boiling point of 248 °C. This is significant due to the work up procedure used in order to analyze reaction conversion. In order to ensure that all small molecules have been removed from the interior of the nanogels they are swollen with an organic solvent (in this case THF) which is then removed, along with any water, under air flow. The *trans*-hexen-1-al will also be removed under these conditions which would produce false conversion results. The higher boiling point of cinnamaldehyde will allow for more accurate results to be obtained. The reaction scheme and the four potential products of this DA reaction can be seen in Scheme 4.3.



Scheme 4.3. A reaction scheme between cyclopentadiene and cinnamaldehyde and the four possible products, the favoured enantiomers according to the mechanism laid out by MacMillan is the *(R)*-enantiomer. The reaction between cyclopentadiene and cinnamaldehyde produces almost equal amounts of *exo* and *endo* products.

The success of the reaction relies on the substrates coming into close proximity with the immobilized catalyst within the nanogel. Therefore, the more hydrophobic the reagents are, the greater the chance of diffusion into the hydrophobic cavity. A way to measure the relative hydrophobicity of compounds is by examining their Log *p*, or partition coefficient. This is the ratio of concentration for a given compound between octanol and water. Log *p* can be predicted based on chemical structure with 80% of molecules within less than 0.5 units.^{34, 35} The Log *p* equation can be seen in Equation 4.1.

$$\text{Log } p = \log \left(\frac{[\text{solute}]_{\text{octanol}}}{[\text{solute}]_{\text{un-ionized water}}} \right) \quad (4.1)$$

By using the predictor, Log *p* for cyclopentadiene and cinnamaldehyde were determined as 1.483 and 2.484 respectively. For comparison, the log *p* values for methanol and *n*-hexane are -0.320 and 3.657 respectively. Therefore, the compounds used for this

reaction are relatively hydrophobic and should congregate within the nanogel. This is further supported from the success of using these types of nanogel structures for an aldol reaction between cyclohexanone and 4-nitrobenzaldehyde; these reagents have log p values of 1.400 and 1.686 respectively. It can therefore be assumed that the reagents are hydrophobic enough to be affected by the concentrator effect and diffuse into the hydrophobic domain resulting in a high local substrate concentration around the catalyst.

In Figure 4.7 the variable nature of the concentration of catalyst and concentration of nanoreactors as a function of DoF is depicted. Situation A has a constant concentration of nanoreactors and volume of nanogel across the series, however this leads to a difference in catalytic loading and therefore catalyst concentration. With situation B identical catalyst loading can be achieved by varying the volume of nanogel added; however this then alters other variables such as volume, number of nanoreactors and catalyst concentration. Some of these variables can be addressed by adding water to the systems as shown in situation C which then gives constant volume and constant catalyst concentration although the number of nanoreactors will nevertheless remain different. Each of these scenarios has been investigated with the series of nanogels and the conversion of the DA reaction monitored to demonstrate catalyst activity.

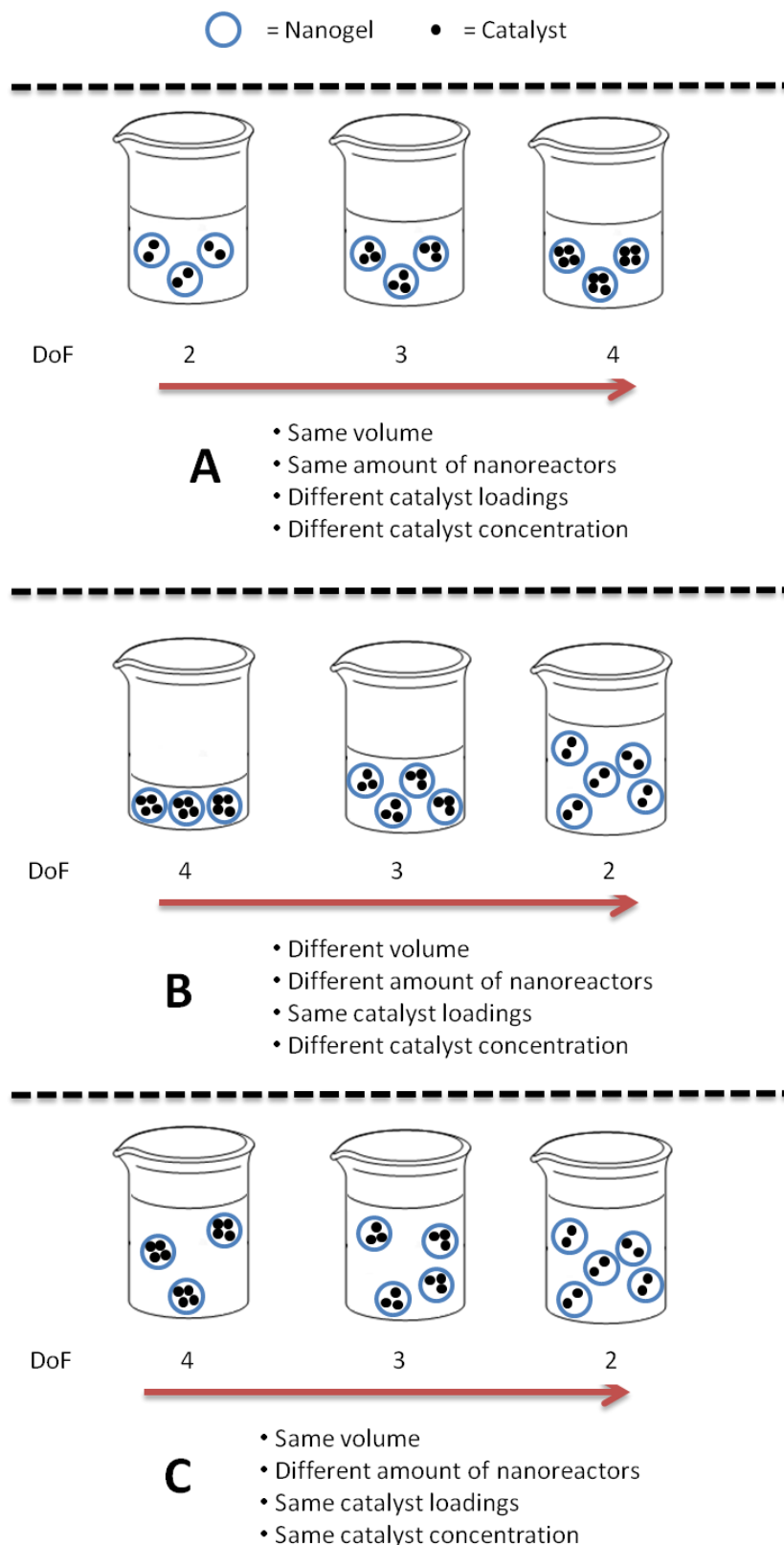


Figure 4.7. A schematic representation of reactions carried out varying the nanogel concentration and catalyst concentration (as affected by the difference in catalyst DoF), represented with arbitrary DoF of 2, 3 and 4.

The first set of reactions were performed fulfilling the criteria of Figure 4.7, situation A. The same volume of nanogels **N 4.1** to **N 4.6**, which have variable DoF, was used for the DA catalysis. There is a clear trend across the series with the higher DoF nanogels reaching the higher conversions after 24 hours. **N 4.6**, the highest DoF nanogel achieved 100% conversion in this time (Table 4.2 Entry 6). This was a predicted result as the higher DoF nanogels have the highest concentration of catalyst in solution (**N 4.5** and **N 4.4** reached 92 and 40% conversion in the same reaction time with **N 4.3** only reaching 5% conversion at 1 mol% catalyst loading). This trend of increasing mol% giving higher conversion has been represented clearly in Figure 4.8. Unfortunately, **N 4.2** and **N 4.1** were not able to catalyze the reaction at all in 24 hours.

Table 4.2. The conversions of DA reaction between cinnamaldehyde and cyclopentadiene catalyzed by nanogels **N 4.1** – **N 4.6** at various mol%, in water (maintaining a volume of 2 mL).

Entry	Nanogel	DoF (%)	mol%	Conversion ^a (%)
1	N 4.1	0.5	0.25	0
2	N 4.2	1	0.5	0
3	N 4.3	2	1	5
4	N 4.4	15	7.2	40
5	N 4.5	20	9.8	92
6	N 4.6	25	12.3	100

^aDetermined by ¹H NMR spectroscopy through comparison of the cinnamaldehyde proton ($\delta = 9.68$ ppm) and the product aldehyde protons ($\delta = 9.54$ ppm and 9.85 ppm)

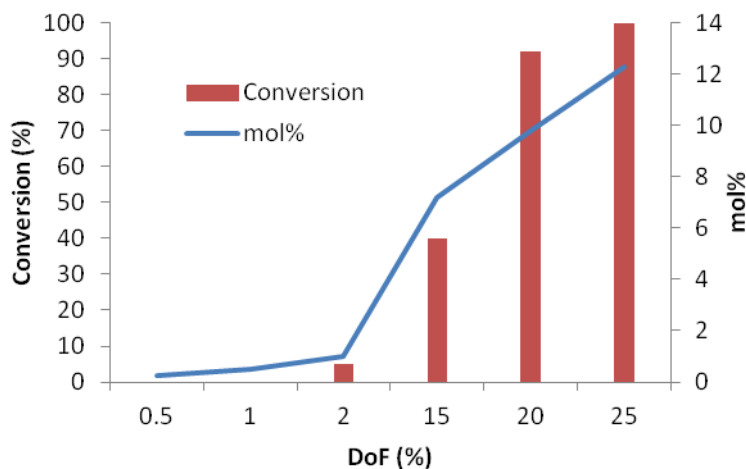


Figure 4.8. A graph demonstrating the clear effect of mol% (blue) on the conversions (red) of the DA reaction between cinnamaldehyde and cyclopentadiene catalyzed by nanogels **N 4.1** – **N 4.6** at various mol%, in water (maintaining a volume of 2 mL).

The kinetics of entry 5, Table 4.2 were then investigated; the results of which can be seen in Figure 4.9 with the selectivities at the time points shown in Table 4.3. In this system it is observed that the high conversion (~90%) was obtained after approximately 6 hours of reaction and the selectivities remain very similar at all time points with *exo:endo* ratios around 1.0:1.3 and *endo* ee of 88%.

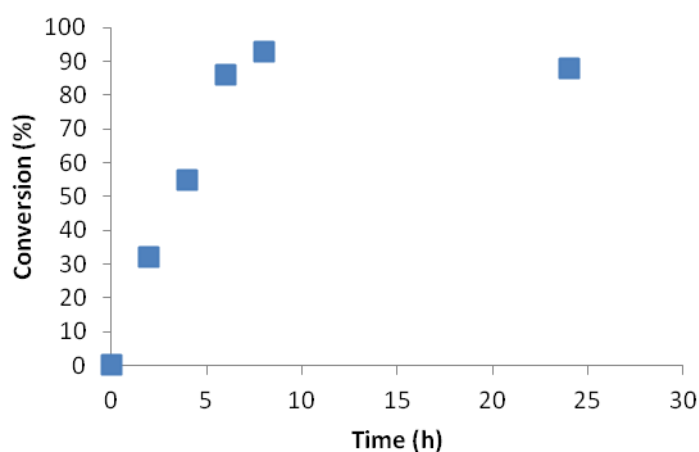


Figure 4.9. Conversion against time for the DA reaction between cyclopentadiene and cinnamaldehyde catalyzed by **N 4.5** in 2 mL giving 9.8 mol% loading.

Table 4.3. The conversions and selectivities for the DA reaction between cyclopentadiene and cinnamaldehyde catalyzed by **N 4.5** in 2 mL giving 9.8 mol% loading.

Time (h)	Conversion ^a (%)	<i>exo:endo</i> ^b	<i>exo ee</i> % ^c	<i>endo ee</i> % ^c
2	32	1.0:1.3	85	88
4	55	1.0:1.3	83	88
6	86	1.0:1.2	82	87
8	93	1.0:1.5	80	88
24	88	1.0:1.5	77	87

^aDetermined by ¹H NMR spectroscopy through comparison of the cinnamaldehyde aldehyde proton ($\delta = 9.68$ ppm) and the product aldehyde protons ($\delta = 9.54$ ppm and 9.85 ppm)

^bDetermined by ¹H NMR spectroscopy through comparison the product aldehyde protons ($\delta = 9.54$ ppm (*exo*) and 9.85 ppm(*endo*))

^cDetermined by chiral GC

Following these results, the volume of nanogels used was varied (Figure 4.7, situation B) in order to obtain the same catalyst loading (5 mol%). This has then altered the catalyst concentration and the number of nanoreactors present, which has been previously shown to have a significant effect.³² **N 4.6** again has the highest conversion despite the lower concentration of nanogels (Table 4.4, Entry 4) compared with the lower DoF nanogels. It is proposed this is a partition coefficient effect between substrates in the water phase and inside the nanogel. This effect has been studied before, with less hydrophobic substrates unwilling to enter the hydrophobic domain resulting in low or no conversion.⁴ As all the reactions detailed in Table 4.6 were conducted using the same volume of reaction substrates, the substrate to water ratio is smallest for **N 4.6**, perhaps explaining its efficiency.

Table 4.4. Conversion of the DA reaction between cinnamaldehyde and cyclopentadiene catalyzed by **N 4.3 – N 4.6** at 5 mol%, determined after 24 h.

Entry	Nanogel	DoF (%)	Amount of Nanogel (mL)	Conversion ^a (%)
1	N 4.3	2	2.000	5
2	N 4.4	15	1.365	26
3	N 4.5	20	1.020	72
4	N 4.6	25	0.815	82

^aDetermined by ¹H NMR spectroscopy through comparison of the cinnamaldehyde aldehyde proton ($\delta = 9.68$ ppm) and the product aldehyde protons ($\delta = 9.54$ ppm and 9.85 ppm)

The last set of experiments focused on achieving the scenario in Figure 4.7, situation C. These experiments were designed to maintain not only the catalyst loading (5 mol% or

1 mol%) but also the substrate to water ratio. This was achieved by diluting the higher DoF nanogels with water to give a constant volume. Firstly, catalysis was carried out at a total nanogel volume of 1.365 mL, matching that of **N 4.4** (Table 4.4, Entry 2), without altering the catalyst loading which remained at 5 mol%. As expected, a drop in conversion was observed for both **N 4.5** and **N 4.6** reaching 60% and 62% conversion respectively in 24 hours (Table 4.5). The more dramatic drop in conversion for **N 4.6** further supports our hypothesis that a partition coefficient effect is involved.

Table 4.5. The conversions of the DA reaction after 24 h between cinnamaldehyde and cyclopentadiene conducted with the nanogels **N 4.4** – **N 4.6** at 5 mol% in the same volume of 1.365 mL. The volume was kept the same by the addition of water to **N 4.5** and **N 4.6**.

Nanogel	DoF (%)	Nanogel Added (mL)	Water Added (mL)	Conversion ^a (%)
N 4.4	15	1.365	0.000	26
N 4.5	20	1.020	0.345	60
N 4.6	25	0.815	0.550	62

^aDetermined by ¹H NMR spectroscopy through comparison of the cinnamaldehyde aldehyde proton ($\delta = 9.68$ ppm) and the product aldehyde protons ($\delta = 9.54$ ppm and 9.85 ppm)

However, as **N 4.5** and **N 4.6** are still outperforming **N 4.4** despite the lower concentration of nanogels, the systems were further diluted to a catalyst loading of 1 mol% in an attempt to make the difference in nanogel concentration more significant. The details of this dilution can be seen Table 4.6. The conversion for **N 4.4** has fallen dramatically to 11%, and even more significantly, the conversion for **N 4.5** and **N 4.6** have fallen to a greater extent. The relative concentration of nanogels must therefore

have an effect at this lower catalytic loading, with the higher concentration of nanogels outperforming the lower concentration with a conversion of 11% compared to 2%.

Table 4.6. Conversion of DA reaction between cinnamaldehyde and cyclopentadiene catalyzed by **N 4.4** – **N 4.6** at 1 mol%, determined after 24 h.

Nanogel	DoF (%)	Nanogel Added (mL)	Water added (mL)	Conversion^a (%)
N 4.4	15	0.275	1.725	11
N 4.5	20	0.255	1.745	2
N 4.6	25	0.205	1.795	8

^aDetermined by ¹H NMR spectroscopy through comparison of the cinnamaldehyde aldehyde proton ($\delta = 9.68$ ppm) and the product aldehyde protons ($\delta = 9.54$ ppm and 9.85 ppm)

The catalysis of **N 4.5** and **N 4.6** have been additionally investigated by altering the catalyst loadings between 1 mol% and 10 mol% (Table 4.7). This was achieved by either altering the nanogel or substrate volume. On increasing the catalyst loading, a corresponding increase in conversion was observed. However, the two methods of achieving the different mol% have not given the same result, with the reactions conducted at the larger volumes always achieving a greater conversion. These higher conversion reactions have been highlighted within Table 4.7. On repeating **N 4.5** at 5 mol% on an increased scale of 2.04 mL improved the conversion slightly to 80% from the 72% observed when using 1.02 mL. The differences in conversion are likely to be as a result of physical changes as the reactions are chemically identical. One possible reason could be the homogeneity of the system as both reactions are carried out using the same size reaction vessels and similar stirrer bars. Thus, it is possible that greater

homogeneity is achieved at greater reaction volumes promoting increased entry of substrates into the hydrophobic cavity.

Table 4.7. The conversions and turnover number (TON) of the DA reaction after 24 h between cinnamaldehyde and cyclopentadiene conducted with the nanogels **N 4.5** and **N 4.6** at various mol%. The changing mol% has been achieved using two different methods either varying the amount of substrate added to a fixed volume of nanogel or by varying the amount of nanogel added to a fixed amount of substrate.

mol%	Conversion ^a (%)	Nanogel Volume (mL)	TON ^b				
				Conversion ^a (%)	Nanogel Volume (mL)	TON ^b	
				Vary Substrate Volume		Vary Nanogel Volume	
N 4.5	1	40	1.020	40	15	0.255	15
	2.5	53	1.020	21	40	0.510	16
	5	72	1.020	15	72	1.020	15
	10	80	1.020	8	95	2.040	10
N 4.6	1	44	0.815	44	28	0.204	28
	2.5	57	0.815	23	48	0.407	20
	5	82	0.815	16	82	0.815	16
	10	60	0.815	6	94	1.630	10

^aDetermined by ¹H NMR spectroscopy through comparison of the cinnamaldehyde aldehyde proton ($\delta = 9.68$ ppm) and the product aldehyde protons ($\delta = 9.54$ ppm and 9.85 ppm)

^bDetermined by the ratio of catalyst to mol% of catalyst

4.3.3 Selectivity

The DA reaction between cinnamaldehyde and cyclopentadiene produces four products, two enantiomers of the *endo* product and two enantiomers of the *exo* product. The relative proportion of these products will be used as a handle to determine how effective the immobilization has been, relative to the unmodified catalyst. As the MacMillan catalysts' enantioselectivity is governed by steric control, placing it within a more confined environment within the nanogel could have both positive and negative effects depending on the orientation.^{36,37} In other words, the polymeric scaffold could enhance steric control if positioned in the correct orientation, but it is more likely that the scaffold will have a negative effect by disturbing the steric control already in place. However, the L-proline system that this work has been based on reported no loss in selectivity for their catalysis. Their system benefits from a free carboxylic acid that can help to direct the catalysis and therefore assist in overcoming any increased sterics from the polymer.

Firstly, the synthesized **M 3.1** shows comparable enantioselectivities to the native MacMillan catalyst, with enantioselectivities of 93% and 88% *endo* ee respectively.³³ This slight fall in selectivity from the reported catalyst to **M 3.1** has been discussed in Chapter 3 but has been attributed to the differing co-catalyst salts. These selectivities and selected nanogel reactions have been detailed in Table 4.8. This has allowed for comparison against the nanogel **N 4.4**, an EMA based nanogel with DoF 15% and a catalyst loading of 5 mol%. The change in selectivity is compared across groups to examine the effects of co-monomer, catalyst loading and DoF.

Table 4.8. The selectivities of the DA reaction after 24 h between cinnamaldehyde and cyclopentadiene. Catalysed by **N 4.4** to which the sets of catalysis are compared. Entries 1 and 2 are the small molecule reaction, entries 3,4 and 5 different co-monomer nanogel, entries 3, 6 and 7 different mol % reaction, entries 3 and 8 different DoF nanogel and entries 3, 9 and 10 different DoF nanogel with the same volume resulting in different mol%.

Entry	Catalyst	Co-monomer	Conversion ^a (%)	mol %	<i>exo:endo</i> ^b	<i>exo ee</i> % ^c	<i>endo ee</i> % ^c
1	MacMillan ³³		99	5	0.8	93	93
2	M 3.1 ^c		62	5	0.8	85	88
3	N 4.4	EMA	26	5	0.8	73	72
4	N 4.7	MMA	40	5	0.7	83	90
5	N 4.8	<i>n</i> BuMA	38	5	0.6	78	85
6	N 4.4	EMA	38	2.5	0.8	66	76
7	N 4.4	EMA	24	1	0.9	58	65
8	N 4.5	EMA	92	9.8	0.9	85	80
9	N 4.6	EMA	100	12.3	0.9	77	79

^aDetermined by ¹H NMR spectroscopy through comparison of the cinnamaldehyde aldehyde proton ($\delta = 9.68$ ppm) and the product aldehyde protons ($\delta = 9.54$ ppm and 9.85 ppm)

^bDetermined by ¹H NMR spectroscopy through comparison the product aldehyde protons ($\delta = 9.54$ ppm (*exo*) and 9.85 ppm(*endo*))

^cDetermined by chiral GC

^dConducted under the reported conditions for the DA reaction catalyzed by the MacMillan catalyst³³

With reference to Table 4.8, the selectivities were found to be highly dependent on the reaction conditions.

It is notable that on placing **M 3.1** within the nanogel, **N 4.4** (entry 3), the enantioselectivity has fallen with *endo* ee% dropping to 72% from 88%. As previously mentioned the catalyst is in a comparatively more crowded environment causing a negative impact on the efficiency of the catalyst. As discussed in Chapter 3 the selectivity of the catalyst is dependent on which face of the catalyst the substrate approaches from, which in turn is governed by the presence of bulkier functionalities, such as a phenyl group in the case of the MacMillan catalyst.^{36, 37} In this environment other polymer units, due to their close proximity, could be impeding the alignment of the substrate and hence diminishing the catalysts control over enantioselectivity.

The effect of co-monomer has been studied with **N 4.7** and **N 4.8** (entries 4 and 5) which have been synthesized with the co-monomers of MMA and *n*BuMA respectively. The change in monomer will alter the hydrophobicity of the environment as well as the carbon bulk present, with MMA offering the least and *n*BuMA the most. Although the glass transition temperature (T_g) of the co-polymer should also be considered as it can be taken as a measure of how dynamic the interior of the nanogel is. The T_g of homopolymers for poly(MMA), poly(EMA) and poly(*n*BuMA) can be seen in Table 4.9. As the carbon chain increases, the T_g decreases from 105 °C for MMA to 20 °C for *n*BuMA; so whilst *n*BuMA has the greatest carbon bulk (i.e. is the most hydrophobic), it may not be providing the greatest steric hindrance as the core is likely to be more

ductile. However the effect of T_g may not be highly significant as the core will be solvated and the polymer is not a pure homopolymer.

Table 4.9. The reported T_g values for the homopolymers of poly(MMA), poly(EMA) and poly(*n*BuMA).³⁸

Polymer	T_g (°C)
PMMA	105
PEMA	65
P <i>n</i> BuMA	20

In the presence of these differing cores the selectivity of the reaction has been altered: *endo* ee% for **N 4.7**, **N 4.4** and **N 4.8**, which are 90, 72 and 85% respectively. As these selectivity results do not follow a linear trend it is possible that the reaction is being affected by both the changing carbon bulk as well as the nature of the core. MMA with the lowest steric bulk has produced the highest selectivity of 90%. This has fallen to 72% when EMA was used as the co-monomer, which has been attributed to an increase in the steric bulk and thus greater interference with the catalyst impeding its native steric control. Both PMMA and PEMA have relatively high T_g 's and therefore the nature of the nanogels are likely to be relatively similar. However, when *n*BuMA was examined, an increase in selectivity compared to the EMA nanogel was observed, despite an increase in carbon chain length. Crucially the T_g of P*n*BuMA is much lower and close to the temperature at which the reaction was carried out (room temperature = 22 °C, T_g = 20 °C). Consequently, the core of the nanogel is likely to be of a different nature to the MMA and EMA core and therefore the fall in T_g could be more significant than the increase in carbon chain length, thus explaining the enhanced selectivity of the *n*BuMA

nanogels. Therefore the affect of temperature on the selectivity, with regards to co-monomer, was also investigated; by conducting the reaction at a lower temperature, 4 °C, the structures of EMA and *n*BuMA should be more comparable. The *endo* ee% for the lower temperature reactions were 85% (EMA) and 87% (*n*BuMA), supporting our hypothesis. Although an increase in selectivity at a lower temperature is expected, the increase in ee% for the *n*BuMA system was much smaller than the EMA system, which could be due to the more rigid nature now likely to be present in the *n*BuMA nanogel.

Entries 6 and 7 show different mol% of the reaction, where a drop in selectivity for low mol% (high concentration of reagents) is observed. At 1 mol% the selectivities of 58% *exo* ee and 65% *endo* ee are observed. This fall in selectivity has been attributed to the higher local concentration of reagents within the nanogel core increasing the steric crowding. Interestingly the conversions do not seem to follow a trend with the highest conversion obtained for 2.5 mol%, however, when the turnover numbers (TON) are examined a clearer trend is observed (1 mol% = 24, 2.5 mol% = 15 and 5 mol% = 5) which shows that the catalyst works more efficiently when at the lowest catalyst loading of 1 mol%.

Entries 8 and 9 examine the effect of different DoF nanogels using the same volume: substrate ratio (resulting in different mol%) (Table 4.2). This means that at higher DoF each catalytic site has less catalytic cycles to perform and is potentially less hindered by the amount of substrate directly around it. The increase in *endo* ee% from 72% at DoF 15% (N 4.4) to 79% DoF 25% (N 4.6) has been attributed to the lower steric crowding around each site. Interestingly the selectivity difference between N 4.5 and N 4.6 is

negligible which has been attributed to achieving a concentration around each site that does not contribute significantly to the selectivity; with the polymeric environment having a greater effect.

Previous work has also demonstrated how catalyst efficiency can be dependent on how isolated it is. With the L-proline immobilization it was found that having a more isolated catalytic site allowed for the formation of the preferred transition state which yielded higher enantioselectivities.³² This effect with L-proline has also been studied by Raja and co-workers who noted that the more isolated catalytic site within a zeolite led to an increase in catalytic activity. The changeable nature of the surroundings with higher or lower loadings altered how hydrophobic the zeolite pore was which also affected the reaction selectivity.³⁹ Site isolation benefits have also been observed in a previous MacMillan immobilization study. Ying and co-workers immobilized the catalyst onto a mesocellular foam (MCF) which showed improved selectivity for both the Friedel-Crafts and DA reactions when the synthesis was manipulated to ensure good spacing between the catalytic sites.²⁹

4.3.4 Hydrophobic effect/concentrator effect

Although there has been a fall in both conversion and selectivity upon placing the MacMillan catalyst within these new nanostructures, one of the main advantages of catalyst immobilization into hydrophobic domains is the concentrator effect, which has therefore been explored. Comparing the reaction at 5 mol% in either 100 μL or 1.38 mL in H_2O shows a significant difference: a fall in conversion from 62% to 0% after 24 hours (Table 4.10). However, **N 4.4** which has 5 mol% of catalyst in 1.38 mL contained within the nanogel reaches 26% conversion over the same time period. By providing a hydrophobic domain within which the substrates would rather reside, a high local concentration of reagents in close proximity to the catalyst is produced. This becomes the equivalent of performing the reaction at a much higher concentration and an improved conversion is obtained.

Table 4.10. Conversions of DA reaction between cinnamaldehyde and cyclopentadiene catalyzed by **M 3.1**, **N 4.4** and **N 4.9** under different conditions, determined after 24 h.

Catalyst	Vol. H ₂ O (mL)	[Catalyst] [M]	mol%	Conversion ^a (%)
MacMillan ³³	<i>b</i>	1.0	5	99
M 3.1	<i>b</i>	1.0	5	62
M 3.1	0.1	0.7	5	62
M 3.1	0.1	0.7	1	29
M 3.1	1.38	0.5×10^{-3}	5	0
N 4.4	1.38	0.5×10^{-3}	5	26
N 4.9	1.38	0.5×10^{-3}	-	0

^a¹H NMR spectroscopy through comparison of the cinnamaldehyde aldehyde proton ($\delta = 9.68$ ppm) and the product aldehyde protons ($\delta = 9.54$ ppm and 9.85 ppm)

^bReactions were conducted in MeOH:H₂O (95:5 v/v%) at 1.0 M

The concentrator effect has further been demonstrated by the kinetics of **M 3.1** in 100 μL of water and **N 4.5** in 1.02 mL at 5 mol%. The conversions were measured from different reactions as sampling the nanogel, with its emulsion type behaviour, lead to anomalous results. The conversions at different time points can be seen in Figure 4.10. The two systems have similar rates of reaction, which as **N 4.5** is 10 times more dilute than **M 3.1** again demonstrates the importance of the concentrator effect and its ability to increase the local concentrations of substrate.

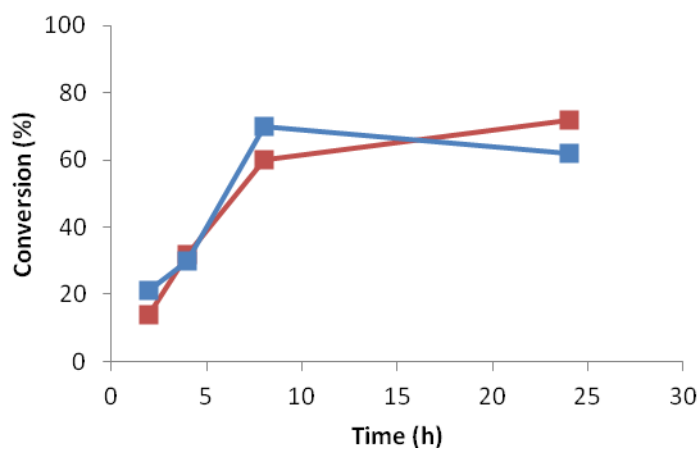
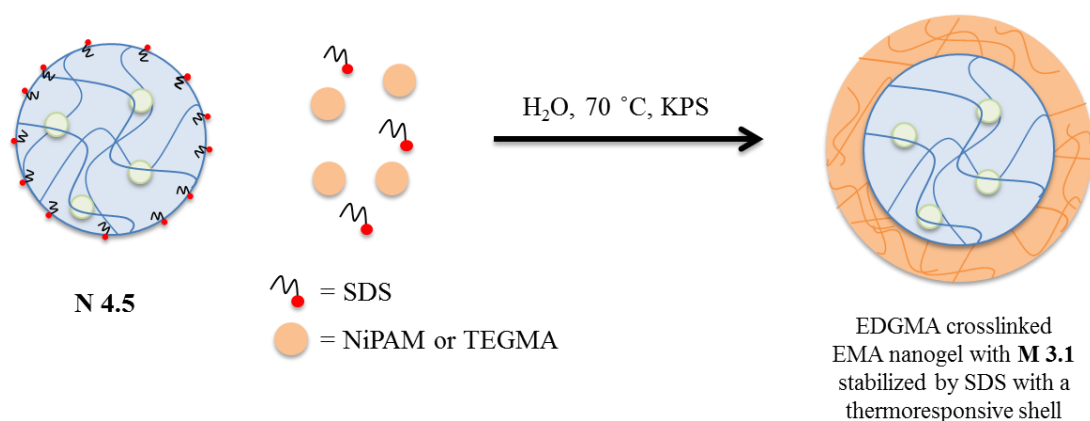


Figure 4.10. The conversion against time of **M 3.1** (blue line) in 100 μL H_2O and **N 4.5** (red line) in 1.02 mL H_2O .

4.3.5 Core-shell nanogels

One of the main reasons that catalyst immobilization is well studied is to increase the potential use of the catalyst which can often be time consuming, toxic, difficult or expensive to prepare.⁵ Immobilization onto insoluble polymeric supports to improve recovery has been used for decades as outlined in a review by Manecke and Stork in 1978.⁴⁰ More recently there has been a shift towards using soluble polymers with the advances in technology in this area. This too has been outlined by a review in 2002 by Bergbreiter which also discusses the separation strategies that are being implemented.⁴¹ A perspective article in 2012 by Cotanda *et al.* discusses the transition into immobilization of catalysts into polymeric nanoreactors as structures for recovery, as they provide other benefits alongside their recycling potential.⁵

In particular, similar nanogel systems have been used for the recovery of L-proline, exploiting a thermo-responsive shell as a stabilizer throughout the recycling cycles.^{32,42} The addition of a cross-linked steric stabilizer as opposed to a static stabilizer such as SDS will allow the nanogel to retain its aqueous solubility even after treatment with organic solvents. This is an important feature to take into account, as the organic substrates need to be extracted from the hydrophobic core after reaction completion. Upon addition of an organic solvent to the aqueous suspension, SDS will become soluble and re-suspension of the hydrophobic nanogel will be difficult. However, by using water soluble shells, re-suspension into water will be possible after removal of the organic substrates from the nanogel core.



Scheme 4.4. A schematic representation of the addition of a shell to a nanogel seed molecule, the synthesis requires addition of a thermo-responsive monomer and a small amount of additional SDS along with initiator.

A similar system was therefore designed for the MacMillan catalyst, using either NiPAM or TEGMA as the water soluble shell with a low CLD of 0.5 wt%. These two monomers are known to exhibit lower critical solution temperature (LCST) behaviour in their polymeric form and are therefore ideal candidates as the growing polymer needs to be hydrophobic at the polymerization temperature (in order to enter the SDS domain) and hydrophilic at the reaction and recycling temperature (in order to stabilize the permanently hydrophobic core). NiPAM was targeted as its ability as a stabilizer had already been demonstrated in the L-proline system. A TEGMA shell was also synthesized due to the known benign affect of the related monomer DEGMA on the catalysis (Chapter 3). TEGMA was used in place of DEGMA as it has a comparatively higher LCST, with poly(DEGMA) around 24 °C²⁶ and poly(TEGMA) around 50 °C.⁴³ A higher LCST was targeted to ensure the shell was hydrophilic at the reaction and recycling temperatures. Details of the synthesized core-shell nanogels can be seen in Table 4.11, along with details of **N 4.5**

Table 4.11. The synthesized nanogels **SN 4.1** – **SN 4.3** detailing the shell monomer, hydrodynamic size (nm) and dispersity (measured by DLS) and average diameter (nm) obtained from TEM.

Nanogel	Shell Monomer	D_H (nm), (\mathcal{D}) ^a	D_{av} (nm) ^b
N 4.5		35 (0.074)	40 ± 7
SN 4.1	NiPAM	151 (0.062)	100 ± 20
SN 4.2	TEGMA	175 (0.172)	190 ± 50
SN 4.3	NiPAM	85 (0.114)	55 ± 10

^aDetermined by DLS

^bDetermined by TEM

N 4.5 (EMA, 20 wt% DoF) was used as the hydrophobic core in all cases yielding poly(EMA)/poly(NiPAM) and poly(EMA)/poly(TEGMA) core-shell nanogels, labelled **SN 4.1** and **SN 4.2** respectively. An increase in nanogel hydrodynamic diameter (D_H) after addition of the thermo-responsive shell from 35 nm to 151 nm and 175 nm for **SN 4.1** and **SN 4.2** was observed, confirming the successful process. The increase was observed at 25 °C for both the original core and the resulting core-shell structures. At this relatively low temperature the shell-forming polymers are expected to be hydrophilic and fully extended in solution, which is reflected in the large particle sizes observed. The DLS data for **SN 4.1** – **SN 4.3** can be seen in Figure 4.11 with corresponding representative TEM images in Figure 4.12.

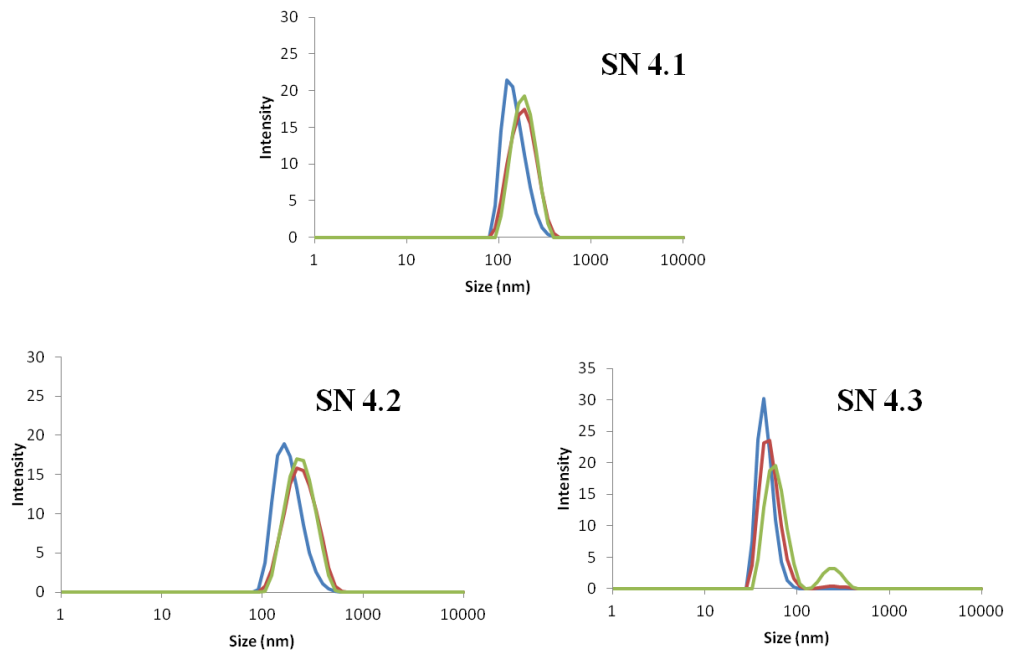
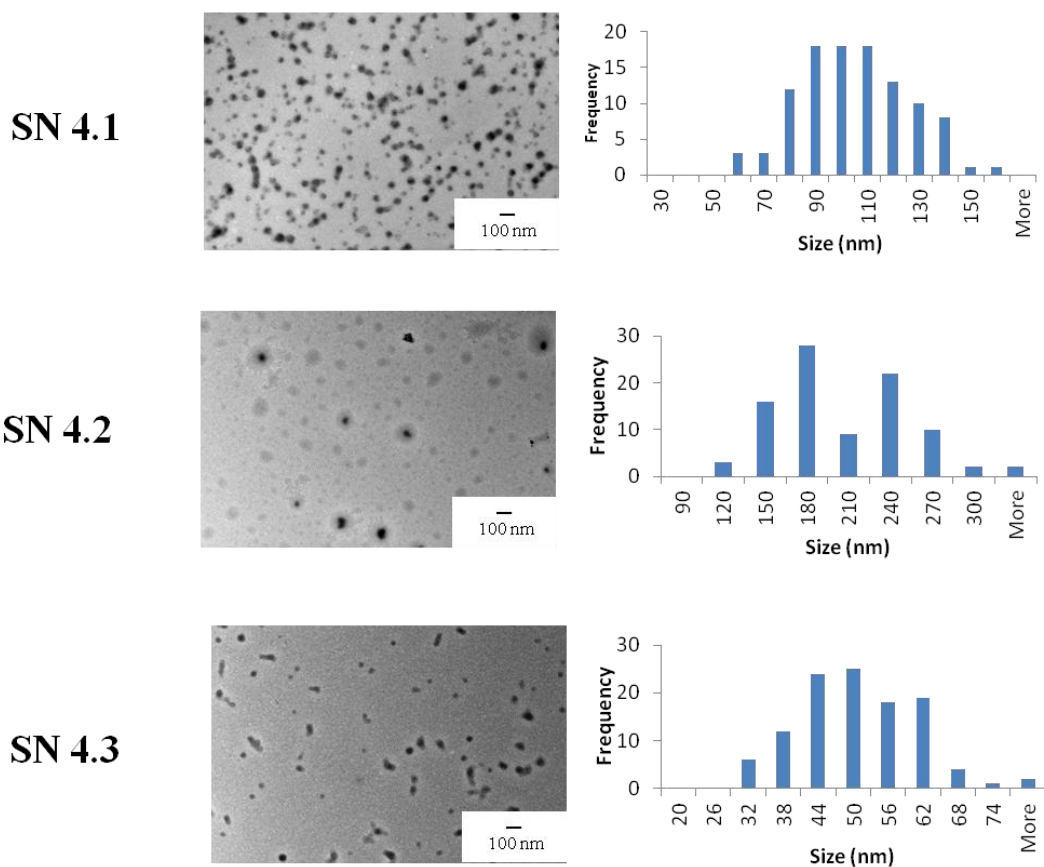


Figure 4.11. Number (blue line), Volume (red line) and Intensity (green line) DLS traces for the nanogels synthesized in this work.



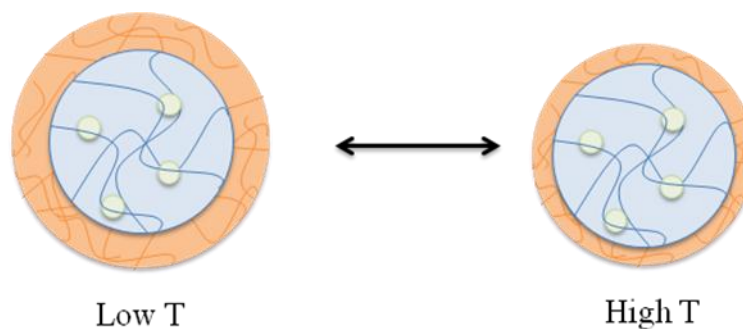


Figure 4.13. A schematic representation of the changeable nature of the shell characteristic at low temperatures (a hydrophilic fully extended polymer) or high temperatures (a hydrophobic collapsed polymer).

The change in the size of the shell can be monitored with variable temperature DLS (Figure 4.14). The collapse (i.e. decreased particle size) for both **SN 4.1** and **SN 4.2** is observed confirming the responsive nature of the core-shell nanogels. A decrease in particle size was first observed at 30 °C and 40 °C for **SN 4.1** and **SN 4.2** respectively, which is in alignment with their homopolymer LCSTs of 28 °C⁴⁴ and 50 °C.⁴³ The non-responsive character of the core nanogel was also recorded for comparison, as shown below.

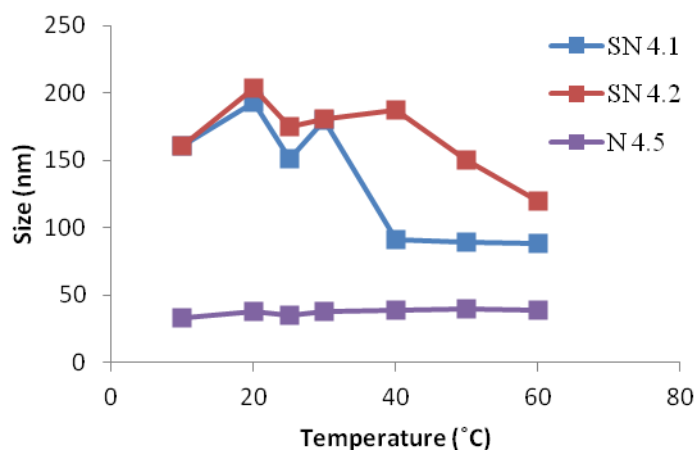


Figure 4.14. Change in particle size with temperature, as determined by DLS for **SN 4.1** (blue line), **SN 4.2** (red line) and **N 4.5** (purple line).

Unfortunately, the shells had a detrimental effect on the activity of the catalyst, with conversions for the DA reaction dropping to $\leq 10\%$ after 24 hours (Table 4.12). In an attempt to increase the conversion, a thinner NiPAM shell was added (**SN 4.3**) to **N 4.5** giving a total diameter of 85 nm compared to the 151 nm of **SN 4.1**. Nevertheless, equally low conversions were noted after 24 hours ($\leq 10\%$). Additionally the nanogels were also concentrated to produce systems with the same catalyst concentration as during the shell synthesis this was effectively diluted. The concentrated systems, **SN 4.1a** and **SN 4.2a** were unable to produce improved conversions with only slight increases observed ($\leq 20\%$) and still below that achieved without the shell.

Table 4.12. Conversion of DA reaction between cinnamaldehyde and cyclopentadiene catalyzed by **SN 4.1**, **SN 4.2** and the more concentrated **SN 4.1a** and **SN 4.2a** at various mol% at rt.

Nanogel	Catalyst loading (mol %)	Conversion^a (%)
SN 4.1	5	10
SN 4.2	5	7
SN 4.1	2.5	8
SN 4.2	2.5	5
SN 4.1a	2.5	0
SN 4.1a	5	13
SN 4.1a	10	13
SN 4.1a	20	30
SN 4.2a	5	18
SN 4.3	5	10

^aH NMR spectroscopy through comparison of the cinnamaldehyde aldehyde proton ($\delta = 9.68$ ppm) and the product aldehyde protons ($\delta = 9.54$ ppm and 9.85 ppm)

The selectivity was also negatively affected by the addition of the shells dropping as low as 50% *endo* ee for **SN 4.1** and 35% *endo* ee for **SN 4.2** (Table 4.13).

Table 4.13. The selectivities of **SN 4.1** and **SN 4.2** for the DA reaction after 24 h between cinnamaldehyde and cyclopentadiene.

Catalyst	<i>exo:endo</i> ^a	<i>exo ee</i> % ^b	<i>endo ee</i> % ^b
SN 4.1	0.7	52	56
SN 4.2	0.7	35	60
SN 4.3	1.3	51	38

^{ab}Determined by ¹H NMR spectroscopy through comparison the product aldehyde protons ($\delta = 9.54$ ppm (*exo*) and 9.85 ppm(*endo*))

^bDetermined by chiral GC

Due to the low activity and selectivity, the potential recovery and reuse of these systems were not investigated.

It was hypothesized that it may be possible to completely switch off the catalysis at elevated temperatures due to the collapsed shell preventing entry of the substrates into the catalyst decorated core. This effect has been noted by the groups of Liu⁴⁵ and Song.⁴⁶ Both have incorporated catalysts into nanoreactors that contain poly(NiPAM): on performing their respective reactions at an elevated temperature, above the LCST of poly(NiPAM) a fall in conversion was observed which both groups attributed to the different nature of the poly(NiPAM) at the elevated temperatures.

Therefore, the DA reaction was performed additionally at 4 °C and 40 °C. A negligible increase in conversion was observed by increasing the reaction temperature from 4 °C to 20 °C for **SN 4.1a** from 10 to 13% (Table 4.14). However, when the temperature was

further increased to 40 °C, above the LCST temperature for the system, no conversion was observed. This is in contrast to the activity of **M 3.1** where 83% conversion was observed even at 40 °C after 24 hours (in 100 μ L of water). Therefore, it is proposed that the lack of catalytic activity for the core-shell nanogels at the higher temperatures is a direct result of the shell polymer becoming hydrophobic and preventing the entry of substrates into the catalytic domain.

Table 4.14. The conversions of the DA reaction after 24 h between cinnamaldehyde and cyclopentadiene conducted with **SN 4.1a** and **SN 4.2a** at various temperatures.

Nanogel	mol%	Temp (°C)	Conversion^a (%)
SN 4.1a	5	4	10
SN 4.1a	5	20	13
SN 4.1a	5	40	0
SN 4.2a	5	4	13
SN 4.2a	5	20	18
SN 4.2a	5	40	12

^a¹H NMR spectroscopy through comparison of the cinnamaldehyde aldehyde proton ($\delta = 9.68$ ppm) and the product aldehyde protons ($\delta = 9.54$ ppm and 9.85 ppm)

4.4 Conclusions

In conclusion, a range of nanoparticles placing the MacMillan catalyst into a unique hydrophobic domain have been synthesized. Due to the ease of synthesis, the DoF of the nanogels and in some cases the co-monomer has been easily varied and the effect of these changes on the catalytic ability has been thoroughly studied. The nanogels are capable of catalyzing the DA reaction between cyclopentadiene and cinnamaldehyde and in order to achieve good conversion it has been shown that a balance between the concentration of nanogels, concentration of catalyst and the substrate to water ratio needs to be struck. In these unique environments the selectivity of the reaction has been compromised with different surroundings causing different effects. These systems do however demonstrate the concentrator effect, a phenomenon that was targeted at the outset of placing the catalyst into a hydrophobic cavity.

4.5 Experimental

4.5.1 Instrumentation

^1H NMR spectra were recorded on a 250 or 300 MHz Bruker DPX FT-NMR spectrometer using deuterated solvents. Chemical shifts are reported as δ in parts per million (ppm) relative to the solvent used (deuterated-DMSO at 2.50 ppm). Enantiomeric excess (ee%) was measured by gas chromatography (GC) on a Varian 450-GC with a 25 m chirasil-Dex chiral column injection temperature 250 °C, column temperature 100 °C, ramp to 174 °C at 2.0 °C min⁻¹. Dialysis tubing was purchased from Spectrum labs with a MWCO of 6 – 8 kDa. Hydrodynamic diameters (D_H) and size distributions were determined by dynamic light scattering (DLS) using a Malvern Zetasizer Nano ZS instrument at 25 °C equipped with a 4 mW He-Ne 633 nm laser and a detector at 173°. All measurements were made in triplicate consisting of 10 runs of 10 s each. Variable temperature DLS measurements were carried out using a temperature increment of 10 °C between 20 °C and 60 °C, consisting of 10 x 10 s runs with a 2 min equilibration time held at each temperature. Size exclusion chromatography (SEC) analyses were performed in *N,N*-dimethylacetamide (DMAc) containing LiBr (1 mg mL⁻¹) at a flow rate of 1.0 mL min⁻¹ at 50 °C, on a set of two PLgel 5 μm mixed-C columns and one guard column. Transmission electron microscopy (TEM) samples were prepared by drop deposition of a 0.1 mg mL⁻¹ polymer solution in water onto copper/carbon grids that had been pre-treated with oxygen plasma and analyzed by using a JEOL TEM-2100 microscope operating at 200 kV. TEM images were taken by Miss Dafni Moatsou.

4.5.2 Methods and Techniques

N-isopropylacrylamide (NiPAM) was recrystallized from methanol and stored at 4 °C. Cyclopentadiene was prepared from dicyclopentadiene purchased from Sigma-Aldrich and was stored at -20 °C. All other chemicals were purchased from Sigma-Aldrich and used without further purification.

M 3.1: The synthesis of **M 3.1** has been outlined in Chapter 3.²⁶

4.5.2.1 Nanogel synthesis

Typical nanogel synthesis: **M 3.1** (0.108 g) (20 wt%) was first dissolved in 800 μ L of CHCl_3 and added to a solution of sodium dodecyl sulfate (SDS) (0.125 g) in 10 mL H_2O . This heterogeneous mixture was then added dropwise to 40 mL of H_2O stirring at 600 rpm in a 250 mL round bottom flask. Ethyl methacrylate (EMA) (0.469 mL), ethylene glycol dimethacrylate (EGDMA) (0.0026 mL) and potassium persulfate (KPS) (5 mg) were also added and the mixture was purged with nitrogen for 10 min before submerging into a preheated oil bath at 70 °C with stirring at 600 rpm overnight. The solution turned to an iridescent solution which was then dialyzed against millipure H_2O to remove any excess SDS.

Core-Shell nanogel synthesis: A typical shell synthesis involved the aforementioned nanogels as seeds for the polymerization; the following procedure is for the addition of a large NiPAM shell. The seed nanogel dispersion (25 mL) was purged by bubbling nitrogen and heated at 70 °C with rapid stirring (600-800 rpm). In another flask, SDS (0.018 g) was dissolved in water (25 mL) and purged with nitrogen. To that, NiPAM

(0.220 g), *N,N'*-methylenebisacrylamide (BIS) (1.3 mg, 0.5 wt%) and KPS (2.5 mg) were added. The monomer mixture was then added slowly to the heated seed nanogel dispersion at no faster than 1 mL min⁻¹. Once the addition was complete, a positive pressure of nitrogen was maintained for the duration of the reaction. The solution was left to stir overnight and then dialyzed against millipure H₂O (MWCO = 6 – 8 kDa) to remove excess reagents.

4.5.2.2 Diels-Alder reaction

A typical DA reaction was carried out as follows: to the calculated amount of nanogel dispersion for a desired mol%, cinnamaldehyde (22 μ L, 1 eq) and cyclopentadiene (30 μ L, 1.5 eq) were added, which was then stirred for 24 h. Over this period, the reaction mixture turned from the iridescent blue solution to yellow. The reagents and products were extracted at the desired time by swelling the hydrophobic nanogels *via* the addition of 3 mL of THF, yielding a clear yellow solution. The THF was then removed under a flow of air and the remaining residues dissolved in deuterated-DMSO and analyzed by ¹H NMR spectroscopy determining reaction conversion and GC determining enantiomeric excess (ee%). Injection temperature 250 °C, column temperature 100 °C, ramp to 174 °C at 2 °C min⁻¹, *exo* isomers t_R = 31.7 and 33.1 min, *endo* isomers t_R = 31.9 and 33.4 min. ¹H NMR (250 MHz, DMSO): δ 9.54 (1H, d, ³ J = 1.8 Hz, C(O)H *exo*), 9.68 (1H, d, ³ J = 7.5 Hz, C(O)H starting material), 9.85 (1H, d, ³ J = 2.2 Hz, C(O)H *endo*). pH of N 4.5 = 3.3.

4.6 References

1. S. Narayan, J. Muldoon, M. G. Finn, V. V. Fokin, H. C. Kolb and K. B. Sharpless, *Angew. Chem. Int. Ed.*, 2005, **44**, 3275-3279.
2. P. Cotanda, A. Lu, J. P. Patterson, N. Petzetakis and R. K. O'Reilly, *Macromolecules*, 2012, **45**, 2377-2384.
3. J. P. Patterson, P. Cotanda, E. G. Kelley, A. O. Moughton, A. Lu, T. H. Epps III and R. K. O'Reilly, *Polym. Chem.*, 2012, **4**, 2033-2039.
4. P. Cotanda and R. K. O'Reilly, *Chem. Commun.*, 2012, **48**, 10280-10282.
5. P. Cotanda, N. Petzetakis and R. K. O'Reilly, *MRS Commun.*, 2012, **2**, 119-126.
6. D. M. Vriezema, M. Comellas Aragones, J. A. A. W. Elemans, J. J. L. M. Cornelissen, A. E. Rowan and R. J. M. Nolte, *Chem. Rev.*, 2005, **105**, 1445-1490.
7. B. Helms and J. M. J. Fréchet, *Adv. Synth. Catal.*, 2006, **348**, 1125-1148.
8. A. Lu and R. K. O'Reilly, *Curr. Opin. Biotechnol.*, 2013, **24**, 639-645.
9. B. Helms, C. O. Liang, C. J. Hawker and J. M. J. Fréchet, *Macromolecules*, 2005, **38**, 5411-5415.
10. R. van Heerbeek, P. C. J. Kamer, P. W. N. M. van Leeuwen and J. N. H. Reek, *Chem. Rev.*, 2002, **102**, 3717-3756.
11. T. Dwars, E. Paetzold and G. Oehme, *Angew. Chem. Int. Ed.*, 2005, **44**, 7174-7199.
12. T. Rispens and J. B. F. N. Engberts, *J. Org. Chem.*, 2002, **67**, 7369-7377.
13. J. Perez-Juste, F. Hollfelder, A. J. Kirby and J. B. F. N. Engberts, *Org. Lett.*, 1999, **2**, 127-130.
14. Z. Ge, D. Xie, D. Chen, X. Jiang, Y. Zhang, H. Liu and S. Liu, *Macromolecules*, 2007, **40**, 3538-3546.

15. A. Lu, P. Cotanda, J. P. Patterson, D. A. Longbottom and R. K. O'Reilly, *Chem. Commun.*, 2012, **48**, 9699-9701.
16. H. Wei and E. Wang, *Chem. Soc. Rev.*, 2013, **42**, 6060-6093.
17. Y. Chi, S. T. Scroggins and J. M. J. Fréchet, *J. Am. Chem. Soc.*, 2008, **130**, 6322-6323.
18. B. Helms, S. J. Guillaudeu, Y. Xie, M. McMurdo, C. J. Hawker and J. M. J. Fréchet, *Angew. Chem. Int. Ed.*, 2005, **44**, 6384-6387.
19. A. W. Bosman, R. Vestberg, A. Heumann, J. M. J. Fréchet and C. J. Hawker, *J. Am. Chem. Soc.*, 2002, **125**, 715-728.
20. T. Terashima, M. Kamigaito, K.-Y. Baek, T. Ando and M. Sawamoto, *J. Am. Chem. Soc.*, 2003, **125**, 5288-5289.
21. E. Huerta, P. J. M. Stals, E. W. Meijer and A. R. A. Palmans, *Angew. Chem. Int. Ed.*, 2012, **52**, 2906-2910.
22. F. Cozzi, *Adv. Synth. Catal.*, 2006, **348**, 1367-1390.
23. N. Haraguchi, Y. Takemura and S. Itsuno, *Tetrahedron Lett.*, 2010, **51**, 1205-1208.
24. T. E. Kristensen and T. Hansen, *Eur. J. Org. Chem.*, 2010, **2010**, 3179-3204.
25. T. E. Kristensen, K. Vestli, M. G. Jakobsen, F. K. Hansen and T. Hansen, *J. Org. Chem.*, 2010, **75**, 1620-1629.
26. B. L. Moore, A. Lu, D. A. Longbottom and R. K. O'Reilly, *Polym. Chem.*, 2012, **4**, 2304-2312.
27. P. Riente, J. Yadav and M. A. Pericas, *Org. Lett.*, 2012, **14**, 3668-3671.
28. S. A. Selkälä, J. Tois, P. M. Pihko and A. M. P. Koskinen, *Adv. Synth. Catal.*, 2002, **344**, 941-945.

29. Y. Zhang, L. Zhao, S. S. Lee and J. Y. Ying, *Adv. Synth. Catal.*, 2006, **348**, 2027-2032.
30. T. Terashima, A. Nomura, M. Ito, M. Ouchi and M. Sawamoto, *Angew. Chem. Int. Ed.*, 2011, **50**, 7892-7895.
31. M. Yan, J. Ge, Z. Liu and P. Ouyang, *J. Am. Chem. Soc.*, 2006, **128**, 11008-11009.
32. A. Lu, D. Moatsou, D. A. Longbottom and R. K. O'Reilly, *Chem. Sci.*, 2012, **4**, 965-969.
33. K. A. Ahrendt, C. J. Borths and D. W. C. MacMillan, *J. Am. Chem. Soc.*, 2000, **122**, 4243-4244.
34. <http://www.molinspiration.com/services/logp.html>
35. A. K. Ghose, V. N. Viswanadhan and J. J. Wendoloski, *J. Phys. Chem. A*, 1998, **102**, 3762-3772.
36. J. F. Austin and D. W. C. MacMillan, *J. Am. Chem. Soc.*, 2002, **124**, 1172-1173.
37. C. H.-M. Larsen, in *Chemistry and Chemical Engineering*, California Institute of Technology, California, 2006.
38. http://www.sigmaaldrich.com/img/assets/3900/Thermal_Transitions_of_Homopolymers.pdf
39. J. Dzierzak, E. Bottinelli, G. Berlier, E. Gianotti, E. Stulz, R. M. Kowalczyk and R. Raja, *Chem. Commun.*, 2010, **46**, 2805-2807.
40. G. Manecke and W. Storck, *Angew. Chem. Int. Ed. Eng.*, 1978, **17**, 657-670.
41. D. E. Bergbreiter, *Chem. Rev.*, 2002, **102**, 3345-3384.
42. R. Arshady, *Colloid. Polym. Sci.*, 1992, **270**, 717-732.

43. S.-I. Yamamoto, J. Pietrasik and K. Matyjaszewski, *J. Polym. Sci. Part A: Polym. Chem.*, 2008, **46**, 194-202.
44. J.-F. Lutz, O. Akdemir and A. Hoth, *J. Am. Chem. Soc.*, 2006, **128**, 13046-13047.
45. X. Huang, Y. Yin, Y. Tang, X. Bai, Z. Zhang, J. Xu, J. Liu and J. Shen, *Soft Matter*, 2009, **5**, 1905-1911.
46. Z. Chen, Z.-M. Cui, C.-Y. Cao, W.-D. He, L. Jiang and W.-G. Song, *Langmuir*, 2012, **28**, 13452-13458.

Chapter 5: Tryptophan as a FRET probe in the study of the effects of polymer structure on the diffusion of small molecules into a cross-linked polymeric nanogels

5.1 Abstract

Having explored the use of nanogels for catalysis reactions in Chapter 4, further investigations into these types of systems have been conducted. A new readily polymerizable monomer based on the amino acid L-tryptophan was synthesized and incorporated into a range of cross-linked polymer particles stabilized in aqueous solution by a surfactant. The relatively easy synthesis of these nanogels has allowed for variables such as cross-linking density (CLD) and co-monomer to be easily changed allowing for a range of nanogels to be synthesized. The fluorescent properties of L-tryptophan with its Forster Resonance Energy Transfer (FRET) pair dansyl amide (DNSA) have been exploited in order to probe the effect of the changing variables of the nanogels on DNSA diffusion. By constantly measuring the L-tryptophan emission after the addition of the FRET pair, the time taken for the molecules to come into close proximity and for FRET to occur (L-tryptophan emission decreases, DNSA emission increases) can be calculated. It has been shown that by increasing the CLD and thus the steric effects around the hydrophobic core, diffusion is slowed from 33 minutes to 53 minutes and by increasing the hydrophobicity/decreasing the T_g of the system, a decrease in diffusion time from 61 minutes to 44 minutes is observed.

5.2 Introduction

The fluorescent properties of the amino acid L-tryptophan are well known and have been exploited in the research of proteins due to its sensitivity to the polarity of its environment.¹⁻⁵ In a more hydrophobic environment L-tryptophan's fluorescence emission becomes more intense and shifts to a shorter wavelength. Additionally, as a result of its aromatic nature, L-tryptophan residues are usually located in the hydrophobic centre of a protein making the change in environment dramatic on structural rearrangements. This makes it a highly useful probe to study conformation changes within proteins and interactions with other molecules. An example of a well-studied protein using L-tryptophan is Staphylococcal nuclease (Snase) which has one L-tryptophan residue with different fluorescent spectra depending on the folded/unfolded nature of the protein, therefore enabling studies of protein structure stability.⁶ The structure of Snase can be seen in Figure 5.1, the tryptophan moiety, highlighted in purple, is the last residue to exhibit order.

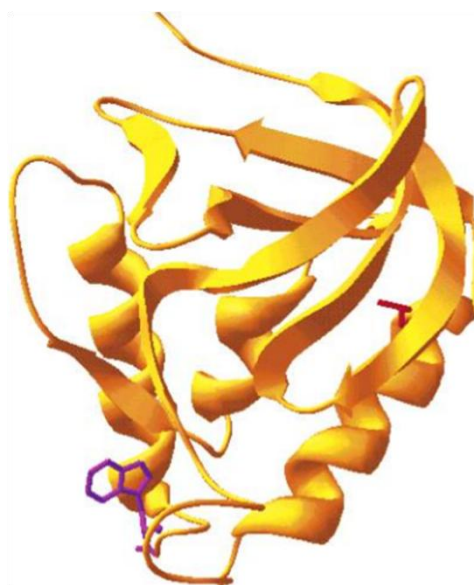


Figure 5.1. A reproduction of the 3D representation of Snase,⁶ the L-tryptophan moiety highlighted in purple is the last residue to exhibit order.

The amino acids L-phenylalanine and L-tyrosine also exhibit fluorescence characteristics but their use in folding experiments is less common than tryptophan's because of their lower extinction coefficients.⁷ Their excitation and emission fluorescence spectra in an aqueous pH 7 solution can be seen in Figure 5.2. Tryptophan also has the further advantage of being selectively excited at $\lambda_{\text{ex}} = 295 \text{ nm}$, an excitation wavelength often used in the literature.⁷

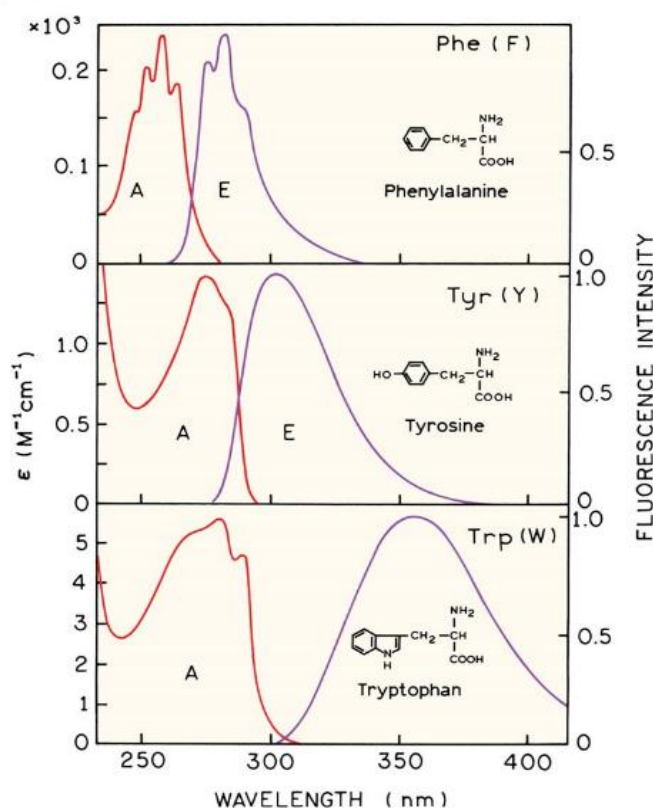


Figure 5.2. A reproduction of the excitation (red line) and emission (purple line) spectra of phenylalanine, tyrosine and tryptophan in an aqueous pH 7 solution.⁷

The use of fluorescence is also prevalent within other areas of self-assembly. In particular it is often used to study the formation of self-assembled structures; as fluorescence is highly dependent on environment, the emission from a probe will change as per its location. Prior to the assembly of the structure the probe will be

nanostructure which includes spheres, cylinders and vesicles. The different ratios of hydrophobic and hydrophilic segments can alter the way the unimer chains pack together during the self-assembly process, which leads to variable structures. This packing parameter is calculated according to Equation 5.1, where p is the packing parameter, v is the volume of the hydrophobic chains, a_0 is the area of the head group and l_c is the length of the hydrophilic tail.

$$p = \frac{v}{a_0 l_c} \quad (5.1)$$

It has been shown that values of $p \leq 1/3$ will give spherical micelles, $1/3 \leq p \leq 1/2$ gives cylindrical micelles and $1/2 \leq p \leq 1$ gives vesicles. This has been shown in Figure 5.3 which has been reproduced from a publication by Blanzas *et al.*¹³

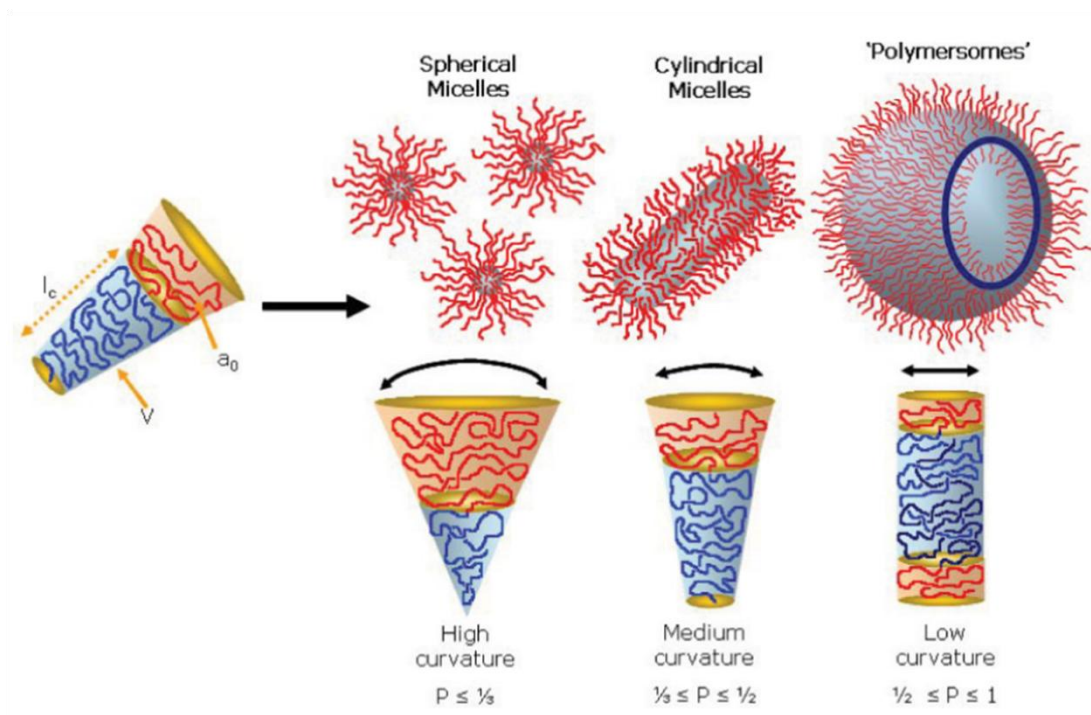
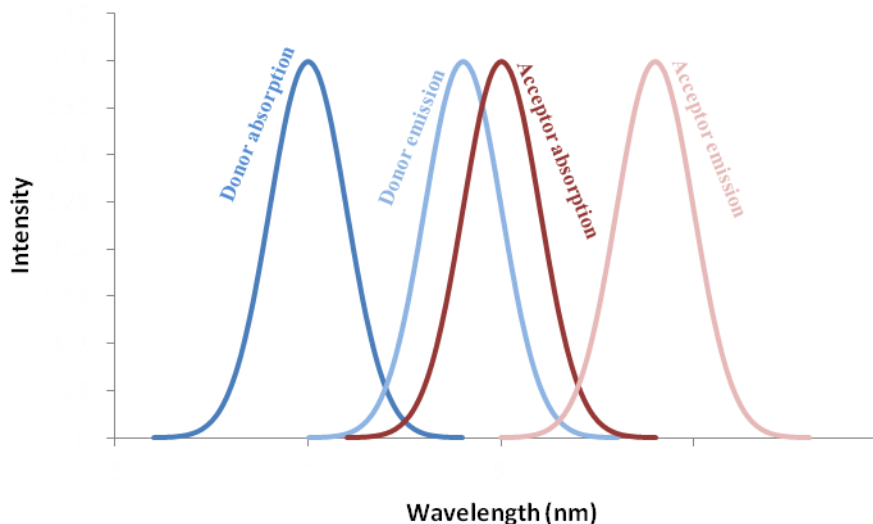


Figure 5.3. A reproduction of a figure which demonstrates how the influence of packing parameters can affect the self-assembled structure.¹³

The main driving force for self-assembly is the decrease of the free energy in the system through removal of unfavourable interactions. Therefore the CMC is strongly dependent of the amount of hydrophobic material present in a system. Consequently one potential drawback of CMC analysis *via* the use of a pyrene probe is that the large, bulky, planar nature of pyrene can arguably alter the CMC of a system as it alters the hydrophobic balance which micelle formation is dependent upon. One alternative method, still utilizing fluorescence, has recently been developed within our group. Small dithiomaleimide molecules have been shown to be fluorescent and can be easily incorporated into polymers and peptides as a fluorescent label which could then be monitored and these fluorescent tags are much less likely to disrupt the systems aggregation behaviour.^{14, 15}

Fluorescence is also commonly used in Forster Resonance Energy Transfer (FRET) studies.¹⁶⁻²³ FRET is the energy transfer between an excited donor molecule and an acceptor molecule. The acceptor molecule absorbs the emitted energy from the donor molecule and fluoresces at a different wavelength. This process is distance dependent with FRET occurring at <10 nm and can therefore be used to study the positioning of particular molecular pairs. A schematic of the FRET process can be seen in Scheme 5.2.



Scheme 5.2. A representative scheme of the FRET process. The donor absorbs radiation and fluoresces at a wavelength which excites the acceptor that in turn emits at a different wavelength.

L-Tryptophan has a number of FRET pairs including folic acid,²¹ ribonucleoside analogues,²² modified amino acids,^{17, 18} and dansyl groups^{16, 19} (which have been used in this work). FRET has been exploited by Gai *et al.* who used *p*-cyanophenylalanine (Phe_{CN}), a modified version of phenylalanine, to monitor peptide structure.¹⁷ Phe_{CN} was incorporated into a 14 residue peptide which also contained L-tryptophan. These two fluorescent molecules are FRET pairs and could therefore provide information on how close the residues were, which is related to their FRET efficiency. Thus, this provided insight into the peptide structure and of the environments of the examined residues. Another example of FRET in the deduction of peptide folding was reported by Deng *et al.* using L-tryptophan and a dansyl group.¹⁶ Their study focused on the peptide transthyretin (TTR) which has been well studied due to its involvement in mental diseases. By attaching the dansyl group to the N-terminal and an L-tryptophan to the C-terminal of the peptide the

kinetics of the formation of amyloid fibrils was studied using fluorescence spectroscopy.

More recently, supramolecular assemblies with fluorescent characteristics have been synthesized.^{4, 24-29} The main aim of these structures has been to provide a handle for the release or uptake of specific molecules. With increased research into the design of nanostructures for specific delivery such as drug delivery, fluorescent properties provide a convenient handle to observe the location and movement of targeted molecules. For instance a fluorescent polymeric micelle based on poly(ethylene glycol) (PEG) and poly(styrene) (PS) has been used to monitor the encapsulation and release of the cancer drug doxorubicin (DOX).²⁴ The PS block was co-polymerized with a unique fluorescent monomer (2-(1,2,3,4,5-pentaphenyl-1H-silol-1-yloxy)ethyl methacrylate) that interacted with DOX as a FRET pair. Therefore, when DOX was encapsulated FRET occurred and the emission for DOX was observed, but on release the emission was solely caused by the fluorescent monomer allowing the location of DOX to be determined in relation to the construct.

L-Tryptophan has also been used as a fluorescent handle within other higher order structures. Mori *et al.* synthesized an amphiphilic block polymer with L-tryptophan forming the hydrophobic block allowing for the assembly of micelle structures.³⁰ L-Tryptophan's fluorescent properties were then used for fluoride ion recognition; an area that is of importance due to implications in drinking water analysis. L-Tryptophan fluorescence within a polymer structure has also been studied by De *et al.* who synthesized a methacrylate based polymer and were also able to demonstrate the low cytotoxicity of the polymers through incubation with HeLa cells. These

fluorescent properties coupled with the biocompatible nature of the polymers makes them potential candidates for drug delivery or siRNA delivery.³¹

Whilst these systems are able to demonstrate the presence or absence of particular molecules, there have been fewer studies on the diffusion of molecules into different structures. With regards to the use of higher order structures such as nanoreactors, the steric effect of increased cross-linking density (CLD) has been noted independently by the Fréchet group³² and Lu *et al.*³³ They both noted that increased steric constraints imposed by higher levels of cross-linking diminished the reaction rates. Other work that has focussed on how structure affects the diffusion out of a micelle has been conducted by Lin *et al.* They have investigated the effect of changing the ratios and block length of micelle structures made from PS and poly(acrylic acid) (PAA) on the release of encapsulated DOX.³⁴ Their work demonstrated that the ratio of PAA:PS affected the release data with higher acrylic acid vs styrene volume ratios showing the slowest release (based on constant polymer concentration).

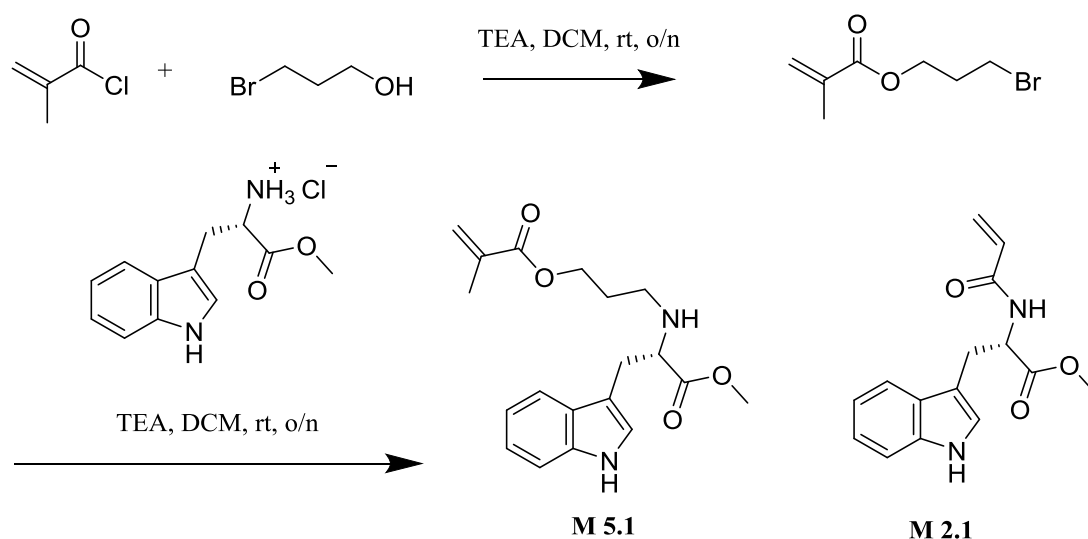
With the increasing use of polymer based structures for catalysis reactions the process of substrates reaching the catalyst is important and the nature and permeability of the polymeric structure surrounding the catalyst needs to be considered. Whilst micelle constructs offer advantages as they are synthesized through the self-assembly of well-defined polymers, their production can often be time-consuming and involve multiple steps, and unless further cross-linking chemistry is performed, their structures are not covalently bonded. Nanogels, however, are synthesized in a one-pot synthesis that can be simultaneously cross-

linked, which enables the formation of stabilized polymeric particles. This straightforward and facile synthesis has allowed for a series of nanogels to be readily prepared altering multiple variables. This Chapter will examine a range of polymeric nanogels incorporating the intrinsically fluorescent amino acid L-tryptophan. By altering variables such as CLD and co-monomer it will be possible to investigate their effect on the diffusion of small molecules into the nanogel core. Through the use of the L-tryptophan FRET pair dansyl amide (DNSA), the diffusion of DNSA into L-tryptophan rich regions has been monitored with time and its dependence on nanogel CLD and co-monomer examined.

5.3 Results and Discussion

5.3.1 Monomer Synthesis

As discussed in Chapter 2, an acrylamide type L-tryptophan monomer (**M 2.1**) has been synthesized. However, the direct polymerization of this functional monomer was difficult and thus a second L-tryptophan monomer **M 5.1** was subsequently designed and synthesized. **M 5.1** is structurally similar to **M 2.1** but is a methacrylate type monomer and has a longer linker between the polymerizable group and the functional L-tryptophan unit. Interestingly, these minor changes to the design resulted in a readily polymerizable monomer. The synthetic route to **M 5.1** is presented in Scheme 5.3 alongside the previously discussed **M 2.1** monomer.



Scheme 5.3. The synthetic route to the L-tryptophan-containing monomer **M 5.1**.

The ^1H NMR and ^{13}C NMR spectra of **M 5.1** can be seen in Figure 5.4 and Figure 5.5 respectively and the high resolution mass spectrometry provided a mass of m/z for $[\text{M} + \text{H}]^+$ of 345.1809, which correlates exactly with the expected mass of 345.1809 m/z for the desired product. The ^1H NMR spectrum showed the expected

chemical shifts and integrations. Proton **h** has a complex splitting pattern that appears as two separate peaks due to the chiral nature of the molecule: the two protons are diastereotopic and therefore their resonances have different chemical shifts.

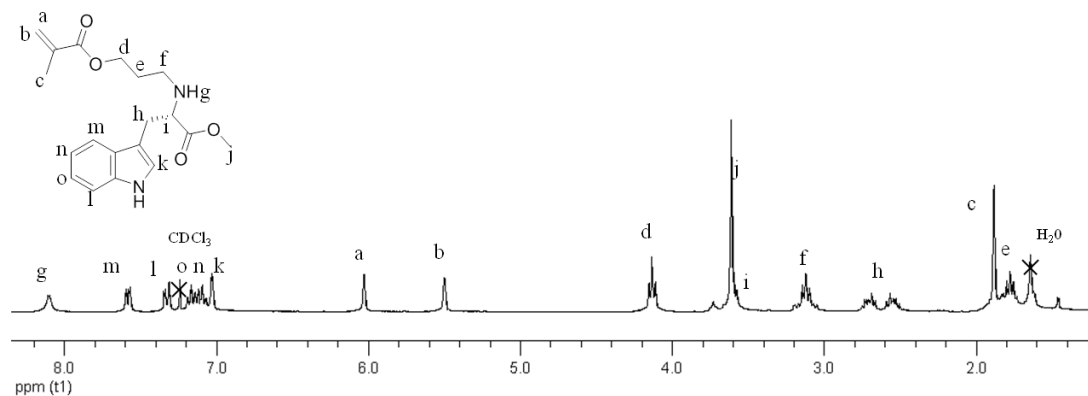


Figure 5.4. ^1H NMR (300 MHz) spectrum of **M 5.1** in CDCl_3 .

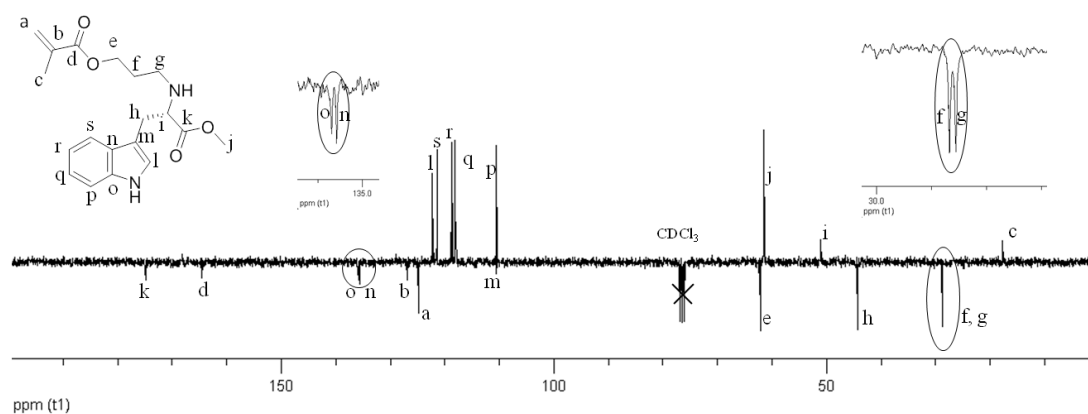


Figure 5.5. ^{13}C NMR (75 MHz) spectrum of **M 5.1** in CDCl_3 , expanded parts of the spectrum are inserted where two peaks have very similar shifts.

Through the use of RAFT **M 5.1** has been polymerized with good control. Homopolymerizations with various concentration, temperature, CTA (2-cyano-2-propyl benzodithioate (**CTA 5.1**) or 2-cyano-2-propyl dodecyl trithiocarbonate (**CTA 5.2**), Figure 5.6) and radical flux are shown in Table 5.1. All conditions have

given good polymerization results, which demonstrate the versatile polymerizable nature of **M 5.1**. The lowest dispersity was achieved for the polymerization carried out at the lowest concentration (0.1 g mL^{-1}), entry 1.

Table 5.1. The range of conditions tested for the polymerization of **M 5.1**, altering temperature, radical flux, CTA and monomer concentration, along with the conversion and \bar{D} of the resulting polymers. The structures of CTA 1 and 2 can be seen in Figure 5.6.

Polymer	[Polymer] (g mL^{-1})	Temp ($^{\circ}\text{C}$)	AIBN	CTA ^a	Time (h)	Conversion ^b (%)	\bar{D} ^c
P 5.1	0.1	70	0.2	1	6	58	1.11
P 5.2	0.2	70	0.2	1	6	59	1.15
P 5.3	0.5	70	0.2	1	6	72	1.16
P 5.4	0.2	70	0.1	1	6	61	1.17
P 5.5	0.2	70	0.3	1	6	68	1.15
P 5.6	0.2	80	0.2	1	6	62	1.16
P 5.7	0.2	70	0.2	2	6	65	1.26
P 5.8	0.2	80	0.2	2	6	80	1.19

^aCTA structures are shown in Figure 5.6

^bDetermined by ^1H NMR spectroscopy

^cDetermined by SEC (DMF, PMMA calibration)

Both a dithiobenzoate (**CTA 5.1**) and a trithiocarbonate (**CTA 5.2**) were tested as CTAs for the polymerization of **M 5.1** as both families are known to be compatible for RAFT mediated methacrylate polymerizations (Figure 5.6).³⁵⁻³⁷ From the results

in Table 5.1, narrower \bar{D} values were obtained from the dithiobenzoate CTA. The effectiveness of a RAFT CTA is dependent on the reactivity of the C=S bond and the reactivity of the formed monomer radical. Dithiobenzoates typically have a higher transfer constant than trithiocarbonates,³⁸ which in these polymerizations seems to have provided greater polymerization control.

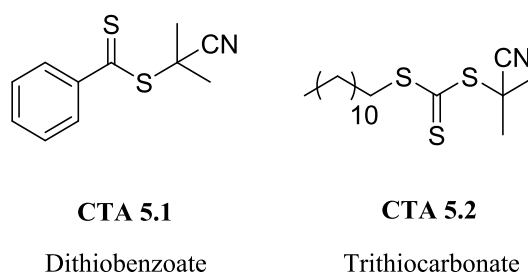


Figure 5.6. Structures of the CTA 5.1 and 5.2 used in the polymerization of **M 5.1**, detailed in Table 5.1.

A typical conversion ^1H NMR spectrum can be seen in Figure 5.7 for the conversion of entry 7 in Table 5.1. The polymer peaks are highlighted with a blue dot and the monomer peaks are labeled. The conversion was calculated by comparing the integration of the monomer vinyl signal, **a**, to the integration of the aromatic region, taking into account the remaining monomer.

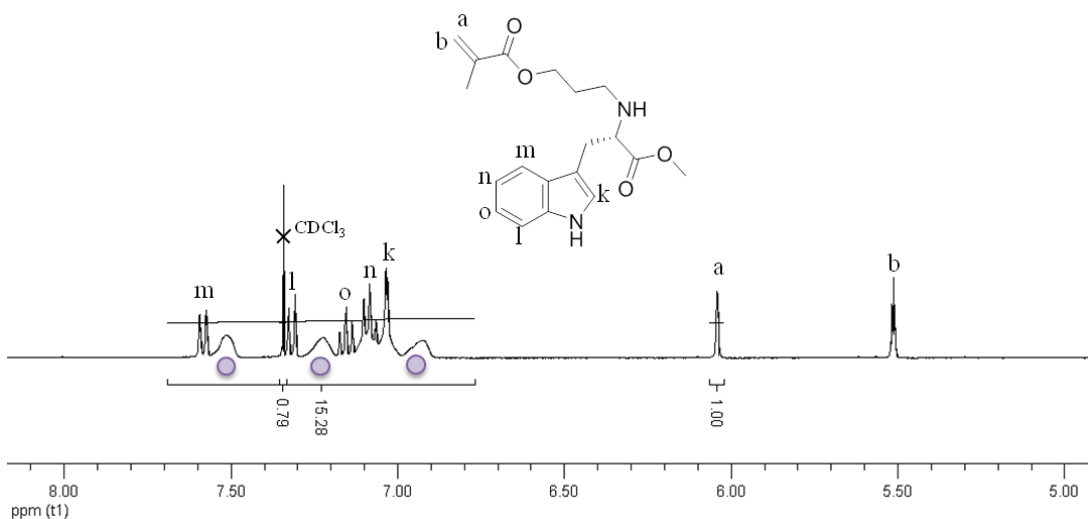


Figure 5.7. ^1H NMR (300 MHz) spectrum of the conversion of **M 5.1** in CDCl_3 with polymeric peaks highlighted and observed monomeric peaks labelled. The conversion was calculated by subtracting the monomer peaks and CDCl_3 peak from the integral and comparing the value to the quantity of monomer still left. e.g. $((15.28-0.79-5)/5) \times (1/(1.898+1))*100\% = 65\%$.

The evolution of molecular weight with respect to time was followed by ^1H NMR spectroscopy and SEC and the data for **P 5.1** (entry 1, Table 5.1) can be seen in Figure 5.8. The straight line in Figure 5.8 is indicative of first order kinetics and therefore a constant concentration of a propagating species in accordance with Equation 5.2. This is indicative of a polymerization with living characteristics, as expected from a RAFT polymerization.

$$\ln \frac{[M]_0}{[M]} = k_p [P^*] t \quad (5.2)$$

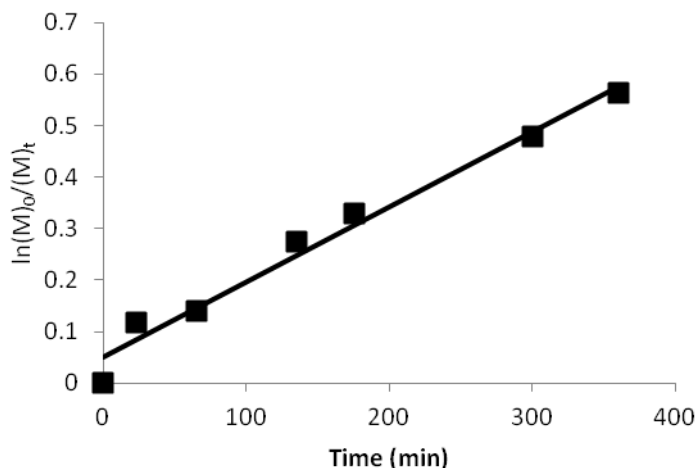


Figure 5.8. A plot of $\ln(M)_0/(M)_t$ against time for the polymerization of **P 5.1**, entry 1 in Table 5.1.

The possibility of co-polymerizing **M 5.1** was also investigated by co-polymerization with both methyl methacrylate (MMA) and ethyl methacrylate (EMA) at molar ratios of 1:1 for **M 5.1** to co-monomer. Analysis of the polymers *via* DMF SEC showed single polymer peaks with D of 1.6 and 1.4 respectively.

Additionally, chain extension of **P 5.1** (homopolymer of **M 5.1**) with MMA was also carried out. **P 5.1** (the macroCTA) and MMA (100 equivalents) were dissolved together in dioxane with a radical flux from AIBN (0.2 equivalents). The polymerization was conducted for 6 hours at 70 °C and conversion analyzed by ^1H NMR spectroscopy (*ca.* 70%) and successful chain extension was confirmed by SEC as seen in Figure 5.9. The low molecular weight tail on the chain-extended polymer is indicative of un-chain-extended macroCTA, which has been attributed to the presence of dead polymer in the system.

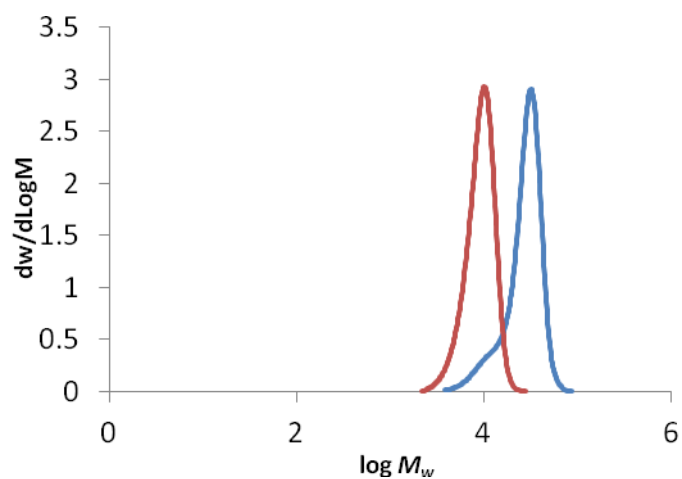
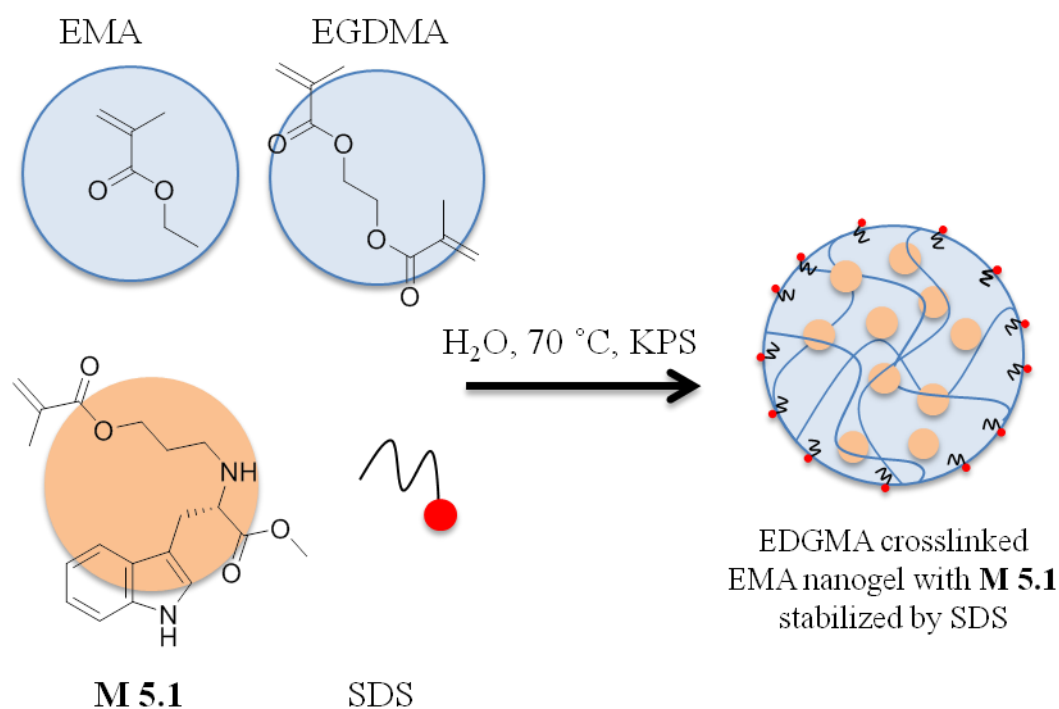


Figure 5.9. SEC trace of **P 5.1** (red line) and the chain extension (blue line) (DMF, PMMA calibration).

These polymerizations have successfully shown that **M 5.1** can be easily homopolymerized, co-polymerized and chain extended; which demonstrates its versatility.

5.3.2 Nanogel synthesis

Nanogels, similar to those in Chapter 4, incorporating the functional monomer **M 5.1** have been synthesized. The functional nanogels were successfully synthesized using emulsion polymerization with a hydrophobic co-monomer and a surfactant stabilizer. A range of nanogels incorporating **M 5.1** at 5 wt% degree of functionalization (DoF) were prepared with varying CLD (0.5 – 25%) and co-monomer (MMA, EMA or *n*-butyl methacrylate (*n*BuMA)). Ethylene glycol dimethacrylate (EGDMA) (0.5 wt%) was used as the cross-linker with sodium dodecylsulfate (SDS) as the surfactant stabilizer. A schematic representation of this synthesis is shown in Scheme 5.4.



Scheme 5.4. A schematic representation of the emulsion polymerization process used in the synthesis of **M 5.1** decorated cross-linked polymeric nanogels stabilized by SDS and cross-linked with EGDMA.

The polymerization has been analyzed by ^1H NMR spectroscopy and SEC to confirm that **M 5.1** has been incorporated into the polymer. In order to analyze the synthesized polymers by these techniques it was necessary to synthesize particles that were not cross-linked in order to solubilize the resulting polymer. This was accomplished by performing an identical nanogel synthesis but omitting the cross-linker. The conversions of the monomers throughout the synthesis were measured by taking samples and then disturbing the SDS stabilization through addition of THF. The solvents were then removed and conversion of **M 5.1** was calculated through the relative amounts of polymer to monomer present in the ^1H NMR spectrum. Conversions of EMA were calculated in a different manner as monomeric EMA was removed simultaneously with the solvent. As emulsion polymerizations typically go to high conversions the EMA conversion in a final ^1H NMR spectrum (24 hours) was taken as 100% conversion. The relative integrations of **M 5.1** polymer to EMA polymer in earlier samples as measured by ^1H NMR spectroscopy could then provide EMA conversion across the time-interval samples. The conversions of the two monomers can be seen in Figure 5.10. Both EMA and **M 5.1** conversions are increasing with time, although **M 5.1** conversion is slightly slower. However, as both monomer conversions increase simultaneously incorporating into the same nanogel co-polymer is likely which has been further demonstrated by SEC analysis.

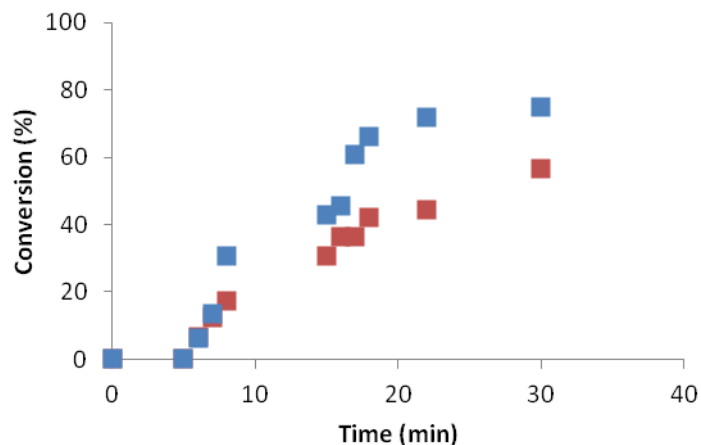


Figure 5.10. Conversions of the monomers in the nanogel with EMA (blue) (relative conversion) and **M 5.1** (red). The integration of monomer: polymer for **M 5.1** was used to determine conversion. As EMA monomer has been removed on removal of THF, the final ^1H NMR spectrum (24 h) was taken to be 100% conversion for EMA and the relative integration of EMA polymer to **M 5.1** polymer was used to determine the conversion of EMA.

The synthesized co-polymers of the nanogel were also characterized by SEC, again through analysis of the non cross-linked nanogel in order that the resulting polymer could be readily solubilized. The UV trace at 309 nm is often used to confirm the presence of the chain transfer end-group in RAFT synthesized polymers. However, in this case there was no RAFT end group present but the trace was found to be equally useful as L-tryptophan absorbs at 309 nm. Thus, UV was used to confirm the incorporation of L-tryptophan into the resultant polymer. The SEC traces can be seen in Figure 5.11. A single well-defined polymer peak was observed with the RI and UV traces almost overlaying, which demonstrates the successful incorporation of L-tryptophan into the co-polymer. Unfortunately, due to the high molecular weight of the co-polymer, accurate molecular weight and \mathcal{D} were not determined as the trace was outside the calibration limit of the instrument.

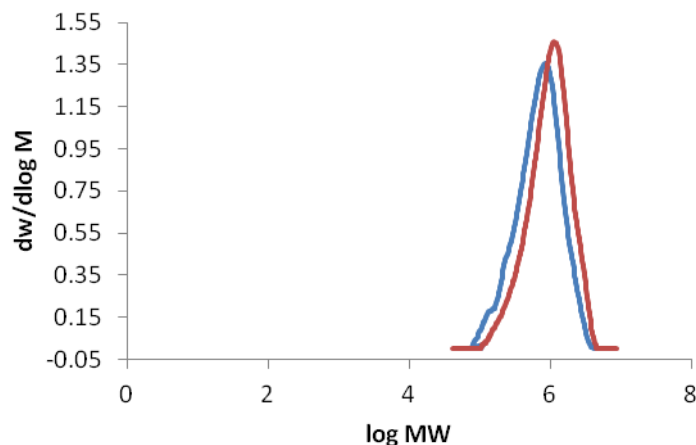


Figure 5.11. SEC trace showing the RI (blue line) and UV 309 nm trace (red line) (DMAC, PMMA calibration).

The use of a photodiode array (PDA) detector also confirmed the presence of L-tryptophan within the nanogel co-polymer as a result of the unique absorption profile of L-tryptophan. In Figure 5.12 the PDA traces on a THF SEC instrument are shown. The top trace shows a unique absorption for the L-tryptophan emission, which elutes after approximately 20 minutes. The bottom trace shows the resulting polymer, which elutes after 10 minutes and shows evidence of L-tryptophan absorption as part of the polymer peak. Whilst the absorptions are not identical due to the different chemical structures of the monomer and polymer, the strong L-tryptophan absorption at 280 nm suggests **M 5.1** is indeed successfully incorporated into the polymeric structure.

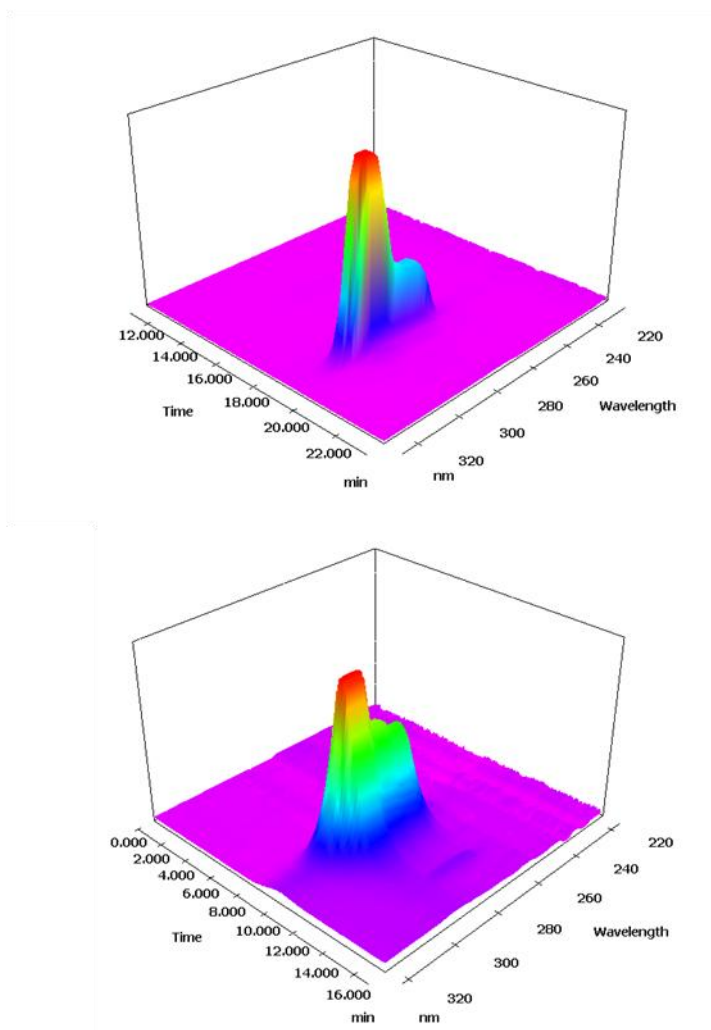


Figure 5.12. PDA analysis from THF SEC showing monomer (top) and nanogel co-polymer (bottom). Left hand axis shows elution time (min), right hand axis shows wavelength (nm) and the vertical axis shows intensity.

The synthesized nanogels have been analyzed by multi-angle dynamic light scattering (DLS) in order to ascertain their sizes and by transmission electron microscopy (TEM) to determine their shape. The details of the synthesized nanogels can be seen in Table 5.2, which indicates their CLD, co-monomer and size measured by multi-angle DLS and TEM.

Table 5.2. The details of the synthesized nanogels **N 5.1** – **N 5.8** including CLD, co-monomer and size.

Nanogel	CLD (%)	Co-monomer	D_H (nm) ^a	D_{av} (nm) ^b
N 5.1	0.5	EMA	26	25 ± 5
N 5.2	5	EMA	20	25 ± 5
N 5.3a^c	10	EMA	18	18 ± 4
N 5.3b^c	10	EMA	16	-
N 5.3c^c	10	EMA	16	-
N 5.4	25	EMA	18	19 ± 4
N 5.5	10	MMA	18	18 ± 4
N 5.6	10	<i>n</i> BuMA	28	25 ± 6
N 5.7	10	EMA	34	27 ± 7
N 5.8	10	EMA	48	34 ± 7

^aMeasured by multi-angle DLS

^bDetermined by TEM

^cThe synthesis of **N 5.3** was performed in triplicate times giving the products a, b and c

The in-solution size measurement of these nanogels was obtained by using multi-angle DLS. Attempts to use a zetasizer DLS were unsuccessful as the programme was unable to analyze the results, possibly due to the fluorescent nature of the nanogels. The correlation function at different angles was taken and by plotting the decay rate (Γ) at each angle against the scattering vector squared (q^2) a straight line graph with gradient equal to the diffusion coefficient (D_T) of the particle can be

obtained, as shown in Figure 5.13. The analysis shown is represented by **N 5.3c** (5 wt% DoF, 10 wt% CLD) and a hydrodynamic diameter (D_H) of 16 nm was found.

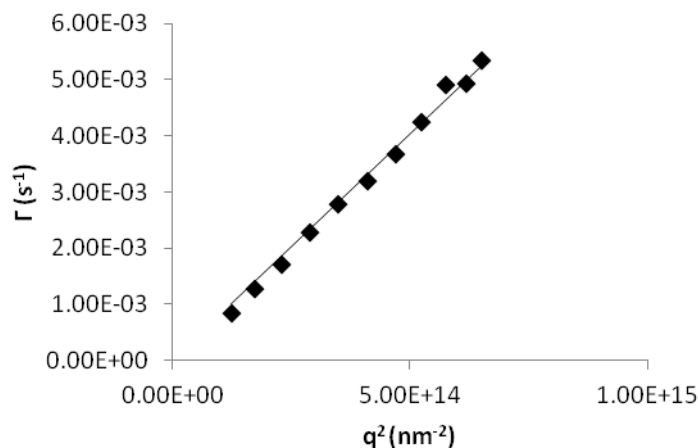


Figure 5.13. A plot of decay time against scattering vector squared for **N 5.3c**. The resulting gradient is the diffusion coefficient of the particles.

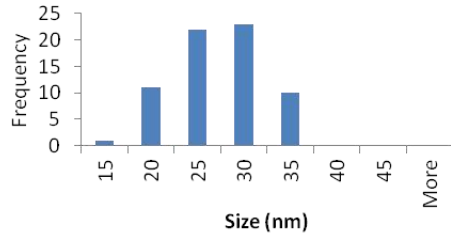
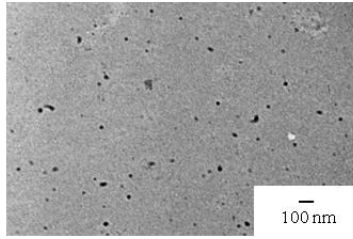
This can then be related to the size of the population or D_H through the Stokes-Einstein equation which can be seen in Equation 5.3.

$$D_T = \frac{k_B T}{6\pi \eta r} \quad (5.3)$$

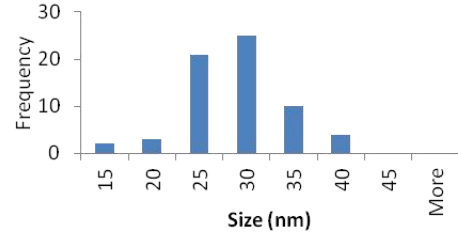
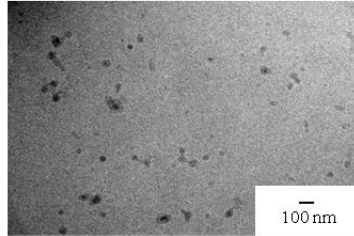
D_T = diffusion coefficient (s $^{-1}$ m 2), k_B = Boltzman constant (m 2 kg s $^{-2}$ K $^{-1}$), T = absolute temperature (K), η = viscosity (kg m $^{-1}$ s $^{-2}$), r = hydrodynamic radius (m).

A representative TEM image of each of the nanogels can be seen in Figure 5.14. The TEM images indicate that the majority of the particles are spherical in nature, although some do deviate from the ideal. However, as TEM requires the particles to be dried to a solid support it is not unusual for the particles to collapse giving them non-spherical appearance.

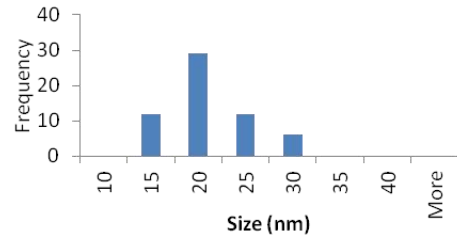
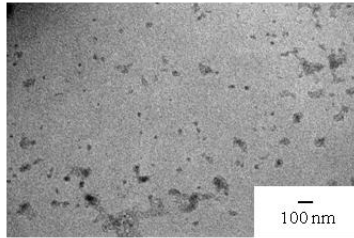
N 5.1



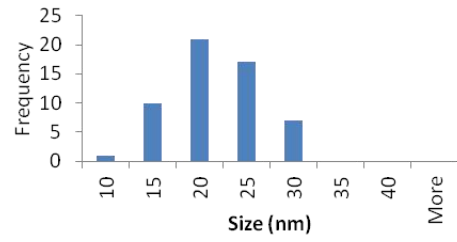
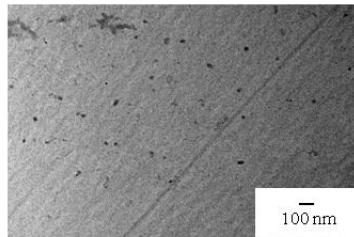
N 5.2



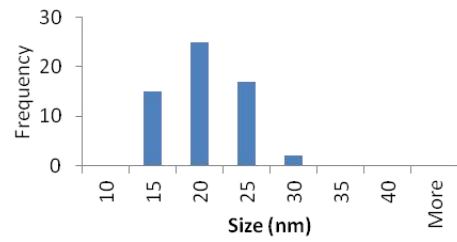
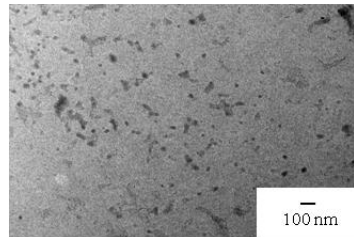
N 5.3



N 5.4



N 5.5



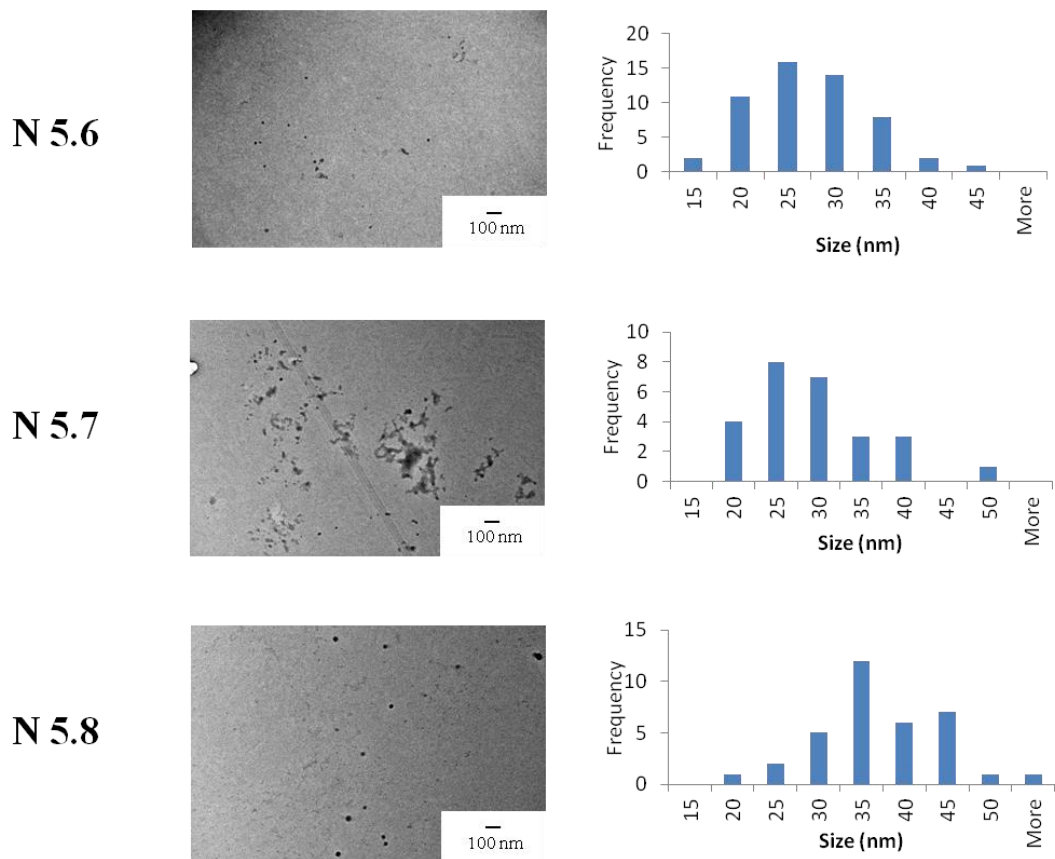


Figure 5.14. Representative TEM images of the synthesized nanogels, which demonstrates the spherical nature of the synthesized particles - scale bar is 100 nm. TEM samples were prepared by drop deposition of a 0.1 mg mL⁻¹ polymer solution in water onto copper/carbon grids that had been pre-treated with oxygen plasma and analyzed by using a JEOL TEM-2100 microscope operating at 200 kV.

5.3.3 Fluorescence investigations

5.3.3.1 L-Tryptophan's fluorescence as a monomer, polymer and nanogel

A commonly exploited characteristic of L-tryptophan is its fluorescent properties. Indeed, the fluorescent properties of L-tryptophan are dramatically influenced by its surrounding environment, which has been used to study protein folding. In this work the fluorescent property of L-tryptophan has been studied across three main areas, in its monomeric form **M 5.1** and when incorporated into a polymer and a nanogel. It is well known that as L-tryptophan is placed within a more hydrophobic domain its fluorescence intensity increases and the emission shifts to a shorter wavelengths.^{2, 3}

The fluorescence emission spectrum ($\lambda_{\text{ex}} = 380$ nm, slit width = 10 nm) of **M 5.1** and **P 5.1** at 1 mg mL⁻¹ in THF can be seen in Figure 5.15. The emission intensity from **P 5.1** is far greater than **M 5.1** and the peak maxima has shifted from $\lambda_{\text{em}} = 450$ nm in **P 5.1** to $\lambda_{\text{em}} = 462$ nm in **M 5.1**; this suggests the L-tryptophan in the polymer is located in a more hydrophobic environment. This change in environment has been attributed to the close proximity of the L-tryptophan units in **P 5.1** as they are bound to a polymer chain, which will be collapsed into a random coil, creating a more hydrophobic environment.

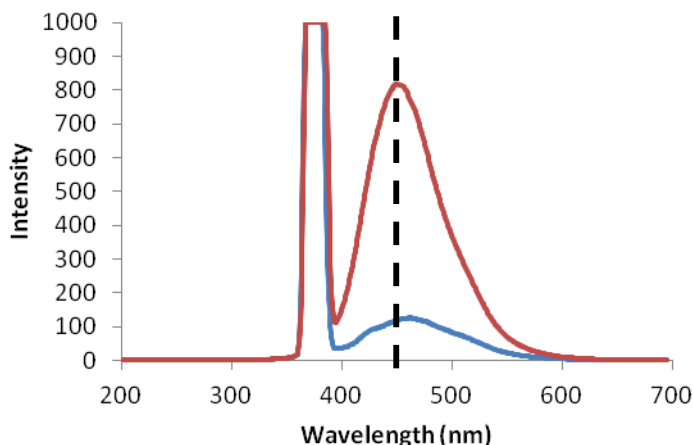


Figure 5.15. The fluorescence spectra ($\lambda_{\text{ex}} = 380 \text{ nm}$, slit width = 10 nm) of **M 5.1** (blue line) and **P 5.1** (red line) in THF at 1 mg mL^{-1} , Rayleigh scattering $\lambda = 380 \text{ nm}$.

The nanogel (**N 5.1**) (5 wt% DoF, 0.5 wt% CLD) was subsequently analyzed using the same fluorescence settings as previously used for **M 5.1** (slit width = 10 nm), although the analysis had to take place in H_2O opposed to THF which was used for the **M 5.1** and **P 5.1** analyses. However, as significant dilution of the nanogel was required to eliminate the turbidity and make the sample suitable for analysis, the concentration of L-tryptophan in solution was $0.0006 \text{ mg mL}^{-1}$ as opposed to 1 mg mL^{-1} previously used for the **M 5.1** and **P 5.1** analyses. The wavelength of maximum absorption had also shifted to a shorter wavelength ($\lambda_{\text{ex}} = 280 \text{ nm}$) which was then used for the excitation. Surprisingly, at this low concentration, the L-tryptophan emission was too great to give a readable result from the fluorescence detector ($>1000 \text{ A.U.}$), which indicates the nanogels exhibit a very high fluorescence intensity (Figure 5.16). By changing the slit width from 10 nm to 2.5 nm on the fluorescence spectrometer, a readable result (*ca.* 400 A. U.) was obtained but unfortunately this increased the noise in the spectrum. This result indicates that L-tryptophan is in a particularly hydrophobic environment which further suggests it is contained within the hydrophobic nanogel core. The maximum emission for

L-tryptophan when located within a nanogel has shifted to a shorter wavelength than compared to when it is present in a polymer ($\lambda_{em} = 420$ nm to $\lambda_{em} = 350$ nm). This change in wavelength is much more significant than that seen on folding and unfolding of proteins which are typically in the order of 10 to 20 nm. This large shift indicates a dramatic change in environment from monomer or polymer in THF to a hydrophobic nanogel in H₂O.³⁹

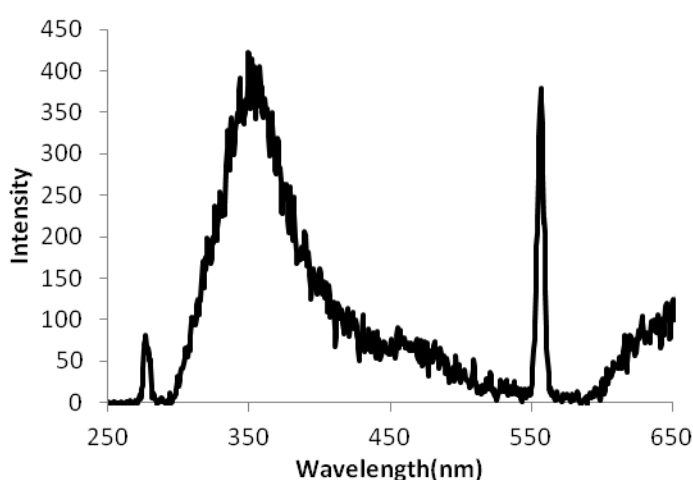


Figure 5.16. Fluorescence spectrum of **N 5.1** ($\lambda_{ex} = 280$ nm, slit width = 2.5 nm), which equates to 0.0006 mg mL⁻¹ **M 5.1** in H₂O, Rayleigh scattering $\lambda = 280$ nm, Raman Scattering $\lambda = 560$ nm in H₂O.

5.3.3.2 L-Tryptophan Degradation

It has been reported that exposure of L-tryptophan to UV-B irradiation at $\lambda_{ex} = 300$ nm leads to a loss of fluorescence, with the presence of oxygen being important to this process.⁴⁰⁻⁴² The loss of L-tryptophan emission coupled with an increase in emission at $\lambda_{em} = 500$ nm could be the formation of the oxidation product *N*-formylkynurenine (NFK); although there are several other oxidation products of L-tryptophan which have been documented by Hoffman *et al.* in 2011, which involve

attack on the indole ring from oxygen.⁴³ These oxidation products can be seen in Figure 5.17.

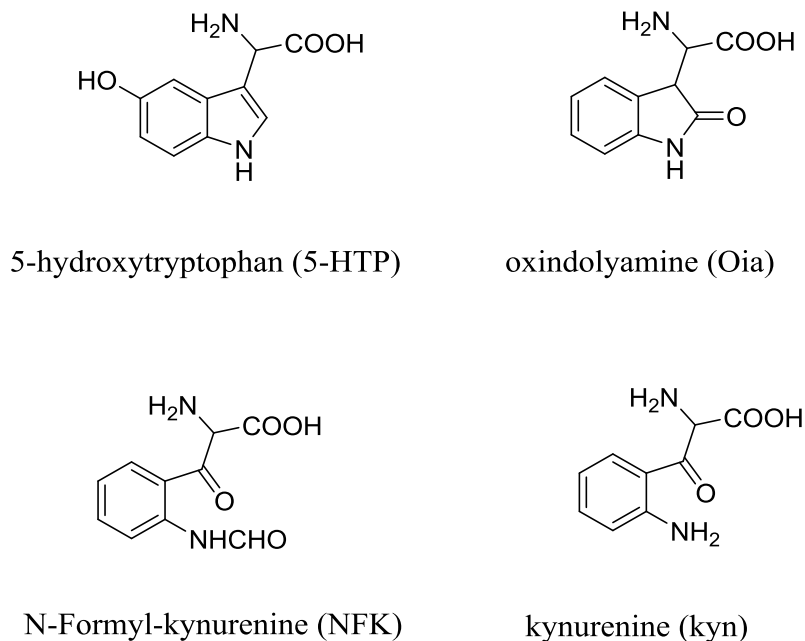


Figure 5.17. Possible photoproducts of L-tryptophan.

A L-tryptophan nanogel (**N 5.3**) (5 wt% DoF, 10 wt% CLD) was exposed to various excitation wavelengths ($\lambda_{\text{ex}} = 225 \text{ nm}$, 260 nm, 270 nm and 280 nm) every 5 minutes and the intensity of the possible photo by-products was recorded at $\lambda_{\text{em}} = 500 \text{ nm}$. Under the conditions (slit width = 10 nm) which were required in order to examine all wavelengths, it was not possible to monitor the loss in fluorescence from the L-tryptophan as the emission intensity was above the detection limit of the instrument (>1000 A.U.). The results can be seen in Figure 5.18. It is clear that at the shorter wavelength of $\lambda_{\text{ex}} = 225 \text{ nm}$ there is hardly any by-product produced whereas upon excitation at $\lambda_{\text{ex}} = 270 \text{ nm}$ more by-product which has fluorescence emission at $\lambda_{\text{em}} = 500 \text{ nm}$ was present; however, it is not certain that by-products that do not fluoresce are not being produced at this shorter excitation wavelength.

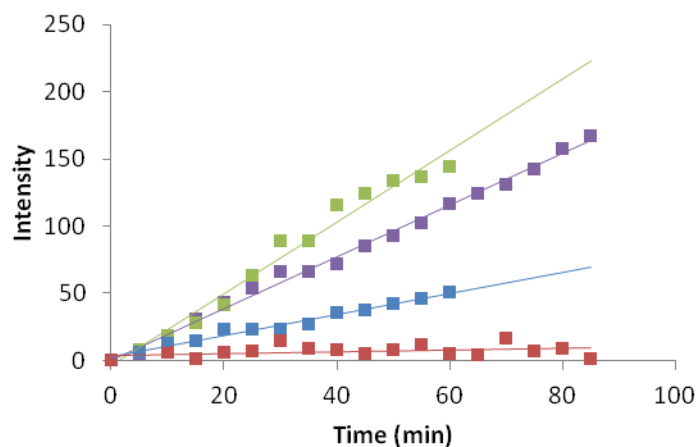
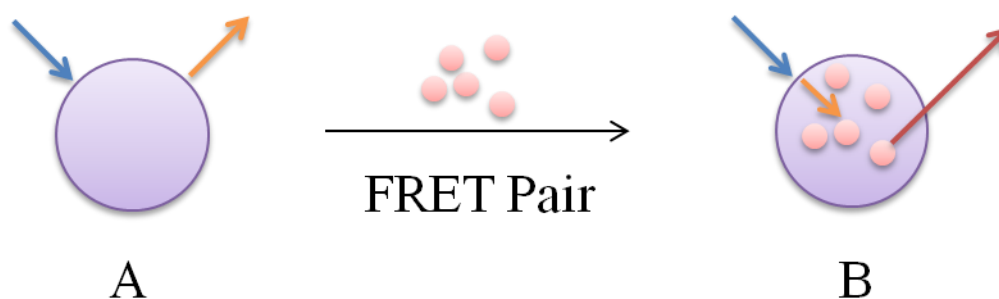


Figure 5.18. The increase of intensity at $\lambda_{em} = 500$ nm of **N 5.3** exciting at either $\lambda_{ex} = 280$ nm (red line), 270 nm (blue line), 260 nm (green line) and 225 nm (purple line) every 5 min (slit width = 2.5 nm). The intensities have been normalized to start at zero to provide a clearer visual comparison.

5.3.4 FRET experiments

With such unique fluorescent properties this L-tryptophan-containing nanogel was further investigated using Forster Resonance Energy Transfer (FRET). A schematic representation can be seen in Scheme 5.5 with the donor molecule represented by **A**, the L-tryptophan-containing nanogel. The acceptor molecule, the FRET pair, can be loaded into the nanogel which gives us **B**, where the FRET pair is close enough (~ 10 nm) to the L-tryptophan for FRET to occur. This process was monitored by the decrease in fluorescence intensity of L-tryptophan and the increase in emission of the acceptor molecule.



Scheme 5.5. A Schematic to represent the FRET interaction between the L-tryptophan-containing nanogel, **A**, and a FRET pair that is loaded into the nanogel.

Dansyl amide (DNSA), a known FRET pair of L-tryptophan, was selected as the FRET acceptor molecule. The fluorescence spectrum of DNSA was recorded in an unfunctionalized EMA nanogel prepared in the same manner as **N 5.3** but without the L-tryptophan monomer in order to study its fluorescence behaviour under conditions close to those of the FRET experiment. The excitation and emission profiles of DNSA under these conditions can be seen in Figure 5.19. The DNSA excitation spectrum in the EMA nanogel overlays with the tryptophan emission spectrum from **N 5.3** (Figure 5.16); with the emission of DNSA at $\lambda_{\text{em}} = 470$ nm and

a maximum absorption at $\lambda_{\text{abs}} = 350$ nm. The absorption at the short wavelengths (< 230 nm) are contributed to by the water in the sample.

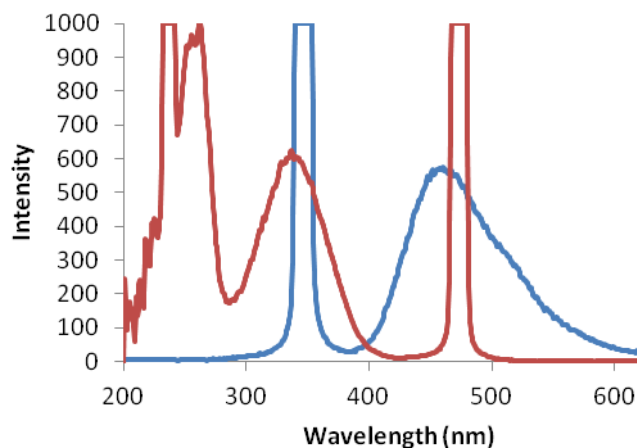
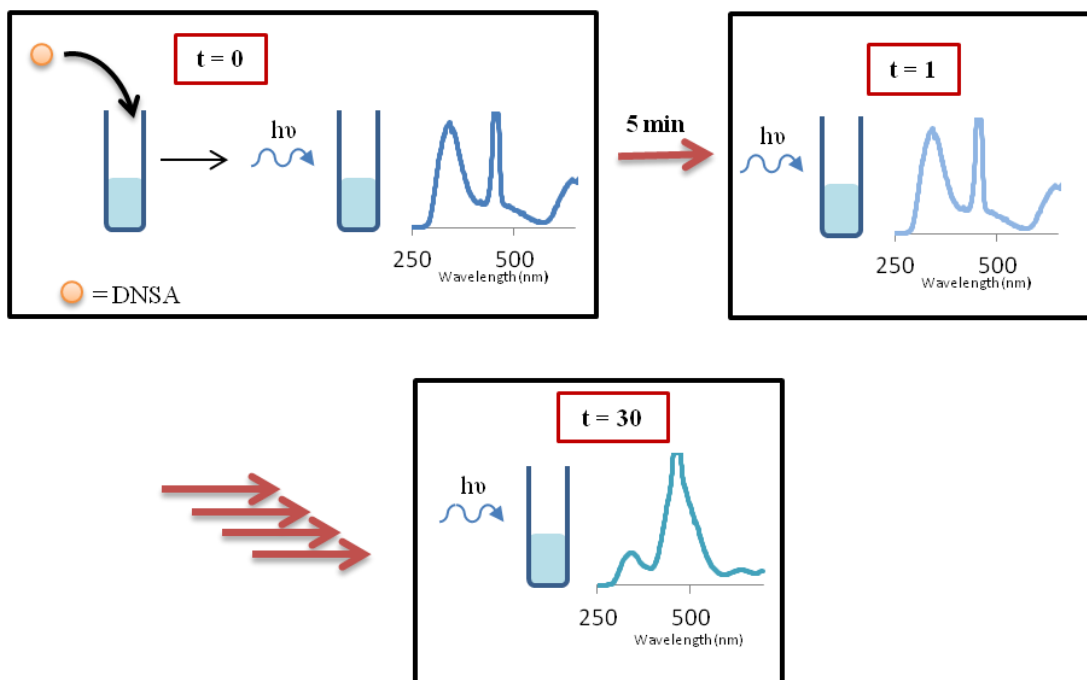


Figure 5.19. The excitation and emission fluorescence spectra of DNSA encapsulated into an unfunctionalized EMA nanogel. The excitation spectrum (red line) is based on emission at $\lambda_{\text{em}} = 470$ nm (Rayleigh scattering $\lambda = 470$ nm, Raman scattering $\lambda = 235$ nm) and the emission spectrum (purple line) was excited at $\lambda_{\text{ex}} = 350$ nm (Rayleigh scattering $\lambda = 470$ nm), slit width = 5 nm.

The migration of DNSA was monitored through the emission spectra of the L-tryptophan nanogel solution ($\lambda_{\text{ex}} = 225$ nm) recorded every 5 minutes after the DNSA was added (5 μL of a 2 mg mL^{-1} solution in THF). The solution was excited at $\lambda_{\text{ex}} = 225$ nm, which is not the maximum absorption of the L-tryptophan, to minimize the formation of fluorescent degradation products. On excitation at $\lambda_{\text{ex}} = 225$ nm the DNSA-containing SDS micelles gave a slight but insignificant (< 20 A.U.) intensity reading. A schematic that demonstrates this experimental procedure can be seen in Scheme 5.6.



Scheme 5.6. A schematic representation of the FRET experimental procedure. At $t = 0$ the DNSA is added to the fluorometer cell that already contains the nanogel solution which is immediately irradiated with light and the spectrum recorded. The fluorescence cell is left in position and irradiated at 5 min intervals and the spectra recorded. Over time the spectra changed giving a lower emission of tryptophan and an increased emission for DNSA.

Over time a decrease in L-tryptophan emission was observed, which was accompanied by an increase in DNSA emission. This emission is unfortunately at a similar wavelength to the fluorescent photo by-product, however, the chosen conditions of the experiment should have minimized this production. Additionally the increase of emission at this wavelength in the presence of DNSA is far greater than in its absence, further confirming it to be DNSA emission. In Figure 5.20 fluorescent spectra can be seen, which demonstrates the change in fluorescent emission during the experiment. The L-tryptophan emission at $\lambda_{em} = 350$ nm has decreased and an emission at a higher wavelength was observed; typical of a FRET experiment. Unfortunately, the Raman scattering peak ($\lambda = 450$ nm) coincides with the DNSA emission peak ($\lambda_{em} = 470$ nm).

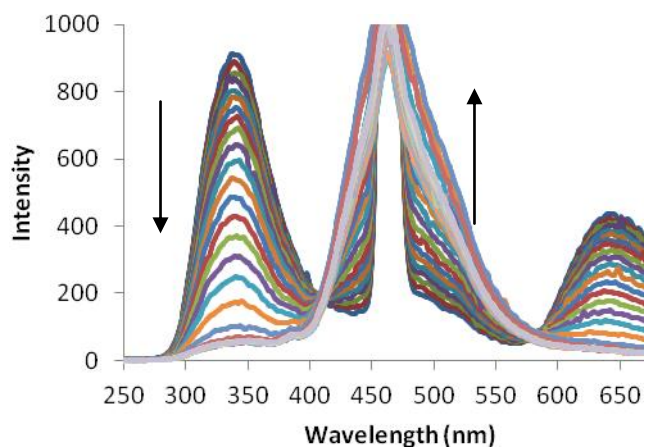


Figure 5.20. Fluorescence spectrum showing **N 5.3** after purging with N_2 with $\lambda_{ex} = 225$ nm recorded every 5 min after addition of DNSA.

By recording the intensity of the L-tryptophan emission every 5 minutes and plotting it against time, a decay plot of the L-tryptophan was produced which showed three distinct periods; a stable period before DNSA had entered the nanogel, a rapid decrease as DNSA quenches the L-tryptophan as it comes into close proximity and lastly a stable period where the emission of L-tryptophan was small. By taking the lines of best fit for these three phases it was possible to calculate the times at which each began. A representation of this graph can be seen in Figure 5.21.

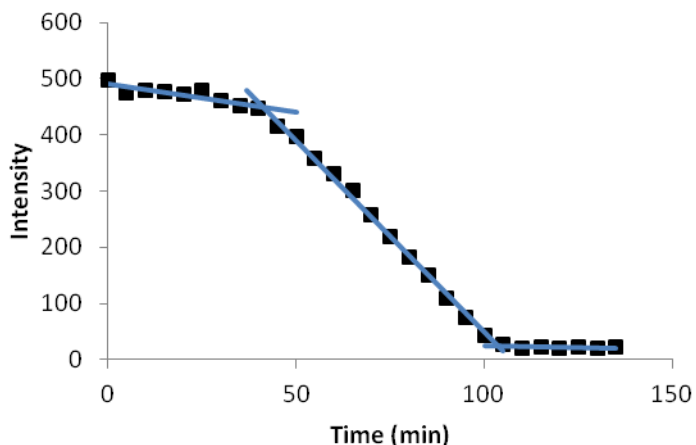


Figure 5.21. A graph showing the decrease in fluorescence intensity of L-tryptophan with time, on addition of DNSA exciting at $\lambda_{\text{ex}} = 225$ nm every 5 min, and the trendlines that have been used to calculate specific times within the graph.

The L-tryptophan emission was used to monitor the occurrence of FRET as opposed to the DNSA emission for a few reasons. The DNSA emission coincides with the Raman scattering peak which is not possible to de-convolute and thus this emission peak was not reliable. Moreover, the DNSA emission may max out the detector and this cannot be adjusted for at the start of the experiment, which is possible for L-tryptophan. Additionally, DNSA will start to quench itself in high concentrations (Figure 5.22 and Figure 5.23); the DNSA emission intensity has been recorded at both $\lambda_{\text{ex}} = 350$ nm (Figure 5.22) and $\lambda_{\text{ex}} = 380$ nm (Figure 5.23) in varying concentrations. Two wavelengths were investigated in order to replicate the λ_{ex} during the FRET experiments ($\lambda_{\text{ex}} = 350$ nm) and also at the maximum absorption found under these conditions (dissolved in THF) ($\lambda_{\text{ex}} = 380$ nm). Therefore at a certain point during the experiment as DNSA enters the nanogel the DNSA emission could start to decline. These factors appear to make the emission of the acceptor molecule less reliable than that of the donor, L-tryptophan, but the qualitative presence of the emission is significant.

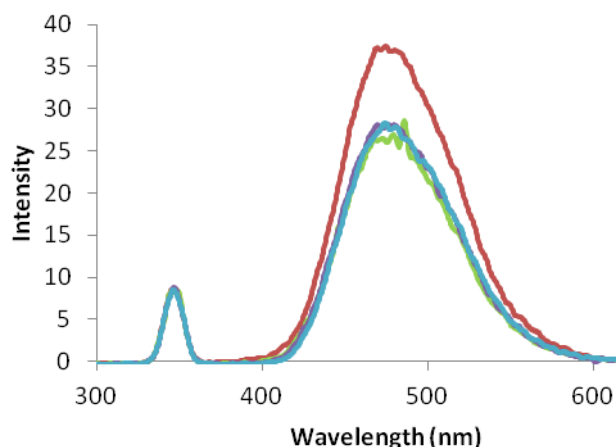


Figure 5.22. The fluorescence intensity of DNSA excited at $\lambda_{\text{ex}} = 350 \text{ nm}$ for 1 mg mL^{-1} (red line), 5 mg mL^{-1} (green line), 10 mg mL^{-1} (purple line), 20 mg mL^{-1} (blue line), in THF (Rayleigh scattering $\lambda = 350 \text{ nm}$).

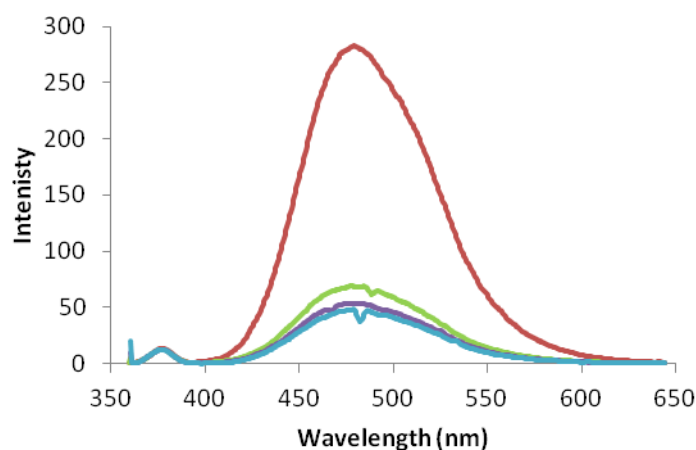


Figure 5.23. The fluorescence intensity of DNSA excited at $\lambda_{\text{ex}} = 380 \text{ nm}$ for 1 mg mL^{-1} (red line), 5 mg mL^{-1} (green line), 10 mg mL^{-1} (purple line), 20 mg mL^{-1} (blue line), in THF (Rayleigh scattering $\lambda = 380 \text{ nm}$).

A typical DNSA emission profile against time can be seen in Figure 5.24. This plot is after addition of DNSA to nanogel **N 5.1** (5 wt% DoF, 0.5 wt% CLD). Overtime the emission intensity of DNSA increases as it diffuses into the nanogel and comes into closer proximity with the L-tryptophan. The profile has a peculiar shape with a sharp increase and decrease in intensity around 100 minutes. This increase and

decrease has been attributed to changing FRET efficiencies caused between the donor and acceptor which can be affected by the acceptors concentration.⁴⁴

Additionally, the self-quenching of DNSA may also have a contributing effect.

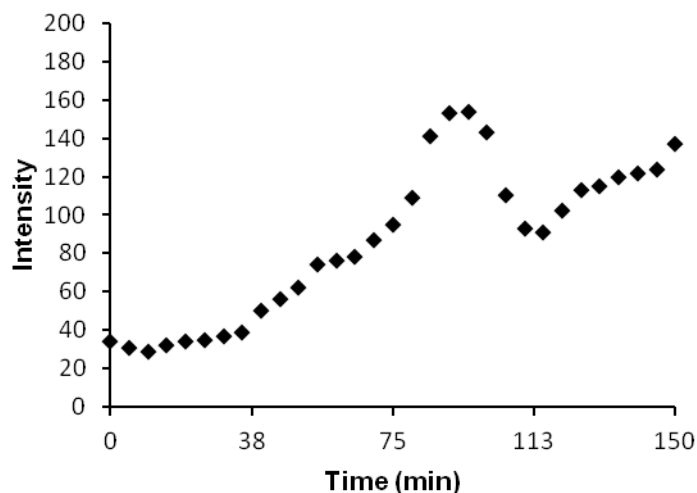


Figure 5.24. A typical DNSA fluorescence emission intensity against time plot. Addition of 5 μL of 2 mg mL^{-1} THF solution to 200 μL of **N 5.1** irradiated at $\lambda_{\text{ex}} = 225 \text{ nm}$ every 5 min.

5.3.4.1 L-Tryptophan nanogel

Initially the emission intensity of L-tryptophan was examined on addition of DNSA across a series of cross-linked nanogels with different CLD, co-monomer and size. As FRET is distance dependent it was hypothesized that the different characteristics of these nanogels would alter the diffusion rate of DNSA into the nanogel core and thus to the L-tryptophan moieties. The data collected for these experiments can be seen in Table 5.3. Nanogels **N 5.1** to **N 5.4** have variable CLD which was achieved by varying the amount of cross-linker, EGDMA, in the reaction from 0.5 wt% to 25 wt%. Nanogels **N 5.5**, **N 5.3** and **N 5.6** have various co-monomers with the same CLD of 10 wt%. Finally the nanogels **N 5.3**, **N 5.7** and **N 5.8** have the same co-monomer of EMA and the same CLD of 10 wt% but were synthesized in the

presence of a different wt% of SDS stabilizer (20 wt%, 13 wt% and 6 wt% respectively) resulting in different particle sizes.⁴⁵ The 1st inflection point (IP), the gradient of the decline and the 2nd IP were all examined to highlight any trends within the data. For these fluorescence measurements the samples were first degassed by bubbling nitrogen into the system through a septum for 5 minutes. 200 μL was removed and placed in the fluorescence cell and 5 μL of a 2 mg mL^{-1} DNSA solution in THF was added giving a molar ratio of 1 L-tryptophan unit to 10 DNSA units. The spectra were then recorded at 5 minute intervals starting at $t = 0$ minutes with slit width at 10 nm.

Table 5.3. The 1st and 2nd IP and gradient of decrease of L-tryptophan emission for the addition of DNSA to the nanogels N 5.1 – N 5.8.

Nanogel	CLD (%)	Co-monomer	Size (nm)	1 st IP (min) ^a	Gradient ^a	2 nd IP (min) ^a
N 5.1	0.5	EMA	26	55	-13.8	127
N 5.2	5	EMA	20	34	-5.6	164
N 5.3	10	EMA	18	48	-13.4	117
N 5.4	25	EMA	18	41	-6.8	179
N 5.5	10	MMA	18	33	-3.0	117
N 5.6	10	<i>n</i> BuMA	28	19	-1.3	764
N 5.7	10	EMA	34	47	-4.94	232
N 5.8	10	EMA	48	55	-4.46	266

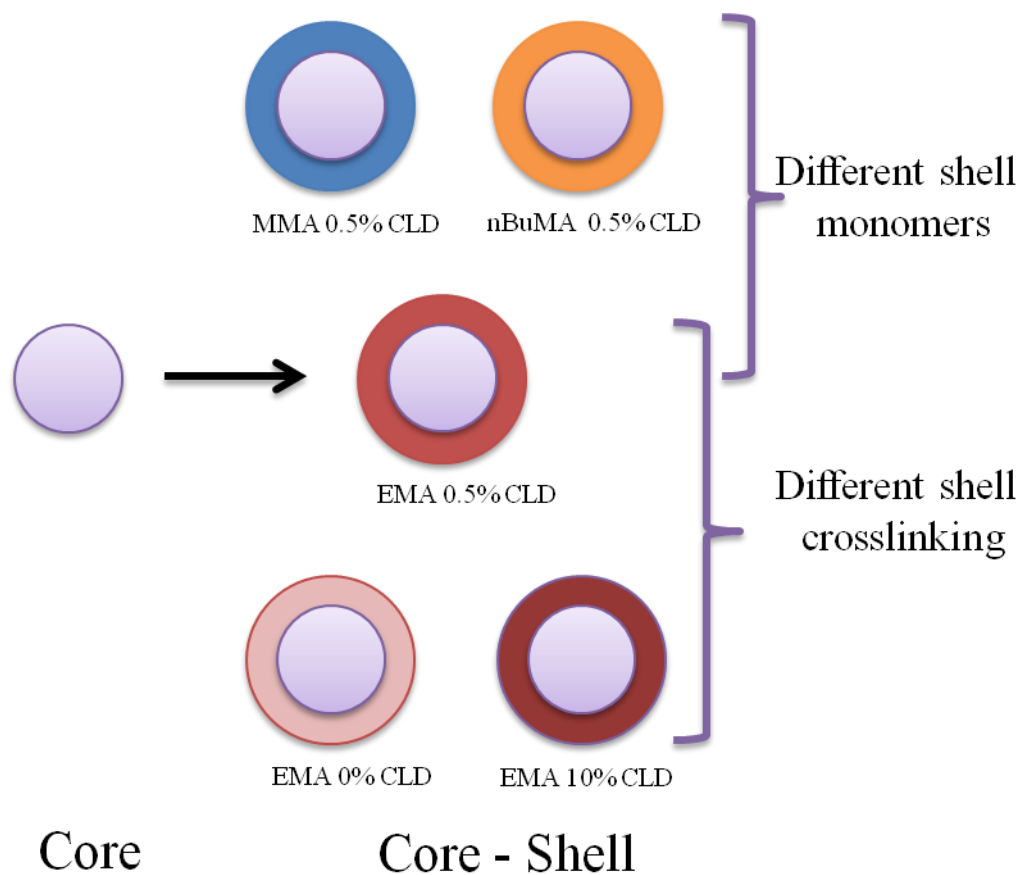
^aMeasured from L-tryptophan emission loss *via* fluorescence spectroscopy

Unfortunately, no obvious trends were observed within the synthesized samples. It was initially anticipated that changes such as CLD and core hydrophobicity would affect the FRET process. For instance, an increase of the CLD would be expected to slow down diffusion of DNSA into the core resulting in an increase in the time required for FRET to initially occur or for full quenching to take place. It was therefore concluded that the current nanogel design did not differentiate the nanogels enough for us to observe a clear difference in fluorescence intensity due to FRET. The L-tryptophan moieties are likely to be found in both the central areas and close

to the particle surface. Consequently it is possible that only diffusion through the SDS shell is required for DNSA to come into contact with the L-tryptophan, and this is the case for all nanogels. A new design was therefore considered which placed the L-tryptophan into a more central core, surrounded by an additional polymer shell in order to examine any differences this may have on the FRET process.

5.3.4.2 L-Tryptophan core-shell nanogels

Core-shell structures were targeted in order to place the L-tryptophan moieties in the central hydrophobic domain.⁴⁶ The already synthesized **N 5.3a-c** were used as seeds in a second, seeded emulsion polymerization of a polymeric shell to yield core-shell type structures. The CLD and monomer of these shells were varied in order to further probe their effects on DNSA diffusion, measured *via* FRET. A schematic of this synthesis can be seen in Scheme 5.7. As the L-tryptophan is placed in a more inaccessible area it was hypothesized that the difference in the polymeric shell would have an effect on the diffusion time of DNSA.



Scheme 5.7. A schematic representation of the structures synthesized through the addition of polymeric shells to a L-tryptophan containing core.

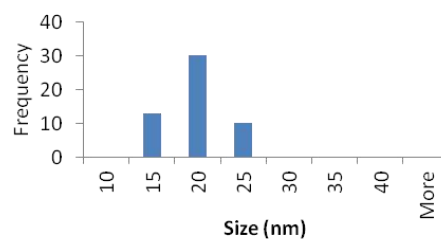
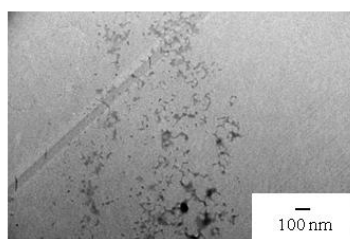
In order to produce this series of core-shell particles, three separate core batches were synthesized to provide the seeds required for shell growth (N 5.3a-c). The core of each of the resulting nanogels is outlined in Table 5.4, along with the shell monomer, shell CLD and the final size of the core-shell nanogels SN 5.1 – SN 5.5. TEM images of these core-shell nanogels can be seen in Figure 5.25.

Table 5.4. Details of synthesized nanogels SN 5.1 – SN 5.5 including parent core, shell monomer and shell CLD.

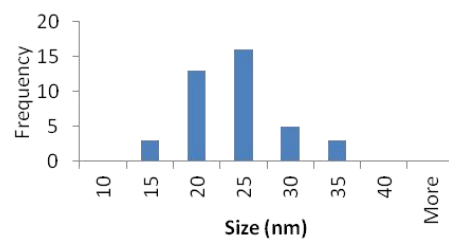
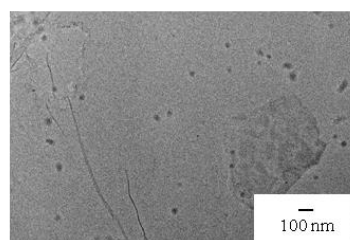
Nanogel	Core Nanogel / Size (nm)	Shell monomer	Shell CLD	D_H (nm) ^a
SN 5.1	N 5.3a / 18	EMA	0	24
SN 5.2	N 5.3b / 16	EMA	0.5	26
SN 5.3	N 5.3b / 16	EMA	10	23
SN 5.4	N 5.3c / 21	MMA	0.5	30
SN 5.5	N 5.3c / 21	<i>n</i> BuMA	0.5	28

^aMeasured by multi-angle DLS

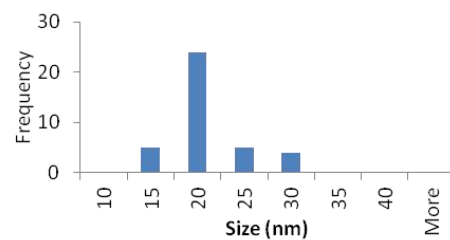
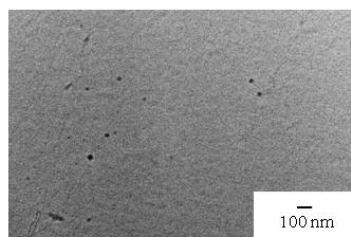
SN 5.1



SN 5.2



SN 5.3



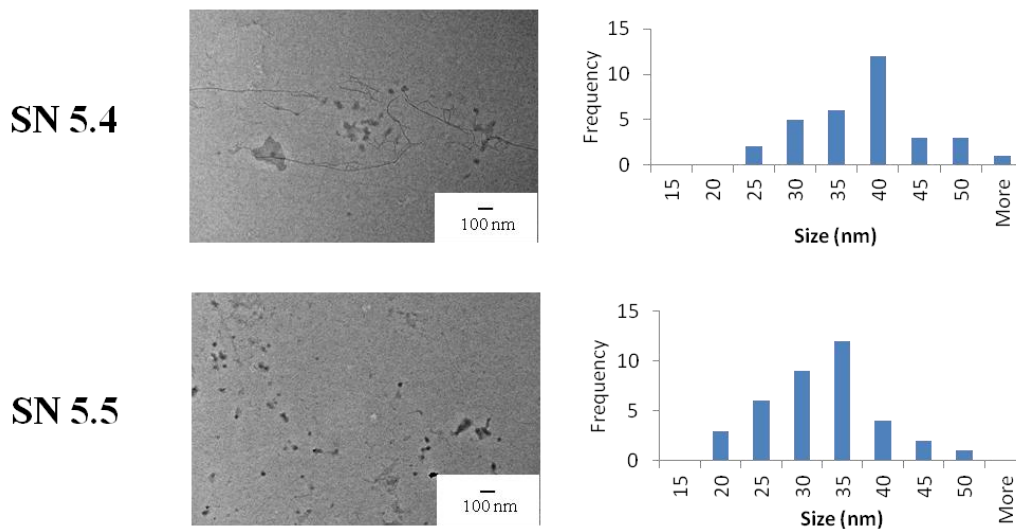


Figure 5.25. Representative TEM images of SN 5.1 – SN 5.5 which demonstrates the spherical nature of the synthesized particles - scale bar is 100 nm. TEM samples were prepared by drop deposition of a 0.1 mg mL^{-1} polymer solution in water onto copper/carbon grids that had been pre-treated with oxygen plasma and analyzed by using a JEOL TEM-2100 microscope operating at 200 kV.

To conduct these fluorescence measurements, the samples were first degassed by bubbling nitrogen into the system through a septum for 5 minutes. $200 \mu\text{L}$ was removed and placed in the fluorescence cell and $1 \mu\text{L}$ of a 2 mg mL^{-1} DNSA solution in THF was added giving a molar ratio of 1 L-tryptophan to 2 DNSA units. The reduction in the amount of DNSA solution added, compared to the previous system, was required to prevent maximum intensity of the DNSA being reached too soon into the experiment. The spectra were then recorded at 5 minute intervals starting at $t = 0$ minutes with the slit width set at 10 nm. Runs were conducted 3 times and then the graphs analyzed before being averaged and the standard deviation calculated. It has been hypothesized that the time of the 1st IP is the point at which the FRET pairs are close enough together for FRET to occur. These time points have been compared across the series of core-shell nanogels.

Table 5.5 shows the fluorescence results for **SN 5.1**, **SN 5.2**, **SN 5.3**, nanogels which share the same shell (EMA) but have different CLDs. The 1st IP increased with increasing shell CLD which was an anticipated result. Increasing the CLD of the shell increases the level of steric hindrance, which will have an effect on the diffusion rate of DNSA; consequently, a shell with 0% CLD should offer the least resistance. At 0% CLD the 1st IP was observed at 33 minutes and changing the CLD to 10 wt% increased the 1st IP time to 54 minutes. However, the difference in the time to reach the 1st IP from 0.5 wt% to 10 wt% CLD is not as significant as expected. Therefore it has been hypothesized that the initial crosslinking causes changes in the structure of the shell, which is of greater significance than further cross-linking.

Table 5.5. The 1st IP results of **SN 5.1-SN 5.3** with addition of DNSA. These nanogels have the same shell, EMA, but have increasing levels of CLD.

Nanogel	Shell CLD	1st IP (min)^a
SN 5.1	0	33 ± 1
SN 5.2	0.5	52 ± 3
SN 5.3	10	54 ± 2

^aDetermined by the decrease in fluorescence intensity by L-tryptophan after addition of DNSA

Table 5.6 shows the results of varying the shell monomer. By changing the shell forming monomer it has been possible to alter the hydrophobicity, steric bulk and T_g of the polymeric shell. Examining the series of MMA to EMA to *n*BuMA the hydrophobicity and steric bulk are increased but the T_g decreases. It is anticipated

that the increase in hydrophobicity and also the decrease in T_g would result in a reduction in the time required to observe the first quench. Nevertheless, the increase in steric bulk may also slow down diffusion of DNSA into the core.

Table 5.6. The 1st IP results of SN 5.4, SN 5.2 and SN 5.5 with addition of DNSA. These nanogels have the same CLD of 0.5% but have a different shell monomer of either MMA, EMA or *n*BuMA.

Nanogel	Shell monomer	T_g (°C)	1 st IP (min) ^a
SN 5.4	MMA	115	59 ± 1
SN 5.2	EMA	65	52 ± 3
SN 5.5	<i>n</i> BuMA	20	45 ± 1

^aDetermined by the decrease in fluorescence intensity by L-tryptophan after addition of DNSA

As the shell monomer becomes more hydrophobic a decrease in the time required to reach the 1st IP was observed, i.e. the longest time was required for DNSA to diffuse through the MMA shell. Therefore, by increasing the hydrophobicity and lowering the T_g of the shell, an increase in the speed of diffusion into the central L-tryptophan rich region was observed. As just mentioned, MMA, the least hydrophobic shell which also has the highest T_g requires the longest time before FRET is observed, 59 minutes. This is decreased to 52 minutes for EMA and 45 minutes for *n*BuMA, which is the most hydrophobic and has a low T_g of 20 °C.

Therefore, variations to the shell such as changing the CLD and hydrophobicity/ T_g of the shell have successfully resulted in a change in DNSA diffusion. By creating a more rigid structure *via* introduction of cross-linking, diffusion of the small molecule was observed. Furthermore, by increasing the hydrophobicity and in this case simultaneously lowering the T_g of the shell, an increase in diffusion of DNSA was observed. The use of L-tryptophan's fluorescent properties has been crucial in this study to examine diffusion of small molecules into polymer nanoparticles with different characteristics. With the increasing use of advanced polymeric systems for a range of applications, including sensing and drug delivery, there is a growing need to understand how polymer structure can affect small molecule diffusion. The incorporation of this new monomer has provided nanogels with in built fluorescence that could act as a model system for future investigations into small molecule diffusion.

5.4 Conclusions

A new monomer based on the amino acid L-tryptophan has been successfully synthesized and was found to be readily polymerizable and therefore has been homopolymerized, co-polymerized and used to form diblock co-polymers. The new monomer has also been incorporated into cross-linked polymeric nanogels which have subsequently been used as seeds in a second polymerization to yield core-shell structures placing the L-tryptophan in a central location. The fluorescent properties of L-tryptophan in the monomer, polymer and nanogel structures have been examined, highlighting the effects that the surrounding environment has on the fluorescence of L-tryptophan, where a more hydrophobic environment returned greater emission intensity. This fluorescent property has been exploited in FRET experiments with L-tryptophan's FRET pair dansyl amide. By monitoring the change in L-tryptophan emission intensity, the effects of CLD and shell monomer in the core-shell nanogels were examined.

5.5 Experimental

5.5.1 Instrumentation

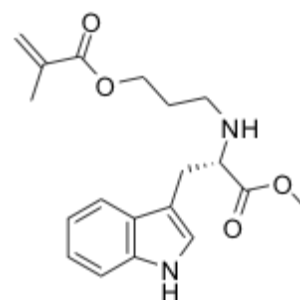
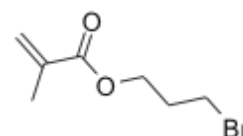
^1H NMR spectra were recorded on a 250 or 300 MHz Bruker DPX FT-NMR spectrometer using deuterated solvents. Chemical shifts are reported as δ in parts per million (ppm) relative to the solvent used (CDCl_3 at 7.26 ppm). Dialysis tubing was purchased from Spectrum labs with a MWCO of 6 – 8 kDa. Hydrodynamic diameters (D_{H}) and size distributions were determined by multi-angle dynamic light scattering (DLS) using an ALV spectrometer which consists of a 22 mW HeNe laser at $\lambda = 632.8$ nm. Measurements were carried out at 20 °C, and recorded at scattering angles between 30 and 150° every 10 or 20°. At least two measurements were run on each angle, each run for at least 60 seconds. The hydrodynamic radius (R_{H}) was then determined by plotting the decay rate (Γ) against the scattering vector squared (q^2), and applying the Stokes-Einstein equation. Size exclusion chromatography (SEC) analyses were performed either in *N,N*-dimethylacetamide (DMAc) containing LiBr (1 mg mL⁻¹) at a flow rate of 1.0 mL min⁻¹ at 50 °C, on a set of two PLgel 5 μm mixed-C columns and one guard column or in THF with 2% triethylamine (TEA) as eluent, with a flow rate of 1.0 mL min⁻¹ on a set of two PLgel 5 μm mixed-D columns, plus one guard column equipped with a PDA detector. Transmission electron microscopy (TEM) samples were prepared by drop deposition of a 0.1 mg mL⁻¹ polymer solution in water onto copper/carbon grids that had been pre-treated with oxygen plasma and analyzed using a JEOL TEM-2100 microscope operating at 200 kV. TEM images were taken by Miss Dafni Moatsou. Fluorescence experiments were carried out on a PerkinElmer LS 55 Fluorescence Spectrometer.

5.5.2 Methods and Techniques

Azo-(*bis*)-isobutyronitrile (AIBN) was purchased from Sigma-Aldrich, recrystallized from methanol and stored in the dark at 4 °C. MMA and EMA used for RAFT polymerizations were filtered through an aluminium oxide column and stored at 4 °C. All other chemicals were purchased from Sigma-Aldrich and used without further purification.

5.5.2.1 Small Molecule synthesis

M 5.1: The first step was conducted according to literature protocol.⁴⁷ 3-Bromopropanol (10 mL, 0.15 mol), TEA (16.7 mL, 0.16 mol) and dichloromethane (DCM, 230 mL) were added to a round bottom flask and stirred in an ice bath. Methacryloyl chloride (11.3 mL, 0.15 mol) was added drop-wise to the stirring solution. After addition, the solution was allowed to warm to room temperature and was stirred overnight. The resulting solution was diluted with methanol (~ 50 mL) and washed with NaHCO₃ and H₂O x 2 before being dried over MgSO₄ and the solvent removed under vacuum. The crude product was purified by column chromatography in petroleum ether: ethyl acetate (90:10) yielding the linker unit, yield = 13.45 g, 42%. ¹H NMR (300 MHz, CDCl₃) δ 1.78 (3H, s, CHH=C(CH₃)), 2.06 (2H, quin, ³J = 6.3 Hz, CH₂CH₂CH₂), 3.32 (2H, t, ³J = 6.6 Hz, CH₂-Br), 4.12 (2H, t, ³J = 6.0 Hz, C(O)OCH₂), 5.41 (1H, s, CHH=CH₃), 5.93 (1H, s, CHH=CH₃).



In the second step L-tryptophan methyl ester (7.3 g, 0.028 mol), TEA (4.65 mL, 0.034 mol) and DMF (100 mL) were stirred together in an ice bath. The linker (5.9 g, 0.028 mol) was added slowly before the reaction was allowed to warm up to room temperature

and stir for 2 days. After this period the solution was diluted with water and extracted into diethyl ether. The organic layers were combined and washed with NaHCO_3 and brine before being dried over MgSO_4 . The solvent was then removed before purification using column chromatography in hexane: ethyl acetate (90:10) to initially remove any unreacted linker and then changing the gradient to 50:50 to collect the desired product. Yield 5.2 g, 54%. ^1H NMR (300 MHz, CDCl_3) δ 1.76 (2H, q, $^3J = 6.6$ Hz, $\text{CH}_2\text{-CH}_2\text{-CH}_2$), 2.63 (2H, m, $^3J = 6.6$ Hz, $\text{CH}_2\text{-Ar}$), 1.88 (3H, s, $\text{CH}_3\text{-CH=CH}_2$), 3.12 (2H, m, $\text{CH}_2\text{-CH}_2\text{-NH}$), 3.59 (1H, t, $^3J = 6.3$ Hz, CH-NH), 3.62 (3H, s, $\text{CH}_3\text{-OC(O)}$), 4.13 (2H, t, $^3J = 6.3$ Hz, $\text{CH}_2\text{-OC(O)}$), 5.49 (1H, s, $\text{CHH=C(CH}_3\text{)}$), 6.02 (1H, s, $\text{CHH=CH(CH}_3\text{)}$), 7.03-7.59 (5H, m, Ar-H). ^{13}C NMR (300 MHz, CDCl_3): δ 17.7($\text{CH}_2\text{=C(CH}_3\text{)}$) 28.5 ($\text{CH}_2\text{-CH}_2\text{-CH}_2\text{-NH}$), 28.7 ($\text{CH}_2\text{-CH}_2\text{-CH}_2\text{-NH}$) 44.3 (Ar- CH_2), 51.1 ($\text{CH}_2\text{-CH-(NH)-COOCH}_3$), 61.5 (COOCH_3), 62.2 ($\text{CH}_2\text{-CH}_2\text{-CH}_2\text{-NH}$), 110.5 (Ar- H), 110.6-122.3 (Ar- H), 124.8 ($\text{CH}_2\text{=C(CH}_3\text{)}$), 126.8 ($\text{CH}_2\text{=C(CH}_3\text{)}$) 135.6 (Ar- H), 135.7 (Ar- H), 164.6 ($\text{CH}_2\text{=CH(CH}_3\text{)CO}$), 174.7 (COOMe). HR ESI-MS: found 345.1809 m/z $[\text{M}+\text{H}]^+$ expected 345.1809. $[\alpha]_D^{25} = +30$.

5.5.2.2 Polymerizations

Homopolymerization: A typical homopolymerization of **M 5.1** to synthesize **P 5.1** was carried out as follows: monomer **M 5.1** (0.05 g, 1.5×10^{-4} mol), 2-cyano-2-propyl benzodithioate (CTA) (6.7×10^{-4} g, 3.1×10^{-6} mol), AIBN (1.0×10^{-4} g, 6.1×10^{-7} mol) and dioxane (0.5 mL) were weighed into an ampoule. The mixture was degassed by 3 freeze-pump-thaw cycles before being back-filled with nitrogen and then heated to 70 °C for 6 h. The polymer was precipitated into cold stirring diethyl ether twice and collected as a pink solid. ^1H NMR (300 MHz, CDCl_3) δ 0.51-2.05

(7H, C(CH₃)CH₂ polymer backbone and CH₂CH₂CH₂NH), 2.55 (2H, m, CH₂CH₂CH₂NH), 3.09 (2H, s, Ar-CH₂), 3.59 (3H, s, CH₃C(O)O), 3.59 (1H, s, CH₂CH), 3.89 (2H, s, CH₂CH₂CH₂NH), 6.92-7.42 (5H, s, Ar-H), 8.91 (1H, s, NH). Conversion by ¹H NMR spectroscopy: 58%. M_n (SEC, DMF, PMMA calibration) = 6.0 kDa, $D = 1.11$.

Copolymerization: In a typical copolymerization, **M 5.1** (0.047 g, 1.45×10^{-4} mol), MMA (0.017 g, 1.45×10^{-4} mol), CTA (0.001 g, 2.89×10^{-6} mol), AIBN (4.7×10^{-5} g, 2.9×10^{-7} mol) were weighed into an ampoule and degassed by 3 freeze-pump-thaw cycles before being back-filled with nitrogen and then heated to 70 °C for 24 h. The polymer was precipitated into cold stirring diethyl ether twice and collected as a yellow solid. ¹H NMR (300 MHz, CDCl₃) δ tryptophan peaks: 0.74-2.03 (7H, C(CH₃)CH₂ polymer backbone and CH₂CH₂CH₂NH), 2.51 (2H, br m, CH₂CH₂CH₂NH), 3.04 (2H, br s, Ar-CH₂), 3.51 (1H, br s, CH₂CH), 3.52 (3H, br s, CH₃C(O)O), 3.66 (2H, br s, CH₂CH₂CH₂NH), 6.91-7.46 (5H, bs, Ar-H), 9.01 (1H, bs, NH) MMA peaks: 0.74-2.03 (7H, C(CH₃)CH₂ polymer backbone), 1.80 (3H, bs, CH₃C(O)O). Conversion by ¹H NMR spectroscopy: **M 5.1** 74% and MMA 87%. M_n (SEC, DMF, PMMA calibration) = 34.9 kDa, $D = 1.60$.

Chain-extension to give a block copolymer: The tryptophan MacroCTA (homopolymer) was synthesized using conditions as described above, **P 5.1** ($M_{n, \text{NMR}} = 14$ kDa) and a representative chain extension with methyl acrylate was carried out as follows: **P 5.1** (0.05 g, 3.6×10^{-6} mol, 1 eq), MMA (40 μ L, 3.6×10^{-4} mol, 100 eq), AIBN (1.2×10^{-4} g, 7.3×10^{-7} mol) and dioxane (1 mL) were weighed into an ampoule. The mixture was degassed by 3 freeze-pump-thaw cycles before being

back-filled with nitrogen and then heated to 70 °C for 6 h. The polymer was precipitated into cold stirring diethyl ether twice and collected as a pink solid. ^1H NMR (300 MHz, CDCl_3) δ tryptophan peaks: 0.51-1.92 (7H, $\text{C}(\text{CH}_3)\text{CH}_2$ polymer backbone and $\text{CH}_2\text{CH}_2\text{CH}_2\text{NH}$), 2.33 (2H, m, $\text{CH}_2\text{CH}_2\text{CH}_2\text{NH}$), 2.91 (2H, s, Ar- CH_2), 3.40 (1H, s, CH_2CH), 3.41 (3H, s, $\text{CH}_3\text{C}(\text{O})\text{O}$), , 3.61 (2H, s, $\text{CH}_2\text{CH}_2\text{CH}_2\text{NH}$), 6.76-7.33 (5H, s, Ar- H), 7.71 (1H, s, NH) MMA peaks: 0.51-1.92 (7H, $\text{C}(\text{CH}_3)\text{CH}_2$ polymer backbone), 1.63 (3H, s, $\text{CH}_3\text{C}(\text{O})\text{O}$). Conversion by ^1H NMR spectroscopy: 70%. M_n (SEC, DMF, PMMA calibration) = 22.9 kDa, $D = 1.24$.

5.5.2.3 Nanogel Synthesis

For a typical synthesis of the L- tryptophan containing nanogel core: SDS (0.156 g, 20 wt%) was dissolved in stirring water (50 mL) at 600 rpm. In a separate vial, **M 5.1** (0.029 g, 5 wt%), EMA (0.534 mL) and EGDMA (0.055 mL, 10 wt%) were mixed without additional solvent. This monomer solution was then added to the stirring SDS/ H_2O solution. The resulting solution was bubbled with nitrogen for 10 min before potassium persulfate (KPS) (5 mg) was added. The mixture was purged with nitrogen for a further 10 min before submerging into a preheated oil bath at 70 °C with stirring at 600 rpm overnight. The solution turned to an iridescent solution and was quenched by cooling to room temperature and exposure to air. The nanogel was then dialyzed against millipure H_2O (MWCO = 6 – 8 kDa) to remove excess SDS.

*For a typical shell synthesis, through a seeded emulsion polymerization process:*⁴⁸

The seed nanogel dispersion (25 mL) was purged with nitrogen and heated at 70 °C with rapid stirring (600-800 rpm). In a separate flask, SDS (0.078 g) was dissolved

in water (25 mL) and also purged with nitrogen. To the SDS/water solution, EMA (0.275 mL), EGDMA (1.2 μL , 0.5 wt%) and KPS (2.5 mg) were added. The monomer/surfactant mixture was then added slowly to the heated nanogel seeds at no faster than 1 mL min^{-1} . Once the addition was complete, a positive pressure of nitrogen was maintained for the duration of the reaction. The solution was left to stir overnight and purified by dialysis against millipure H_2O (MWCO = 6 – 8 kDa) to remove excess reagents and SDS.

5.5.2.4 Fluorescence experiments

Fluorescence investigations into monomer, polymer and nanogel: The solutions were prepared at the prescribed concentrations in THF, apart from the nanogel which was analyzed without alteration i.e. in water. A pre-scan method was initially used to determine the maximum absorption wavelength which was then used for the fluorescence recording. **M 5.1** was excited at 345 nm and emission was recorded at 420 nm. The RAFT polymer was excited at 388 nm and emission recorded at 405 nm. The nanogel was excited at 280 nm and emission recorded at 350 nm. For the monomer and polymer samples, an excitation and emission slit width of 10 nm was used, which was reduced for nanogel samples to 2.5 nm.

FRET experiments for core nanogels were carried out as follows: the nanogel solution was diluted by a factor of 10 prior to use. The system was excited at 225 nm using a 2.5 nm slit width for emission and excitation. A solution of DNSA at 2 mg mL^{-1} in THF was prepared and degassed using nitrogen. The nanogel sample was also degassed by bubbling with nitrogen. 200 μL of the nanogel solution was removed and placed in the fluorescence cuvette to which 5 μL of the DNSA solution was added and the fluorescence programme started. After a short time delay, which

is the same for all experiments, the first spectrum was recorded $t = 0$ min. One spectrum was recorded at 5 min intervals until the same intensity was recorded at least 10 times, after which the tryptophan emission was regarded as fully quenched. The same FRET procedure was used to investigate the core-shell nanogels, but using a slit width of 10 nm rather than 2.5 nm and adding 1 μL of the DNSA solution.

5.6 References

1. P. R. Callis and T. Liu, *J. Phys. Chem. B*, 2004, **108**, 4248-4259.
2. J. T. Vivian and P. R. Callis, *Biophys. J.*, 2001, **80**, 2093-2109.
3. Y. Chen and M. D. Barkley, *Biochemistry*, 1998, **37**, 9976-9982.
4. D. K. Smith and L. Müller, *Chem. Commun.*, 1999, 1915-1916.
5. A. Kessler, O. Menendez-Aguirre, J. Hinrichs, C. Stubenrauch and J. Weiss, *Faraday Discuss.*, 2013, **166**, 399-416.
6. C. A. Royer, *Chem. Rev.*, 2006, **106**, 1769-1784.
7. J. Lakowicz, *Principles of fluorescence spectroscopy*, Springer, New York, 2006.
8. S. B. La, T. Okano and K. Kataoka, *J. Pharm. Sci.*, 1996, **85**, 85-90.
9. C. L. Zhao, M. A. Winnik, G. Riess and M. D. Croucher, *Langmuir*, 1990, **6**, 514-516.
10. I. Astafieva, K. Khougaz and A. Eisenberg, *Macromolecules*, 1995, **28**, 7127-7134.
11. A. V. Kabanov, I. R. Nazarova, I. V. Astafieva, E. V. Batrakova, V. Y. Alakhov, A. A. Yaroslavov and V. A. Kabanov, *Macromolecules*, 1995, **28**, 2303-2314.
12. M. Wilhelm, C. L. Zhao, Y. Wang, R. Xu, M. A. Winnik, J. L. Mura, G. Riess and M. D. Croucher, *Macromolecules*, 1991, **24**, 1033-1040.
13. A. Blanazs, S. P. Armes and A. J. Ryan, *Macromol. Rapid Commun.*, 2009, **30**, 267-277.
14. M. P. Robin, P. Wilson, A. B. Mabire, J. K. Kiviaho, J. E. Raymond, D. M. Haddleton and R. K. O'Reilly, *J. Am. Chem. Soc.*, 2013, **135**, 2875-2878.

15. M. P. Robin, A. B. Mabire, J. C. Damborsky, E. S. Thom, U. H. Winzer-Serhan, J. E. Raymond and R. K. O'Reilly, *J. Am. Chem. Soc.*, 2013, **135**, 9518-9524.
16. W. Deng, A. Cao and L. Lai, *Biochem. Biophys. Res. Commun.*, 2007, **362**, 689-694.
17. M. J. Tucker, R. Oyola and F. Gai, *J. Phys. Chem. B*, 2005, **109**, 4788-4795.
18. S. J. Miyake-Stoner, A. M. Miller, J. T. Hammill, J. C. Peeler, K. R. Hess, R. A. Mehl and S. H. Brewer, *Biochemistry*, 2009, **48**, 5953-5962.
19. S. J. Nannepaga, R. Gawalapu, D. Velasquez and R. Renthal, *Biochemistry*, 2003, **43**, 550-559.
20. H. Sahoo, D. Roccatano, M. Zacharias and W. M. Nau, *J. Am. Chem. Soc.*, 2006, **128**, 8118-8119.
21. U. S. Mote, S. R. Patil, S. H. Bhosale, S. H. Han and G. B. Kolekar, *J. Photochem. Photobiol., B*, 2011, **103**, 16-21.
22. Y. Xie, T. Maxson and Y. Tor, *J. Am. Chem. Soc.*, 2010, **132**, 11896-11897.
23. H. Sahoo, D. Roccatano, A. Hennig and W. M. Nau, *J. Am. Chem. Soc.*, 2007, **129**, 9762-9772.
24. J.-I. Chen and W.-C. Wu, *Macromol. Biosci.*, 2013, **13**, 623-632.
25. Y. Koda, T. Terashima, A. Nomura, M. Ouchi and M. Sawamoto, *Macromolecules*, 2011, **44**, 4574-4578.
26. W. Wang, Y. Zhang, Q. Yang, M. Sun, X. Fei, Y. Song, Y. Zhang and Y. Li, *Nanoscale*, 2013, **5**, 4958-4965.
27. C. Grazon, J. Rieger, R. Meallet-Renault, B. Charleux and G. Clavier, *Macromolecules*, 2013, **46**, 5167-5176.

28. Z. Xing, J. Zhang, X. Li, W. Zhang, L. Wang, N. Zhou and X. Zhu, *J. Polym. Sci., Part A: Polym. Chem.*, 2013, **51**, 4021-4030.
29. T. Xing, B. Lai and L. Yan, *Macromol. Chem. Phys.*, 2013, **214**, 578-588.
30. H. Mori, E. Takahashi, A. Ishizuki and K. Nakabayashi, *Macromolecules*, 2013, **46**, 6451-6465.
31. S. G. Roy, R. Acharya, U. Chatterji and P. De, *Polym. Chem.*, 2013, **4**, 1141-1152.
32. V. Rodionov, H. Gao, S. Scroggins, D. A. Unruh, A.-J. Avestro and J. M. J. Fréchet, *J. Am. Chem. Soc.*, 2010, **132**, 2570-2572.
33. A. Lu, D. Moatsou, D. A. Longbottom and R. K. O'Reilly, *Chem. Sci.*, 2013, **4**, 965-969.
34. L. Y. Lin, N. S. Lee, J. Zhu, A. M. Nystrom, D. J. Pochan, R. B. Dorshow and K. L. Wooley, *J. Controlled Release*, 2011, **152**, 37-48.
35. J. Chiefari, Y. K. Chong, F. Ercole, J. Krstina, J. Jeffery, T. P. T. Le, R. T. A. Mayadunne, G. F. Meijs, C. L. Moad, G. Moad, E. Rizzardo and S. H. Thang, *Macromolecules*, 1998, **31**, 5559-5562.
36. R. T. A. Mayadunne, E. Rizzardo, J. Chiefari, J. Krstina, G. Moad, A. Postma and S. H. Thang, *Macromolecules*, 2000, **33**, 243-245.
37. J. Chiefari, R. T. A. Mayadunne, C. L. Moad, G. Moad, E. Rizzardo, A. Postma and S. H. Thang, *Macromolecules*, 2003, **36**, 2273-2283.
38. C. L. McCormick and A. B. Lowe, *Acc. Chem. Res.*, 2004, **37**, 312-325.
39. S. Khorasanizadeh, I. D. Peters, T. R. Butt and H. Roder, *Biochemistry*, 1993, **32**, 7054-7063.
40. C. R. Caldwell, *Plant Physiol.*, 1993, **101**, 947-953.

41. R. L. Jensen, J. Arnbjerg and P. R. Ogilby, *J. Am. Chem. Soc.*, 2012, **134**, 9820-9826.
42. J. R. Lakowicz and G. Weber, *Biochemistry*, 1973, **12**, 4171-4179.
43. T. Todorovski, M. Fedorova and R. Hoffmann, *J. Mass Spectrom.*, 2011, **46**, 1030-1038.
44. M. Lunz, A. L. Bradley, V. A. Gerard, S. J. Byrne, Y. K. Gun'ko, V. Lesnyak and N. Gaponik, *Phys. Rev. B*, 2011, **83**, 115423.
45. C. S. Chern, *Prog. Polym. Sci.*, 2006, **31**, 443-486.
46. R. Arshady, *Colloid. Polym. Sci.*, 1992, **270**, 717-732.
47. H. J. Spijker, A. J. Dirks and J. C. M. van Hest, *Polymer*, 2005, **46**, 8528-8535.
48. C. D. Jones and L. A. Lyon, *Macromolecules*, 2000, **33**, 8301-8306.

Conclusions

Due to the advances in polymerization technology polymers containing functional monomers based on the amino acids L-tyrosine and L-tryptophan have been synthesized. The facile incorporation of these amino acids into polymeric structures has allowed for their properties of chiral resolution, catalysis and fluorescence to be studied and utilized.

L-Tyrosine has been used as the starting material for the synthesis of a unique monomer incorporating both methacrylate functionality and the MacMillan catalyst. This novel monomer has then been immobilized into both co-polymers synthesized *via* RAFT polymerization and cross-linked nanogels synthesized *via* emulsion polymerization. Its catalytic activity in these two systems has been investigated through the use of the DA reaction. The polymers have allowed for the *pseudo*-continuous use of the catalyst whilst the nanogels offered benefits from the concentrator effect; although the selectivity of the catalyst was compromised when immobilized into the nanogel. L-Tryptophan has been examined for both its chiral resolution ability and its fluorescent character. The monomer and polymer of both enantiomers of tryptophan were studied as a potential chiral resolver and were shown to have different strength interactions with the enantiomers of 1'-bi-2-naphthol. L-Tryptophan was also immobilized within a cross-linked nanogel and used in FRET studies with its FRET pair dansyl amide to probe the effects of cross linking density and co-monomer on small molecule diffusion.

The facile incorporation of amino acids into these different types of structures has allowed for various applications to be examined. Amino acids represent a readily available class of chiral starting materials that have a range of properties and potential applications. The advances in polymerization technologies has allowed for these properties, in some instances, to be enhanced and immobilized, potentially opening up routes to new advanced materials.